Doctorate in Cognitive Sciences
CIMeC Center for Mind/Brain Sciences
Università degli studi di Trento

Finding the missing connection

Diffusion-based tractography reconstruction of the acoustic radiation and other applications

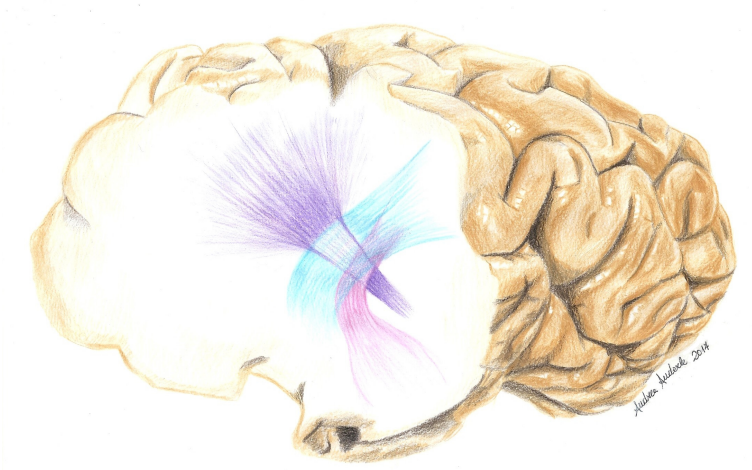

PhD Candidate:
Chiara Maffei

Supervisor:
Prof. Jorge Jovicich

Acknowledgments

I would like to start by acknowledging all those that have contributed to this dissertation.

Without any doubts, I want to start by thanking my supervisor Professor Jorge Jovicich for having been the best supervisor one PhD student can possibly ever have. I want to thank him for his constant support, his generosity, his trust and mentorship over these three years. I am deeply grateful for everything he has done for me.

I would also like to thank Professor Gabriele Miceli for his guidance over my academic growth. Professor Miceli has supervised me during my master thesis work, and we kept working together during my PhD. I am thankful for the stimulating discussions we had over these years and for his contagious passion and enthusiasm for research.

I am particularly indebted to Doctor Silvio Sarubbo. I am very grateful for the chance I had to collaborate with him during my PhD. The validation part of my work would not have been possible without his precious collaboration. The experience he offered me is invaluable for me.

I would then like to thank my reviewing committee members: Laurent Petit and Mara Cercignani for their time, interest, and helpful comments and suggestions.

Last but not least, I want to thank all my friends and colleagues that have shared with me the everyday joys and sorrows of a researcher's life: Henrietta Howells, Ekaterina Delikishkina, Fleur Van Ierschot, Ludovico Minati, Ceren Battal, Domenico Zacà, Mohamed Rezk, Isabella Giachetti. None of this work would have been possible without their invaluable support.

Contents

List of Figures

List of Tables

Chapter 1

Introduction

1.1 Background and motivation

"To say that the white matter is but a uniform substance like wax in which there is no hidden contrivance, would be to low an opinion of nature's finest masterpiece. We are assured that wherever in the body there are fibers, they everywhere adopt a certain arrangement among themselves, created more or less according to the functions for which they are intended...all the diversity of our sensation and our movements depends upon this. We admire the skillful construction...where each of these fibers, confined in a small space, functions without confusion and without disorder." (Nicolaus Steno 1669)

For many years, much of our knowledge on cognitive brain functions has been linked to the modular paradigm, in which brain areas are postulated to act as independent processors for specific cognitive functions. In the second half of the 19th century however, neuro-anatomical research extended from the cortical surface to the sub-cortical white matter and interest in the connectivity of the human brain started off. These first investigations revealed the brain as a heterogeneous ensemble of interconnected regions, far from being composed of isolated modules (Catani, Mesulam, 2008). A new paradigm slowly emerged that emphasized the idea of different brain areas working together in large-scale networks. It became clear that the function of a complex system cannot be deduced from a list of its components. "The relation among components introduces attributes that are not contained in the list of constituent elements" (Mesulam M: Preface. In Fiber pathways of the brain. Edited by Schmahmann JD PD. New York: Oxford University Press; 2006).

At the base of these definitions stands the key idea that what describes a function is not its cortical location but its unique profile of interrelated underlying connections. In 1993 Francis Crick and Edward Jones published an editorial in Nature entitled "Backwardness of human neuroanatomy". Their intention was to "make a wide audience aware" of how little is known about the anatomy of the human brain, and to highlight the ur-

gent need for "new methods to solve this problem" (Catani, 2007). A year later, in 1994, Basser et al. (Basser et al., 1994) published their seminal paper where they described, for the first time, diffusion tensor imaging (DTI). A real breakthrough came with the development of this technique to study the organization of the white matter in the living human brain. With DTI it was possible, for the first time, to infer neuro-anatomical information of microstructural brain tissue. One of the main applications of DTI has been since then the three-dimensional computerized reconstruction of white-matter fiber trajectories, called "tractography" (Mori et al., 1999). This technique allowed exploring the anatomy of the main white matter pathways in humans *in-vivo* and non-invasively.

Since then, many steps have been taken in diffusion-based tractography and many white matter bundles have been over the years described and correlated with different cognitive abilities (Catani et al., 2005), in the effort to chart the relation between human brain anatomy, brain function, and behaviour within the same individual (Pestilli, 2015). However, as any other method, tractography is not without limitations: the strong dependence of this technique on acquisition and algorithm parameters makes it highly variable, and prevents the reliable reconstruction of some major white matter bundles. The need to enlarge the anatomical knowledge of the brain is as strong today as it was twenty years ago.

1.2 Research summary

This dissertation is divided into three main parts.

Part I (Chapters 2-3) provides a basic overall introduction to the investigation of brain white matter architecture through the use of diffusion MRI methods. Chapter 2 focuses on the basic principles of diffusion and on how we can model and quantify the displacement of water molecules in the human brain. Chapter 3 introduces diffusion-based tractography, considering the applications and limitations of this technique.

Part II (Chapters 4-6) presents the work that I view as the main contribution of this dissertation, which focuses on the topographic and tractography characterization of a main projection sensory pathway, the acoustic radiation (AR).

In the first chapter of Part II (Chapter 4), a review of the available topographical knowledge of the acoustic radiation in non-human primates and humans is provided. Chapter 5 describes a study that provides novel topographical knowledge of the AR through Klinger's post-mortem blunt dissection and diffusion-based tractography. Chapter 6 provides a characterization of AR tractography results in relation to acquisition and analysis variables and the construction of a probabilistic atlas of the AR. Chapter 7 provides an example of AR investigation in a specific population of congenitally deaf subjects.

Part III (Chapter 8) describes preliminary analyses of diffusion tractography applications on other white matter bundles of the human brain. The first study aims at characterizing optic radiation (OR) differences between early blind, late blind and age & gender matched healthy sighted subjects. The second study of chapter 8 describes a study aimed at characterizing the middle longitudinal fasciculus (MdLF) to investigate

its role in audio-visual integration in patients affected by word deafness after suffering from an ischemic stroke in the left hemisphere.

1.3 Original contributions

Chapter 4 constitutes a theoretical review on the topography and tractography literature of the acoustic radiation conceived by my advisor (Jorge Jovicich) and me.

Chapter 5 was made possible by the collaboration with the S.Chiara Hospital in Trento (Dr. Silvio Sarubbo, Dr. Franco Chioffi) and the Bambino Gesu Hospital (Dr. Alessandro de Benedictis). Franco Chioffi made the specimens available for scientific investigation, Silvio Sarubbo performed the post-mortem blunt micro-dissections, and Alessandro de Benedictis collected and processed the images of the dissections. I conducted the diffusion MRI data processing and tractography analysis, and Silvio Sarubbo, Jorge Jovicich and I shared responsibility for production of the manuscript, which is now published in the journal Brain Structure and Function with the title: "Topography of the human acoustic radiation as revealed by *ex-vivo* fibers micro-dissection and *in-vivo* diffusion-based tractography" (Maffei et al., 2017).

Chapter 6 was performed in collaboration with Silvio Sarubbo (S. Chiara Hospital in Trento) and my supervisor Jorge Jovicich. Silvio Sarubbo contributed with his anatomical expertise and topographical knowledge of the AR, I processed the diffusion data and conducted all the analyses, and me and Jorge Jovicich shared responsibility for the production of the manuscript. Part of this work was presented as a poster at the OHBM conference (C. Maffei, J. Jovicich. Effects of acquisition and tractography parameters on the reconstruction of the acoustic radiation. OHBM 2016, 22nd Annual Scientific Meeting. Geneva (CH), June 2016. Poster Presentation.), and we are now working to ultimate the study and submit the manuscript for publication.

Chapter 7 constitutes a very preliminary investigation of a project we are working on. The project is carried on in collaboration with colleagues at our center (Stefania Benetti and Olivier Collignon). Stefania Benetti and Olivier Collignon recruited the subjects and acquired the MRI data. I conducted the pre-processing of the data and the preliminary investigation.

Chapter 8 includes two different projects. The first one, on the anatomy of the optic radiation in blind subjects, was performed in collaboration with colleagues at our center (Center for Mind/Brain Sciences (CIMeC)) (Olivier Collignon, Ceren Battal), and Institute of Psychology (IPSY) and of Neurosciences (IoNS); University of Louvain-la-Neuve; Belgium (Mohamed Toaffik, Stefania Mattioni, Tehvide Hicret), as well as members of our own lab (Jorge Jovicich). Stefania Mattioni and Ceren Battal recruited the subjects and collected the MR imaging data. Mohamed Toaffik and Tehvide Hicret performed the parcellation and the manual editing in Freesurfer. I was responsible for the processing of the diffusion MRI data and the production of the manuscript draft. Part of the study was presented as a poster at the ISMRM conference (Chiara Maffei, Isabella Giachetti, Stefania Mattioni, Ceren Battal, Mohamed Rezk, Olivier Collignon, and Jorge Jovicich. How does blindness onset impact on the structure of the optic

radiation? ISMRM 25th Annual Meeting & Exhibition. Honolulu, (USA), April 2017) and we are now working to ultimate the study and submit the manuscript for publication.

The second project, on the anatomy of the middle longitudinal fasciculus in stroke patients, is an extension of the abstract I submitted to the 25th Annual Meeting of the Organization for Human Brain Mapping in 2017, entitled: "Is the Middle Longitudinal Fasciculus involved in audio-visual integration?". The work was conducted in collaboration with Gabriele Miceli (CIMeC) and the colleagues at the Brain and Spine Institute, Hôpital de la Salpêtrière, Paris, France (Laurent Cohen, Katarzyna Siuda-Krzywicka, Sami Abboud, Paolo Bartolomeo). They collected the imaging data of patient GAB and controls, while Gabriele Miceli collected the imaging data of patient FO and controls. I collected behavioural data and processed the diffusion MRI data. Part of the study was presented as a poster at the OHBM conference (C. Maffei, J. Jovicich, L. Cohen, K. Siuda-Krzywicka, S. Abboud, P. Bartolomeo, G. Miceli. Is the middle longitudinal fasciculus involved in audio-visual integration? OHBM 2017, 23nd Annual Scientific Meeting. Vancouver (CA), June 2017) and we are now working to ultimate the study and submit the manuscript for publication.

1.4 Scientific production

Publications

- Chiara Maffei, Rita Capasso, Giulia Cazzolli, Flavio Dell'Acqua, Marco Catani, Gabriele Miceli, "Pure word deafness following left temporal damage: behavioral and tractography evidence from a new case". Accepted for publication on Cortex.
- Chiara Maffei, Jorge Jovicich, Alessandro De Benedictis, Franco Chioffi, and Silvio Sarubbo. "Topography of the acoustic radiation as revealed by ex-vivo fiber dissections and in-vivo diffusion-based tractography". Brain Structure and Function, 2017 (in press).
- Chiara Maffei, Guadalupe Soria, Alberto Prats-galino, Marco Catani, "Imaging white-matter pathways of the auditory system with diffusion imaging tractography" in G.G. Celesia and Hickok (edited by), The Human Auditory System: Fundamental Organization and Clinical Disorders, Amsterdam: Elsevier B.V., 2015. - (HANDBOOK OF CLINICAL NEUROLOGY). - ISBN: 9780444626301

Conference Abstracts

- C. Maffei, J. Jovicich, L. Cohen, K. Siuda-Krzywicka, S. Abboud, P. Bartolomeo, G. Miceli. Is the middle longitudinal fasciculus involved in audio-visual integration? OHBM 2017, 23nd Annual Scientific Meeting. Vancouver (CA), June 2017. Poster Presentation.

- Chiara Maffei, Jorge Jovicich, Alessandro De Benedictis, Franco Chioffi, and Silvio Sarubbo. Topography of the acoustic radiation as revealed by ex-vivo fiber dissections and in-vivo diffusion-based tractography. ISMRM 25th Annual Meeting & Exhibition. Honolulu, (USA), April 2017. Oral Presentation.
- Chiara Maffei, Isabella Giachetti, Stefania Mattioni, Ceren Battal, Mohamed Rezk, Olivier Collignon, and Jorge Jovicich. How does blindness onset impact on the structure of the optic radiation? ISMRM 25th Annual Meeting & Exhibition. Honolulu, (USA), April 2017. Poster Presentation.
- C. Maffei, Rita Capasso, Giulia Cazzolli, Flavio Dell'Acqua, Marco Catani and Gabriele Miceli. The neural underpinnings of pure word deafness following left temporal damage. 54th Annual Academy of Aphasia. Llandudno, Wales (UK), October 2016. Poster Presentation.
- C. Maffei, J. Jovicich. Effects of acquisition and tractography parameters on the reconstruction of the acoustic radiation. OHBM 2016, 22nd Annual Scientific Meeting. Geneva (CH), June 2016. Poster Presentation.
- C. Maffei, J. Jovicich. Reconstruction of the human acoustic radiation tract: an investigation of diffusion acquisition and tractography algorithm factors. Italian Chapter of the International Society for Magnetic Resonance Imaging in Medicine Annual Meeting. Bologna (IT), February, 2016. Poster Presentation.
- C. Maffei, F. Dell'Acqua, J. Jovicich. Effects of b-value on spherical deconvolution characterization of the corpus callosum. ESMRMB 2015, 32nd Annual Scientific Meeting. Edinburgh (UK), October 2015. Oral presentation.

Invited Talks

- Sherbrooke Connectivity Imaging Lab, Sherbrooke (CA), June 2017. Host: Maxime Descoteaux. Title: "Reconstructing the Acoustic Radiation Using Diffusion-based Tractography".
- Athinoula A. Martinos Center for Biomedical Imaging, Boston (USA), June 2017. Host: Anastasia Yendiki. Title: "Topography of the Acoustic Radiation Revealed by Post-mortem Dissections and Diffusion-based Tractography".
- Neurodegenerative Diseases Institute, Neurofunctional Imaging Group, Bordeaux (FR), February 2017. Host: Laurent Petit. Title: "A missing Connection".
- Ospedale "S.Maria del Carmine", U.O. di Neurologia e Riabilitazione Neurologica, Rovereto (IT), December 2016. Host: Giorgio Rossi.

Awards

- ISMRM Magna cum Laude Merit Award for the work "Topography of the acoustic radiation as revealed by ex-vivo fiber dissections and in-vivo diffusion-based tractography" presented at the ISMRM 25th Annual Meeting & Exhibition, April 2017.
- Trainee Educational Stipend Award. ISMRM 25th Annual Meeting & Exhibition, 2017.
- Student Support Program Award. ESMRMB 2015, Edinburgh.
- Scholarship for Merit, M.Sc. Cognitive Science, University of Trento. Awarded for outstanding achievement throughout the entire course of study. September 2014.

Bibliography

Basser P J, Mattiello J, LeBihan D. MR diffusion tensor spectroscopy and imaging. // Biophysical journal. 1994. 66, 1. 259–267.

Catani Marco. From hodology to function // Brain. 2007. 130, 3. 602–605.

Catani Marco, Jones Derek K., Ffytche Dominic H. Perisylvian language networks of the human brain // Annals of Neurology. 2005. 57, 1. 8–16.

Catani Marco, Mesulam Marsel. What is a disconnection syndrome? // Cortex. 2008. 44, 8. 911–913.

Maffei Chiara, Jovicich Jorge, De Benedictis Alessandro, Corsini Francesco, Barbareschi Mattia, Chioffi Franco, Sarubbo Silvio. Topography of the human acoustic radiation as revealed by ex vivo fibers micro-dissection and in vivo diffusion-based tractography // Brain Structure and Function. sep 2017. 1–11.

Mori S, Crain B J, Chacko V P, Zijl P C van. Three-dimensional tracking of axonal projections in the brain by magnetic resonance imaging. // Annals of neurology. 1999. 45, 2. 265–269.

Pestilli Franco. Test-retest measurements and digital validation for in vivo neuroscience // Scientific Data. 2015. 2. 140057.

Chapter 2

Measuring Water Diffusion

2.1 The mathematical basis of diffusion

On a molecular level, nothing stands still. Water molecules inside and outside our cells are moving randomly in constant thermal agitation, a phenomenon known as "Brownian motion" (from the botanist Robert Brown that discovered this phenomenon in 1827), or simply "diffusion". This movement is defined as the constant random displacement of particles due to physical factors such as temperature, or pressure from high concentration to low concentration regions. In this process, the trajectory of each water molecule in an unrestricted medium can be thus described as a "random walk", meaning that a molecule stays in a particular position for a fixed time, T_0, before moving to a new random location T_1. Given that this is a random process, it is certainly impossible to predict the position of each of these molecules after a given time window. However, in the glorious 1905, Einstein used a probabilistic framework to show that one aspect of this random behaviour could be characterized (Einstein, 1905). He proposed that, provided the number of particles is sufficiently large, and provided they can diffuse freely, at a fixed temperature, the squared displacement of molecules from their starting point, averaged all the molecules in the sample, is directly proportional to the observation time (or diffusion time τ). This relationship is given by Einstein's equation:

$$X^2 = 2D\tau \tag{2.1}$$

where X^2 is the average mean-squared displacement of particles during a diffusion time τ, and D is the diffusion coefficient. D constitutes the constant of proportionality, which depends on the size of the molecules, the temperature and the viscosity of the medium. In free water, during a given time interval, the distribution of X^2 takes the form of a Gaussian distribution, with the peak being at zero displacement and being equal probability to displace in any direction from the origin (Figure 2.1).

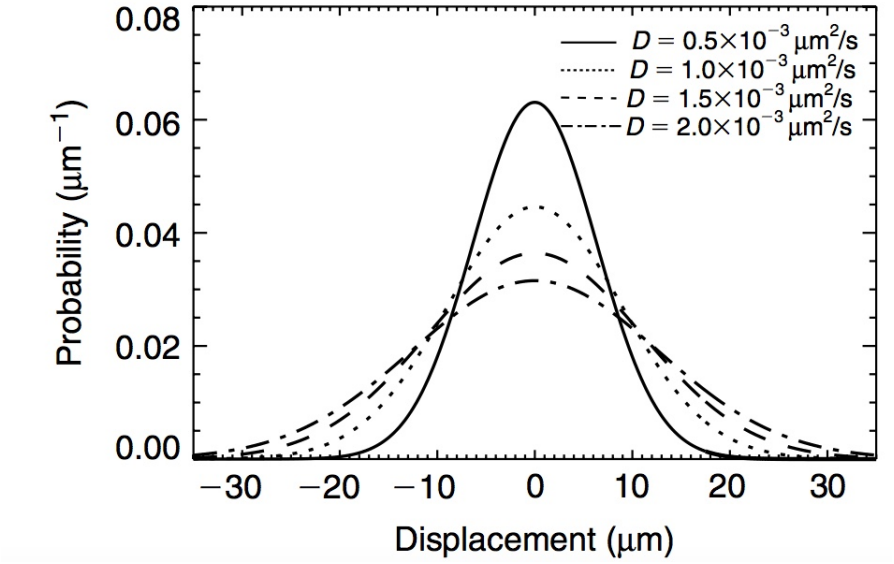

Figure 2.1: Gaussian Diffusion. The figure displays the diffusion process in the form of a Gaussian distribution. The displacement is plotted for different values of D at a fixed diffusion time τ of $40ms$. Larger D leads to broader displacement probability profiles (taken from Johansen-Berg, Behrens (2009)).

2.2 Diffusion in the brain

In the human brain, water molecules are not completely free to move because several physical barriers hinder their diffusion. These barriers are mainly constituted by cell membranes, axons, macro-molecules, and cytoskeleton. Because of the presence of these obstacles, water molecules need to find a way to diffuse around them and thus the displacement distance increases less with the increase of diffusion time, compared to unrestricted diffusion. As the diffusion time increases, an increasing fraction of water molecules strikes the boundaries and the effects of the obstacles become predominant. It follows that in a fixed period of time, the overall displacement and, therefore, the diffusion coefficient (D), are reduced in brain tissue compared to free water. This is the reason why to describe diffusion in brain tissue, we generally refer to the apparent diffusion coefficient (ADC), to reflect the fact that several biological barriers hinder water diffusion (Le Bihan et al., 1986). The ADC in the brain is 2 to 10 times smaller than in free water.

Inside the brain, molecules of water are distributed between extra-cellular and intra-cellular spaces. In general, diffusion in the extra-cellular space happens more freely, since in the intra-cellular space it is more likely to encounter cell walls, organelles, macro-molecules, *etc.*. High viscosity, macro-molecular crowding, and restriction effects have been proposed to explain diffusion reduction in the intra-cellular space. For extracellular space, tortuosity effects are considered. Because of the presence of different obstacles,

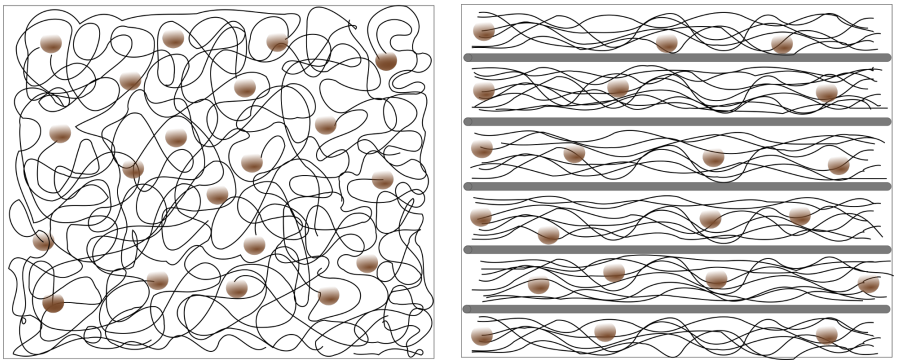

Figure 2.2: Isotropic and Anisotropic Diffusion. The figure shows a schematic representation of isotropic and anisotropic diffusion in the brain. In isotropic tissues (grey matter, CSF) water molecules can diffuse with equal probability along all directions (left panel), while in anisotropic tissues (white matter) the water molecules can more freely diffuse along the direction of axonal fibers than across them (right panel).

water molecules must take longer paths to cover a given distance, since they have to diffuse around cells that are not totally permeable to them (Beaulieu, 2002).

The brain tissue is mainly subdivided into white matter, grey matter, and cerebrospinal fluid (CSF). The grey matter is composed by neurons and glia cells, while the myelinated axonal filaments connecting the neurons constitute the white matter. These components limit the free diffusion of water in two very different ways: in the CSF and to some extent in the grey matter, where physical properties are identical in all directions, the diffusion of water molecules is reduced equally along all orientations. This is thus defined isotropic tissue (from Greek *iso*=equal and *tropos*=direction) and isotropic diffusion (Figure 2.2). In the CSF, barriers to water diffusion are sparser, and thus the overall displacement length is larger than in grey matter, where cell walls and membrane are more densely packed. White matter tissue on the contrary, is anisotropic (non-isotropic); here the well-organized axonal filaments allow displacement of water molecules preferentially along their fibers rather than perpendicularly to them. The exact cause of this anisotropy remains under debate (Beaulieu et al., 1996; Johansen-Berg, Behrens, 2009). However studies show this is mainly due to the presence of cellular membranes, with some contributions from myelination and axons packing (Beaulieu, 2002). Given that the tissue microstructure properties clearly affect the diffusion of water molecules, we can think of the diffusion process as an indirect probe of the structures that alter this displacement per unit time. Diffusion weighted magnetic resonance imaging (DW-MRI) takes advantage of these differences in tissue properties to indirectly acquire information on the microstructural anatomy of the human brain.

2.3 Diffusion MRI acquisition

In 1985, at the international ISMRM conference in London, Denis Le Bihan, at that time doctoral student in physics in France (Le Bihan, Breton, 1985), presented the world-first diffusion weighted images (DWI). This technique is a variant of conventional magnetic resonance imaging (MRI) that is sensitive to the displacement of water molecules inside a voxel, in a given period of time.

The sensitivity of the MR signal to molecular diffusion measured through spin-echo sequences was first observed by Edwin Hahn (Hahn, 1950). He reported a reduction of the signal following dephasing of spins caused by translational diffusion in an inhomogeneous magnetic field. A few years later, Carr, Purcell (1954) proposed a mathematical and physical framework to directly use Hahn's spin-echo sequence to measure the random molecular diffusion. Given that a spin's processional frequency is determined by the local magnetic field (as stated by the Larmor equation), when a magnetic field is applied spins at different locations experience different magnetic fields, and so they precess at different angular frequencies. This means that a particle experiencing a magnetic field at a particular time and position, will suffer a phase shift after moving to another location, that will influence the MR signal.

After a decade, Stejskal, Tanner (1965) introduced the pulse-gradient spin-echo sequence (PGSE) scheme that made modern diffusion MRI measurements possible, and that remains today the standard scheme to sensitize the MR signal to diffusion. This framework replaced the constant magnetic field used by Carr and Purcell (constant field gradient approach) (Carr, Purcell, 1954) with short duration gradient pulses, which allowed to clearly distinguish between the encoding time (δ, pulse duration) and the diffusion time (Δ, interval between the two pulses) (Figure 2.3). The two gradient pulses are applied one after excitation and one before signal sampling; the water molecules subject to motion during this time-frame emit a radiofrequency signal with slightly different phases, causing signal attenuation in the resulting images (Johansen-Berg, Behrens, 2009). Voxels with higher diffusion will lose more signal than voxels with low diffusion: the faster the diffusion, the greater the loss of signal. These voxels will then appear darker (hypo-intense) in the final image. This attenuation depends in the first place on the magnetic field gradient pulses used for diffusion encoding and gradient pulses used for spatial encoding. This diffusion weighted contrast can be fit to a mono-exponential model through the Stejskal-Tanner equation:

$$S_i = S_0 e^{-b*D} \tag{2.2}$$

where S_i is the diffusion-weighted signal observed at a given voxel along direction i, S_0 is the signal measured at the same location but with no diffusion gradient applied, and D is the diffusion coefficient. The term b is the b-value (Le Bihan, Breton, 1985), which is a function of the strength, duration, and temporal spacing of the diffusion gradients. The b-value (measured in s/mm^2) characterizes the diffusion weighting and is defined

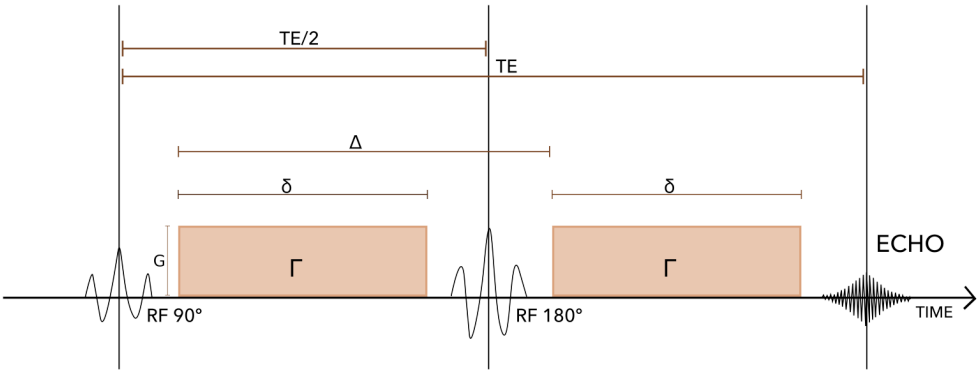

Figure 2.3: Diffusion MRI Acquisition Scheme. Scheme of the Pulse Gradient Spin Echo sequence is represented. The scanner maintains an approximately homogeneous magnetic field H_0 over the sample to which the spins (precessing hydrogen nuclei) align to. The horizontal line represents the time from the first pulse (echo time (TE)). The first 90° radio-frequency (RF) pulse tips the spins in the transversal plane perpendicular to H_0. H_0 inhomogeneities cause the spins to precess at different phases so that net magnetization decays. The second 180° RF pulse centred at time $TE/2$ negates the phase of the spins, and in the absence of diffusion gradients the net magnetization is restored and MR signal received. The diffusion-weighting gradients (r) offset the spin phase by a linear function of the spin position, adding an extra phase on the complex magnetization that depends on spin location, gradient strength (G), and gradient duration (δ). In case of stationary spin the phase offset of Γ_1 is cancelled out by Γ_2 because of the 180° RF pulse negation. However, if a spin moves from position r_1 to r_2 between the two RF pulses it retains a residual phase offset of $q(r_2 - r_1) = qx$, where x is the spin displacement.

as:

$$b = \gamma^2 G^2 \delta^2 (\Delta - \delta/3) \tag{2.3}$$

where γ is a physical constant known as the gyromagnetic ratio, G is the amplitude of the gradient, is the duration in milliseconds, and is the interval between the two gradients (Figure 2.3). Given that, as already mentioned, diffusion in the brain is not free, the diffusion coefficient D in (2.2) is replaced by the statistical entity ADC (Le Bihan et al., 1986) in:

$$Si = S_0 e^{-b*ADC_i} \tag{2.4}$$

where ADC_i is the ADC along the diffusion encoding gradient in direction $G_i = [x_i, y_i, z_i]$. The ADC has been introduced to bridge the distance between the micro scale of the physical molecular diffusion process and what can be measured at the MRI voxel scale (Le Bihan, Johansen-Berg, 2012). The ADC is intended to summarize at the voxel level those hidden physical processes that happen at much smaller scales. In this sense, the ADC depends not only on the actual diffusion coefficient, but also on experimental and hardware related parameters that affect the measurement at the voxel level. From this formula it can be seen that raising the b-value increases the loss of signal S and, similarly, higher ADC values result in lower signal.

Until the late 80s, however, no information about directionality of tissue microstructure could be inferred. Michael Moseley and his group made a great discovery in the cat brain (Moseley et al., 1990), proposing a new method where the information obtained from diffusion measurements was made to be orientation-dependent. They found that the diffusion coefficient is higher when measured along white matter fibres than perpendicular to them. The signal loss is thus related to diffusion-related displacement only in the direction of the applied diffusion gradient. In regions with isotropic diffusion, the diffusion-weighted intensity would be the same in all directions, but in anisotropic regions the signal is different depending on the direction of the applied gradient. It follows that, when the measured volume contains ordered tissue, a single ADC is no longer enough to characterize the behaviour of water molecules, since this will strictly depend on the applied direction. It was then suggested that measuring diffusion along at least the three principal axes could characterize regions of anisotropic diffusion. For the case of multiple diffusion directions (three in this case) 2.4 becomes:

$$S_i = S_0 e^{-b* \frac{ADC_1 + ADC_2 + ADC_3}{3}} \tag{2.5}$$

Here the resulting ADC represents the average ADC values along the three directions. It became clear that this orientation-dependent feature could be used to determine and map the orientation of white matter fibers in the human brain, assuming the direction of the fibers was parallel to the direction of the fastest diffusion of water molecules.

2.4 Reconstruction from diffusion MRI

In 1994 Basser, Mattiello and Le Bihan published their seminal paper on diffusion tensor imaging (DTI) (Basser et al., 1994), a method to fully describe water mobility profiles along different axes and determine orientation of fiber tracts . The tensor model provides a mathematical way to describe the Gaussian water diffusion in three-dimensional space. Mathematically the tensor is represented by a 3×3 symmetric matrix:

$$D = \begin{bmatrix} D_{xx} & D_{xy} & D_{xz} \\ D_{xy} & D_{yy} & D_{yz} \\ D_{xz} & D_{yz} & D_{zz} \end{bmatrix} \tag{2.6}$$

where the diagonal elements correspond to the displacement along the three axes, and the off-diagonal elements correspond to the correlation between displacements along those axes. As the diffusion tensor is symmetrical, by acquiring at least six diffusion weighted directions and a non-diffusion weighted volume the tensor can be computed. By extending equation 2.2, the diffusion behaviour of water molecules can be modelled by the tensor representation in 2.6. The diffusion tensor can be visualized as an ellipsoid, which describes the three-dimensional geometric profile of the distance travelled by the water molecules in a given diffusion time. The size and the shape of the ellipsoid are defined by the three eigenvalues $(\lambda_1, \lambda_2, \lambda_3)$ while the spatial orientation is described by the three eigenvectors (ν_1, ν_2, ν_3) (Figure 2.4).

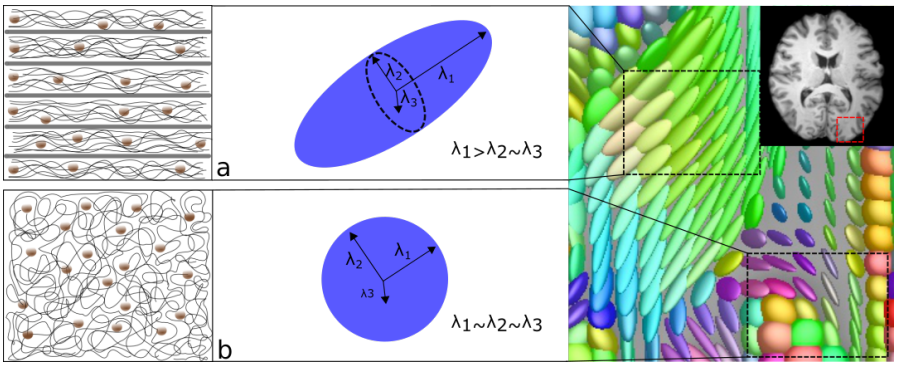

Figure 2.4: The Tensor Model. The image shows the profile of the tensor for anisotropic and isotropic configurations. In anisotropic tissue the tensor assumes a cigar-shape, while in isotropic tissue the tensor resembles a sphere. On the right a particular of the brain is shown with the tensor model fit at each voxel.

At each voxel of the acquired DWI volume, the tensor model is fit to the data. In biological tissues the tensor can vary between three possible configurations: (1) axial anisotropy (where λ_1 is greater than λ_2 and λ_3), which is typical of voxels containing highly organized parallel fibers (white matter); (2) planar anisotropy (when λ_1 is sim-

ilar to $\lambda_3 2$ and greater than λ_3), which is common in voxels containing, for example, crossing or diverging fibers; and (3) isotropy (when all three eigenvalues are similar), which is commonly observed, for example, in the CSF (Figure 2.4). In every voxel, the tensor shape encodes the three-dimensional information on the water diffusion profile. In addition, quantitative metrics can be derived from the tensor and used to described microstructure organization at the voxel level. The mean diffusivity (MD) is the mean of the three eigenvalues and describes average diffusivity of water inside the voxel ($MD = (\lambda_1\lambda_2\lambda_3)/3$). The fractional anisotropy (FA) is a normalized index that varies from 0 to 1 (where 0 means fully isotropic tissue and 1, fully anisotropic) and represents the degree of anisotropy of the biological tissue. The FA is a measure of how one of the three eigenvectors differs from the other, based on the eigenvalues:

$$FA = \sqrt{\frac{(\lambda_1 - \lambda_2)^2 + (\lambda_2 - \lambda_3)^2 + (\lambda_1 - \lambda_3)^2}{2({\lambda_1}^2 + {\lambda_2}^2 + {\lambda_3}^2)}} \tag{2.7}$$

In addition to MD and FA, axial diffusivity (AD) and radial diffusivity (RD) can be extracted to determine water molecule displacement along a direction parallel or perpendicular to the main orientation of fibers, respectively. These metrics provide important additional information on the underlying microstructure of the tissue compared to simple dMRI: FA index provides rotationally invariant information on the anisotropy of p, and the principal eigenvector v1 provides information on the principal orientation of fibres. However, the neuro-biological interpretation of these measures remains difficult (Jones, Cercignani, 2010), and it might be confounded by factors that are not related to the microstructural properties of the tissue, but to the limits of the model itself.

2.5 Beyond the tensor model

If we consider the size of a single axon ($0.3-5\mu$m) and the common low resolution of DWI (2 to 3 mm), it becomes evident that two or more differently oriented fiber populations are very likely to be present within the same voxel. However, the DTI reconstructs only one tensor per voxel, thus being an oversimplification of reality. The portion of spins inside the voxel that experience diffusion-driven displacement of R over time Δ is defined as:

$$P(R, \Delta) = nR/Nspin \tag{2.8}$$

where Nspin is the total number of spins inside a voxel. P is called the displacement distribution function or probability density function (PDF) of spin displacement within a voxel. Given that R represents the displacement in 3D, P (R,Δ) captures the 3D diffusion process of spins within the voxel (Van et al., 2010). DTI computes the tensor starting from the assumption that p is a zero-mean trivariate Gaussian distribution (Jbabdi,

Johansen-Berg, 2011). The Gaussian function has ellipsoidal contours which can have only a single peak, resulting in the tensor model being able to describe only one main fiber orientation per voxel. Nevertheless, Jeurissen et al. (Jeurissen et al., 2013) revealed that voxels that contain multiple fiber orientations can be detected in over 90 of white matter voxels, a much higher percentage of what previously reported (70-90%) (Behrens et al., 2007). In these voxels, a single tensor is not a suitable representation of the underlying fiber orientation and the closest Gaussian approximation to p would contain no useful information on the true nature of p and the principal eigenvector will no longer correspond to any of the underlying orientation of the fiber tracts present (Assaf et al., 2004). It becomes thus clear that the tensor model represents an oversimplification of reality and a poor fit to the data. In these regions, the tensor model will estimate an erroneous orientation profile causing tensor-derived measures such as fractional anisotropy to be unreliable or misleading (Jones, 2008). For example, FA values will decrease significantly in such regions of complex fiber configuration, because of the inability of the tensor to fully characterize the complexity of the underlying anatomy.

Several different descriptive models have been then developed to account for more complex fiber architectures and describe the intricate relation between microstructure and signal. These include Q-ball imaging (Tuch, 2004) (QBI), diffusion spectrum imaging (Wedeen et al., 2005), hybrid models (Jansons, Alexander, 2003), and spherical deconvolution (Dell'Acqua et al., 2013, 2010; Tournier et al., 2007, 2004). These alternatives to the tensor model can be broadly divided into two macro categories based on how they approach the DW data: model-free approaches, in which the three-dimensional displacement probability profile is obtained directly from the diffusion signal (dODF) (Wedeen et al., 2005), and model-based approaches in which the measured diffusion signal is fitted with a chosen model that assumes *a-priori* a discrete number of fiber orientations and generates for each voxel an estimation of the fiber orientation distribution function (fODF)(Dell'Acqua et al., 2007). These models have been proven capable of correctly and reliably describing white matter pathways in crossing fibers regions that the tensor model was unable to (Behrens et al., 2007).

Model-based approaches

Instead of modelling a single preferred diffusion direction (as in the tensor model), model-based methods define a number of directions. A simple generalization of the tensor is constituted by multi-tensor models which replace p with a mixture of Gaussian densities in the presence of n fiber population per voxel, assuming n is known (Alexander, 2005). Each population is modelled by a different tensorial distribution and the total p per voxel is the sum of the Gaussians weighted by the volume fraction occupied by each population. A simplified case of the multi-tensor scenario is the ball and stick model (Behrens et al., 2003), which assumes that molecules inside the voxel belong to one of two populations: a hindered (modelled by a stick) and a free component (modelled by a ball). However, the choice of the number of directions represents a limitation to the model: in voxels with only one fiber orientation fitting a $n = 2$ model will cause a loss of specificity. Furthermore, even when the number of fibers chosen is correct, the model

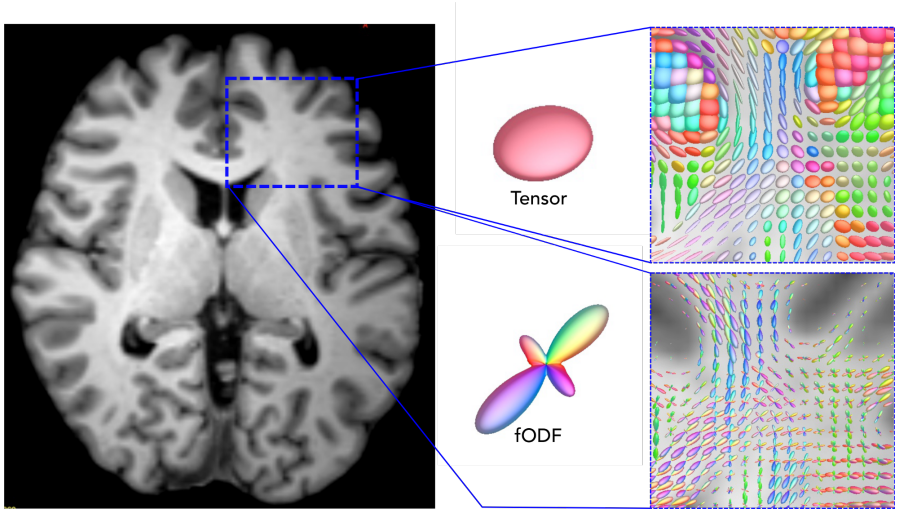

Figure 2.5: Beyond the Tensor Model. The figure illustrates the comparison of the tensor and spherical deconvolution model reconstruction of the diffusion profile for a region of the human brain with complex fiber configuration.

estimation is still limited by the fact that the underlying biological tissue is more complex than just a sum of Gaussian processes.

Inside the model-based approaches, a class of models go under the category of spherical deconvolution methods (Dell'Acqua et al., 2007; Tournier et al., 2007, 2004). These methods generalize the multi-tensor approaches considering a distribution of fiber orientations rather than a discrete number, which is allowed to tend to infinity. The assumption is that the diffusion signal can be approximated by the sum of the signals emanating from each of the fibre populations present in the sample. These approaches generate for each voxel an estimation of the fiber orientation distribution function (fODF) from the diffusion profile. The signal is expressed as the convolution of the fODF with the response from a single fibre. The normalized signal from a population of crossing fibers can be then written as:

$$S(\Theta, \phi) = R(\Theta) \otimes F(\Theta, \phi) \tag{2.9}$$

where F (Θ, ϕ) is the fODF and R (Θ) is the response function for a single fiber population aligned with the z-axis (Minati, Węglarz, 2007). The fODF provides information on the fraction of fibers that are aligned along the direction (Θ, ϕ), expressed in spherical coordinates:

$$F(\Theta, \phi) = \frac{\delta(\Theta_1, \phi_1)}{2} + \frac{\delta(\Theta_2, \phi_2)}{2} \tag{2.10}$$

where $\delta(\Theta_1, \phi_1)/2$ is a Dirac delta function pointing along the direction of the population 1 and weighted by its respective volume fraction (Tournier et al., 2004). This technique can successfully reconstruct the diffusion profile correctly without the need of *a priori*

information on the number of fiber populations present inside the voxel. The different peaks of the fOD function provide the information on the orientation, the direction, and the weight of the fibers in each voxel. However, one limitation to these methods is their susceptibility to noise, which often results in spurious peaks in the recovered fODF (Parker et al., 2013). If the fODF is a delta function, then its value should be zero for all other orientations. However, in the presence of noise this value actually fluctuates around zero, creating random positive and negative side lobes. Several regularization solutions have been introduced to correct for this, imposing a non-negativity constrain (Alexander, 2005; Dell'Acqua et al., 2007; Tournier et al., 2007). We refer to these methods as constrained spherical deconvolution (CSD) methods. A second limitation is the assumption that the response function is the same for every voxel of the brain and for all fiber populations. However different regions of the brain might have different diffusion properties, resulting in white matter fibers with different characteristics. Some groups have suggested solutions to overcome this limitation (Anderson, 2005; Schultz, Groeschel, 2013).

Model-free approaches

Model-free approaches characterize the water molecular displacement by using a diffusion orientation distribution function (dODF). These models try to extract the ODF without imposing a particular distribution to p. The ODF is a metric of how likely fibers within a voxel orient in a certain direction (Tuch, 2004; Wedeen et al., 2005). The estimate of the dODF does not require any assumption about its form and is derived directly from the diffusion characteristics of the fibers. In other words, these methods, instead of reconstructing the fiber orientations *per se*, attempt to recover the complete diffusion profile. These methods include diffusion spectrum imaging (DSI) (Wedeen et al., 2005) and q-ball imaging (QBI) (Tuch, 2004). DSI reconstructs a discrete representation of p directly from DW measurements on a regular grid of wavenumbers via a fast Fourier transform. The ODF is the radial projection of p onto the unit sphere and has peaks in the direction of the ridges of p which provide information on the underlying fibre orientations. An important limitation of DSI is related to MRI acquisition time. In order to recover the ODF without applying any *a priori* model of p, DSI needs a high number of measurements to be acquired at high b-values. This requires very long MR scanning times, making the resultant data more susceptible to head motion artefacts and less compatible for clinical applications. Advances in MRI technology (high number of head RF channels together with imaging acceleration strategies) are promising solutions to these limitations (Setsompop et al., 2013).

In the attempt to lower the DSI requirements, Q-ball methods (QBI) approximate the ODF using spherical acquisition schemes, instead of a 3D Cartesian grid like DSI. Although still requiring a high number of diffusion directions and high b-value for the Funk Radon transform approximation to be valid (Tuch, 2004), this number is smaller than DSI and still allows QBI to probe tissue structure without any modelling of p. However, the approximation of the dODF introduces some blurring and reduces angular resolution and precision of peaks directions. Fiber orientations are extracted from the

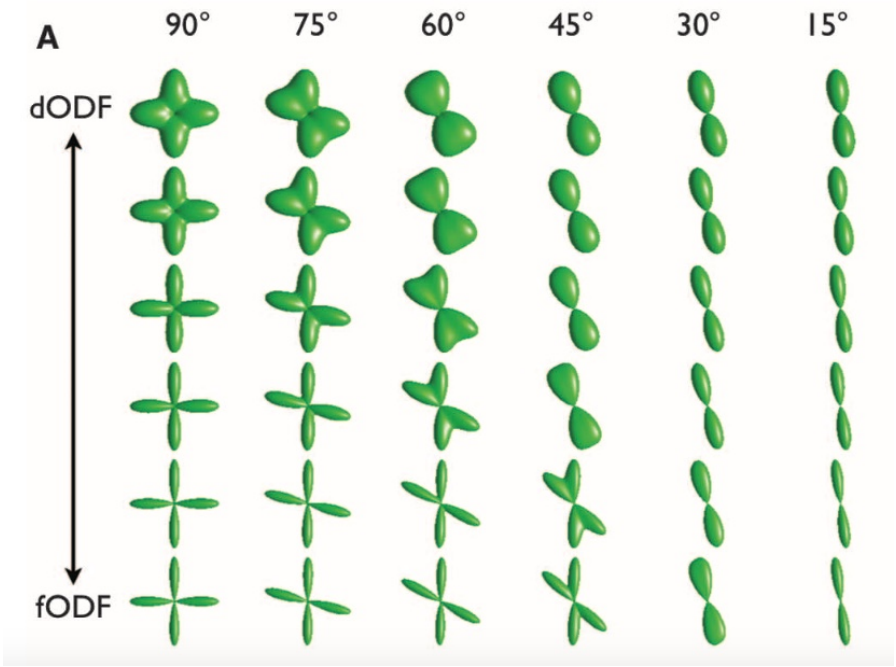

Figure 2.6: Angular Resolution. The image shows the ODFs profiles for different angles, in a continuum from the parametric fODF to the non-parametric dODF. The angular profile of the different ODFs determines the ability to separate crossing populations of fibers inside the voxel. For 90° crossing all ODFs are able to distinguish two orientations, whereas for lower angles, only sharper ODF profiles are able to resolve the crossing (Dell'Acqua, Catani, 2012).

directions of p along which the probability of displacement is higher. Due to the nature of diffusion, these regions will be relatively broad, leading to biases in the estimation of fiber orientations. Alternative methods have been proposed to improve the angular resolution of the ODF obtained through QBI by applying a sharpening deconvolution transform (Descoteaux et al., 2009).

Nevertheless, the angular resolution (*i.e.*, the ability to resolve crossing fibres at smaller angles) that can be obtained with non-parametric models remains lower than what we can obtain with spherical deconvolution methods. For orthogonal crossing, all profiles are able to distinguish two orientations, whereas for lower angles, only sharper profiles are able to resolve the crossing (Figure 2.6). Moreover, fiber reconstruction through SD/CSD methods is achievable at lower b-values and acquisition protocols that are closer to those used in conventional DTI acquisitions (Tournier et al., 2008). While non-parametric models require the acquisition of DW images with gradients applied over a range of different orientations and amplitudes, spherical deconvolution methods use data acquired through the HARDI acquisition protocol (Tuch et al., 2002), where a

relatively high number of uniformly distributed DW directions are applied at a constant b-value, allowing for a focus on the angular frequency information of the signal.

2.6 Summary

Water molecules constantly diffuse in a random fashion due to physical processes. In organic matter, this displacement is restricted by obstacles and assumes different diffusivity profiles on the basis of the surrounding tissue properties. In the brain, the highly myelinated and well organized axonal fibers that constitute the white matter will make it easier for water molecules to diffuse along than across them.

It is thus possible to indirectly acquire information about the microstructure of brain tissue by observing the water displacement distribution. The introduction of diffusion MRI made it possible to obtain this unique information non-invasively and *in-vivo*. Successively, the formalism introduced by the diffusion tensor enlarged the possibilities and applications of diffusion MRI, providing rotationally invariant quantitative measures that could be used to compare microstructural organization across individuals. However, it has became clear that this model was an oversimplification of reality and more advanced models have been put forward. Among these, spherical deconvolution models are capable of providing good angular resolution at clinically feasible acquisition protocols, making them particularly suitable for the investigation of the white matter architecture in the human brain. The work in this thesis is focused mostly on the use of spherical deconvolution as a method of reconstructing the acoustic radiation in the human brain using diffusion MRI.

Assuming that the direction of least hindrance to diffusion aligns with the direction of the fibers, it becomes possible to recover information on the architecture of the white matter fibers of the brain. The process of virtually reconstructing the trajectories of the white matter bundles of the brain starting from DWI data is called tractography, and it is discussed in the next chapter.

Bibliography

Alexander Daniel C. Multiple-fiber reconstruction algorithms for diffusion MRI // Annals of the New York Academy of Sciences. 1064, 1. dec 2005. 113–133.

Anderson Adam W. Measurement of fiber orientation distributions using high angular resolution diffusion imaging // Magnetic Resonance in Medicine. nov 2005. 54, 5. 1194–1206.

Assaf Yaniv, Freidlin Raisa Z., Rohde Gustavo K., Basser Peter J. New modeling and experimental framework to characterize hindered and restricted water diffusion in brain white matter // Magnetic Resonance in Medicine. nov 2004. 52, 5. 965–978.

Basser P J, Mattiello J, LeBihan D. MR diffusion tensor spectroscopy and imaging. // Biophysical journal. 1994. 66, 1. 259–267.

Beaulieu C, Does M D, Snyder R E, Allen P S. Changes in water diffusion due to Wallerian degeneration in peripheral nerve. // Magnetic resonance in medicine. oct 1996. 36, 4. 627–31.

Beaulieu Christian. The basis of anisotropic water diffusion in the nervous system - A technical review. nov 2002. 435–455.

Behrens T. E J, Berg H. Johansen, Jbabdi S., Rushworth M. F S, Woolrich M. W. Probabilistic diffusion tractography with multiple fibre orientations: What can we gain? // NeuroImage. 2007. 34, 1. 144–155.

Behrens T E J, Johansen-Berg H, Woolrich M W, Smith S M, Wheeler-Kingshott C a M, Boulby P a, Barker G J, Sillery E L, Sheehan K, Ciccarelli O, Thompson a J, Brady J M, Matthews P M. Non-invasive mapping of connections between human thalamus and cortex using diffusion imaging. // Nature neuroscience. 2003. 6, 7. 750–757.

Carr Hy, Purcell Em. Effects of Diffusion on Free Precession in Nuclear Magnetic Resonance Experiments // Physical Review. 1954. 94, 3. 630–638.

Dell'Acqua F, Rizzo G, Scifo P, Clarke R a, Scotti G, FAzio F. A ModelBased Deconvolution Approach to Solve Fiber Crossing in DiusionWeighted MR Imaging // Biomedical Engineering, IEEE Transactions on. 2007. 54, 3. 462472.

Dell'Acqua Flavio, Catani Marco. Structural human brain networks: hot topics in diffusion tractography. // Current opinion in neurology. 2012. 25, 4. 375–83.

Dell'Acqua Flavio, Scifo Paola, Rizzo Giovanna, Catani Marco, Simmons Andrew, Scotti Giuseppe, Fazio Ferruccio. A modified damped Richardson-Lucy algorithm to reduce isotropic background effects in spherical deconvolution // NeuroImage. 2010. 49, 2. 1446–1458.

Dell'Acqua Flavio, Simmons Andrew, Williams Steven C R, Catani Marco. Can spherical deconvolution provide more information than fiber orientations? Hindrance modulated orientational anisotropy, a true-tract specific index to characterize white matter diffusion // Human Brain Mapping. 2013. 34, 10. 2464–2483.

Descoteaux Maxime, Deriche Rachid, Knösche T, Anwander Alfred. Deterministic and Probabilistic Tractography Based on Complex Fiber Orientation Distributions // IEEE Transactions on Medical Imaging. 2009. 28, 2. 269–286.

Einstein A. Uber die von der molekularkinetischen Theorie der warme gefordete Bewegung von in ruhenden Flussigkeiten suspendierten Teilchen. // Ann Physik. 1905. 4. 549–560.

Hahn E. L. Spin echoes // Physical Review. nov 1950. 80, 4. 580–594.

Jansons Kalvis M, Alexander Daniel C. Persistent angular structure: new insights from diffusion magnetic resonance imaging data // Inverse Problems. 2003. 19, 5. 1031–1046.

Jbabdi Saad, Johansen-Berg Heidi. Tractography: Where Do We Go from Here? // Brain Connectivity. 2011. 1, 3. 169–183.

Jeurissen Ben, Leemans Alexander, Tournier Jacques Donald, Jones Derek K., Sijbers Jan. Investigating the prevalence of complex fiber configurations in white matter tissue with diffusion magnetic resonance imaging // Human Brain Mapping. 2013. 34, 11. 2747–2766.

Johansen-Berg Heidi, Behrens Timothy E J. Diffusion MRI, from quantitative measures to in-vivo neuroanatomy. 2009.

Jones Derek K. Studying connections in the living human brain with diffusion MRI // Cortex. 2008. 44, 8. 936–952.

Jones Derek K, Cercignani Mara. Twenty-five pitfalls in the analysis of diffusion MRI data // NMR in Biomedicine. 2010. 23, 7. 803–820.

Le Bihan , Breton . Imagerie de diffusion in vivo par resonance magnetique nucleaire // Compte-Rendus de l'Academie de Sciences Paris. 1985. 301. 1109–1112.

Le Bihan D, Breton E, Lallemand D, Grenier P, Cabanis E, Laval-Jeantet M. MR imaging of intravoxel incoherent motions: application to diffusion and perfusion in neurologic disorders. // Radiology. nov 1986. 161, 2. 401–407.

Le Bihan Denis, Johansen-Berg Heidi. Diffusion MRI at 25: Exploring brain tissue structure and function. jun 2012. 324–341.

Minati Ludovico, Węglarz Władysław P. Physical foundations, models, and methods of diffusion magnetic resonance imaging of the brain: A review // Concepts in Magnetic Resonance Part A. sep 2007. 30A, 5. 278–307.

Moseley Me, Cohen Y, Kucharczyk J. Diffusion Weighted MR Imaging of anisotropic water diffusion in cat nervosu system // Radiology. 1990. 187. 439–446.

Parker G D, Marshall D, Rosin P L, Drage N, Richmond S, Jones D K. A pitfall in the reconstruction of fibre ODFs using spherical deconvolution of diffusion MRI data // NeuroImage. jan 2013. 65. 433–448.

Schultz Thomas, Groeschel Samuel. Auto-calibrating spherical deconvolution based on ODF sparsity // Lecture Notes in Computer Science (including subseries Lecture Notes in Artificial Intelligence and Lecture Notes in Bioinformatics). 8149 LNCS, PART 1. 2013. 663–670.

Setsompop K., Kimmlingen R., Eberlein E., Witzel T., Cohen-Adad J., McNab J. a., Keil B., Tisdall M. D., Hoecht P., Dietz P., Cauley S. F., Tountcheva V., Matschl V., Lenz V. H., Heberlein K., Potthast A., Thein H., Van Horn J., Toga A., Schmitt F., Lehne D., Rosen B. R., Wedeen V., Wald L. L. Pushing the limits of in vivo diffusion MRI for the Human Connectome Project // NeuroImage. 2013. 80. 220–233.

Stejskal E. O., Tanner J. E. Spin Diffusion Measurements: Spin Echoes in the Presence of a Time-Dependent Field Gradient // The Journal of Chemical Physics. jan 1965. 42, 1. 288–292.

Tournier J. Donald, Calamante Fernando, Connelly Alan. Robust determination of the fibre orientation distribution in diffusion MRI: Non-negativity constrained super-resolved spherical deconvolution // NeuroImage. may 2007. 35, 4. 1459–1472.

Tournier J. Donald, Calamante Fernando, Gadian David G., Connelly Alan. Direct estimation of the fiber orientation density function from diffusion-weighted MRI data using spherical deconvolution // NeuroImage. 2004. 23, 3. 1176–1185.

Tournier J.-Donald, Yeh Chun-Hung, Calamante Fernando, Cho Kuan-Hung, Connelly Alan, Lin Ching-Po. Resolving crossing fibres using constrained spherical deconvolution: Validation using diffusion-weighted imaging phantom data // NeuroImage. aug 2008. 42, 2. 617–625.

Tuch David S. Q-ball imaging // Magnetic Resonance in Medicine. dec 2004. 52, 6. 1358–1372.

Tuch David S., Reese Timothy G., Wiegell Mette R., Makris Nikos, Belliveau John W., Wedeen Van J. High angular resolution diffusion imaging reveals intravoxel white matter fiber heterogeneity // Magnetic Resonance in Medicine. oct 2002. 48, 4. 577–582.

Van Anh T, Granziera Cristina, Bammer Roland. An introduction to model-independent diffusion magnetic resonance imaging. // Topics in magnetic resonance imaging : TMRI. dec 2010. 21, 6. 339–54.

Wedeen Van J., Hagmann Patric, Tseng Wen Yih Isaac, Reese Timothy G., Weisskoff Robert M. Mapping complex tissue architecture with diffusion spectrum magnetic resonance imaging // Magnetic Resonance in Medicine. 2005. 54, 6. 1377–1386.

Chapter 3

Diffusion-based MRI Tractography

3.1 Introduction

The previous chapter introduced diffusion MRI as a methods of characterizing water diffusion in a tissue. One of the major applications of this technique has been the three-dimensional reconstruction of white matter fibre trajectories. In the brain, ensembles of axonal fibres following the same course and connecting the same cortical or subcortical regions are called bundles. The computerized process of reconstructing bundles in 3D from a set of DW images is called tractography. The tractography algorithm pieces together the underlying information about the diffusion displacement contained in every voxel through continuous lines called streamlines.

The main assumption underpinning tractography is that the principal diffusion direction aligns with the orientation of the fibres contained within each voxel (Jbabdi, Johansen-Berg, 2011). The second assumption in tractography consists in the inference of an anatomic continuity from voxel to voxel. On the basis of these two fundamental assumptions, the tracking algorithm follows the direction of maximum diffusion from a given voxel into a neighboring voxel, allowing the reconstruction of three-dimensional trajectories of fibre bundles.

The result of this process, outlined in this chapter, can give colourful images of the white matter connections of the human brain (Figure 3.1). Such beautiful images, however, carry serious limitations for their interpretation. This chapter describes the available tractography algorithms and their different applications, while also highlighting important limitations present in the methods.

3.2 Tractography before tractography

The birth of diffusion-based tractography (Conturo et al., 1999; Mori et al., 1999) opened previously unforeseen possibilities to look into the white matter organization of the human brain *in-vivo*, non-invasively and within short clinical acquisition protocols.

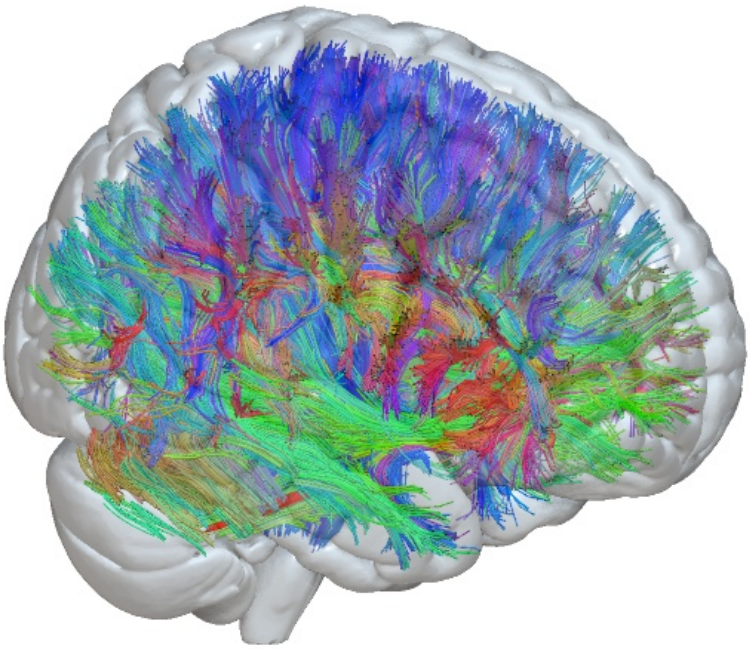

Figure 3.1: Whole Brain Tractography. The figure shows an example of a whole brain tensor-based tractography reconstruction together with a mesh of the human brain. The colours encode the diffusion direction: red=right-left, blu=inferior-superior, green=anterior-posterior. The image is generated using SurfIce and the available example data (https://www.nitrc.org/projects/surfice/).

Before the introduction of tractography techniques, individual anatomy of white matter connections could be investigated only after death. The interest in the connectivity of the human brain took off in the 19th century. In this time the spreading of associationism lead neuroanatomical research to extend from the cortical surface to the subcortical white matter pathways (Catani et al., 2013). Theodor Hermann Meynert (1833-1892), a German anatomist and psychiatrist, divided the white matter into three principal categories, that are still used and accepted today: association fibres, that link cortical regions of the same hemisphere, projection fibres, that connect cortical and subcortical regions, and commissural fibres, connecting the two hemispheres. Famous neurologists like Jules Dejerine (1849-1917) and Carl Wernicke (1848-1905), through their single case studies identified classic neurological syndromes such as conduction aphasia, pure word deafness, and pure alexia, and showed that proper functioning of the human brain can be disrupted through disconnection of the white matter pathways alone (Dejerine, 1895; Lichteim, 1885). These first investigations revealed that these pathways form the underlying structure to transfer information between different brain regions and are thus fundamental in the understanding of brain function in both normal and diseased brains. (Catani, Mesulam, 2008; Geschwind, 1965).

Despite the quality of the topographical descriptions of these anatomists, a comprehensive representation of the fibre systems of the human brain was still lacking due to methological limitations in dealing with specimens (Zemmoura et al., 2015). A methodological revolution came through with the introduction of Klingler's freezing-defrosting. This technique allowed to investigate the white matter bundles maintaining their three-dimensional anatomical relationships with adjacent bundles. The admirable dissection work of Josef Klingler made it possible to clearly name and define major fibre systems of the human brain (Ludwig, Klingler, 1956) (Figure 3.2).

Most of our knowledge about the topography of long-range white matter connections comes from the work of these anatomists. The introduction of tractography techniques allowed us to carry on the inquiry into the complex organization of the brain white matter *in-vivo* and non-invasively.

3.3 Tractography algorithms

The two main assumptions underpinning tractography applications are that the principal diffusion direction aligns with the orientation of the fibres contained within each voxel, and that continuity from voxel to voxel is anatomically legitimated (Jbabdi, Johansen-Berg, 2011). On the basis of these two fundamental assumptions, the tracking algorithm follows the direction of the least hindrance to diffusion from a given voxel into a neighbouring voxel, following some user-defined heuristics. The way this process is carried out and its results depends on the parameters and on the type of algorithms employed. Tractography algorithms mainly divide in deterministic and probabilistic methods, and into local and global approaches. This section introduces the user-defined choices that have to be made and the different possible approaches in tractography algorithms.

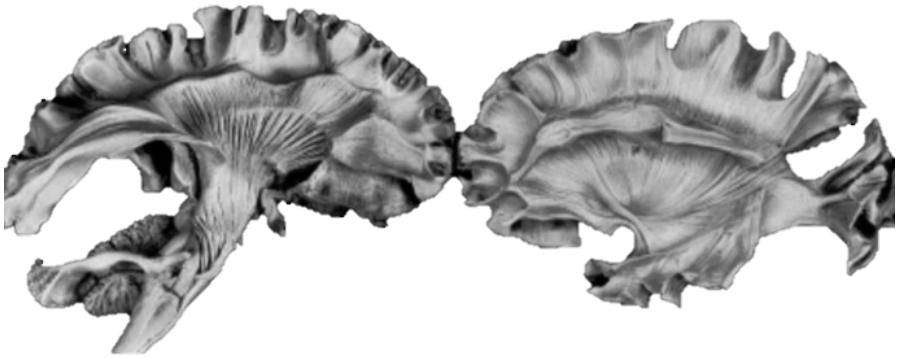

Figure 3.2: Klingler's Dissections. Illustration of Klinger's dissections (Ludwig, Klingler, 1956).

Tract start, continuation and termination criteria

The reconstruction of the streamlines requires the determination of specific user-defined parameters for starting, continuing or stopping the tracking. Tractography can be initiated from one or more user-defined regions of interest (ROIs), that can be either anatomically or functionally defined, or from the entire brain. In the latter case, the selection of voxels to be used can be constrained to those belonging to the white matter or the interface between the grey and the white matter by use of a binary mask. The seeding strategy can also vary from determining a precise number of seeds per voxel, to randomly seeding throughout the brain, to fixing a specific number of streamlines that we want to be generated.

The algorithm can then proceed by stepping out from the starting position along the orientation estimated at that point, with a fixed user-specified step size. The sub-voxel estimation of the continuous underlying fibre orientation at any location in the 3D space within the DW volume is obtained using interpolation. The simplest method to obtain an estimate of this orientation at any location is to use nearest-neighbour interpolation (the desired white matter orientation is approximated as that of the nearest voxel), but other methods, such as trilinear interpolation and third order B-splines are also commonly used (Pajevic et al., 2002). Other differences in tractography implementations relate to the propagation algorithm used. These can be first-order Euler integration procedures (following the eigenvector for a fixed step size), second-order (the tangent is used for half step and then a new tangent is calculated), and fourth order (the weighted average of four estimated tangents is used at each step) Runge-Kutta integration (Basser et al., 2000).

Among stopping criteria, the most widely used heuristics is to apply an FA threshold (usually < 0.2), to avoid tracking through regions that do not contain white matter fibres (*e.g.*, lateral ventricles). However, since FA is tensor-derived, it suffers from model limitations and might be unreliable in some regions of the brain. For this reason, tissue segmentation maps derived from T1-weighted images are now more often used. Another

Step	Parameters	Effect
MRI Acquisition	Voxel size b-value DW Directions	Location accuracy and Angular Resolution
Low-level diffusion model	Tensor Multitensor Spherical deconvolution Model-free	Accuracy of the reconstructed fibre orientation distribution
Tractography approach	Deterministic Probabilistic	False Negatives False Positives
Tractography Parameters	Step size Starting strategy Seeding strategy Propagation criteria Stopping criteria	Sensitivity and specificity of the tractography reconstructions

Table 3.1: Parameter choices that affect diffusion tractography results. The table lists key acquisition and analysis parameters that can be manipulated by the user at different steps of the processing pipeline, and what they affect in the reconstruction process.

common stopping rule is represented by the maximum angle between two contiguous diffusion directions (usually $< 45^{o}$). The aim is to prevent "unfeasible" turns in path propagation and reduce artefactual tract reconstructions (Jones, Callan, 2003). Recently more advanced stopping criteria have been introduced taking advantage from the anatomical information coming from other imaging modalities, to guide the tractography algorithm and avoid tracing into anatomically implausible regions (Girard et al., 2014). More specific exclusion masks can also be used.

Different combinations of these parameters will lead to very different tractography outcomes (Girard et al., 2014). Ultimately, the best combination would lead to more accurate 3D reconstructions that minimize the number of false positive and false negative. In tractography we refer to false positive when an anatomically implausible connection is created. For example, two adjacent tensors belonging to different pathways are joined together by the tractography algorithm. On the contrary, false-negative artefacts occur when the tractography algorithm is unable to reconstruct pathways that truly exist. This usually occurs in regions with high density of crossing fibres, where the encoding diffusion model fails to provide a clear indication of the directionality of the underlying fibres.

Deterministic and probabilistic algorithms

Quality of the estimation of the fibre orientation depends on a number of factors, which include the signal noise in the DWI data, partial volume effects (i.e., loss of signal due to the limited resolution of the imaging system and the inability to separate different

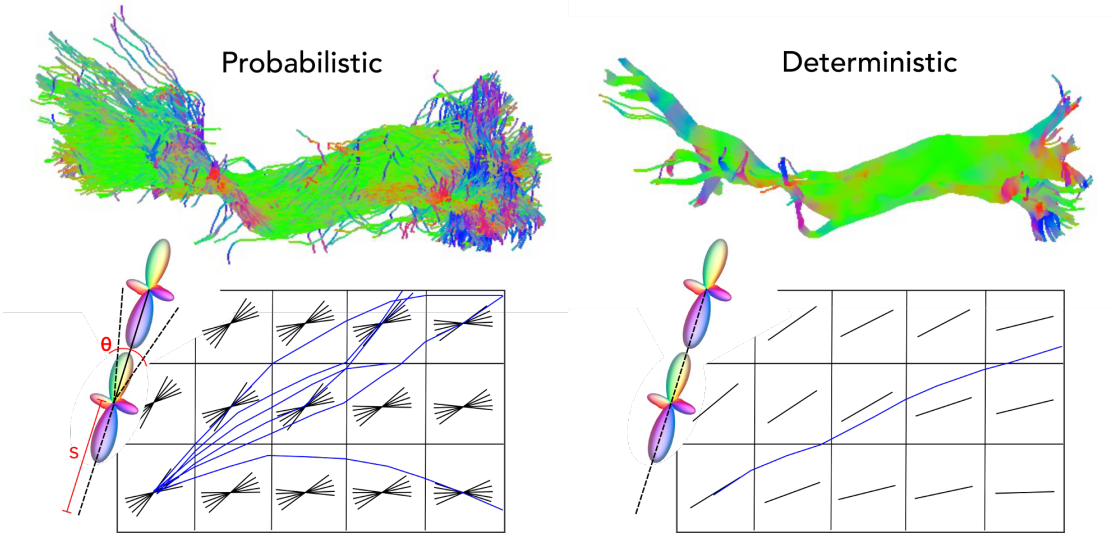

Figure 3.3: Probabilistic and Deterministic Tractography. Differences between probabilistic and deterministic approaches are shown. Top: reconstruction of the inferior fronto-occipital fasciculus (IFOF) using a probabilistic and a deterministic approach starting from the same low-level spherical deconvolution model (performed in Mrtrix3). Bottom: cartoons describing tractography propagation behaviors in the two approaches. Particulars of the fODF are also shown: s=step size, θ=curvature threshold.

tissues within a voxel), and the inaccuracy of the chosen diffusion model. Initial work in the field focused on deterministic approaches (Conturo et al., 1999; Mori et al., 1999) and was later extended to probabilistic methods (Behrens et al., 2003). Deterministic tractography extracts only one main trajectory estimate from the underlying diffusion orientation. The estimated fibre direction is assumed to represent the best estimate to propagate streamlines. However, no indication of the confidence that one can assign to the reconstructed trajectory is provided. This makes these methods sensitive to the estimated principal direction, and highly susceptible to noise in the DWI data. To overcome this and better deal with noise in the estimated diffusion profile, probabilistic methods have been introduced (Behrens et al., 2007).

Unlike deterministic tractography, probabilistic methods generate multiple solutions to reflect the "uncertainty" of the estimated fibre orientation (Behrens et al., 2003). Instead of providing a single estimate of the fibre path, probabilistic methods give the probability distribution of that estimate. At every voxel, a probability distribution of the orientations is estimated and connections are traced thousands of time, each time using a slightly different orientation, chosen from a pool of likely orientations (Figure 3.3). It should be noted that the high probability of a connection does not provide confidence on the probability of the underlying true anatomical connectivity. Often, artefactual trajectories have very high probability, similar to true anatomic pathways. Low-quality

data-sets might generate highly reproducible reconstructions, although anatomically inaccurate. In general, while deterministic approaches are prone to a higher number of false-negative artefacts, probabilistic methods generate more false-positive reconstructions.

Both probabilistic and deterministic methods, initially used in the context of the tensor model, have been adapted to work with more advanced models that can detect multiple fibre populations per voxel. In this case, the subsequent diffusion direction can be chosen on the basis of different criteria, the most common of which is the closest to the current direction (Behrens et al., 2007), but sometimes all possible directions are explored (Descoteaux et al., 2009).

Local and global approaches

Both deterministic and probabilistic approaches described above belong to the definition of local tractography. Other algorithms exist that are based on a global approach. Global tractography algorithms tend to find the fibre configuration that best explains the data, directly operating on the DWI data. Unlike streamline methods that use only local information to determine the trajectories, global approaches move to a global goodness-of-fit of the entire candidate tractogram. This method transforms tractography into a global optimization problem and makes it less sensitive to local effects, such as noise and modelling errors (O'Donnell et al., 2002; Sotiropoulos et al., 2010). However, these approaches are extremely computationally demanding and require further validation.

3.4 Tractography applications

Reconstructing virtual white matter pathways' trajectories *in-vivo* allows to explore the structural connectivity of the brain across large numbers of individuals or over time, and to correlate this information with functional and behavioural data. In the past decade, several groups have implemented different tractography techniques to investigate cognitive functions (Catani et al., 2005; Saur et al., 2010), neurodegenerative diseases (Stebbins, Murphy, 2009), plasticity mechanisms (Schotten et al., 2012; Shu et al., 2009), psychiatric disorders (Mulert et al., 2012; Rudie et al., 2013), and to inform neurosurgical planning (Chen et al., 2015; Wu et al., 2007). Here we focus on the two most common applications of tractography, namely the characterization of white matter tracts as well as the parcellation of grey matter in terms of white matter connectivity.

The first and most widely implemented use of streamline tractography so far has been the localization and quantitative investigation of specific white matter bundles. Many studies focused on localizing and naming the major known and unknown fibre tracts of the human brain (Catani et al., 2012; Makris et al., 2009; Yeatman et al., 2014). This is usually achieved by isolating certain bundles through *in-vivo* virtual dissections (Catani, Mesulam, 2008) on the basis of prior anatomical knowledge of the trajectories of these bundles. Following this process, most major white matter tracts of the human brain have been reconstructed with results comparable to *post-mortem* dissections (Lawes et al., 2008) (Figure 3.4). This use of tractography became extremely important

in neurosurgical applications. In the recent years, the employment of diffusion-based tractography reconstructions for pre-surgical mapping has become common practice in most clinics (Chen et al., 2009; Wu et al., 2007). Here, the 3D profiles of the tracts are used to make decisions on resection boundaries, with the final aim of sparing fundamental brain functions like language.

Once specific white matter bundles have been isolated, it is possible to use them as (ROIs) and extract quantitative measures from them, such as those that can be easily obtained from the tensor model (FA, MD, RD, AD). We usually refer to this method as tractometry (Figure 3.4b). This application permits to characterize the microstructural properties of tissue in the normal and pathological brain, to provide quantitative measurements for group comparisons or individual case studies, and to correlate tractography results with behavioural or clinical scores (Forkel et al., 2014; Schotten et al., 2012).

Using these methods, neuroscientists have tried to answer questions about the connectivity of the human brain and the strength and integrity of its connections, somehow assuming that the reconstructions obtained with the tractography algorithm reflect true anatomical connections and the state of their connectivity. However, the interpretation of these indices is not always straightforward, especially in regions containing fibre crossing (Wheeler-Kingshott, Cercignani, 2009). In such regions, for example, a decrease in FA is likely to not be related to any integrity loss of the fibres (Dell'Acqua, Catani, 2012). The lack of specificity of current diffusion indices is mainly related to partial volume effects. In other words, it is related to the fact that at the voxel level (typical volume of $8mm^3$), diffusion properties are the average result of multiple co-existing fibre populations. Recent methods have tried to bridge the gap between the voxel level and fibre level, introducing quantitative measures that are related to single fibre population in a voxel (Raffelt et al., 2012, 2017). These methods constitute a promising step forward in combining microstructural and tractography information. On another front, recent technological improvements in MRI technology (strong magnetic gradients, high number of RF channels and fast imaging techniques) allow to reduce partial volume effects by reducing voxel size, while still allowing data acquisition in reasonable clinical times (Setsompop et al., 2013). Reducing voxel size has the side effect of reducing the signal-to-noise ratio (SNR), thus, such approaches have better uses at high-field systems (Sepehrband et al., 2017).

A second application of tractography has been its implementation as a tool to functionally parcellate the grey matter. If we assume white matter connections transfer information between specific cortical regions and subserve specific brain functions, and that we can reconstruct these connections with some confidence, it follows that we can try to parcellate the cortex on the basis of its connections. Several studies have shown successful and robust parcellation of the cortical and subcortical regions using this technique (Behrens et al., 2003; Klein et al., 2009) (Figure 3.4).

More recently, tractography has been used to build connectivity matrices of the entire brain, to study the macrostructural organization of the human brain at the network level (Calabrese et al., 2015; Hagmann et al., 2008; Pestilli et al., 2014; Sporns, 2013; Sporns et al., 2005; Heuvel van den, Sporns, 2011). The standard routine to map structural brain

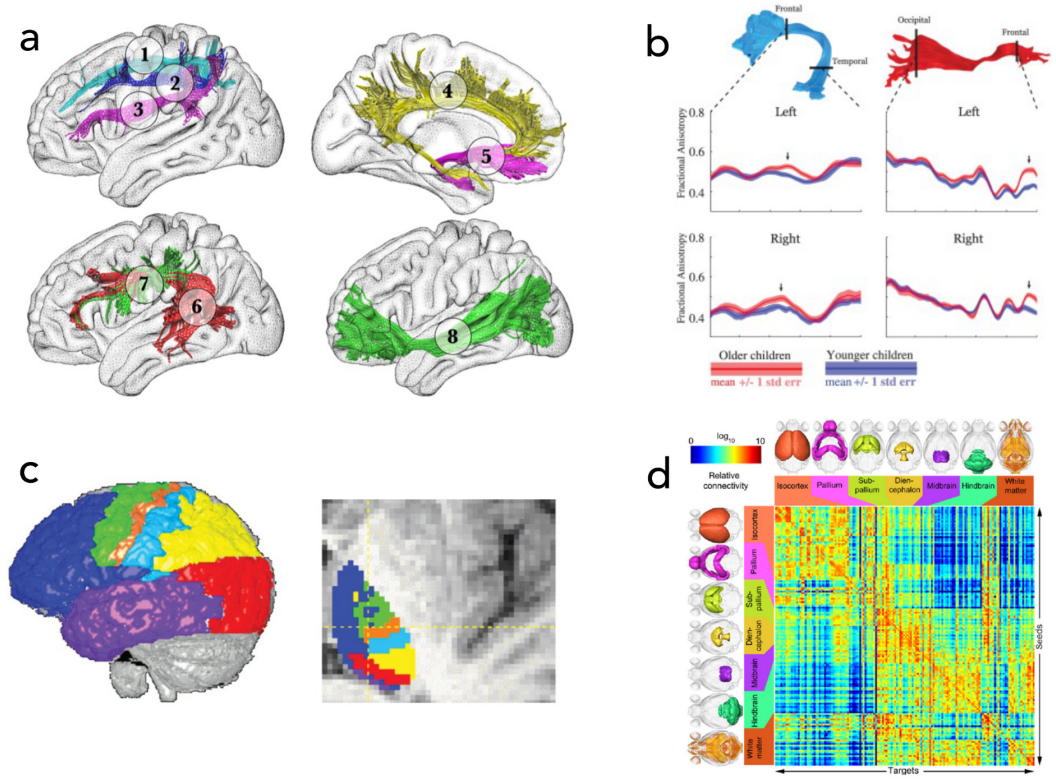

Figure 3.4: Tractography Applications. The figure shows different applications of diffusion-based tractography: a) localization of major fibre bundles in the human brain (1. Superior longitudinal fasciculus (SLF) I, 2. SLF II, 3. SLF III, 4. Cingulum, 5. Uncinate, 6. Arcuate fasciculus (AF), 7. Anterior portion of the AF, 8. Inferior fronto-occipital fasciculus (Rojkova et al., 2016). b) quantification of fractional anisotropy index along the streamline bundle (Yeatman et al., 2012). c) parcellation of the thalamus based on its connections with the cortex obtained through multi-tensor probabilistic tractography (Behrens et al., 2003). d) probabilistic tractography connectome of the mouse brain (Calabrese et al., 2015).

connectomes is a three-step process. First, the brain cortex is subdivided into discrete, spatially contiguous parcels on the basis of either functional or anatomical information. Second, tractography (usually probabilistic) is used to identify white matter fascicles connecting all the pairs of nodes. Finally, terminations of individual fascicles are used to build a matrix of brain connections (Figure 3.4d). White matter tracts and the brain areas they connect compose a large-scale network called the connectome. In this network, the reconstructed trajectories are used to define properties of the connections (or edges) and nodes of the network (brain areas). These networks and their properties can be used to characterize the effects of developmental variations, abnormalities, neurodegenerative diseases, or traumatic brain injury.

Despite the successful application of diffusion-based tractography techniques into both neurobiological and clinical research, a significant gap exists between histological studies and current *in-vivo* neuroimaging methods. As a result, tractography still presents several limitations that prevent it from becoming a completely reliable tool in clinical settings.

3.5 Tractography limitations

While acknowledging that to-date tractography is the only tool at our disposal to investigate the white matter architecture *in-vivo* and non-invasively, it is important to be aware of its limitations in order to ask the right scientific questions and better interpret the outcomes. Inaccuracies in the virtual white matter bundle reconstructions may arise from a variety of user-defined choices, including the low-level diffusion model, the tractography algorithm, and MRI acquisition parameters and related noise. Below we review some of the key confounds in diffusion-based tractography.

Diffusion model choice issues

As previously mentioned, failures to correctly estimating the fibre direction depend on the signal noise, the partial volume effects, and the inaccuracy of the chosen diffusion model. The availability of new diffusion models that can deal with multiple fibre trajectories inside the voxel has been crucial to describe tracts that were not visible using the tensor model, (*e.g.*, the lateral projections of the corpus callosum (Behrens et al., 2007; Dell'Acqua, Catani, 2012; Descoteaux et al., 2009). However, even though these models allow to overcome many inherent limitations of the diffusion tensor, in voxels with highly complex fibres configurations mis-estimates of connectivity due to modelling errors are still present in tractography results, preventing their reliability. This is mainly due to the fact that, given the coarse resolution of dMRI, many different configurations contribute to the signal of the same imaging voxel and can have very similar resulting diffusion profiles. Fanning, kissing, bending and adjacent fibres would result in the same 3D diffusion profile, preventing the tractography algorithm from knowing the exact underlying structure (Figure 3.5) (Jbabdi, Johansen-Berg, 2011; Tournier et al., 2011). Moreover, some of these fibres configurations are asymmetric by nature, while the diffusion profile is always symmetric, and so are the diffusion data. Recent attempts to overcome this

and account for asymmetric structures have been made by Bastiani et al. (2017) and Rowe et al. (2013).

Error propagation issues

Complex fibre configurations are intrinsic to DWI, because of its coarse resolution compared to the anatomical structures under investigation. When one corrupt orientation is encountered, the tracking algorithm may erroneously merge it with adjacent streamline bundles, leading to false positive and false negative reconstructions at the same time (Tournier et al., 2011). Even small deviation from the true diffusion profile can cause streamlines to take erroneous directions, leading to incorrect reconstruction outcomes. Because of the local nature of most tractography algorithms, the error tends to spread and propagate along the reconstruction process. This error can be enhanced by the interpolation method used. First Euler integration methods have been shown to overshoot in highly curved regions due to the finite step size (Lazar, Alexander, 2003), while Runge Kutta methods minimize this error (Basser et al., 2000).

The presence of systematic bias in the estimation of fibre orientations severely affects the reliability of tractography results. This is particularly important for clinical applications, such as neurosurgical planning, where precision is fundamental to make decisions on surgical resections.

Tract termination issues

To improve the accuracy and precision of tractography reconstructions, anatomical information can be included in the reconstruction process (Girard et al., 2014; Smith et al., 2012). However, while determining the location of bundles can be achieved with fairly good results, especially for major white matter bundles, extracting the precise termination of connections in the cortex is still very challenging. When tracking, macroscopic termination criteria are used (*e.g.* white matter binary mask, edge of the brain, white matter-grey matter (WM-GM) interface) that are inherently affected by limits of the spatial resolution, partial volume effects and noise. As a result, streamline endpoints do not necessarily reflect the endpoints of the tracts (Alexander, 2005; Jbabdi, Johansen-Berg, 2011). This limitation makes it difficult to clearly delineate region-to-region connectivity and poses limits to the construction of connectome matrices, which are based on tract terminations. When streamlines do not reach the WM/GM interface they are excluded from the structural connectivity analysis (Hagmann et al., 2008). Some methods have been recently proposed that use the entire information from the bundle and not just the termination to build the connectome (Caiafa, Pestilli, 2017).

MRI data acquisition issues

Ultimately, the results always depend on the quality of the diffusion data. The choice of the b-factor, the number of DW directions, the spatial resolution, and the SNR are all factors that will affect the accuracy and the precision of the tractography reconstructions (Dell'Acqua et al., 2010; Jones et al., 1999; Tournier et al., 2008). The limited spatial resolution of common dMRI acquisitions can represent a great confound because of the

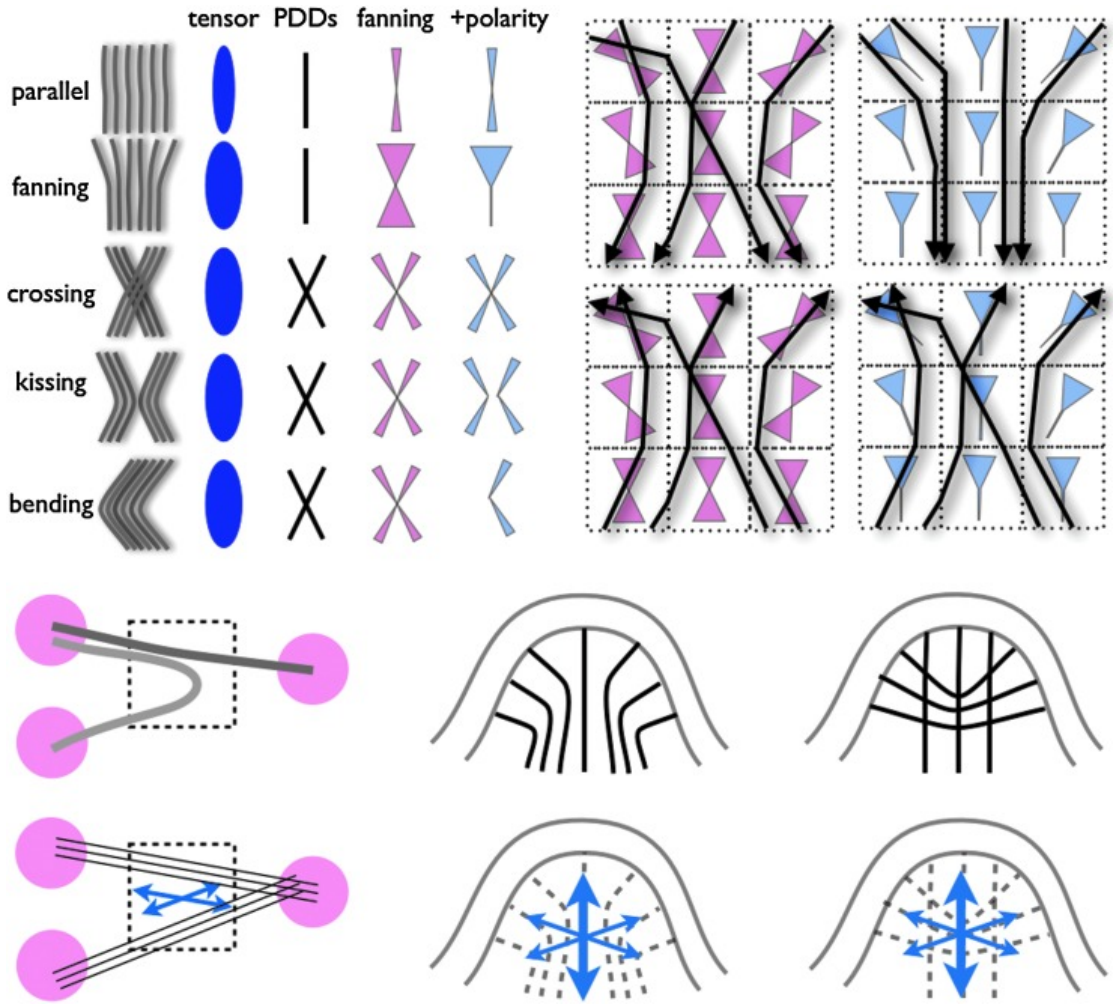

Figure 3.5: Tractography Limitations. Schematic illustrations of ambiguities in mapping diffusion to axon geometry, and their consequences for tractography. Top left: Different fibre configurations can lead to a similarly oriented tensor. The tensor's principal diffusion direction (PDD) is the same for all cases, but modeling crossing fibres helps distinguish a few of the cases. Modeling fibre fanning separates the top two geometries. Further, modeling the polarity of a fanning can help separate all cases. Top right: Illustration of the asymmetry in tracking when fanning polarity is modeled locally. Bottom left: Illustration of a case of kissing fibres, where the local model is one of crossing fibres. Tractography will lead to jumping between the tracts, causing false positives. Bottom right: Case of ambiguities near the cortex. Both axon configurations lead to the same diffusion profile (and hence the same tracking results), but have very different implications in terms of the actual connectivity (Jbabdi, Johansen-Berg, 2011).

presence of many different tissue types in the same voxel (partial volume effect). This can result in missing real connections, or in merging fibres belonging to two different populations. An increase in spatial resolution improves the accuracy of distinguishing neighbouring structures in the brain (O'Halloran et al., 2013). High angular resolution is necessary to precisely model diffusion inside the voxel and distinguish different fibres orientations. Angular resolution is improved by increasing the b-factor and/or the number of DW directions. For moderate b-values many directions are needed (*e.g.* 90), whereas this number can be lowered for higher b-values (Vos et al., 2016). However, increasing one of these parameters might come at the expense of the other, or of the acquisition time, which may lead to higher head motion sensitivity, and to protocols not easily applicable in clinical settings. A critical issue is, thus, how to optimize acquisition parameters for a clinically acceptable acquisition time (Calabrese et al., 2014; Sepehrband et al., 2017). Studies investigating the best trade-offs between angular and spatial resolution (Zhan et al., 2012; Calabrese et al., 2014) suggest tractography benefits the most from angular resolution (Vos et al., 2016).

Tractography validation issues

Given the high dependency of tractography reconstructions on models, data quality, and user-defined parameters, it is central that the outcomes are validated before inferring general principles of brain organization derived from their application. However, another important limitation of tractography is the absence of a gold standard to compare tractography results with. Validation of tractography has been achieved through different methods: animal models, physical phantoms, *post-mortem* studies in humans, and more recently developed computational methods. However, each of these methods presents with its own limitations. While phantoms have been used to test low-level diffusion models mimicking different possible fibre configuration, building realistic phantoms is challenging and the result is a rather simplified model of white matter architecture. It follows that acquisition and tractography parameters that work well on a phantom might not be directly applicable to *in-vivo* data. Renewed interest has grown in the last years in using Klinger's method (Ludwig, Klingler, 1956) to validate tractography results, and the course of several white matter bundles has been validated using this method (De Benedictis et al., 2016; Maldonado et al., 2013; Sarubbo et al., 2015). This technique has the advantages of providing direct visualization of the fibres without losing their 3D coherence. However, it doesn't allow to see the fibre crossing, it requires experienced operators, and it has a lower spatial resolution than histology. Histology, while allowing for very high resolution, is prone to geometric distortion in the registration process (Dauguet et al., 2007). More recently, other techniques have been used for anatomical validation, like optical coherence tomography (OCT), which allows for high spatial resolution and does not suffer from artefacts introduced by specimen slicing (Magnain et al., 2014; Wang et al., 2011). All these methods are clearly not available *in-vivo*. Recently computational methods to attest the strength of the evidence of a tract in a specific data-set have been developed (Pestilli et al., 2014). These methods evaluate a tractogram on the basis of of how well it fits the underlying diffusion data.

3.6 Summary

Tractography allows to look into the white matter architecture of the human brain *in-vivo* and non-invasively following a short MR acquisition protocol. To date, no other imaging modality or tool is available to achieve this goal. However, by its very nature diffusion tractography is indirect, inaccurate and difficult to quantify. While neuroscientist would like to be able to question the integrity and the strength of connections, tractography does not provide a direct measure of connectivity in the human brain. While it is easy to be captured by the pretty and colourful pictures that can be obtained with tractography, we must not forget the importance that the methodological component exerts on producing these images. It is fundamental to be aware of the limitations of diffusion-based tractography, so that these methods can be wisely applied to investigate brain anatomy in neurobiological and clinical contexts .

While tractography has been proven successful in the reconstruction of major white matter association bundles, it is still challenging to go beyond these brain "highways". The next chapter focuses on a particular white matter tract, the acoustic radiation, which due to its anatomy is particularly challenging to characterize using diffusion tractography.

Bibliography

Alexander Daniel C. Multiple-fiber reconstruction algorithms for diffusion MRI // Annals of the New York Academy of Sciences. 1064, 1. dec 2005. 113–133.

Basser Peter J, Pajevic Sinisa, Pierpaoli Carlo, Duda Jeffrey, Aldroubi Akram. In vivo fiber tractography using DT-MRI data // Magnetic Resonance in Medicine. oct 2000. 44, 4. 625–632.

Bastiani Matteo, Cottaar Michiel, Dikranian Krikor, Ghosh Aurobrata, Zhang Hui, Alexander Daniel C., Behrens Timothy E., Jbabdi Saad, Sotiropoulos Stamatios N. Improved tractography using asymmetric fibre orientation distributions // NeuroImage. sep 2017. 158. 205–218.

Behrens T E J, Berg H Johansen, Jbabdi S, Rushworth M F S, Woolrich M W. Probabilistic diffusion tractography with multiple fibre orientations: What can we gain? // NeuroImage. 2007. 34, 1. 144–155.

Behrens Timothy E J, Woolrich M W, Jenkinson Mi, Johansen-Berg H, Nunes R G, Clare S, Matthews P M, Brady J M, Smith S M. Characterization and Propagation of Uncertainty in Diffusion-Weighted MR Imaging // Magnetic Resonance in Medicine. 2003. 50, 5. 1077–1088.

Caiafa Cesar F, Pestilli Franco. Multidimensional encoding of brain connectomes // Scientific Reports. 2017. 7, 1. 11491.

Calabrese Evan, Badea Alexandra, Coe Christopher L., Lubach Gabriele R., Styner Martin A., Johnson G. Allan. Investigating the tradeoffs between spatial resolution and diffusion sampling for brain mapping with diffusion tractography: Time well spent? // Human Brain Mapping. 2014. 5685, February 2013. n/a–n/a.

Calabrese Evan, Badea Alexandra, Cofer Gary, Qi Yi, Johnson G. Allan. A Diffusion MRI tractography connectome of the mouse brain and comparison with neuronal tracer data // Cerebral Cortex. nov 2015. 25, 11. 4628–4637.

Catani Marco, Dell'Acqua Flavio, Vergani Francesco, Malik Farah, Hodge Harry, Roy Prasun, Valabregue Romain, Thiebaut de Schotten Michel. Short frontal lobe connections of the human brain // Cortex. 2012. 48, 2. 273–291.

Catani Marco, Jones Derek K., Ffytche Dominic H. Perisylvian language networks of the human brain // Annals of Neurology. 2005. 57, 1. 8–16.

Catani Marco, Mesulam Marsel. What is a disconnection syndrome? // Cortex. 2008. 44, 8. 911–913.

Catani Marco, Thiebaut de Schotten Michel, Slater David, Dell'Acqua Flavio. Connectomic approaches before the connectome // NeuroImage. oct 2013. 80. 2–13.

Chen Xiaolei, Weigel Daniel, Ganslandt Oliver, Buchfelder Michael, Nimsky Christopher. Prediction of visual field deficits by diffusion tensor imaging in temporal lobe epilepsy surgery // NeuroImage. 2009. 45, 2. 286–297.

Chen Zhenrui, Tie Yanmei, Olubiyi Olutayo, Rigolo Laura, Mehrtash Alireza, Norton Isaiah, Pasternak Ofer, Rathi Yogesh, Golby Alexandra J., O'Donnell Lauren J. Reconstruction of the arcuate fasciculus for surgical planning in the setting of peritumoral edema using two-tensor unscented Kalman filter tractography // NeuroImage: Clinical. 2015. 7. 815–822.

Conturo T E, Lori N F, Cull T S, Akbudak E, Snyder A Z, Shimony J S, McKinstry R C, Burton H, Raichle M E. Tracking neuronal fiber pathways in the living human brain. // Proceedings of the National Academy of Sciences of the United States of America. aug 1999. 96, 18. 10422–7.

Dauguet Julien, Peled Sharon, Berezovskii Vladimir, Delzescaux Thierry, Warfield Simon K., Born Richard, Westin Carl Fredrik. Comparison of fiber tracts derived from in-vivo DTI tractography with 3D histological neural tract tracer reconstruction on a macaque brain // NeuroImage. aug 2007. 37, 2. 530–538.

De Benedictis Alessandro, Petit Laurent, Descoteaux Maxime, Marras Carlo Efisio, Barbareschi Mattia, Corsini Francesco, Dallabona Monica, Chioffi Franco, Sarubbo Silvio. New insights in the homotopic and heterotopic connectivity of the frontal portion of the human corpus callosum revealed by microdissection and diffusion tractography // Human Brain Mapping. dec 2016. 37, 12. 4718–4735.

Dejerine J. Anatomie des Centres Nerveux. Reuff. Paris, 1895.

Dell'Acqua Flavio, Catani Marco. Structural human brain networks: hot topics in diffusion tractography. // Current opinion in neurology. 2012. 25, 4. 375–83.

Dell'Acqua Flavio, Scifo Paola, Rizzo Giovanna, Catani Marco, Simmons Andrew, Scotti Giuseppe, Fazio Ferruccio. A modified damped Richardson-Lucy algorithm to reduce isotropic background effects in spherical deconvolution // NeuroImage. 2010. 49, 2. 1446–1458.

Descoteaux Maxime, Deriche Rachid, Knösche T, Anwander Alfred. Deterministic and Probabilistic Tractography Based on Complex Fiber Orientation Distributions // IEEE Transactions on Medical Imaging. 2009. 28, 2. 269–286.

Forkel Stephanie J, Thiebaut de Schotten Michel, Dell'Acqua Flavio, Kalra Lalit, Murphy Declan G M, Williams Steven C R, Catani Marco. Anatomical predictors of aphasia recovery: a tractography study of bilateral perisylvian language networks. // Brain : a journal of neurology. jul 2014. 137, Pt 7. 2027–39.

Geschwind N. Disconnection syndromes in animals and man // Brain. 1965. 88. 237–644.

Girard Gabriel, Whittingstall Kevin, Deriche Rachid, Descoteaux Maxime. Towards quantitative connectivity analysis : reducing tractography biases // NeuroImage. 2014. 98. 266–278.

Hagmann Patric, Cammoun Leila, Gigandet Xavier, Meuli Reto, Honey Christopher J, Wedeen Van J, Sporns Olaf. Mapping the Structural Core of Human Cerebral Cortex // PLoS Biology. jul 2008. 6, 7. e159.

Heuvel Martijn P. van den, Sporns Olaf. Rich-Club Organization of the Human Connectome // Journal of Neuroscience. 2011. 31, 44.

Jbabdi Saad, Johansen-Berg Heidi. Tractography: Where Do We Go from Here? // Brain Connectivity. 2011. 1, 3. 169–183.

Jones D K, Horsfield M A, Simmons A. Optimal strategies for measuring diffusion in anisotropic systems by magnetic resonance imaging. // Magnetic resonance in medicine. sep 1999. 42, 3. 515–25.

Jones Jeffery A, Callan Daniel E. Brain activity during audiovisual speech perception: an fMRI study of the McGurk effect. // Neuroreport. jun 2003. 14, 8. 1129–33.

Klein Arno, Andersson Jesper, Ardekani Babak A., Ashburner John, Avants Brian, Chiang Ming-Chang, Christensen Gary E., Collins D. Louis, Gee James, Hellier Pierre, Song Joo Hyun, Jenkinson Mark, Lepage Claude, Rueckert Daniel, Thompson Paul, Vercauteren Tom, Woods Roger P., Mann J. John, Parsey Ramin V. Evaluation of 14 nonlinear deformation algorithms applied to human brain MRI registration // NeuroImage. jul 2009. 46, 3. 786–802.

Lawes I Nigel C, Barrick Thomas R, Murugam Vengadasalam, Spierings Natalia, Evans David R, Song Marie, Clark Chris A. Atlas-based segmentation of white matter tracts of the human brain using diffusion tensor tractography and comparison with classical dissection. // NeuroImage. jan 2008. 39, 1. 62–79.

Lazar Mariana, Alexander Andrew L. An error analysis of white matter tractography methods: synthetic diffusion tensor field simulations // NeuroImage. oct 2003. 20, 2. 1140–1153.

Lichteim L. On aphasia // Brani. 1885. 7. 433–484.

Ludwig E, Klingler J. Atlas Cerebri Humani (The Inner Structure of the Brain Demonstrated on the Basis of Macroscopical Preparations). Boston, 1956.

Magnain Caroline, Augustinack Jean C., Reuter Martin, Wachinger Christian, Frosch Matthew P., Ragan Timothy, Akkin Taner, Wedeen Van J., Boas David A., Fischl Bruce. Blockface histology with optical coherence tomography: A comparison with Nissl staining // NeuroImage. jan 2014. 84. 524–533.

Makris Nikos, Papadimitriou George M., Kaiser Jonathan R., Sorg Scott, Kennedy David N., Pandya Deepak N. Delineation of the middle longitudinal fascicle in humans: A quantitative, in vivo, DT-MRI study // Cerebral Cortex. 2009. 19, 4. 777–785.

Maldonado Igor Lima, De Champfleur Nicolas Menjot, Velut St??phane, Destrieux Christophe, Zemmoura Ilyess, Duffau Hugues. Evidence of a middle longitudinal fasciculus in the human brain from fiber dissection // Journal of Anatomy. 2013. 223, 1. 38–45.

Mori S, Crain B J, Chacko V P, Zijl P C van. Three-dimensional tracking of axonal projections in the brain by magnetic resonance imaging. // Annals of neurology. 1999. 45, 2. 265–269.

Mulert Christoph, Kirsch Valerie, Whitford Thomas J., Alvarado Jorge, Pelavin Paula, McCarley Robert W., Kubicki Marek, Salisbury Dean F., Shenton Martha E. Hearing voices: A role of interhemispheric auditory connectivity? // World Journal of Biological Psychiatry. 2012. 13, 2. 153–158.

O'Donnell Lauren, Haker Steven, Westin Carl-Fredrik. New Approaches to Estimation of White Matter Connectivity in Diffusion Tensor MRI : Elliptic PDEs and Geodesics in a Tensor-Warped Space // Miccai. 2002. 1. 459–466.

O'Halloran R. L., Aksoy M., Van A. T., Bammer R. 3D isotropic high-resolution diffusion-weighted MRI of the whole brain with a motion-corrected steady-state free precession sequence // Magnetic Resonance in Medicine. aug 2013. 70, 2. 466–478.

Pajevic Sinisa, Aldroubi Akram, Basser Peter J. A continuous tensor field approximation of discrete DT-MRI data for extracting microstructural and architectural features of tissue. // Journal of magnetic resonance (San Diego, Calif. : 1997). jan 2002. 154, 1. 85–100.

Pestilli Franco, Yeatman Jason D, Rokem Ariel, Kay Kendrick N, Wandell Brian A. Evaluation and statistical inference for human connectomes. // Nature methods. 2014. 11, 10. 1058–63.

Raffelt David, Tournier J. Donald, Rose Stephen, Ridgway Gerard R., Henderson Robert, Crozier Stuart, Salvado Olivier, Connelly Alan. Apparent Fibre Density: A novel measure for the analysis of diffusion-weighted magnetic resonance images // NeuroImage. 2012. 59, 4. 3976–3994.

Raffelt David A, Tournier J. Donald, Smith Robert E, Vaughan David N, Jackson Graeme, Ridgway Gerard R, Connelly Alan. Investigating white matter fibre density and morphology using fixel-based analysis // NeuroImage. jan 2017. 144, Pt A. 58–73.

Rojkova K., Volle E., Urbanski M., Humbert F., Dell'Acqua F., Thiebaut de Schotten M. Atlasing the frontal lobe connections and their variability due to age and education:

a spherical deconvolution tractography study // Brain Structure and Function. apr 2016. 221, 3. 1751–1766.

Rowe Matthew, Zhang Hui Gary, Oxtoby Neil, Alexander Daniel C. Beyond crossing fibers: Tractography exploiting sub-voxel fibre dispersion and neighbourhood structure // Lecture Notes in Computer Science (including subseries Lecture Notes in Artificial Intelligence and Lecture Notes in Bioinformatics). 7917 LNCS. 2013. 402–413.

Rudie J.D., Brown J.A., Beck-Pancer D., Hernandez L.M., Dennis E.L., Thompson P.M., Bookheimer S.Y., Dapretto M. Altered functional and structural brain network organization in autism // NeuroImage: Clinical. 2013. 2. 79–94.

Sarubbo Silvio, De Benedictis Alessandro, Milani Paola, Paradiso Beatrice, Barbareschi Mattia, Rozzanigo Umbero, Colarusso Enzo, Tugnoli Valeria, Farneti Marco, Granieri Enrico, Duffau Hugues, Chioffi Franco. The course and the anatomo-functional relationships of the optic radiation: a combined study with post mortem dissections and in vivo direct electrical mapping. // Journal of anatomy. jan 2015. 226, 1. 47–59.

Saur Dorothee, Schelter Björn, Schnell Susanne, Kratochvil David, Küpper Hanna, Kellmeyer Philipp, Kümmerer Dorothee, Klöppel Stefan, Glauche Volkmar, Lange Rüdiger, Mader Wolfgang, Feess David, Timmer Jens, Weiller Cornelius. Combining functional and anatomical connectivity reveals brain networks for auditory language comprehension // NeuroImage. 2010. 49, 4. 3187–3197.

Schotten Michel Thiebaut De, Cohen Laurent, Amemiya Eduardo, Braga Lucia W, Dehaene Stanislas, Yvette Gif, Paris-sud France Université. Learning to Read Improves the Structure of the Arcuate Fasciculus // Cerebral Cortex. 2012. 3. 1–7.

Sepehrband Farshid, O'Brien Kieran, Barth Markus. A time-efficient acquisition protocol for multipurpose diffusion-weighted microstructural imaging at 7 Tesla // Magnetic Resonance in Medicine. feb 2017.

Setsompop K., Kimmlingen R., Eberlein E., Witzel T., Cohen-Adad J., McNab J. a., Keil B., Tisdall M. D., Hoecht P., Dietz P., Cauley S. F., Tountcheva V., Matschl V., Lenz V. H., Heberlein K., Potthast A., Thein H., Van Horn J., Toga A., Schmitt F., Lehne D., Rosen B. R., Wedeen V., Wald L. L. Pushing the limits of in vivo diffusion MRI for the Human Connectome Project // NeuroImage. 2013. 80. 220–233.

Shu Ni, Liu Yong, Li Jun, Li Yonghui, Yu Chunshui, Jiang Tianzi. Altered anatomical network in early blindness revealed by diffusion tensor tractography. // PloS one. sep 2009. 4, 9. e7228.

Smith Robert E., Tournier Jacques-Donald, Calamante Fernando, Connelly Alan. Anatomically-constrained tractography: Improved diffusion MRI streamlines tractography through effective use of anatomical information // NeuroImage. 2012. 62, 3. 1924–1938.

Sotiropoulos Stamatios N., Bai Li, Morgan Paul S., Constantinescu Cris S., Tench Christopher R. Brain tractography using Q-ball imaging and graph theory: Improved connectivities through fibre crossings via a model-based approach // NeuroImage. feb 2010. 49, 3. 2444–2456.

Sporns Olaf. Making sense of brain network data // Nature Methods. may 2013. 10, 6. 491–493.

Sporns Olaf, Tononi Giulio, Kötter Rolf. The Human Connectome: A Structural Description of the Human Brain // PLoS Computational Biology. sep 2005. 1, 4. e42.

Stebbins G T, Murphy C M. Diffusion tensor imaging in Alzheimer's disease and mild cognitive impairment. // Behavioural neurology. 2009. 21, 1. 39–49.

Tournier J.-Donald, Yeh Chun-Hung, Calamante Fernando, Cho Kuan-Hung, Connelly Alan, Lin Ching-Po. Resolving crossing fibres using constrained spherical deconvolution: Validation using diffusion-weighted imaging phantom data // NeuroImage. aug 2008. 42, 2. 617–625.

Tournier Jd, Mori S, Leemans a. Diffusion Tensor Imaging and Beyond // Magnetic Resonance in .... 2011. 65, 6. 1532–1556.

Vos Sjoerd B., Aksoy Murat, Han Zhaoying, Holdsworth Samantha J., Maclaren Julian, Viergever Max A., Leemans Alexander, Bammer Roland. Trade-off between angular and spatial resolutions in in vivo fiber tractography // NeuroImage. apr 2016. 129. 117–132.

Wang Hui, Black Adam J., Zhu Junfeng, Stigen Tyler W., Al-Qaisi Muhammad K., Netoff Theoden I., Abosch Aviva, Akkin Taner. Reconstructing micrometer-scale fiber pathways in the brain: Multi-contrast optical coherence tomography based tractography // NeuroImage. oct 2011. 58, 4. 984–992.

Wheeler-Kingshott Claudia A.M., Cercignani Mara. About "axial" and "radial" diffusivities // Magnetic Resonance in Medicine. may 2009. 61, 5. 1255–1260.

Wu Jin-Song, Zhou Liang-Fu, Tang Wei-Jun, Mao Ying, Hu Jin, Song Yan-Yan, Hong Xun-Ning, Du Gu-Hong. Clinical evaluation and follow-up outcome of diffusion tensor imaging-based functional neuronavigation // Neurosurgery. nov 2007. 61, 5. 935–949.

Yeatman Jason D, Dougherty Robert F, Myall Nathaniel J, Wandell Brian A, Feldman Heidi M. Tract profiles of white matter properties: automating fiber-tract quantification. // PloS one. 2012. 7, 11. e49790.

Yeatman Jason D., Weiner Kevin S., Pestilli Franco, Rokem Ariel, Mezer Aviv, Wandell Brian a. The vertical occipital fasciculus: A century of controversy resolved by in vivo measurements // Proceedings of the National Academy of Sciences. 2014. 111, 48. E5214–E5223.

Zemmoura I, Vons J, Velut S, Destrieux C. From Vesalius to tractography. // Journal of neurosurgical sciences. dec 2015. 59, 4. 309–25.

Zhan Liang, Franc Daniel, Patel Vishal, Jahanshad Neda, Jin Yan, Mueller Bryon A, Bernstein Matt A, Borowski Bret J, Jack Clifford R, Toga Arthur W, Lim Kelvin O, Thompson Paul M, Thompson Paul M. How do spatial and angular resolution affect brain connectivity maps from diffusion MRI? // Proceedings. IEEE International Symposium on Biomedical Imaging. 2012. 1–6.

Chapter 4

A missing connection: a topographical review of the acoustic radiation

4.1 Introduction

The acoustic radiation (AR) represents a highly-myelinated group of axonal projections belonging to the auditory system of primates, and constitutes one of the main sensory pathways of the brain, carrying auditory information from the thalamus to the cortex. The connectivity pattern of these auditory fibres has been described in some detail in cytoarchitectonic and myeloarchitectonic studies of non-human primates (Hackett et al., 1998; Mesulam, Pandya, 1973; Morel et al., 1993; Polyak, 1932) and, at a more macroscopic level, in a few histological studies in humans (Bürgel et al., 2006; Flechsig, 1920; Pfeifer, 1920). However, the information obtained from non-human primate studies cannot be directly transferred to the human brain, and it has mostly focused on the cytoarchitectonic aspects of the auditory cortices and their intrinsic connectivity, with little emphasis on the topography of the AR itself. In humans, invasive techniques have very restricted application, and little information can be drawn from old myeloarchitectonical studies.

The advent of diffusion tractography (Chapter 3) has made it possible to investigate the anatomy of the major white matter bundles of the human brain *in-vivo* and non-invasively (Catani et al., 2002; Lawes et al., 2008). However, the AR constitutes a notable exception in this sense. This primary sensory bundle is largely absent from most tractography studies investigating audition and language, and from human white matter atlases (Thiebaut de Schotten et al., 2011). This is mainly due to the intrinsic anatomical characteristics of these fibres that meet the current limits of dMRI tractography methods (Maffei et al., 2015; Jones, Cercignani, 2010). The diffusion-based tractography recon-

struction of the AR remains at present highly challenging, discouraging its anatomical investigation in humans *in-vivo*. Successful reconstruction of the human auditory tract *in-vivo* is of great importance for both clinical applications (e.g. pre-surgical mapping, stroke patients) and basic neurobiological research. Reliably revealing the 3D characteristics of this tract would help in correlating the anatomical and the functional aspects of audition and in studying human-only cognitive functions such as language, both in healthy and pathological conditions. The aim of this chapter is to bring together the available information on the topography of the AR from primate studies, with particular emphasis on the anatomical features that make this tract extremely challenging for the state of the art dMRI tractography techniques. Old and recent studies on the anatomy of the AR will be reviewed, and some recent attempts to reconstructing the AR using diffusion-based tractography methods will be discussed. Finally, open questions in the field will be presented and possible future research directions considered.

4.2 The auditory system

The anatomical and functional organization of the human auditory system has been in large part inferred from animal studies, because of restricted application of invasive procedures in humans (Hackett et al., 2001, 1998; Kaas, Hackett, 2000). Although comparative studies have shown similar features across human and non-human primates, cortical and subcortical architectonic differences and cognitive dissimilarities exist (Passingham, 2009; Schmahmann et al., 2007; Thiebaut de Schotten et al., 2012). It is thus important to understand the similarities and dissimilarities between the species and consider the potential uniqueness of the human auditory system, in relation to the ability of perceiving and processing language-specific stimuli. This section reviews the organization of the auditory system at the subcortical and cortical level, comparing human and non-human primates anatomy.

The auditory aystem

The auditory system of mammalian is a complex network of subcortical and corticocortical projections that encodes and transmits stimuli coming from the acoustic environment enabling humans and other animals to detect sounds, determine sounds direction, discriminate sounds sources, and communicate. The acoustic signal is first received and processed by an ensemble of nerve axons that start at the auditory nerve (AN) (Figure 4.1). The AN conveys action potentials in response to neurotransmitters released by the hair cells in the cochlea. This information is transmitted to the bilateral cochlear nuclei (CN), the first auditory relay of the brain stem. This is divided in a ventral (VCN) and a dorsal (DCN) part. The cellular and nerve fibres organization of the VCN is similar between humans and other mammals, while that of the DCN exhibits notable inter-species variation (Brugge, 2013). The signal is transformed and transmitted from this station to higher auditory centres via three main ascending pathways: the dorsal acoustic stria (of Monakov), the intermediate acoustic stria (of Held), and the ventral acoustic stria (trapezoid body). The next auditory relay is the superior olivary complex (SOC), which,

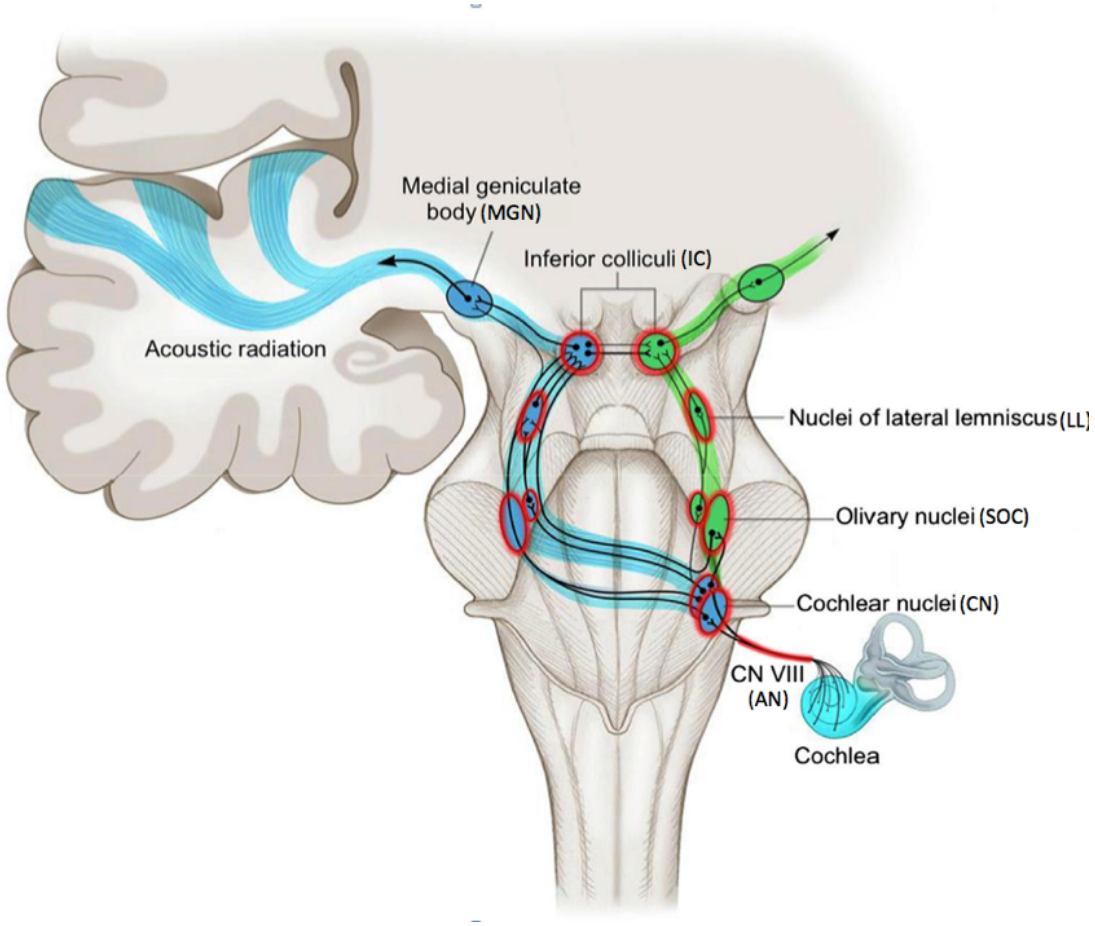

Figure 4.1: The Auditory System. The image shows the schematic representation of the ascending human auditory system. Ipsi-lateral (green) and contro-lateral (blue) connections from the cochlea to the auditory cortex are shown, with the auditory relays of the brain stem highlighted in red. Image adapted from: https://pharmaceuticalintelligence.com.

receiving inputs from both ears, is the primary site for binaural interactions and thus important for localizing sounds on the horizontal plane. Axons arising in the SOC form the lateral lemniscus (LL) projecting to the inferior colliculus (IC), which works as intermediate operator, integrating the information arising from the multiple auditory centres of the brainstem. From the IC the auditory information reaches the medial geniculate nucleus of the thalamus (MGN) through the tecto-thalamic lemniscal pathway (Figure 4.1). From here, projection fibres leave to contact ipsilateral cortical auditory regions in the temporal lobe. These thalamo-cortical neurons form the acoustic radiation (AR).

The auditory cortex

The extent and organization of the auditory projection cortex (areas of neo-cortex contacted by MGB neurons) has been extensively investigated in both humans and non-human primates (Hackett et al., 2001; Moerel et al., 2014). From an anatomical perspective, this is defined as the area of the cortex that receives significant inputs from the MGN. It is located in the temporal lobe, on the lateral and dorsal surfaces, corresponding to the superior temporal gyrus (STG) and superior temporal plane (TP), respectively, some of the latter buried deep within the Sylvian fissure. In monkeys three hierarchically organized regions are distinguished: a core (primary cortex), a belt (secondary cortex) and a para-belt region (association cortex) (Hackett et al., 1998; Kaas, Hackett, 2000; Mesulam, Pandya, 1973). The core region occupies a portion of the caudal superior temporal plane and it is characterized by a dense population of small granule cells (*e.g.*, koniocortex). This area is surrounded by a narrow belt region, and a third more lateral region that occupies the dorsal surface of the superior temporal gyrus. This latter para-belt is generally considered to be a higher-order auditory region or auditory association cortex (Hackett et al., 1998), that integrates auditory with non-auditory multisensory information. These cortical regions are further internally subdivided based on micro-anatomical and functional differences, and their connectivity to cortical and sub-cortical structures (Hackett et al., 2001). The monkey auditory core has been divided in auditory area 1 (AI), rostral field (R), and sometimes a rostro-temporal field (RT) on the base of the functional response these areas have to frequencies (Merzenich, Brugge, 1973) (Figure 4.2a).

Post-mortem studies in humans delineate homologous regions with a primary auditory cortex (PAC) (or auditory core) (Brodmann area 41) located on the transverse temporal gyrus of Heschl (HG), a belt region (Brodmann area 42), and other auditory association areas identified in the planum polare (PP) on the STG anterior to HG and in the planum temporale (PT), posterior to the HG (Brodmann area 22-42) (Morosan et al., 2001) (Figure 4.2b). Brodmann identified a fourth area 52 at the most medial end of HG, at the transition between the auditory cortex and the insula (Brodmann, 1909). The transverse temporal gyrus of Heschl (HG) lies diagonally across the superior temporal plane, hidden in the depth of the Sylvian fissure (SF) (Figure 4.2c). This structure is new on an evolutionary perspective: it is absent in macaque monkey and can be found only in some chimpanzees' brain (Hackett et al., 2001; Moerel et al., 2014). It is defined anteriorly by the transverse sulcus (TS) of the temporal lobe, which unites medially to

the circular sulcus of the insula, and posteriorly by the Heschl's sulcus (HS). There might be a second HS (or sulcus intermedius) if two HG gyri are present. On the sagittal and coronal slices the HG appears as a protrusion of the superior temporal plane (STP), with variable shapes like an omega, a mushroom or a heart (Abdul-Kareem, Sluming, 2008; Marie et al., 2015). The core area is located on the posterior medial part of HG -and part of a second HG if present- occupying half of the gyral volume (Rademacher et al., 2001). As in non-human primates, it is composed by densely packed granular neurons and it has a well-developed layer IV (Brugge, 2013; Seldon, 1981), reflecting dense thalamic axonal inputs. Just as in monkeys, belt and para-belt regions are involved in the integration of higher order functions, and in humans are largely responsible for processing language-related information (Scott, Johnsrude, 2003).

This macro-anatomical correspondence between monkeys and humans is lost at finer level of area definitions. Disagreement on number, location and functions of human auditory areas still exists, resulting in different groups using different functional parcellation schemes and nomenclatures. The internal anatomical subdivision of the human primary and secondary auditory cortices is at present not completely understood. Several groups have tried to elucidate this with the aim of building a common framework of reference (Baumann et al., 2013; Clarke, Rivier, 1998; Da Costa et al., 2011; Fullerton, Pandya, 2007; Moerel et al., 2014; Seldon, 1981; Tardif, Clarke, 2001; Wallace et al., 2002).

Intrinsic anatomical connectivity in the auditory system

Importantly, cortical areas are also heavily interconnected by reciprocal connections. This intrinsic connectivity has been widely investigated in non-human primates (Hackett et al., 1998; Kaas, Hackett, 2000; Galaburda, Pandya, 1983) and to a lesser extent in humans. Experiments using the anterograde and retrograde tracer DiI in humans (Tardif, Clarke, 2001) suggest that intrinsic connections within the primary auditory areas mainly involve nearby regions, whereas in surrounding regions (belt and para-belt), connections spread to more distant areas and may play an important role in the integration of different auditory features. Consistently, in monkeys the core has dense reciprocal connections with adjacent areas of the core and belt, but few, if any, with the parabelt or more distant areas. The belt region receives input from the core and from the dorsal and medial divisions of the MGN, and has also dense connections to adjacent parabelt areas. The parabelt receives inputs from the belt but has fewer –if any- connections to the core area, suggesting hierarchical organization of the auditory cortical regions (Hackett et al., 1998; Kaas, Hackett, 2000). This connection pattern suggest a serial process of information from the core to belt to parabelt to further regions, and its is been interpreted as evidence for a processing hierarchy (Kaas et al., 1999; Rauschecker et al., 1997).

Tonotopic organization

This hierarchical organization is reflected in the tonotopic arrangement of the cortical auditory regions. Along the path from the cochlea to the cortex, the auditory information is tonotopically organized, meaning that frequencies are spatially ordered. This tonotopic arrangement is preserved at all levels of the auditory system, from the lower

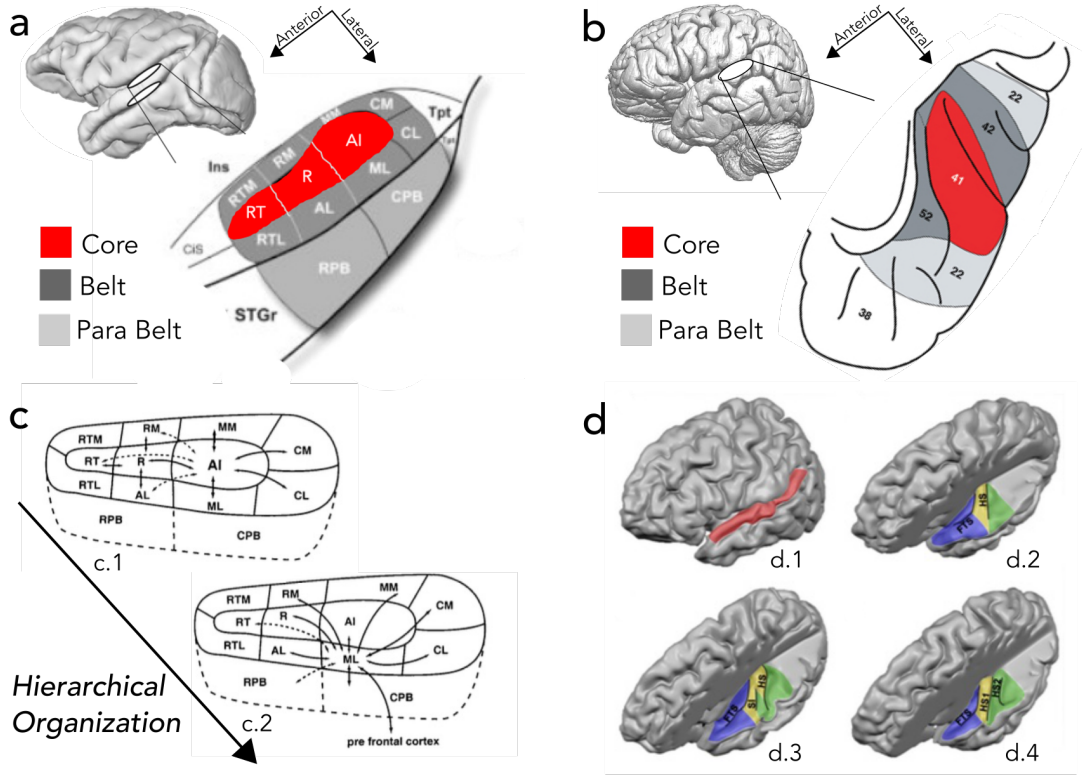

Figure 4.2: The Auditory Cortex. The figure shows the organization of the auditory cortex in humans and non-human primates. a: Subdivision of the auditory cortex in monkeys into core, belt, parabelt and cytoarchitectonical regions (modified from (Hackett, 2011)). b: Subdivision of the auditory cortex in the human brain into core, belt, and parabelt areas. Corresponding Brodman regions are also shown (modified from (Hackett, 2011)). The difference in the gradient of the auditory cortex can be noticed. In monkeys is an anterior-posterior gradient, while in humans is a medio-lateral one. c: Intrinsic connectivity of the auditory cortex in monkeys. The core regions have reciprocal connections with core and belt regions (c.1). Belt regions have connections with other belt regions and more distant centers (c.2) (modified from (Kaas, Hackett, 2000)). d: Lateral view of the left hemisphere with STG highlighted in red (d.1). d2-4 show superior view of the supratemporal plane in the case of a single Heschl's gyrus (d.2), two Heschl's gyri with incomplete separation (d.3), and two Hescl's gyri. HG is shown in yellow, planum polare (PP) in blue, planum temporale (PT) in green (taken from (Moerel et al., 2014)).

subcortical structures to the higher cortical auditory regions, and constitutes one of the most remarkable features of the auditory system. In primates, tonotopic maps can be found in the core auditory region and in a number of areas in the belt region (Merzenich, Brugge, 1973), whereas auditory cortex beyond the belt cannot be well characterized in terms of tonotopical organization. In humans, the same strong tonotopic organization of AI can be revealed in HG (Howard et al., 1996; Liegeois-Chauvel et al., 1991), considered for this reason the main location of A1. However, no widespread consensus on the exact part of the tonotopic gradient to be assigned to the core exists (Baumann et al., 2013).

Even if no definitive agreement on parcellations schemes and tonotopic organization exists, the combination of animal research, post-mortem studies in humans, and functional magnetic resonance imaging (fMRI) (Humphries et al., 2010; Dijk van, Langers, 2013) methods allowed to obtain a comprehensive view on the functional and anatomical organization of this complex system. Compared to its cortical counterparts, the white matter components of the auditory system have attracted less attention. This review will focus in particular on the very last part of the ascending auditory system, which is composed of complex of axons projecting from the medial geniculate of the thalamus (MGN) to the cortex of the temporal lobe. These thickly myelinated fibres constitute the acoustic radiation (AR) (Figure 4.1).

4.3 The anatomy of the acoustic radiation

Knowledge on the AR topography in humans mainly comes from anatomical pioneering investigations in the beginning of the 20^{th} century (Flechsig, 1920; Pfeifer, 1920; Dejerine, 1895). After these first studies, to the best of our knowledge, virtually no additional information on this structure has been reported in humans. Most neuroanatomical books tend to only report schematic drawings of this pathways.

This section reviews old and more recent studies that investigated the connectivity pattern and the topography of this bundle in non-human primates and humans, aiming at building a more complete profile of the anatomy of this tract across the two species.

4.3.1 The acoustic radiation in non-human primates

The anatomical connections between the thalamus and the auditory cortex in the temporal lobe have been investigated in animals using different invasive techniques. These fibres stem from the medial geniculate nucleus (MGN) of the thalamus, as first described by Monakow (1882) on the basis of experimental lesion studies in rabbits. What is less clear is the location and extension cortex these fibres connect to. Using retrograde degeneration techniques Minkowski (1923) showed that only ablation of the superior temporal gyrus (STG) caused degeneration in the MGN. Polyak (1932) in his Marchi axonal degeneration studies concluded that the fibres of the auditory system are distributed almost exclusively within the supra-temporal plane, where they terminate at a posteromedial bulge he homologized with the transverse gyrus of Heschl in humans. Similarly, Walker confirmed that projections from the MGN contact a very specific area on the posterior

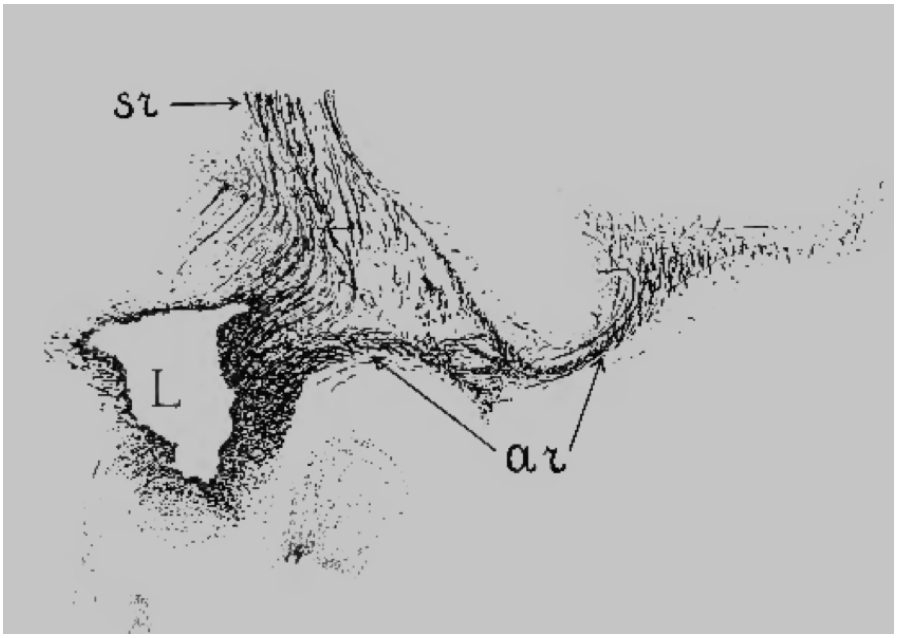

Figure 4.3: The Acoustic Radiation in Non-human Primates. The image shows the lesion (L) of the posterior thalamus in a rhesus monkey, from where numerous thalamocortical (sr) and auditory fibres (ar) emerge. The AR is visible here in its entire length up to its termination on the lip of the Sylvian fissure. Adapted from Polyak (1932).

part of the Sylvian fissure, which he named a "rudimentary transverse gyrus" (Walker, 1937).

Successively, studies showed that different parts of the medial geniculate body projected to different parts of the auditory cortex. In particular, (Mesulam, Pandya, 1973) used silver impregnation techniques in the rhesus monkey to show that the more anterior part of the parvocellular subdivision of the MGN projects to primary auditory areas. Rauschecker et al. (1997) confirmed that core regions receive dense and direct thalamic inputs from the ventral MGN and that these connections appear to be in parallel, so that ablation of one area does not deactivate the others. While the ventral division of the MGN connect to primary regions, its posterior and medial divisions have been found to connect in parallel to auditory association areas, bypassing primary auditory regions (Rauschecker et al., 1997). These connections form the extralemniscal (or non-classical) auditory pathway. Neurons of this pathway show less sharp responses to sounds and are responsive also to other sensory stimulation, such as touch. The dorsal division also projects to other regions of the brain like the lateral nucleus of the amygdala (Moller, 2006).

In addition to connections from the MGN, primary auditory regions seem to receive non-MGN inputs from the suprageniculate nucleus (SG), the posterior nuclear complex

(PCN) and the pulvinar (Kaas, Hackett, 2000; Rauschecker et al., 1997). Conversely, Mesulam & Pandya (1973) (Mesulam, Pandya, 1973) found that in some cases projections of the MGN were found in the superior and inferior Sylvian fossa, the insula, and the parietal operculum.

Taken together, these studies mainly focused on connectivity aspects between the MGN and the auditory projection cortical territory, while scarce attention has been paid to the topographical characteristics of the tract itself. Polyak (1932) (Polyak, 1932) gave us one of the first and most detailed descriptions of the topography and course of this tract in monkeys. He describes a dense bundle of closely assembled fibres that leaves the MGN, turns laterally and cross the most ventral portion of the internal capsule immediately above the lateral geniculate body (LGN). Here these fibres are distinguishable from somato-sensory fibres by their being a strong bundle in a nearly horizontal orientation. Then the AR bends ventrally and reaches the external capsule by passing through the ventral edge of the posterior putamen. Here it meets other projection and association bundles before finally reaching the white matter of the superior temporal convolution close to the Sylvian fissure (Figure 4.3). Overall, he describes the auditory radiation as a regularly arranged projection system, where fibres lie parallel to one another to gradually diverge only when approaching the cortex.

4.3.2 The acoustic radiation in humans

The early information we have about the anatomy of the AR in the human brain dates back to the old myeloarchitectonical observations of the pioneers in this field (Dejerine, 1895; Flechsig, 1920; Pfeifer, 1920). Flechsig, Pfeifer, and Dejerine reported the anatomy of this bundle in their maps (Figure 4.4). These classical topographical descriptions of the AR locate these fibres at the posterior ventral part of the thalamus, where the MGN is located. The AR leaves the MGN and pursue an antero-lateral direction passing through the posterior portion of the internal capsule, proceeding along the corona radiata, curving around the inferior portion of the circular sulcus of the insula before finally reaching the transverse temporal gyrus of Heschl (Dejerine, Serieux, 1897; Flechsig, 1920) where they enter in a ventral-to-dorsal direction (Pfeifer, 1920) (Figure 4.4).

These old maps from Dejerine and Flechsig, while being of invaluable historical importance, cannot be used to extract precise anatomical information that can be applied to modern brain atlases or neuroimaging studies. More recently, radiological information about the AR white matter anatomy was obtained in human post-mortem myelin-stained sections (Bürgel et al., 2006; Rademacher et al., 2002). This study is of great importance as it represents the main reference framework for *in-vivo* imaging studies. This study confirmed the classical topographical description of the acoustic fibres: they leave the MGN and take a rostro-caudal and upward course in the lateral direction, passing close to the posterior margin of the internal capsule and the ventral rim of the insula, to finally contact large portions of HG (Figure 4.5). As previously noted by Pfeifer and Polyak, the authors noticed that the AR does not enter the lenticular nucleus, and runs dorsally to the optic radiation (OR). This intimate relation with the optic tract has been described

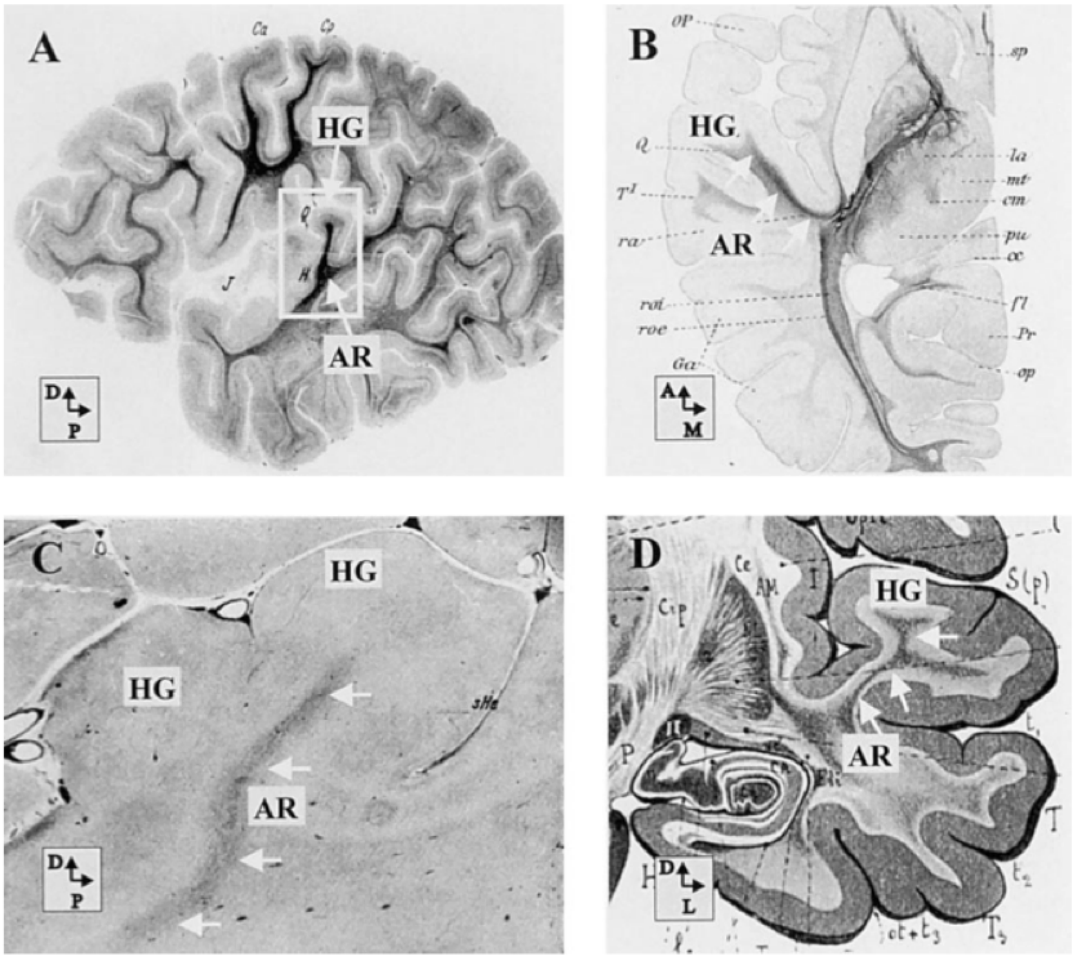

Figure 4.4: The Acoustic Radiation in Humans. The image shows some examples of old myeloarchitectonic studies. A) Sagyttal myelin-stained section showing the AR and HG (Pfeifer, 1920). B) Axial myelin-stained section trough the temporal and occipital lobes showing the medial to lateral extent of the AR (Flechsig, 1920). C) Sagittal myelin-stained section showing the AR projecting to a portion of HG (Pfeifer, 1920). D) Coronal section of the temporal lobe showing the course of the AR as depicted in Dejerine's atlas (Dejerine, 1895). Image adapted from (Rademacher et al., 2002).

in the past by Dejerine who defined this region of close proximity between AR and OR as "carefur sensitive" (Dejerine, 1895). Polyak also describes this region stating that the optic and the acoustic radiation while lying close together are completely separated: the auditory radiation being more frontal, crosses at a right angle above the visual radiation, while the latter takes a caudal sagittal direction (Polyak, 1932).

Overall, the topographical description of the AR in humans resembles the description of this tract in non-human primates. However, compared to non-human primates, the human cortical surface of the auditory regions presents with additional gyri and higher inter subjects and interhemispheric variability (Galaburda et al., 1978; Hackett et al., 2001) that might affect the AR anatomy. Burgel and colleagues found major variability in the localization of the AR between subjects and hemispheres. This variability is particularly evident at the origin of the radiation, *i.e.*, as it leaves the MGN (Bürgel et al., 2006). Differences in the stereotaxic position of the AR showed that right AR is consistently localized more anteriorly than left AR. However, in contrast with previous morphometric reports (Penhune et al., 1996; Rademacher et al., 2001; Seldon, 1981; Economo v., Horn, 1930) no significant asymmetries in the volume of the tract between hemispheres was found.

While in non-human primates, connections to/from different cortical regions have been investigated, studies in humans almost exclusively focused on connections between MGN and HG. However, recent evidence shows the existence of a non-classical extra-lemniscal pathway that runs parallel to the classic pathway and projects to secondary association regions, and other regions of the brain like the limbic system, similarly to results in non-human primates (Keifer et al., 2015). In addition, according to Flechsig, these fibres are divisible into two bundles, one of which ascends near the external capsule and enters the auditory cortex from the superior and posterior side, while the other courses for some distance in the company of the occipito-thalamic radiations, then passing behind and below the fossa sylvii where it pierces the bases of the second and third temporal convolutions to arrive at the transverse temporal gyrus or gyri.

These differences in cortical anatomy between the two species and the variability of cortical and subcortical structures across subjects and hemispheres in humans raise interesting questions on the relationship that might exist between these differences and human-only language abilities.

4.4 The acoustic radiation in tractography studies

The diffusion-based 3D reconstruction of the AR is at present highly challenging, and this tract is largely missing from tractography investigations. Several studies used diffusion imaging methods to investigate the white matter of the auditory system, but they are mostly limited to the extraction of quantitative diffusion metrics from atlas-derived regions of interest (ROIs) (Chang et al., 2004; Lee et al., 2007; Lin et al., 2008; Wu et al., 2009). To the best of our knowledge, only a few studies could actually recover the 3D profile of the AR using tractography techniques (Behrens et al., 2007; Berman et al., 2013; Crippa et al., 2010; Javad et al., 2014; Profant et al., 2014) (Figure 4.6). Why

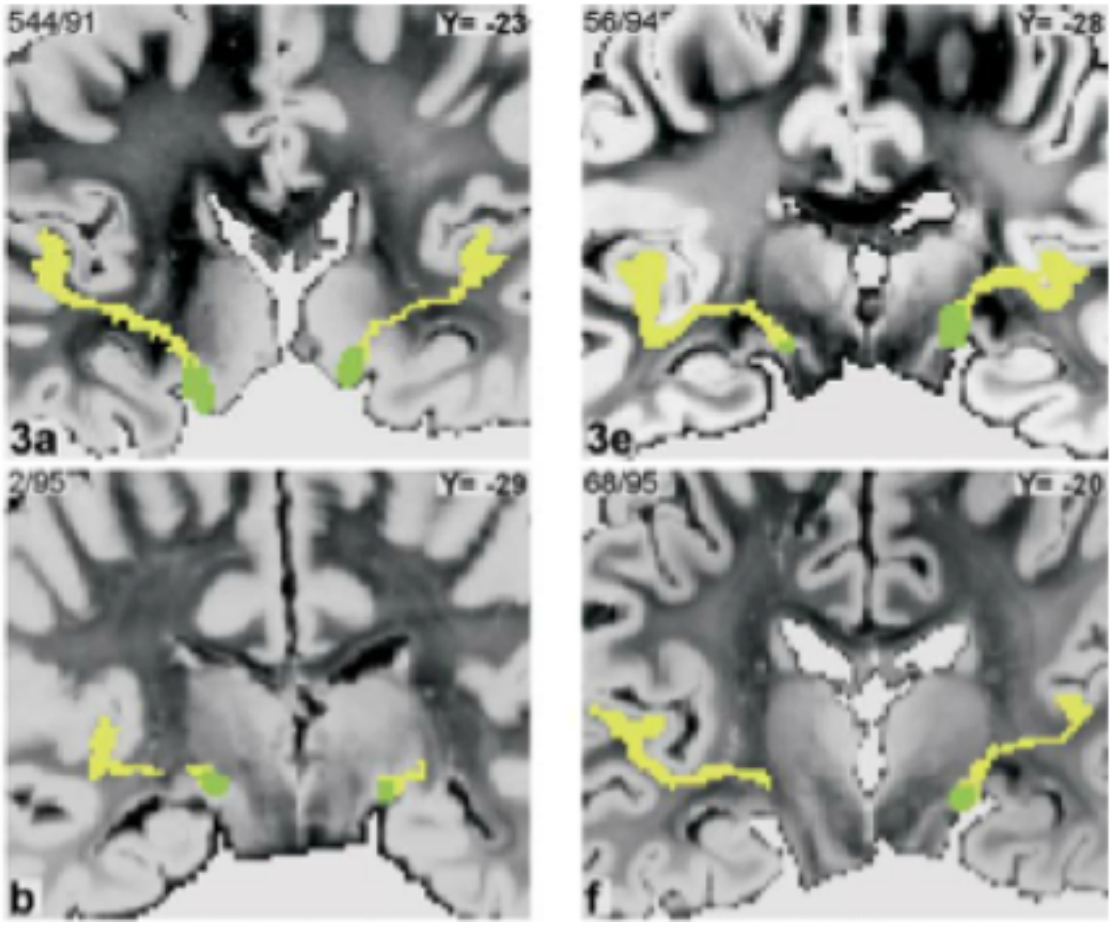

Figure 4.5: The Acoustic Radiation in Humans. Coronal sections of four individual brains with marked acoustic radiation (yellow) and medial geniculate bodies (green). Coronal sections at the level of the medial geniculate body, which projects to the Heschl's gyrus via the acoustic radiation. Image adapted from (Bürgel et al., 2006).

is it so difficult to reconstruct the course of the AR using tractography methods? The acoustic radiation is a highly variable, small tract that crosses major association bundles drawing sharp curves on its way. This anatomical profile and the location of the AR make the 3D reconstruction of this tract a methodological challenge for diffusion-based tractography.

In its course from the MGN to the cortex, the AR describes a typical "S"-shape, as visible in Figure 4.5, and below HG these fibres change direction at a very sharp angle of about 60◦ (Bürgel et al., 2006). This was delineated earlier also by Pfeifer and Polyak, who described a twist of the AR near the cortex. This anatomical profile, made of sharp angles, is difficult to detect for the tractography algorithms, which prefer long straight association bundles.

The location of the AR is also particularly challenging for the tractography algorithm. In its medio-lateral course from the MGN to the HG these fibres lie in a nearly horizontal position and for this reason cross some of the major association bundles that run within the temporal lobe (Berman et al., 2013). Resolving crossing fibres remains a well-known challenge in diffusion MRI (Tuch et al., 2002; Tournier et al., 2004; Dell'Acqua, Catani, 2012) (Chapter 3). The tensor is capable of characterizing only one main fibre orientation per voxel and it has been shown to constantly fail in regions where voxels contain complex fibres architectures (Behrens et al., 2007; Jbabdi, Johansen-Berg, 2011). The impact of this limitation is particularly evident for non-dominant tracts, given that the orientation produced by the tensor will be in most cases close to the largest contributing direction (Tournier et al., 2011). The tensor has been proven incapable of reconstructing the 3D profile of the AR: its streamlines are either truncated when entering voxels containing major antero-posterior orientations or erroneously embedded in the reconstruction of these major association temporal bundles, and no streamlines contacting HG are reconstructed (Behrens et al., 2007; Berman et al., 2013; Crippa et al., 2010).

Together with the shape and location, we also have to consider the size and variability of the auditory structures. The HG shows great variability across subjects and hemispheres (Rademacher et al., 2001; Marie et al., 2015) and the MGN is a very small structure, varying from 74 to 183 mm^3 (Kitajima et al., 2015), that is difficult to locate in neuroimaging data and that is also highly variable across individuals (Rademacher et al., 2002). This poses difficulties in the selection of the regions of interest (ROIs) used to seed the tractography algorithm or to perform virtual dissections of the AR. Extraction of the MGN structure from brain atlases is unlikely to provide a good match for all subjects, and given the small dimensions of the MGN, this could severely affect the final tractography results.

Using a multitensor-based probabilistic model (Behrens et al., 2003) Behrens et al. (2007) were able to visualize the course of the AR from the MGN to the cortex. This first tractography reconstruction of the auditory tract correctly shows the typical S-shape reported in post-mortem observations (Figure 4.6A). Reconstructed streamlines leave the thalamus, arch around the posterior part of the internal capsule and finally reach HG. Using the same model three more studies could reconstruct the profile of the auditory tract (Crippa et al., 2010; Javad et al., 2014; Profant et al., 2014), in some case with

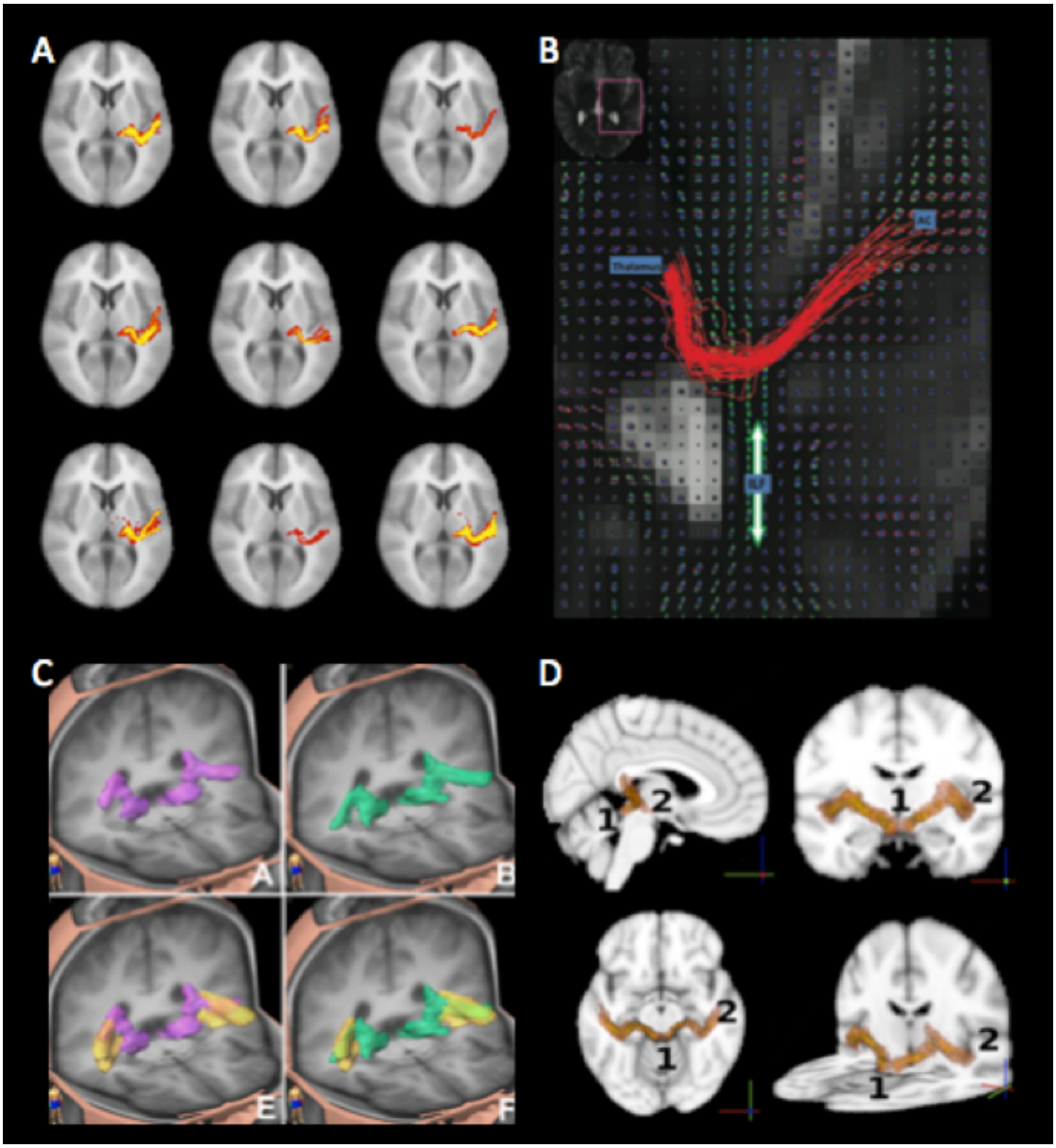

Figure 4.6: The Acoustic Radiation in Tractography Studies. The image shows the tractographic reconstruction of the AR in different studies. A) Probabilistic reconstruction of the AR in 9 subjects (Behrens et al., 2007). B) Probabilistic reconstruction of the AR in one subject (Berman et al., 2013). C) Probabilistic reconstruction of the group auditory tracts connecting the IC to the sound area (light purple) and the pith area (green). In yellow the tracts from the stereotactic histological atlas of Burgel (Bürgel et al., 2006) are shown (Javad et al., 2014). D) Probabilistic reconstruction of the average group auditory fibres connecting the IC (1) to the auditory cortex (2) (Crippa et al., 2010).

low reproducibility. Crippa et al. reconstructed the connection profile of the auditory pathways from the inferior culliculus (IC) to the MGN, up to the auditory cortex (Figure 4.6D). The authors also investigated a non-classic extralemniscal connection between the MGN and the amygdala, that has been associated to tinnitus (Moller, A. R., Moller, M. B., & Yokota, 1992). Similarly, Javad et al. differentiated between sub-components of the acoustic radiation (Figure 4.6C). They combined functional magnetic resonance imaging (fMRI) and diffusion MRI to identify auditory connections to pitch, sound, and melody areas of the auditory cortex. Berman (Figure 4.6B) used a q-ball model to successfully reconstruct the auditory connections between MGN and HG (Berman et al., 2013).

The overall reconstructed 3D profiles from these studies are in agreement with the macro-anatomical landmarks defined by classic studies, and more recent investigations. However, they are still highly variable across subjects, and lack reproducibility. All these studies used probabilistic tractography methods, and up to now no study using diffusion tractography *in-vivo* has been able to reconstruct the AR with deterministic algorithms. While deterministic methods reconstruct a single fibre trajectory per voxel, probabilistic tractography accounts for uncertainty in the data producing a distribution of orientations for each voxel. In this way probabilistic methods are often able to overcome limitations related to the quality of the data, low-level models and tractography algorithms, succeeding in situations where the deterministic methods fail. However, it remains unknown how these three factors –data quality, model, and tractography algorithm- affect the reconstruction the AR, both with deterministic and probabilistic methods. A better understanding of the influence of acquisition and algorithm parameters choice on the AR reconstruction will help to build a more reliable tractography framework in which we can study the anatomy of this tract in humans *in-vivo*. Moreover, the detailed topography of the AR and its relationship with the other neighboring white matter bundles remains to be clarified.

4.5 Characterization of the acoustic radiation: functional and clinical implications

The reliable reconstruction of the AR in humans *in-vivo* may help explore the neuroanatomical and functional mechanisms underlying auditory processing and language comprehension. In addition, the precise characterization of the AR may provide information useful to clinical applications, such as in hearing and speech disorders, recovery from damage, as well as in interventions that can damage the AR, such as brain surgery or radiation treatments.

Language and auditory perception

The ability to communicate through language is quintessentially human. However, the anatomical organization and the functional mechanisms underlying speech comprehension in the brain are still not completely understood. The acoustic information that reaches the primary auditory cortex via the AR fibres is then processed within neu-

ral networks that depend on cortico-cortical short- and long-range connections within the temporal lobe, between both temporal lobes, and connections involving parietal and frontal regions, as schematized in the dual-stream model (Friederici, 2009; Hickok, Poeppel, 2007; Saur et al., 2008). It is unclear, in this processing network, where language-specific processing start (could it involve the thalamus and brainstem auditory nuclei, for instance), and what is the role of the auditory structures in speech perception (Zatorre et al., 2002). Some theories have put forward the idea that the left auditory cortex is specialized in processing temporal cues that are fundamental for speech comprehension (Poeppel, 2003), and that this language-specific encoding might start at the subcortical level (Hornickel et al., 2009). It would be extremely important to understand the role of the AR in conveying relevant auditory information from sub-cortical processing stations. In relation to this, it would be important to understand whether the AR exhibits a degree of leftward lateralization in its volume, as demonstrated for some of the other WM bundles implicated in language processing (Catani, 2007). Reports on the topographic variability of the temporal auditory regions have been known for some time (Galaburda et al., 1978; Economo v., Horn, 1930). Macroscopic volumetric difference in total white matter volume have been found, with larger volume in the left than in the right HG (Penhune et al., 1996). Even if tract-specific histological investigation of the AR did not reveal hemispheric lateralization of this bundle (Bürgel et al., 2006), more studies are needed to clarify the issue, and understand, if this differs from the organization of the AR in non-human primates.

Successful reconstruction of the AR could possibly reveal other, non-classical routes of this tract, if they exist. Evidence for non-HG connections in monkeys is available (Mesulam, Pandya, 1973), and some preliminary tractography studies suggest non-classical connections to the amygdala (Crippa et al., 2010).

Language and auditory disorders

At present, studies investigating the auditory pathways in patients mainly relied on white matter ROI measurements (Lee et al., 2007; Lin et al., 2008). However, ROIs only outline a portion of the underlying white matter bundles and may not be representative of the entire tract, and it may even include information from other adjacent white matter bundles. Successful and reliable reconstruction of the AR *in-vivo* would allow us to investigate the anatomy of this tract in patients with hearing and language disorders, and thus to correlate structural to functional information.

Damage to the acoustic radiation or/and the auditory cortices, following brain infarct or traumatic injury, most often result in rare syndromes, such as auditory agnosia, amusia, and pure word deafness (Shivashankar et al., 2001; Simons, Ralph, 1999; Slevc et al., 2011). The post-stroke lesion profile and the symptomatology in these cases are usually very variable. However, understanding how extensively the AR is affected by these types of lesion may be critical to helping shed light on the functional-structural relationships for linguistic and non-linguistic sound processing in the human brain. In these cases, clarifying whether a language-related asymmetry exist in the AR, may help predict recovery of language or more general auditory functions in affected individuals

(Forkel et al., 2014).

In deaf subjects volumetric studies have outlined differences in grey and white matter of the auditory regions, compared to hearing subjects (Shibata, 2007), but to the best of our knowledge, no specific study on the acoustic radiation in deaf subjects has been conducted up to date. Tractography reconstruction of the AR could help to understand whether these fibres undergo structural reorganization in case of auditory deprivation.

Surgical planning

Shedding light on the functional and anatomical characteristics of the auditory fibres reaching the cortex, especially in their implication in linguistic mechanisms, would be important in case of tumor and epilepsy surgery (Farshidfar et al., 2014; Wu et al., 2007). The 3D reconstruction of major white matter bundles is employed to plan and guide resections during surgery. In this context, virtual dissections have almost exclusively focused on language and motor structures (Chen et al., 2015). The reason why these fibres haven't received much attention in the surgical literature might be related to the fact that most of the auditory processing actually happens subcortically, and even complete damage to these fibres does not lead to deafness. However, fine auditory processing, music perception, and even normal language comprehension might depend on the integrity of these projections. The reliable reconstruction of the AR might be critical for cases of temporal lobe resection, in order to minimize post-operative deficits in these domains.

Brain radiation oncology planning

X-ray therapy (XRT) is today the standard of care for most brain tumours. However, XRT can damage brain tissue, causing neurocognitive deficits in different cognitive domains. This is mainly due to incidental irradiation of healthy brain tissue, and radiation-induced injury (Makale et al., 2016). The implementation of neuroimaging techniques is gaining importance for avoiding such complications, and tailoring radiotherapy based on intra-treatment response (Wong et al., 2017). Studies have shown XRT side effects in both grey matter (Bahrami et al., 2017) and white matter (Connor et al., 2017). It is however still unclear how various regions of the brain are differentially sensitive to radiation injury (Connor et al., 2017). Tractography could be useful for targeting specific WM bundles, and for understanding what are the XRT effects on different white matter pathways, in order to figure out if specific doses constraints for white matter can be set (Kawasaki et al., 2017).

4.6 Open questions

Diffusion-based MRI tractography constitutes a powerful tool for investigating the anatomy of the auditory tract in humans, and the only one available to achieve this *in-vivo* and non-invasively. However, applications of these methods are still restricted by a number of methodological challenges, and the reliable and reproducible reconstruction of this, and other complicated bundles, remains challenging. Few studies have shown that using a multi-fibre model and a probabilistic approach is sufficient to reconstruct the 3D profile

of the AR (Behrens et al., 2007; Berman et al., 2013), with results that are in agreement with the classic topographical description of this tract at a macro-anatomical level (Bürgel et al., 2006). However, these reconstructions still suffer from high variability across subjects and studies, and are limited to probabilistic approaches. Future research should focus on how to possibly improve the accuracy and the precision of the tractography reconstruction of this bundle, and on validating the results at a micro-anatomical scale. This task involves addressing a variety of issues on different but related fronts: MRI acquisition and diffusion modelling, tractography analysis, and validation.

MR Acquisition and Diffusion Modeling Issues

The final outcome of any tractography reconstruction crucially depends on the MRI acquisition scheme and the low-level diffusion model. Because of the fibre crossing, multi-fibre models are necessary to detect the AR. These more advanced models rely on HARDI (high angular resolution diffusion imaging) acquisition schemes, that are characterized by a relative high number of diffusion weighted gradient directions and high b-values to improve the angular contrast (Tuch et al., 2002). Even though spherical deconvolution models have shown to provide good results in terms of angular resolution at clinically feasible protocols (Dell'Acqua et al., 2010; Tournier et al., 2008), it remains unclear how the MRI acquisition parameter and diffusion model choices affect the reconstruction of secondary and more difficult bundles like the AR.

In evaluating the effects of MRI acquisition parameters, spatial resolution should also be taken into consideration, in order to obtain the best trade-off between angular and spatial resolution, while retaining a good signal to noise ratio (SNR). Methodological improvements in MRI technology shows promising results for how these limitations of diffusion results may be pushed (Setsompop et al., 2013; Sepehrband et al., 2017). Such results need further validation from larger studies as the tools become more widely available.

Tractography analysis issues

The quality of the available diffusion data will affect the choice of tractography algorithm type. Probabilistic approaches are better at dealing with low angular resolution data and at overcoming tracking limitations in difficult regions, *i.e.* regions with complex fibre architecture, low SNR, and partial volume effects (Behrens et al., 2007; Descoteaux et al., 2009). Future research should address how to achieve AR reconstructions with deterministic algorithms. Regarding tractography parameters, it is becoming clearer in diffusion imaging that there cannot be a set of parameters that it is ideal to reconstruct all white matter bundles of the human brain (Takemura et al., 2016). Further studies are needed to establish whether there are optimal tractography parameters for the reconstruction of the AR.

Beside the algorithm type and parameters to be used, reconstruction accuracy can be improved implementing recently developed techniques to use anatomical knowledge to inform tractography (Girard et al., 2014; Smith et al., 2012; St-Onge et al., ????). Tractography reconstructions are still challenging for streamlines terminations. This

uncertainty is compounded by the dispersion of axons in grey matter, by the u-fibre system, and by partial volume effects (Reveley et al., 2015). As these techniques improve, reconstructed streamlines terminations could be combined with functional MRI to provide critical insights into the functional subdivision of the auditory cortex, the borders of which are still not clearly defined. Finally, global approaches to tractography exist (Chapter 3), that might provide better results in the case of the acoustic radiation (Christiaens et al., 2015).

Validation issues

A challenge of diffusion tractography is the validation of its results, which can show limitations in well-known tracts (Thomas et al., 2014). In a scenario where limited topographical knowledge is available and diffusion-based reconstructions are still difficult to obtain, validation of tractography results is particularly important. Being aware of the anatomical characteristics of the tract provides us with the underlying ground truth on which methodological decisions, aimed at solving potential limitations of the tractographic reconstruction process, can be made.

Validation of tractography reconstructions can be provided by *ex-vivo* MR acquisition methods (Soria et al., 2011). Using this approach the topography of the acoustic radiation has been recently investigated (Maffei et al., 2015). However, tractography reconstructions from *ex-vivo* data are still subject to some limitations of the tractography techniques. Validation of tractography can also be achieved by gross anatomical post-mortem dissections (De Benedictis et al., 2016; Maldonado et al., 2013; Martin et al., 2010; Sarubbo et al., 2015) (Chapter 3. To our knowledge, no study has used this technique to investigate the topography of the AR.

4.7 Summary

Successful *in-vivo* tractographic reconstruction of the human auditory tracts is of great importance for clinical applications (*e.g.* pre-surgical mapping) as well as for basic research. Thus, characterization of the auditory tracts would allow the investigation of anatomy and function in the same individual, both in health (for example to study the role of these tracts in language processing) and in disease (for example to study how the integrity of this tract relates to cognitive deficits). However, in order to obtain reliable reconstructions of the AR across subjects and protocols, it is important on the one hand to better understand how dMRI acquisition and tractography reconstruction strategies affect the tract's characterization, and on the other to obtain validation of the tractography reconstructions.

Bibliography

Abdul-Kareem Ihssan A, Sluming Vanessa. Heschl Gyrus and Its Included Primary Auditory Cortex: Structural MRI Studies in Healthy and Diseased Subjects // J. Magn. Reson. Imaging. 2008. 28. 287–299.

Bahrami Naeim, Seibert Tyler M., Karunamuni Roshan, Bartsch Hauke, Krishnan AnithaPriya, Farid Nikdokht, Hattangadi-Gluth Jona A., McDonald Carrie R. Altered Network Topology in Patients with Primary Brain Tumors After Fractionated Radiotherapy // Brain Connectivity. jun 2017. 7, 5. 299–308.

Baumann Simon, Petkov Christopher I, Griffiths Timothy D. A unified framework for the organization of the primate auditory cortex. // Frontiers in systems neuroscience. 2013. 7, April. 11.

Behrens T. E J, Berg H. Johansen, Jbabdi S., Rushworth M. F S, Woolrich M. W. Probabilistic diffusion tractography with multiple fibre orientations: What can we gain? // NeuroImage. 2007. 34, 1. 144–155.

Behrens T E J, Johansen-Berg H, Woolrich M W, Smith S M, Wheeler-Kingshott C a M, Boulby P a, Barker G J, Sillery E L, Sheehan K, Ciccarelli O, Thompson a J, Brady J M, Matthews P M. Non-invasive mapping of connections between human thalamus and cortex using diffusion imaging. // Nature neuroscience. 2003. 6, 7. 750–757.

Berman J. I., Lanza M. R., Blaskey L., Edgar J. C., Roberts T. P L. High angular resolution diffusion imaging probabilistic tractography of the auditory radiation // American Journal of Neuroradiology. 2013. 34, 8. 1573–1578.

Brugge John F. Anatomy and physiology of auditory pathways and cortex // Handbook of Clinical Neurophysiology. 2013. 2, 25–52.

Bürgel Uli, Amunts Katrin, Hoemke Lars, Mohlberg Hartmut, Gilsbach Joachim M, Zilles Karl. White matter fiber tracts of the human brain: Three-dimensional mapping at microscopic resolution, topography and intersubject variability // NeuroImage. 2006. 29, 4. 1092–1105.

Catani Marco. From hodology to function // Brain. 2007. 130, 3. 602–605.

Catani Marco, Howard Robert J, Pajevic Sinisa, Jones Derek K. Virtual in vivo interactive dissection of white matter fasciculi in the human brain. // NeuroImage. 2002. 17, 1. 77–94.

Chang Yongmin, Lee S H, Lee Y J, Hwang M J, Bae S J, Kim M N, Lee J, Woo Seongku, Lee Heejung, Kang D S. Auditory neural pathway evaluation on sensorineural hearing loss using diffusion tensor imaging // Neuroreport. aug 2004. 15, 11. 1699–1703.

Chen Zhenrui, Tie Yanmei, Olubiyi Olutayo, Rigolo Laura, Mehrtash Alireza, Norton Isaiah, Pasternak Ofer, Rathi Yogesh, Golby Alexandra J., O'Donnell Lauren J. Reconstruction of the arcuate fasciculus for surgical planning in the setting of peritumoral edema using two-tensor unscented Kalman filter tractography // NeuroImage: Clinical. 2015. 7. 815–822.

Christiaens Daan, Reisert Marco, Dhollander Thijs, Sunaert Stefan, Suetens Paul, Maes Frederik. Global tractography of multi-shell diffusion-weighted imaging data using a multi-tissue model // NeuroImage. 2015. 123. 89–101.

Clarke S., Rivier F. Compartments within human primary auditory cortex: evidence from cytochrome oxidase and acetylcholinesterase staining // Eur J Neurosci. 1998. 10, 2. 741–5.

Connor Michael, Karunamuni Roshan, McDonald Carrie, Seibert Tyler, White Nathan, Moiseenko Vitali, Bartsch Hauke, Farid Nikdokht, Kuperman Joshua, Krishnan Anitha, Dale Anders, Hattangadi-Gluth Jona A. Regional susceptibility to dose-dependent white matter damage after brain radiotherapy // Radiotherapy and Oncology. may 2017. 123, 2. 209–217.

Crippa Alessandro, Lanting Cris P, Dijk Pim van, Roerdink Jos B T M. A diffusion tensor imaging study on the auditory system and tinnitus. // The open neuroimaging journal. 2010. 4. 16–25.

Da Costa Sandra., Zwaag Wietske. van der, Marques Jose. P., Frackowiak Richard. S. J., Clarke Stephanie., Saenz Melissa. Human Primary Auditory Cortex Follows the Shape of Heschl's Gyrus // Journal of Neuroscience. 2011. 31, 40. 14067–14075.

De Benedictis Alessandro, Petit Laurent, Descoteaux Maxime, Marras Carlo Efisio, Barbareschi Mattia, Corsini Francesco, Dallabona Monica, Chioffi Franco, Sarubbo Silvio. New insights in the homotopic and heterotopic connectivity of the frontal portion of the human corpus callosum revealed by microdissection and diffusion tractography // Human Brain Mapping. dec 2016. 37, 12. 4718–4735.

Dejerine J. Anatomie des Centres Nerveux. Reuff. Paris, 1895.

Dejerine J., Serieux P. Un cas de surdite verbale pure terminee par sensorielle suivi d'autopsie. // Compte-Rendus des Seances de la Societe de Diologie. 1897. 10. 1074–1077.

Dell'Acqua Flavio, Catani Marco. Structural human brain networks: hot topics in diffusion tractography. // Current opinion in neurology. 2012. 25, 4. 375–83.

Dell'Acqua Flavio, Scifo Paola, Rizzo Giovanna, Catani Marco, Simmons Andrew, Scotti Giuseppe, Fazio Ferruccio. A modified damped Richardson-Lucy algorithm to reduce isotropic background effects in spherical deconvolution // NeuroImage. 2010. 49, 2. 1446–1458.

Descoteaux Maxime, Deriche Rachid, Knösche T, Anwander Alfred. Deterministic and Probabilistic Tractography Based on Complex Fiber Orientation Distributions // IEEE Transactions on Medical Imaging. 2009. 28, 2. 269–286.

Dijk Pim van, Langers Dave R M. Mapping tonotopy in human auditory cortex. // Advances in experimental medicine and biology. 2013. 787. 419–25.

Economo C. v., Horn L. Über Windungsrelief, Maße und Rindenarchitektonik der Supratemporalfläche, ihre individuellen und ihre Seitenunterschiede // Zeitschrift für die gesamte Neurologie und Psychiatrie. dec 1930. 130, 1. 678–757.

Farshidfar Zahra, Faeghi Fariborz, Mohseni Mostafa, Seddighi Afsoun, Kharrazi Homayoun Hadizadeh, Abdolmohammadi Jamil. Diffusion tensor tractography in the presurgical assessment of cerebral gliomas. // The neuroradiology journal. feb 2014. 27, 1. 75–84.

Flechsig P. Anatomie des menschlichen Gehirns und Rucken-marks auf myellogenetischer Grundlage. Georg Thieme Verlag, Leipzig: Erster Band, 1920.

Forkel Stephanie J, Thiebaut de Schotten Michel, Dell'Acqua Flavio, Kalra Lalit, Murphy Declan G M, Williams Steven C R, Catani Marco. Anatomical predictors of aphasia recovery: a tractography study of bilateral perisylvian language networks. // Brain : a journal of neurology. jul 2014. 137, Pt 7. 2027–39.

Friederici Angela D. Pathways to language: fiber tracts in the human brain // Trends in Cognitive Sciences. apr 2009. 13, 4. 175–181.

Fullerton Barbara C., Pandya Deepak N. Architectonic analysis of the auditory-related areas of the superior temporal region in human brain // The Journal of Comparative Neurology. oct 2007. 504, 5. 470–498.

Galaburda Albert M., LeMay M, Kemper T L, Geschwind N. Right-left asymmetrics in the brain. // Science (New York, N.Y.). feb 1978. 199, 4331. 852–6.

Galaburda Albert M., Pandya Deepak N. The intrinsic architectonic and connectional organization of the superior temporal region of the rhesus monkey // Journal of Comparative Neurology. dec 1983. 221, 2. 169–184.

Girard Gabriel, Whittingstall Kevin, Deriche Rachid, Descoteaux Maxime. Towards quantitative connectivity analysis : reducing tractography biases // NeuroImage. 2014. 98. 266–278.

Hackett T A, Preuss T M, Kaas J H. Architectonic identification of the core region in auditory cortex of macaques, chimpanzees, and humans. // The Journal of comparative neurology. dec 2001. 441, 3. 197–222.

Hackett T A, Stepniewska I, Kaas J H. Thalamocortical connections of the parabelt auditory cortex in macaque monkeys. // The Journal of comparative neurology. oct 1998. 400, 2. 271–86.

Hackett Troy A. Information flow in the auditory cortical network // Hearing Research. 2011. 271. 133–146.

Hickok Gregory, Poeppel David. The cortical organization of speech processing. // Nature reviews. Neuroscience. may 2007. 8, 5. 393–402.

Hornickel Jane, Skoe Erika, Kraus Nina. Subcortical laterality of speech encoding. // Audiology {&} neuro-otology. 2009. 14, 3. 198–207.

A chronic microelectrode investigation of the tonotopic organization of human auditory cortex. // . 1996. 724. 260–264.

Humphries Colin, Liebenthal Einat, Binder Jeffrey R. Tonotopic organization of human auditory cortex. // NeuroImage. apr 2010. 50, 3. 1202–11.

Javad Faiza, Warren Jason D, Micallef Caroline, Thornton John S, Golay Xavier, Yousry Tarek, Mancini Laura. Auditory tracts identified with combined fMRI and diffusion tractography. // NeuroImage. jan 2014. 84. 562–74.

Jbabdi Saad, Johansen-Berg Heidi. Tractography: Where Do We Go from Here? // Brain Connectivity. 2011. 1, 3. 169–183.

Jones Derek K, Cercignani Mara. Twenty-five pitfalls in the analysis of diffusion MRI data // NMR in Biomedicine. 2010. 23, 7. 803–820.

Kaas J H, Hackett T A. Subdivisions of auditory cortex and processing streams in primates. // Proceedings of the National Academy of Sciences of the United States of America. oct 2000. 97, 22. 11793–9.

Kaas Jon H, Hackett Troy A, Tramo Mark Jude. Auditory processing in primate cerebral cortex // Current Opinion in Neurobiology. 1999. 9, 2. 164–170.

Kawasaki Kohei, Matsumoto Masanobu, Kase Masayuki, Nagano Osamu, Aoyagi Kyoko, Kageyama Takahiro. Quantification of the radiation dose to the pyramidal tract using tractography in treatment planning for stereotactic radiosurgery // Radiological Physics and Technology. aug 2017. 1–8.

Keifer Orion P, Gutman David, Hecht Erin, Keilholz Shella, Ressler Kerry J, Ressler Kerry. A Comparative Analysis of Mouse and Human Medial Geniculate Nucleus Connectivity: A DTI and Anterograde Tracing Study // Neuroimage. January. 2015. 15, 105. 53–66.

Kitajima M., Hirai T., Yoneda T., Iryo Y., Azuma M., Tateishi M., Morita K., Komi M., Yamashita Y. Visualization of the Medial and Lateral Geniculate Nucleus on Phase Difference Enhanced Imaging // American Journal of Neuroradiology. 2015. 36, 9.

Lawes I Nigel C, Barrick Thomas R, Murugam Vengadasalam, Spierings Natalia, Evans David R, Song Marie, Clark Chris A. Atlas-based segmentation of white matter tracts of the human brain using diffusion tensor tractography and comparison with classical dissection. // NeuroImage. jan 2008. 39, 1. 62–79.

Lee Young Ju, Bae Sung Jin, Lee Sang Heun, Lee Jae Jun, Lee Kyu Yup, Kim Myoung Nam, Kim Yong Sun, Baik Seung Kug, Woo Seongku, Chang Yongmin. Evaluation of white matter structures in patients with tinnitus using diffusion tensor imaging // Journal of Clinical Neuroscience. 2007. 14, 6. 515–519.

Liegeois-Chauvel C, Musolino A, Chauvel P. Localization of the Primary Auditory Area in Man // Brain. 1991. 139–153.

Lin YuChun, Wang JiunJie, Wu CheMing, Wai YauYau, Yu JenFang, Ng ShuHang. Diffusion tensor imaging of the auditory pathway in sensorineural hearing loss: Changes in radial diffusivity and diffusion anisotropy // Journal of Magnetic Resonance Imaging. 2008. 28, 3. 598–603.

Maffei Chiara, Soria Guadalupe, Prats-Galino Alberto, Catani Marco. Imaging white-matter pathways of the auditory system with diffusion imaging tractography // Handbook of Clinical Neurology. 2015. 129. 277–288.

Makale Milan T., McDonald Carrie R., Hattangadi-Gluth Jona A., Kesari Santosh. Mechanisms of radiotherapy-associated cognitive disability in patients with brain tumours // Nature Reviews Neurology. dec 2016. 13, 1. 52–64.

Maldonado Igor Lima, De Champfleur Nicolas Menjot, Velut St??phane, Destrieux Christophe, Zemmoura Ilyess, Duffau Hugues. Evidence of a middle longitudinal fasciculus in the human brain from fiber dissection // Journal of Anatomy. 2013. 223, 1. 38–45.

Marie D, Jobard G, Crivello F, Perchey G, Petit L, Mellet E, Joliot M, Zago L, Mazoyer B, Tzourio-Mazoyer N. Descriptive anatomy of Heschl's gyri in 430 healthy volunteers, including 198 left-handers. // Brain structure & function. mar 2015. 220, 2. 729–43.

Martin Randi C., Hamilton A. Cris, Slevc L. Robert. fMRI of Speech Production in a Case of Pure Word Deafness // Procedia - Social and Behavioral Sciences. dec 2010. 6. 29–30.

Merzenich M M, Brugge J F. Representation of the cochlear partition of the superior temporal plane of the macaque monkey. // Brain research. feb 1973. 50, 2. 275–96.

Mesulam Marsel M, Pandya Deepak N3. The projections of the medial geniculate complex within the sylvian fissure of the rhesus monkey // Brain Research. 1973. 60. 315–333.

Minkowski M. Etude sur les connexions anatomiques des circonvolutions rolandiques // Arch. Neurol. Psychiat. 1923. 12. 227–68.

Moerel Michelle, De Martino Federico, Formisano Elia. An anatomical and functional topography of human auditory cortical areas // Frontiers in Neuroscience. jul 2014. 8. 225.

Moller, A. R., Moller, M. B., & Yokota M. Some forms of tinnitus may involve the extralemniscal auditory pathway.pdf // The Laryngoscope. oct 1992. 102, 10. 1165–1171.

Moller A.R. Hearing : Anatomy, Physiology, and Disorders of the Auditory System. 2006.

Morel A., Garraghty P. E., Kaas J. H. Tonotopic organization, architectonic fields, and connections of auditory cortex in macaque monkeys // The Journal of Comparative Neurology. sep 1993. 335, 3. 437–459.

Morosan P., Rademacher J., Schleicher A., Amunts K., Schormann T., Zilles K. Human Primary Auditory Cortex: Cytoarchitectonic Subdivisions and Mapping into a Spatial Reference System // NeuroImage. 2001. 13, 4. 684–701.

Passingham Richard. How good is the macaque monkey model of the human brain? // Current opinion in neurobiology. feb 2009. 19, 1. 6–11.

Penhune V B, Zatorre R J, Macdonald J D. Interhemispheric Anatomical Differences in Human Primary Auditory Cortex : Probabilistic Mapping and Volume Measurement from Magnetic Resonance Scans // Cerebral Cortex. 1996. 6. 661–672.

Pfeifer R. Myelogenetisch-anatomische Untersuchungen uber das kortikale Ende der Horleitung // Abh. math. phys. Kl. sachs. Akad. Wiss. 1920. 37. 1–54.

Poeppel David. The analysis of speech in different temporal integration windows: Cerebral lateralization as 'asymmetric sampling in time' // Speech Communication. 2003. 41, 1. 245–255.

The Main Afferent Fiber Systems of the Cerebral Cortex in Primates, VoL 2. // . 1932. 370.

Profant O., Škoch A., Balogová Z., Tintěra J., Hlinka J., Syka J. Diffusion tensor imaging and MR morphometry of the central auditory pathway and auditory cortex in aging // Neuroscience. 2014. 260. 87–97.

Rademacher J, Bürgel U, Zilles K. Stereotaxic localization, intersubject variability, and interhemispheric differences of the human auditory thalamocortical system. // NeuroImage. sep 2002. 17, 1. 142–60.

Rademacher J., Morosan P., Schormann T., Schleicher A., Werner C., Freund H.-J., Zilles K. Probabilistic Mapping and Volume Measurement of Human Primary Auditory Cortex // NeuroImage. 2001. 13, 4. 669–683.

Rauschecker J P, Tian B, Pons T, Mishkin M. Serial and parallel processing in rhesus monkey auditory cortex. // The Journal of comparative neurology. 1997. 382, 1. 89–103.

Reveley Colin, Seth Anil K., Pierpaoli Carlo, Silva Afonso C., Yu David, Saunders Richard C., Leopold David A., Ye Frank Q. Superficial white matter fiber systems impede detection of long-range cortical connections in diffusion MR tractography // Proceedings of the National Academy of Sciences. may 2015. 112, 21. E2820–E2828.

Sarubbo Silvio, De Benedictis Alessandro, Milani Paola, Paradiso Beatrice, Barbareschi Mattia, Rozzanigo Umbero, Colarusso Enzo, Tugnoli Valeria, Farneti Marco, Granieri Enrico, Duffau Hugues, Chioffi Franco. The course and the anatomo-functional relationships of the optic radiation: a combined study with post mortem dissections and in vivo direct electrical mapping. // Journal of anatomy. jan 2015. 226, 1. 47–59.

Saur Dorothee, Kreher Björn W, Schnell Susanne, Kümmerer Dorothee, Kellmeyer Philipp, Vry Magnus-Sebastian, Umarova Roza, Musso Mariacristina, Glauche Volkmar, Abel Stefanie, Huber Walter, Rijntjes Michel, Hennig Jürgen, Weiller Cornelius. Ventral and dorsal pathways for language. // Proceedings of the National Academy of Sciences of the United States of America. 2008. 105, 46. 18035–40.

Schmahmann Jeremy D., Pandya Deepak N., Wang Ruopeng, Dai Guangping, D'Arceuil Helen E., De Crespigny Alex J., Wedeen Van J. Association fibre pathways of the brain: Parallel observations from diffusion spectrum imaging and autoradiography // Brain. 2007. 130, 3. 630–653.

Scott Sophie K., Johnsrude Ingrid S. The neuroanatomical and functional organization of speech perception // Trends in Neurosciences. feb 2003. 26, 2. 100–107.

Seldon H L. Structure of human auditory cortex. I. Cytoarchitectonics and dendritic distributions. // Brain research. dec 1981. 229, 2. 277–94.

Sepehrband Farshid, O'Brien Kieran, Barth Markus. A time-efficient acquisition protocol for multipurpose diffusion-weighted microstructural imaging at 7 Tesla // Magnetic Resonance in Medicine. feb 2017.

Setsompop K., Kimmlingen R., Eberlein E., Witzel T., Cohen-Adad J., McNab J. a., Keil B., Tisdall M. D., Hoecht P., Dietz P., Cauley S. F., Tountcheva V., Matschl V., Lenz V. H., Heberlein K., Potthast A., Thein H., Van Horn J., Toga A., Schmitt F., Lehne D., Rosen B. R., Wedeen V., Wald L. L. Pushing the limits of in vivo diffusion MRI for the Human Connectome Project // NeuroImage. 2013. 80. 220–233.

Shibata D. K. Differences in brain structure in deaf persons on MR imaging studied with voxel-based morphometry // American Journal of Neuroradiology. 2007. 28, 2. 243–249.

Shivashankar N, Shashikala H R, Nagaraja D, Jayakumar P N, Ratnavalli E. Pure word deafness in two patients with subcortical lesions // Clinical Neurology and Neurosurgery. 2001. 103, 4. 201–205.

Simons JS, Ralph MA Lambon. The auditory agnosias // Neurocase. 1999. 5. 379–406.

Slevc L Robert, Martin Randi C, Hamilton A Cris, Joanisse Marc F. Speech perception, rapid temporal processing, and the left hemisphere: a case study of unilateral pure word deafness. // Neuropsychologia. jan 2011. 49, 2. 216–30.

Smith Robert E., Tournier Jacques-Donald, Calamante Fernando, Connelly Alan. Anatomically-constrained tractography: Improved diffusion MRI streamlines tractography through effective use of anatomical information // NeuroImage. 2012. 62, 3. 1924–1938.

Soria Guadalupe, De Notaris Matteo, Tudela Raúl, Blasco Gerard, Puig Josep, Planas Anna M., Pedraza Salvador, Prats-Galino Alberto. Improved Assessment of Ex Vivo Brainstem Neuroanatomy With High-Resolution MRI and DTI at 7 Tesla // Anatomical Record. 2011. 294, 6. 1035–1044.

Surface tracking from the cortical mesh complements diffusion MRI fiber tracking near the cortex. // . ????

Takemura Hiromasa, Caiafa Cesar F., Wandell Brian A., Pestilli Franco. Ensemble Tractography // PLoS Computational Biology. 2016. 12, 2. 1–22.

Tardif E, Clarke S. Intrinsic connectivity of human auditory areas: a tracing study with DiI. // The European journal of neuroscience. 2001. 13, 5. 1045–1050.

Thiebaut de Schotten Michel, Dell'Acqua Flavio, Valabregue Romain, Catani Marco. Monkey to human comparative anatomy of the frontal lobe association tracts // Cortex. jan 2012. 48, 1. 82–96.

Thiebaut de Schotten Michel, Ffytche Dominic H, Bizzi Alberto, Dell'Acqua Flavio, Allin Matthew, Walshe Muriel, Murray Robin, Williams Steven C, Murphy Declan G M, Catani Marco. Atlasing location, asymmetry and inter-subject variability of white matter tracts in the human brain with MR diffusion tractography. // NeuroImage. jan 2011. 54, 1. 49–59.

Thomas Cibu, Ye Frank Q., Irfanoglu M. Okan, Modi Pooja, Saleem Kadharbatcha S., Leopold David A., Pierpaoli Carlo. Anatomical accuracy of brain connections derived from diffusion MRI tractography is inherently limited // Proceedings of the National Academy of Sciences. nov 2014. 111, 46. 16574–16579.

Tournier J Donald, Calamante Fernando, Gadian David G, Connelly Alan. Direct estimation of the fiber orientation density function from diffusion-weighted MRI data using spherical deconvolution // NeuroImage. 2004. 23, 3. 1176–1185.

Tournier J.-Donald, Yeh Chun-Hung, Calamante Fernando, Cho Kuan-Hung, Connelly Alan, Lin Ching-Po. Resolving crossing fibres using constrained spherical deconvolution: Validation using diffusion-weighted imaging phantom data // NeuroImage. aug 2008. 42, 2. 617–625.

Tournier Jacques-Donald, Mori Susumu, Leemans Alexander. Diffusion tensor imaging and beyond. // Magnetic resonance in medicine. jun 2011. 65, 6. 1532–56.

Tuch David S., Reese Timothy G., Wiegell Mette R., Makris Nikos, Belliveau John W., Wedeen Van J. High angular resolution diffusion imaging reveals intravoxel white matter fiber heterogeneity // Magnetic Resonance in Medicine. oct 2002. 48, 4. 577–582.

Walker A E. The Projection of the Medial Geniculate Body to the Cerebral Cortex in the Macaque Monkey. // Journal of anatomy. apr 1937. 71, Pt 3. 319–31.

Wallace Mark N, Johnston Peter W, Palmer Alan R. Histochemical identification of cortical areas in the auditory region of the human brain. // Experimental brain research. apr 2002. 143, 4. 499–508.

Wong Kee H, Panek Rafal, Bhide Shreerang A, Nutting Christopher M, Harrington Kevin J, Newbold Katie L. The emerging potential of magnetic resonance imaging in personalizing radiotherapy for head and neck cancer: an oncologist's perspective // The British Journal of Radiology. mar 2017. 90, 1071. 20160768.

Wu C. M., Ng S. H., Wang J. J., Liu Tien Chen. Diffusion tensor imaging of the subcortical auditory tract in subjects with congenital cochlear nerve deficiency // American Journal of Neuroradiology. 2009. 30, 9. 1773–1777.

Wu Jin-Song, Zhou Liang-Fu, Tang Wei-Jun, Mao Ying, Hu Jin, Song Yan-Yan, Hong Xun-Ning, Du Gu-Hong. Clinical evaluation and follow-up outcome of diffusion tensor imaging-based functional neuronavigation // Neurosurgery. nov 2007. 61, 5. 935–949.

Zatorre Robert J., Belin Pascal, Penhune Virginia B. Structure and function of auditory cortex: music and speech. // Trends in cognitive sciences. jan 2002. 6, 1. 37–46.

Chapter 5

Topography of the human acoustic radiation as revealed by *ex-vivo* fibres micro-dissection and *in-vivo* diffusion-based tractography

5.1 Introduction

As discussed in the previous chapters, very little is known about the structure and topography of the acoustic radiation, and the diffusion-based tractography reconstruction of this bundle remains extremely challenging. In this scenario, validation of tractography results is crucial.

Being aware of the anatomical characteristics of the tract provides us with an underlying ground truth on which methodological decisions, aimed at solving potential limitations of the tractographic reconstruction process, can be made. Validation of tractography reconstruction can be provided by post-mortem human data, either in the form of gross anatomical dissections (Klingler, 1935) or *ex-vivo* MR acquisition (Soria et al., 2011). The spreading of diffusion-based tractography techniques has renewed the interest for blunt micro-dissections of human WM (De Benedictis et al., 2016; Fernández-Miranda et al., 2015; Martino et al., 2010; Sarubbo et al., 2015; Wang et al., 2016). The unique details on the course and topographical organization of the WM bundles provided by blunt micro-dissections constitute, in fact, the minimal available ground truth to improve the methodological processes and overcome the limits of tractography reconstructions. In this study, we combined blunt micro-dissection and advanced diffusion-based tractography methods with the following goals: i) to provide, for the first time to our knowledge, a detailed and multimodal anatomical description of the course and terminations of the AR in humans; ii) to characterize the topography of this bundle in respect to the other

neighboring tracts. Results obtained with *ex-vivo* dissections and *in-vivo* tractography are compared and integrated, and limitations discussed.

5.2 Methods

Post-mortem dissections

Four human cerebral hemispheres (two right) were prepared according to the modified Klinger's preparation previously described (Sarubbo et al., 2016, 2015), in the context of the Structural and Functional Connectivity Lab project of the Division of Neurosurgery of "S. Chiara" Hospital, (Trento APSS, Italy). Microdissection (5x) was performed by an expert anatomist and neurosurgeon (Dr. Silvio Sarubbo) The AR was approached posteriorly starting a layer-by- layer dissection from the posterior third of the superior temporal sulcus (STS) and its elongation in the inferior parietal lobe (IPL) (Sarubbo et al., 2016).

U-fibres connecting the supramarginal gyrus (SMG) and the angular gyrus (AG) with the cortices of the posterior two-thirds of the STS were removed (Figure 5.1a). The stem of the vertical portion of the superior longitudinal fasciculus (SLF) was highlighted and cut (Figure 5.1b), demonstrating the temporal portion of the arcuate fascicle (AF) (Figure 5.1c). The deepest portion and the most ventral fibres of the AF, connecting the frontal lobe to the posterior third of STG (Figure 1D), were removed to highlight the posterior thalamic radiation (PTR) and the AR fibres projecting to Heschl's gyrus (HG). AR were progressively demonstrated in a medio-lateral direction, preserving portion of neighboring projection [PTR, somato-sensorial, external capsule, internal capsule (respectively, SS, EC, IC) and association (AF, SLF)] fibres.

Diffusion tractography

Diffusion and structural data of four subjects provided by the Human Connectome Project database were analyzed using Mrtrix3 (Tournier et al., 2012). Data was previously preprocessed as described in (Fan et al., 2015). The HARDI multi-shell dataset is composed of four shells ($1000-3000-5000-10000 s/mm^2$) for a total of 552 directions at an isotropic spatial resolution of $1.25mm$. A multi-shell multi-tissue constrained spherical deconvolution algorithm (Jeurissen et al., 2014) was fit to the data and anatomically-constrained (Smith et al., 2012) probabilistic tractography (ACT) was performed at following parameters: $0.75mm$ step-size, 45° angle threshold, 2000 seeds/voxel. The structural T1-weighted image of each subject was registered to the diffusion space using the up-sampled fractional anisotropy map in Ants (Klein et al., 2009). After registration, the T1 weighted image of each subject was segmented in FSL using FAST (Zhang et al., 2001) and FIRST (Patenaude et al., 2012) to create a five- tissue-type image to be used for ACT. The left and right thalamus were segmented in FSL using FIRST on each subject's T1 and the HG was carefully manually defined in each subject's hemisphere. Tractography was randomly initiated from every voxel in the thalamus and HG was used as target region: only streamlines leaving the thalamus and entering HG were retained. To investigate the spatial relationship of the AR with adjacent association and

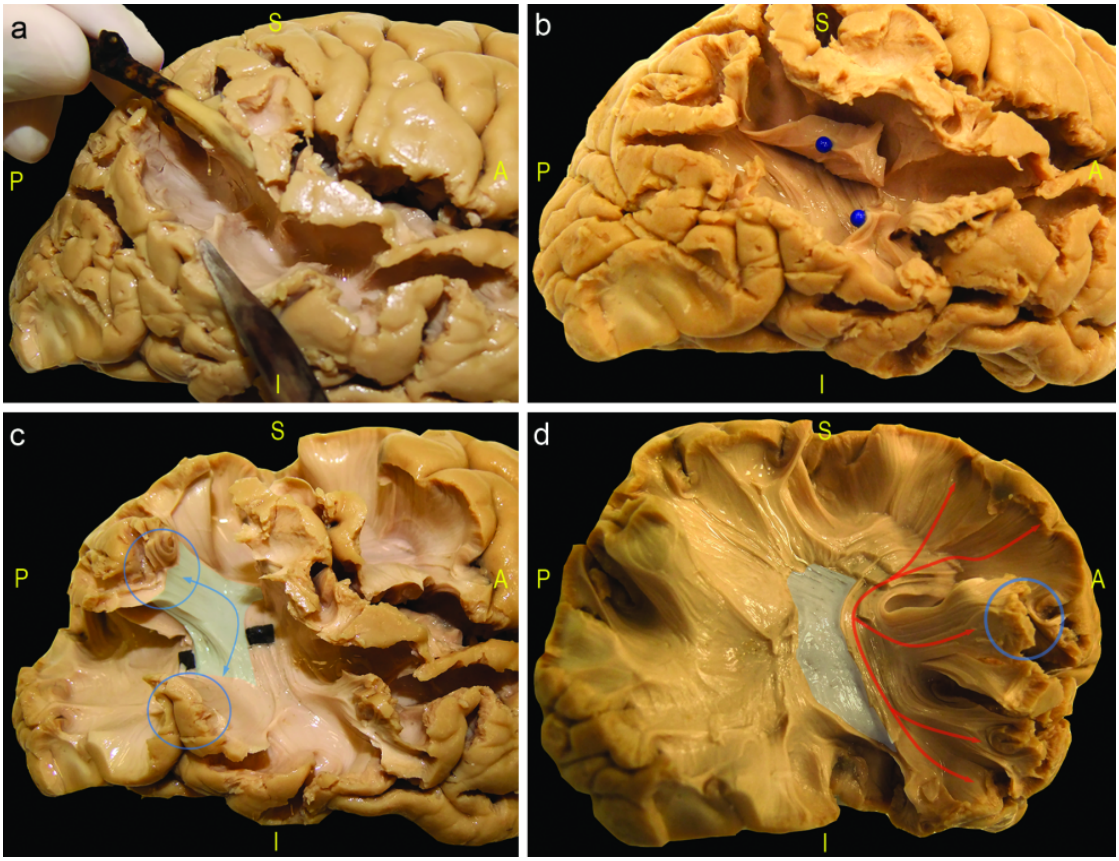

Figure 5.1: Blunt Dissections. These pictures show the different layer-by-layer step of dissection to AR. a) Removal of the compact and homogeneous layer of U-fibres connecting the IPL to the posterior third of STS (the decorticated area at the center of the anatomical scene of this panel). b) In this panel we demonstrated and cut the stem of the indirect posterior component of the SLF, lifted up by two blue pins at the two extremities of the cut. c) In a deeper layer we demonstrated the Wernicke's fascicle (highlighted in light blue, with blue arrows and circles showing the main fibres course and terminations, respectively). This bundle is more superficial and posterior to the layer of AF stem, highlighted in this picture by the black tag. d) Finally, after removal of Wernicke's fascicle we completely exposed the course of AF (red arrows), running above the EC (light blue), and we highlighted the terminations in the most posterior portion of STG (blue circle) and bordering the posterior portion of the middle third of the AR fibres. AF: arcuate fascicle; AR: acoustic radiation; EC: external capsule; IPL: inferior parietal lobule; SLF: superior longitudinal fascicle; STG: superior temporal gyrus; STS: superior temporal sulcus.

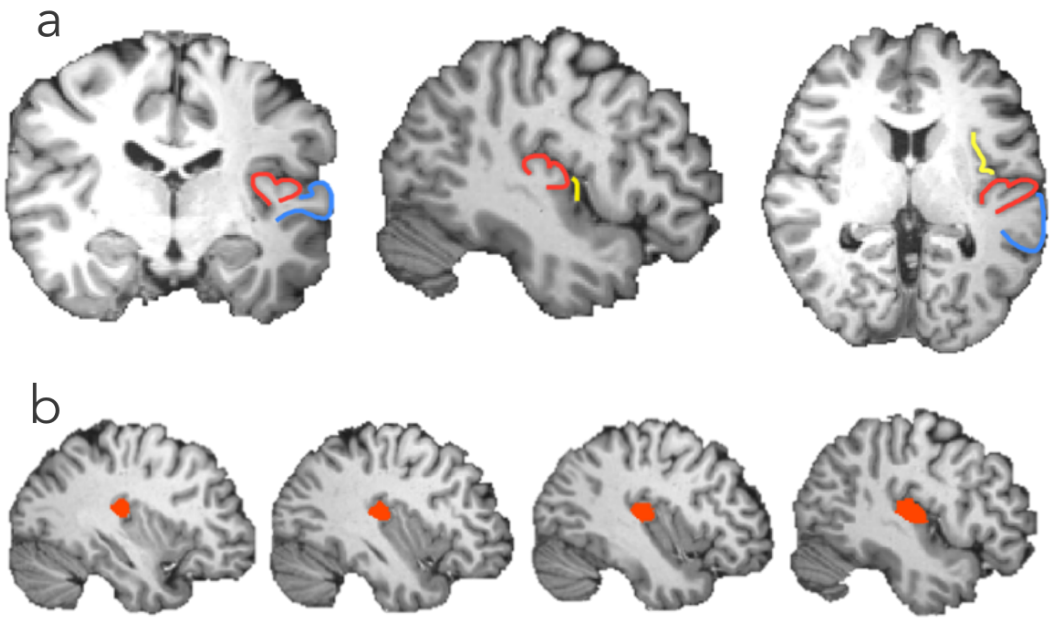

Figure 5.2: Heschl's Gyrus Segmentation. a) T1 weighted image of one representative subject displaying boundaries of left HG (red), left planum temporale (blu) and left insular cortex (yellow). Images are displayed in radiological convention. b) The image shows the selection of HG on different sagittal slice, from the more medial to the more lateral one.

projection tracts, whole brain tractography was also performed in one subject at following parameters: $0.75mm$ step-size, 45° angle threshold, 1000 seeds/voxel. Tractography was initiated from every voxel in a white matter brain mask segmented in FSL using FAST. From these data, using a two region of interest (ROI) approach (Catani et al., 2005, 2003), the streamlines of the posterior thalamic radiation (PTR), the AF, the somato-sensorial fibres (SS), and the inferior longitudinal fasciculus (ILF) were virtually dissected in fibreNavigator (Chamberland et al., 2014). For the PTR, the segmented thalamus and a big ROI encompassing the white matter of the occipital and parietal lobe were used; for the AF a ROI was defined to encompass the fibres lateral to the corona radiate and medial to the cortex as previously described (Catani et al., 2002); to dissect the anterior indirect SLF a first ROI was placed on the inferior frontal gyrus and a second one in the anterior parietal cortex; to dissect the posterior indirect SLF a ROI was placed on the posterior middle temporal gyrus and a second ROI on the posterior portion of the inferior parietal lobe; to reconstruct the IC a single ROI was placed around its posterior arm; for the EC a ROI is defined on the axial slice around the white matter of the external capsule; for the ILF the occipital lobe ROI was used and a second ROI was placed in the white matter of the temporal pole.

Heschl's gyrus segmentation

The Heschl's gyrus (or transverse temporal gyrus) exhibits a highly variable morphology, not only across brains but also hemispheres: size, shape and location of this anatomical structure change enormously. For this reason it is hard to obtain a correct automatic segmentation from software, and a good overlap from atlas regions.

For this study we decided to manually delineate Heschl's gyrus on the T1 weighted image of each subject. In order to improve accuracy of the results accuracy the same region of interest (ROI) was drawn five times for each subject and each hemisphere, after wide investigation of anatomical literature. Accuracy was then measured by calculating the Dice coefficient between successive drawn ROIs, and mean and standard deviation were calculated (Table 5.1). The Dice coefficient was calculated as the volume of the overlapping voxels relative to the volume (v) of the two ROIs ($2 * v(1 \cap 2)/(v1) + (v2)$). A Dice coefficient of 0.0 corresponds to no overlap between the two segmentations, while a Dice coefficient of 1.0 corresponds to identical regions of interest. The Dice coefficient was computed for each region in the testing set and mean and standard deviation reported.

The HG lies diagonally across the superior temporal plane in the depth of the lateral Sylvian fissure. It is defined anteriorly by the transverse sulcus (TS) of the temporal lobe, which unites medially to the circular sulcus of the insula, and posteriorly by the Heschl's sulcus (HS). There might be a second HS (or sulcus intermedius) if two HG gyri are present (Figure 5.2)(Abdul-Kareem, Sluming, 2008; Marie et al., 2015). On the sagittal and coronal slices the HG appears as a protrusion of the superior temporal plane (STP), with variable shapes including a single omega, a mushroom or a heart. On the transverse section HG appears to be a gyrus traversing antero-laterally from a point posterior to the insula to the convexity.

In every subject HG was first identified on the sagittal slice and its borders were marked for every slice from the first medial slice where HG becomes visible as a protrusion of the STP to the more lateral slice where it disappears. Once defined on the sagittal slice its shape was followed and refined on the axial slice, carefully following the grey matter near to the transverse sulcus and Heschl's sulcus. As a last step the coronal plane was checked. Both grey matter and white matter were included in the segmentation, and, if present, the second gyrus was included as well.

5.3 Results and discussion

After removal of the ventral fibres of the AF we exposed a texture of vertical and transverse fibres. Medially, we followed the compact and vertical layer of the projections fibres running from the thalamus to the post-central cortex. Antero-laterally to the stem of the AF we exposed a transverse layer of fibres belonging to the AR and starting from the postero-lateral portion of the thalamus (MGN) (Figure 5.3).

Blunt micro-dissections demonstrated a typical course of the AR. The proximal portion of the AR is characterized by a postero-lateral arching course. In the middle portion of the AR fibres run in an antero-lateral direction, fanning out in the distal portion up to the whole cortex of HG. We defined these three portions as *genu*, *stem* and *fan*.

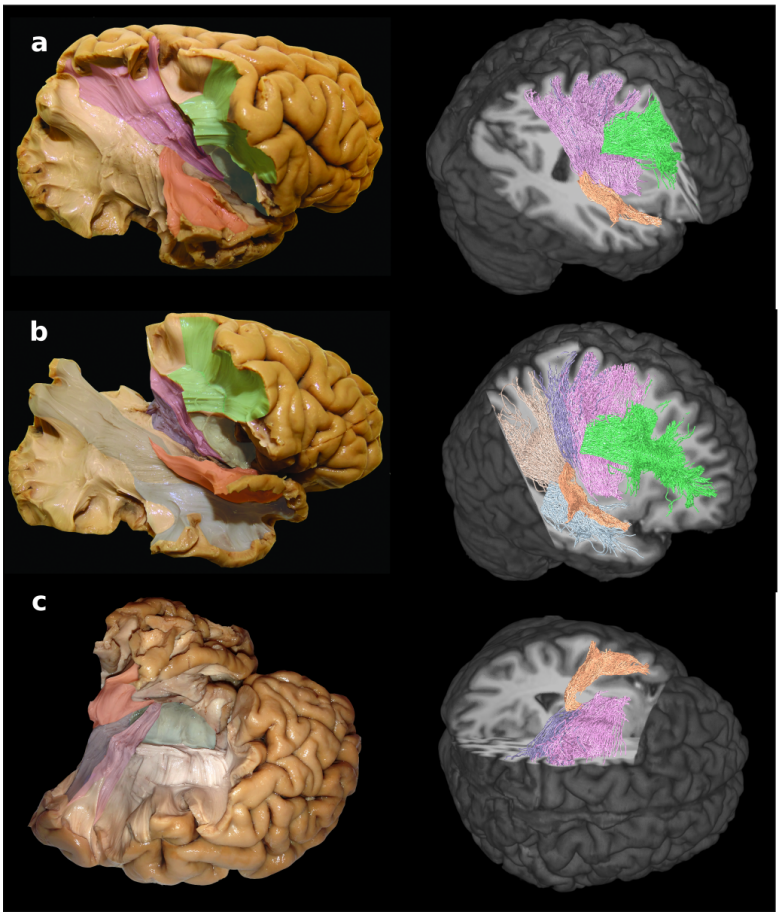

Figure 5.3: Comparison of Dissection and Tractography Results. The figure shows the results from post-mortem micro-dissections and 3D tractography reconstructions. a) The full latero-anterior arching course of AR (orange) was demonstrated from the postero-lateral thalamus to the cortex of the HG. The close relationship with the vertical fibres of the EC (pink) and AF (green) is shown. b) The different layers of WM crossing the course of the AR at the parieto-temporal junction are shown, including: the horizontal fibres of the AF/SLF (indirect anterior portion) complex (green); the vertical fibres of external capsule (pink); the fibres of the PTR (light brown), strongly intermingled with the proximal portion of the AR; the dorsal portion of the ILF (light blue) bordering inferiorly the fan of AR. c) superior view of a left hemisphere showing the relationship between the AR (orange) and internal (purple) and external (pink) capsule fibres. AF: arcuate fascicle; AR: acoustic radiation; EC: external capsule; HG: Heschl's gyrus; IC: internal capsule; ILF: inferior longitudinal fascicle; SLF: superior longitudinal fascicle; PTR: posterior thalamic radiation; WM: white matter.

Subject	**Manual segmentation reproducibility (Dice** $mean \pm sd$**)**	
	Heschl gyrus (right hemisphere)	Heschl gyrus (left hemisphere)
s1	0.82 ± 0.02	0.84 ± 0.03
s2	0.83 ± 0.02	0.84 ± 0.02
s3	0.80 ± 0.03	0.83 ± 0.02
s4	0.81 ± 0.03	0.81 ± 0.04
Mean	0.82 ± 0.01	

Table 5.1: Heschl's gyrus manual segmentation reproducibility. Manual segmentations of the Heschl's gyrus were derived from 3D T1 data, 5 times in each of 4 different subjects on each brain hemisphere. For each subject and hemisphere the table reports the Dice coefficient of 3D spatial overlap as the mean and standard deviation (*sd*) of all 10 pairwise combinations. The grand total mean for both hemispheres is also reported.

The *genu* represents the most critical portion during the AR exposition. In this region, in fact, we highlighted a dense intermingling with the vertical fibres projecting to the somato-sensorial (SS) cortex and with the fibres of the PTR (Figure 5.3-5.4). The stem is located just in front of the AF stem, bordering posteriorly the postero-superior margin of the circular sulcus of the insula (Figure 5.4). The fan constitutes the roof of the WM of the posterior third of the temporal lobe.

Ultra-high b-value and CSD tractography allowed the reconstruction of the AR profile in all the subjects (Figure 5.5). In accordance to blunt micro-dissections and previous literature (Bürgel et al., 2006), these streamlines originate as a compact bundle at the level of the MGN and move in a postero-lateral (*genu*) and antero-lateral (*stem* and *fan*) direction, fanning out in the grey matter of HG (Figure 5.5). On the coronal plane we observed a straight medio-lateral course of these fibres from the origin to the cortical termination. Tractography reconstructions confirmed the origin and terminations of this bundle are located on the same plane and highlighted a typical S-shape course (Bürgel et al., 2006), due to AR fibres arching around the postero-superior portion of the circular sulcus of the insula.

Both blunt micro-dissection and tractography techniques show AR fibres terminating in the grey matter of HG. Terminations of AR are located in the upper cortex of the posterior temporal lobe. While blunt micro-dissections clearly highlighted the core of termination of AR at the level of HG, the 3D streamlines reconstruction was quite noisy in all the subjects at this level, and some streamlines were not stopping in HG, but continuing outside the gyral borders in the antero-posterior direction (Figure 5.5).

Anatomical relationships with neighbouring pathways

Results of *in-vivo* tractography and *ex-vivo* dissections showed the intricate anatomical relationships of the AR with the other bundles of this region. Over the whole tra-

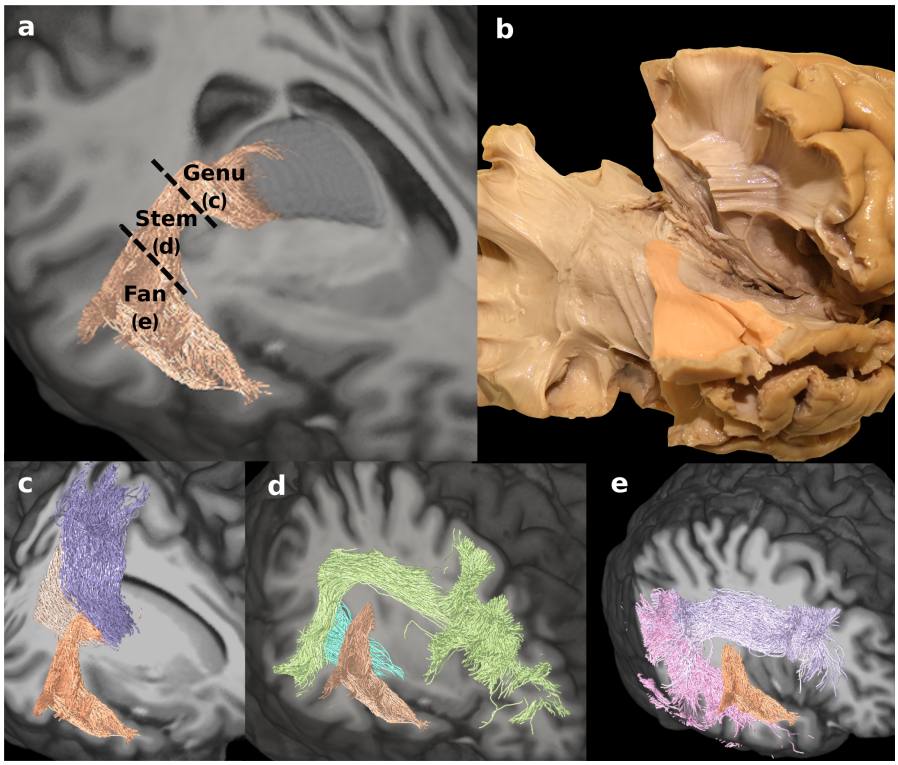

Figure 5.4: The Three Portions of the Acoustic Radiation. The figure shows the three portions of the AR – *genu, stem, and fan*- and their relationships with neighboring WM bundles. a, b) The three portions of the AR are shown on the 3D tractography reconstruction of a representative subject (a) and on a dissected brain (b). In both panels, AR course is colored in pink. In the tractography reconstruction labels defining the three portion of AR course (*genu, stem* and *fan*) are showed. In the dissection image a dotted line highlight the superior and postero-superior course of the circular sulcus of the insula. c, d, e) The panels show the details of the relationships of the three portions with the other pathways. From left to right, (c) the fibres of the *genu* are intermingled with the fibres of PTR (light brown) and, particularly, with the thalamic fibres projecting to the somato-sensorial cortex (purple); (d) the stem is close to the AF (green) and ILF (light blue), (e) the fan is very close to the terminations fibres of the indirect anterior SLF (violet) and indirect posterior portion of SLF (pink). F) In this dissection picture we highlighted the emergence of PTR (purple arrow) and AR (green arrow) fibres from the thalamus (TH), which are separated by a blue tag, highlighting the high fibres crossing at this level. In particular, the intermingling between transversal directions makes the distinction between these two contingents of fibres particularly hard at the origin from the thalamus. AF: arcuate fascicle; AR: acoustic radiation; ILF: inferior longitudinal fascicle; PTR: posterior thalamic radiation; SLF: superior longitudinal fascicle; TH: thalamus.

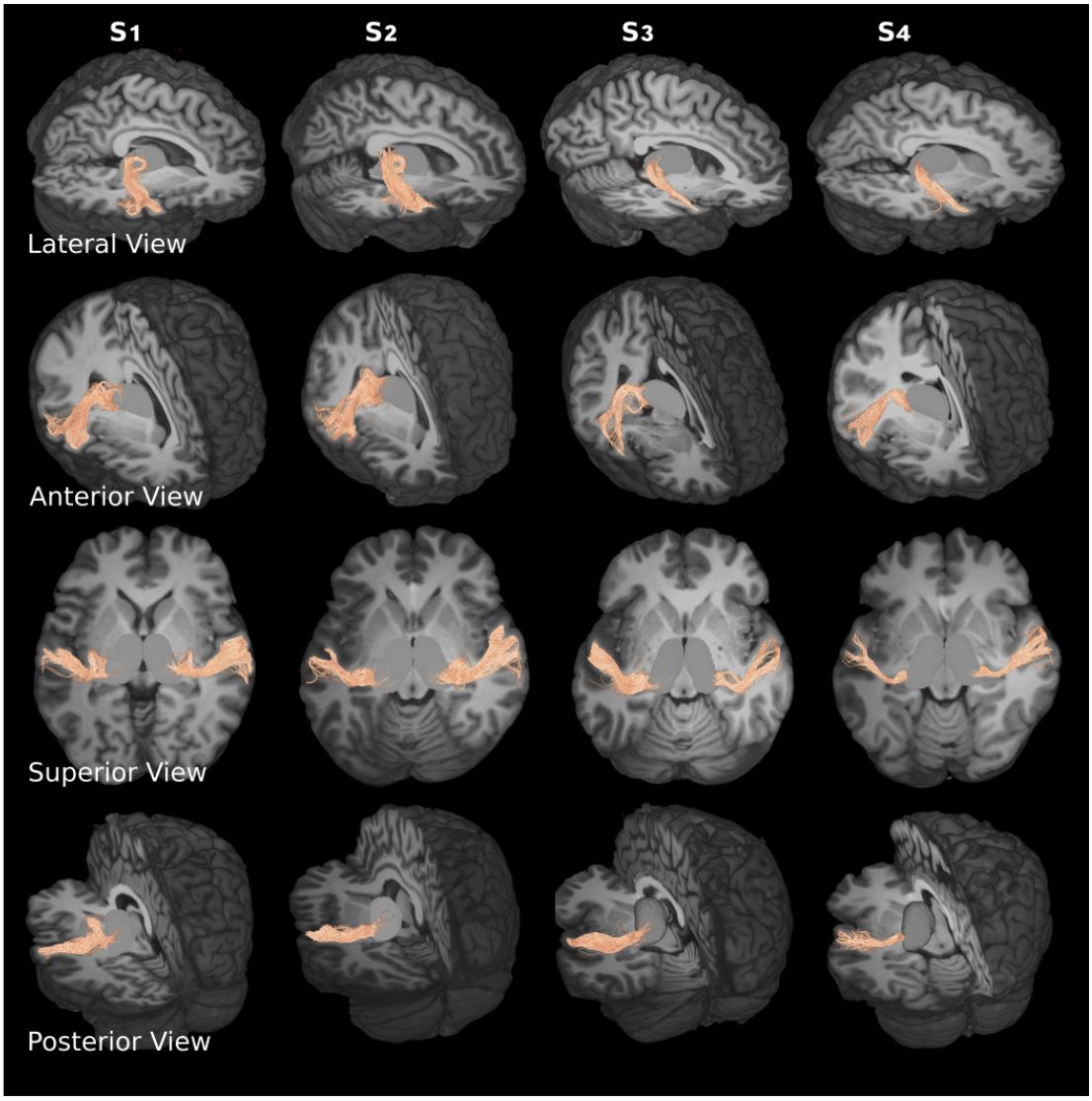

Figure 5.5: Acoustic Radiation Tractography Results. 3D reconstruction of the right and left AR in four healthy subjects (S1, S2, S3, S4). The course of the AR is shown from top to bottom rows in lateral, anterior, superior, and posterior views. The tractography reconstruction is overlaid on the corresponding T1 anatomical scan of each subject. AR: acoustic radiation.

jectory between the MGN to HG, the AR fibres cross major association and projection pathways of the human brain, and are in close proximity with others (Figure 5.3-5.4). In the proximal portion, both techniques confirmed the strong intermingling between the AR running in a lateral direction and the vertical fibres of IC and PTR (Figure 5.3a-b), including those projecting to the somato-sensory cortex. The middle third of the AR runs anteriorly to the AF stem, below the ventral portion of the fronto-parietal course of the AF and the anterior indirect SLF (also known as SLF III). Anteriorly to the AR we highlighted, from the medial to lateral: IC fibres, EC fibres, claustro-opercular sub-insular fibres and the insular cortices; posteriorly, from medial to lateral: the PTR fibres (including the optic radiation), the ILF, the AF, and the indirect posterior portion of the SLF (Figure 5.3-5.4). When comparing tractography results, AR terminations appear to be in close proximity (anterior and above) to the terminations of the most ventral streamlines.

Comparison of dissection and tractography results

Blunt micro-dissections and tractography show comparable results in the reconstruction of the AR profile. Both techniques show AR fibres stemming at the posterior lateral thalamus, moving lateral, arching around the posterior circular sulcus of the insula, moving antero-lateral and terminating in the upper cortex of the posterior temporal lobe. However notable differences between techniques are also visible, which highlight current limitations of diffusion tractography. At the level of the *genu*, where the AR crosses the IC fibres, some of the reconstructed streamlines follow erroneous vertical directions creating implausible false positive artefacts (Figure 5.6). At this level, the dense fibres crossing makes also the blunt dissection very hard to perform, particularly in disentangling between the AR and the vertical thalamic fibres (Figure 5.4d). At the fan level, while blunt micro- dissections clearly highlighted the core of termination of AR at the level of HG, the 3D tractography reconstruction was quite noisy in most of the subjects, and some streamlines did not stop in HG, but continued outside the gyral borders in the antero-posterior direction (Figure 5.6). This artefact was less visible when tractography was initiated in the HG and the thalamus was targeted. However, in this case, tractography was noisier at the thalamus, where many false positive artefacts were visible (Figure 5.7). Overall, reverse seeding doesn't seem to improve the AR reconstruction, particularly at the level of the crossing with the vertical thalamic fibres, where the same artefacts are visible.

Discussion and limitations

To the best of our knowledge, this is the first study revealing the anatomical features and topography of the AR in the human brain to combine *ex-vivo* (blunt micro-dissections) and *in-vivo* (diffusion tractography) data. Both methods showed the unique transversal trajectory of the AR running from the midline to the lateral convexity of the posterior portion of the superior temporal lobe. No other anatomical structure with the same orientation has been described in this region, excluding bi- hemispherical connections of the corpus callosum in human (Westerhausen et al., 2009) and non-human

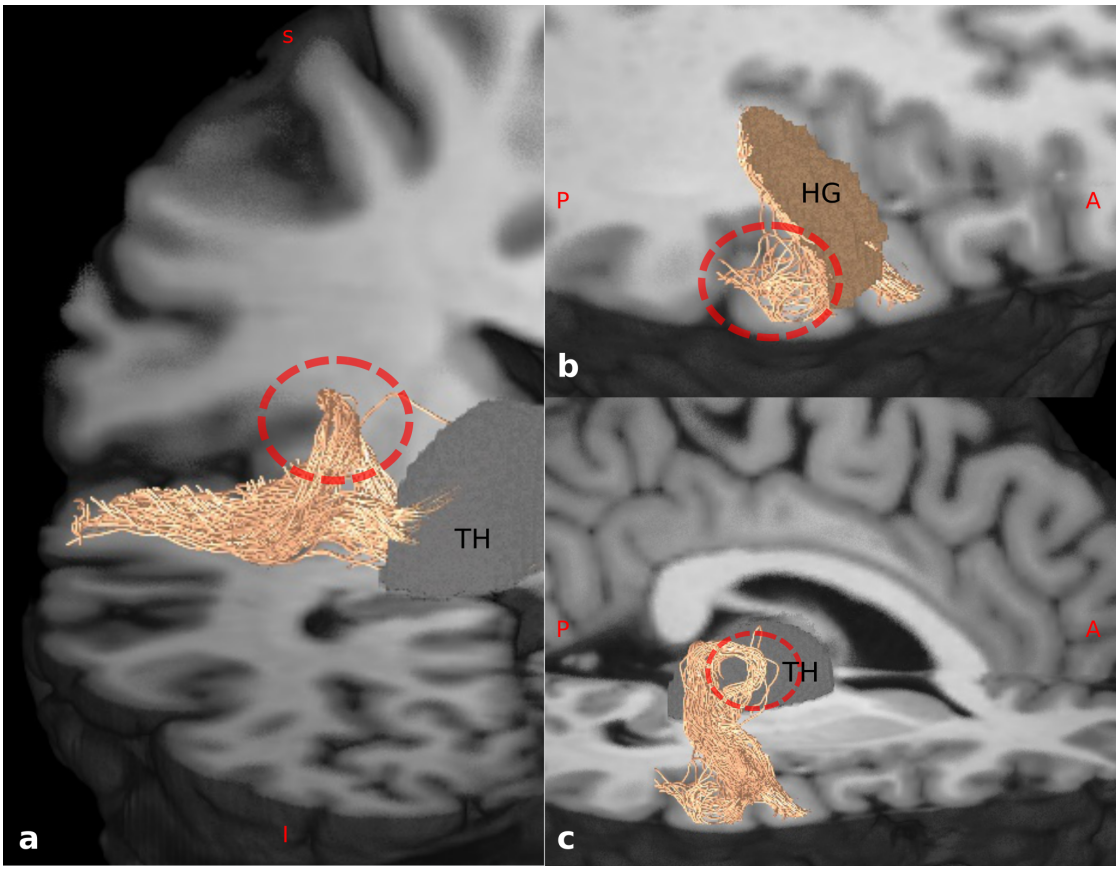

Figure 5.6: Acoustic Radiation Tractography Artefacts. The image highlights the false positive artefacts of the tractograhy reconstructions when compared to post-mortem dissections. a) Posterior view of the AR. The red circle highlights streamlines following erroneous vertical directions. b) Superior view of the AR at the termination in HG. A 3D reconstruction of the HG ROI is shown. The red circle highlights streamlines exiting the ROI and continuing in an antero-posterior direction along the cortex. c) Lateral view of the AR. The red circle highlights a loop at the level of the thalamus. A 3D reconstruction of the thalamus is also shown.

primates (Schmahmann, Pandya, 2006). For this reason, over its course from the thalamus to the HG, the AR crosses several association and projection bundles.Near the *genu* (proximal portion) of the AR, after the emergence from the MGN, these fibres cross in a medio-lateral direction a compact layer of vertical thalamo-cortical fibres. Intermingling this thick and compact wall, AR fibres form a highly organized structure at the level of the stem. Here these cross medio-laterally with the peri-sylvian association pathways, with a prevalent antero-posterior horizontal course. In the *genu* and stem portions, the AR is in close proximity of PTR, OR, EC, claustro-opercular fibres (*genu*), AF, indirect anterior SLF (*stem*). Even at the termination site (HG), these fibres are adjacent to the terminations of different and multi-directional associative pathways (e.g. AF, SLF, etc.). The complex fibre architecture of this region, with a high density of crossing, kissing, and bending fibres, represents an open challenge for diffusion-based tractography techniques (Dell'Acqua, Catani, 2012). The high angular resolution multi-shell HCP data and CSD-based probabilistic tractography has revealed the capability of reconstructing the profile of the AR bundle with results comparable to blunt dissections. However, when compared with *ex-vivo* results, 3D reconstructions still present with two main limitations. At the level of the crossing with the thalamic cortical fibres, some AR streamlines are likely to be truncated or may follow incorrect vertical directions, creating false positive artefacts. At the cortical termination site in HG the accuracy of the tractography is not always optimal, with some streamlines not stopping in HG and continuing outside the gyral borders in the antero-posterior direction along the cortex. Lack of precision in determining streamlines terminations at the cortex constitutes a limit in diffusion-based tractography techniques. When tracking, macroscopic termination criteria are used (e.g. white matter binary mask; edge of the brain, white matter-grey matter interface) that are inherently affected by limits in spatial resolution, partial volume effects and noise. As a result, streamlines end points not necessarily reflect the endpoints of the tracts (Alexander, 2005; Schmahmann, Pandya, 2006; Jbabdi, Johansen-Berg, 2011).

When tractography is performed in the opposite direction (latero-medial), the same artefacts are visible at the thalamus, with streamlines exiting its borders. More investigation is needed to understand if a combination of the two, or the implementation of better termination strategies, would help to obtain more precise 3D reconstructions of the AR. Solving the crossing between the AR and the compact vertical thalamic fibres represents the main obstacle in attempts at AR reconstruction using tractography methods. Most of the available clinical diffusion protocols and tractography pipelines may not be able to solve this, resulting in the AR being absent from the final reconstruction. The use of probabilistic tractography may help to overcome some of the limitations related to the diffusion model or tractography algorithm (Behrens et al., 2007; Descoteaux et al., 2009). However, these methods are also more prone to false positive artefacts than deterministic ones. Being aware of the exact anatomical borders of the bundle, as highlighted by blunt dissections, is a crucial requirement for the interpretation of tractography results and for excluding non-reliable reconstructions. Reliable *in-vivo* reconstruction of the AR would help to shed a light on the mechanisms underlying auditory and language comprehension in humans. The anatomical and topographical description of the AR that emerged from

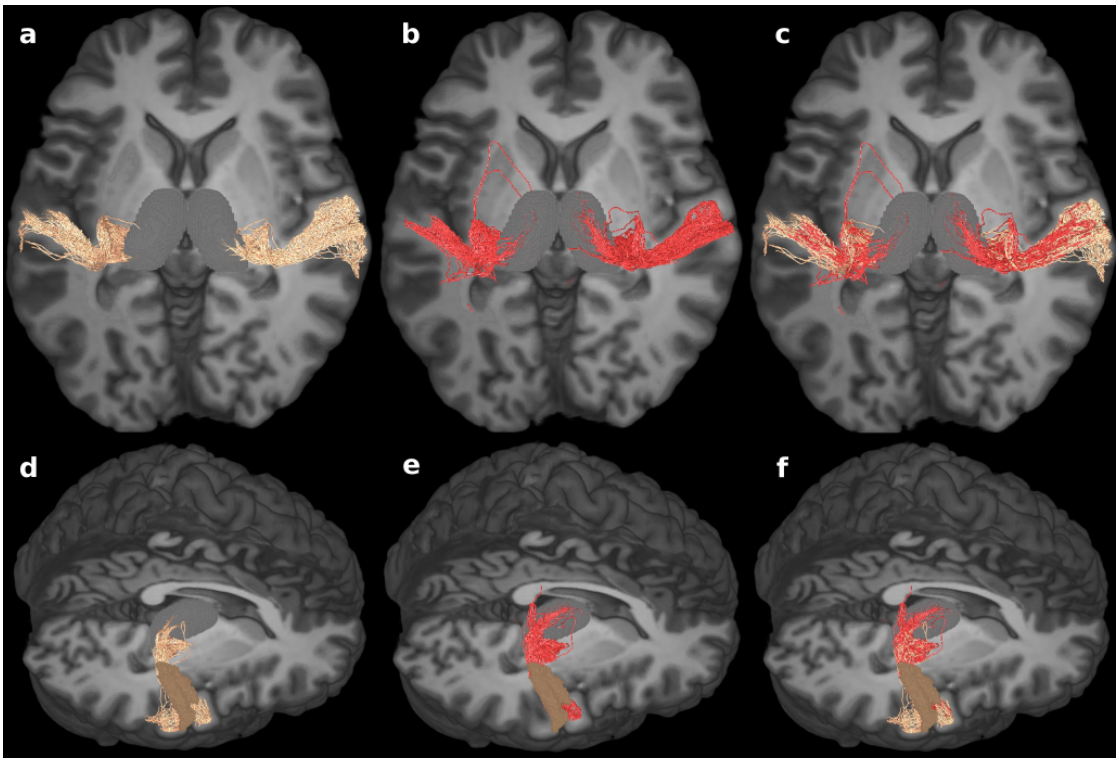

Figure 5.7: Reverse Tractography. The image shows the comparison of tractography results for different seeding strategies for one representative subject. Top: superior view of the reconstruction of the AR. a) tractography was seeded in the thalamus and the HG was used as including ROI. b) tractography was seeded from HG and the thalamus used as inclusion ROI. c) results of the two seeding strategies are show. Bottom: Superolateral view of the AR for the different seeding strategies. A 3D reconstruction of the HG is shown (brown).

this study may reflect the anatomo-functional link between auditory sensorial input and language elaboration, especially considering the close proximity of the AR terminations with the major language bundles of the dorsal peri-sylvian network at the junction between the posterior temporal lobe and inferior parietal lobule (a crucial hub for semantic and articulatory/phonological integration). In the widely accepted dual streams model of language processing (Hickok, Poeppel, 2007; Saur et al., 2008) the AF/SLF system is considered the anatomical structure mediating the elaboration of auditory inputs, before this is passed to the auditory-motor interface for speech processing (Catani et al., 2005; Duffau et al., 2014). This auditory information is brought into the system via the fibres of the AR. In this highly integrated and distributed network, an appreciation of the structural neuroanatomy is crucial for the comprehension of the different steps of processing between sensory perception and conceptual representations (Hickok, Poeppel, 2004). Investigating the functional substrates of this structure will help understand the degree of linguistic specificity of the AR and auditory territories. Current theories assume that the auditory stimulus is computed asymmetrically even at very early stages, with the left hemisphere being specialized in processing fast temporal changes that are not language-specific but are indispensable for speech processing, and the right hemisphere being specialized in spectral analysis that might be more important for music perception (Zatorre et al., 2002). Disentangling the role of the AR pathways in speech processing and music perception would be particular relevant for example in syndromes in which the level of language-specificity of the deficit is still unclear (*e.g.* pure word deafness) (Saffran et al., 1976; Stefanatos et al., 2005). In this scenario and considering also the evolution of brain surgery towards functional tailored resections, the anatomy of the AR is even more crucial for the most complete surgical planning, in order to avoid functional impairments in domains involving auditory processing (*e.g.* language, music, etc.). Investigating the functional substrates of this structure will help understand the degree of linguistic specificity of the AR and auditory territories. In conclusion, combining blunt micro-dissections and diffusion-based tractography allows for the precise topography of the AR to be delineated. This will be crucial in the guidance of reconstruction and in evaluating the reliability of tractography dissection of this structure. Finally, the neuroanatomical organization of this pathway as showed in this study suggests how primary auditory processing is integrated with high-level linguistic and non-linguistic cognitive processing. This may provide new directions for research into linguistic processing, with clinical relevance for the interpretation of symptoms, the improvement of treatments, and the surgical preservation of a fundamental sensory function of the human being.

Bibliography

Abdul-Kareem Ihssan A., Sluming Vanessa. Heschl gyrus and its included primary auditory cortex: Structural MRI studies in healthy and diseased subjects // Journal of Magnetic Resonance Imaging. aug 2008. 28, 2. 287–299.

Alexander Daniel C. Multiple-fiber reconstruction algorithms for diffusion MRI // Annals of the New York Academy of Sciences. 1064, 1. dec 2005. 113–133.

Behrens T. E J, Berg H. Johansen, Jbabdi S., Rushworth M. F S, Woolrich M. W. Probabilistic diffusion tractography with multiple fibre orientations: What can we gain? // NeuroImage. 2007. 34, 1. 144–155.

Bürgel Uli, Amunts Katrin, Hoemke Lars, Mohlberg Hartmut, Gilsbach Joachim M, Zilles Karl. White matter fiber tracts of the human brain: Three-dimensional mapping at microscopic resolution, topography and intersubject variability // NeuroImage. 2006. 29, 4. 1092–1105.

Catani Marco, Howard Robert J, Pajevic Sinisa, Jones Derek K. Virtual in vivo interactive dissection of white matter fasciculi in the human brain. // NeuroImage. 2002. 17, 1. 77–94.

Catani Marco, Jones Derek K, Donato Rosario, Ffytche Dominic H. Occipito-temporal connections in the human brain. // Brain : a journal of neurology. sep 2003. 126, Pt 9. 2093–107.

Catani Marco, Jones Derek K., Ffytche Dominic H. Perisylvian language networks of the human brain // Annals of Neurology. 2005. 57, 1. 8–16.

Chamberland Maxime, Whittingstall Kevin, Fortin David, Mathieu David, Descoteaux Maxime. Real-time multi-peak tractography for instantaneous connectivity display // Frontiers in Neuroinformatics. 2014. 8, May. 1–15.

De Benedictis Alessandro, Petit Laurent, Descoteaux Maxime, Marras Carlo Efisio, Barbareschi Mattia, Corsini Francesco, Dallabona Monica, Chioffi Franco, Sarubbo Silvio. New insights in the homotopic and heterotopic connectivity of the frontal portion of the human corpus callosum revealed by microdissection and diffusion tractography // Human Brain Mapping. dec 2016. 37, 12. 4718–4735.

Dell'Acqua Flavio, Catani Marco. Structural human brain networks: hot topics in diffusion tractography. // Current opinion in neurology. 2012. 25, 4. 375–83.

Descoteaux Maxime, Deriche Rachid, Knösche T, Anwander Alfred. Deterministic and Probabilistic Tractography Based on Complex Fiber Orientation Distributions // IEEE Transactions on Medical Imaging. 2009. 28, 2. 269–286.

Duffau Hugues, Moritz-Gasser Sylvie, Mandonnet Emmanuel. A re-examination of neural basis of language processing: Proposal of a dynamic hodotopical model from data provided by brain stimulation mapping during picture naming // Brain and Language. apr 2014. 131. 1–10.

Fan Qiuyun, Witzel Thomas, Nummenmaa Aapo, Van Dijk Koene R.A., Van Horn John D., Drews Michelle K., Somerville Leah H., Sheridan Margaret A., Santillana Rosario M., Snyder Jenna, Hedden Trey, Shaw Emily E., Hollinshead Marisa O., Renvall Ville, Zanzonico Roberta, Keil Boris, Cauley Stephen, Polimeni Jonathan R., Tisdall Dylan, Buckner Randy L., Wedeen Van J., Wald Lawrence L., Toga Arthur W., Rosen Bruce R. MGH–USC Human Connectome Project datasets with ultra-high b-value diffusion MRI // NeuroImage. 2015.

Fernández-Miranda Juan C., Wang Yibao, Pathak Sudhir, Stefaneau Lucia, Verstynen Timothy, Yeh Fang-Cheng. Asymmetry, connectivity, and segmentation of the arcuate fascicle in the human brain // Brain Structure and Function. may 2015. 220, 3. 1665–1680.

Hickok Gregory, Poeppel David. Dorsal and ventral streams: a framework for understanding aspects of the functional anatomy of language // Cognition. may 2004. 92, 1-2. 67–99.

Hickok Gregory, Poeppel David. The cortical organization of speech processing. // Nature reviews. Neuroscience. may 2007. 8, 5. 393–402.

Jbabdi Saad, Johansen-Berg Heidi. Tractography: Where Do We Go from Here? // Brain Connectivity. 2011. 1, 3. 169–183.

Jeurissen Ben, Tournier Jacques-Donald, Dhollander Thijs, Connelly Alan, Sijbers Jan. Multi-tissue constrained spherical deconvolution for improved analysis of multi-shell diffusion MRI data // NeuroImage. 2014. 103. 411–426.

Klein Arno, Andersson Jesper, Ardekani Babak A., Ashburner John, Avants Brian, Chiang Ming-Chang, Christensen Gary E., Collins D. Louis, Gee James, Hellier Pierre, Song Joo Hyun, Jenkinson Mark, Lepage Claude, Rueckert Daniel, Thompson Paul, Vercauteren Tom, Woods Roger P., Mann J. John, Parsey Ramin V. Evaluation of 14 nonlinear deformation algorithms applied to human brain MRI registration // NeuroImage. jul 2009. 46, 3. 786–802.

Klingler J. Erleichterung der makroskopischen Praeparation des Gehirns durch den Gefrierprozess // Schweiz Arch Neurol Psychiatr. 1935. 36. 247–256.

Marie D, Jobard G, Crivello F, Perchey G, Petit L, Mellet E, Joliot M, Zago L, Mazoyer B, Tzourio-Mazoyer N. Descriptive anatomy of Heschl's gyri in 430 healthy volunteers, including 198 left-handers. // Brain structure & function. mar 2015. 220, 2. 729–43.

Martino Juan, Vergani Francesco, Robles Santiago Gil, Duffau Hugues. New Insights Into the Anatomic Dissection of the Temporal Stem With Special Emphasis on the Inferior Fronto-occipital Fasciculus // Operative Neurosurgery. mar 2010. 66, 3 Suppl Operative. ons4–ons12.

Patenaude Brian, Smith Stephen M, Kennedy David, Jenkinson Mark. A Bayesian model of shape and appearance for subcortical brain segmentation // Neuroimage. 2012. 56, 3. 907–922.

Saffran E M, Marin O S, Yeni-Komshian G H. An analysis of speech perception in word deafness. // Brain and language. apr 1976. 3, 2. 209–28.

Sarubbo Silvio, De Benedictis Alessandro, Merler Stefano, Mandonnet Emmanuel, Barbareschi Mattia, Dallabona Monica, Chioffi Franco, Duffau Hugues. Structural and functional integration between dorsal and ventral language streams as revealed by blunt dissection and direct electrical stimulation // Human Brain Mapping. nov 2016. 37, 11. 3858–3872.

Sarubbo Silvio, De Benedictis Alessandro, Milani Paola, Paradiso Beatrice, Barbareschi Mattia, Rozzanigo Umbero, Colarusso Enzo, Tugnoli Valeria, Farneti Marco, Granieri Enrico, Duffau Hugues, Chioffi Franco. The course and the anatomo-functional relationships of the optic radiation: a combined study with post mortem dissections and in vivo direct electrical mapping. // Journal of anatomy. jan 2015. 226, 1. 47–59.

Saur Dorothee, Kreher Björn W, Schnell Susanne, Kümmerer Dorothee, Kellmeyer Philipp, Vry Magnus-Sebastian, Umarova Roza, Musso Mariacristina, Glauche Volkmar, Abel Stefanie, Huber Walter, Rijntjes Michel, Hennig Jürgen, Weiller Cornelius. Ventral and dorsal pathways for language. // Proceedings of the National Academy of Sciences of the United States of America. 2008. 105, 46. 18035–40.

Schmahmann JD, Pandya DN. Fiber pathways of the brain. Oxford, New York: Oxford University Press, 2006.

Smith Robert E., Tournier Jacques-Donald, Calamante Fernando, Connelly Alan. Anatomically-constrained tractography: Improved diffusion MRI streamlines tractography through effective use of anatomical information // NeuroImage. 2012. 62, 3. 1924–1938.

Soria Guadalupe, De Notaris Matteo, Tudela Raúl, Blasco Gerard, Puig Josep, Planas Anna M., Pedraza Salvador, Prats-Galino Alberto. Improved Assessment of Ex Vivo Brainstem Neuroanatomy With High-Resolution MRI and DTI at 7 Tesla // Anatomical Record. 2011. 294, 6. 1035–1044.

Stefanatos Gerry A, Gershkoff Arthur, Madigan Sean. On pure word deafness, temporal processing, and the left hemisphere. // Journal of the International Neuropsychological Society : JINS. jul 2005. 11, 4. 456–70; discussion 455.

Tournier J. Donald, Calamante Fernando, Connelly Alan. MRtrix: Diffusion tractography in crossing fiber regions // International Journal of Imaging Systems and Technology. 2012. 22, 1. 53–66.

Wang Xuhui, Pathak Sudhir, Stefaneanu Lucia, Yeh Fang-Cheng, Li Shiting, Fernandez-Miranda Juan C. Subcomponents and connectivity of the superior longitudinal fasciculus in the human brain // Brain Structure and Function. may 2016. 221, 4. 2075–2092.

Westerhausen R., Gruner R., Specht K., Hugdahl K. Functional Relevance of Interindividual Differences in Temporal Lobe Callosal Pathways: A DTI Tractography Study // Cerebral Cortex. jun 2009. 19, 6. 1322–1329.

Zatorre Robert J., Belin Pascal, Penhune Virginia B. Structure and function of auditory cortex: music and speech. // Trends in cognitive sciences. jan 2002. 6, 1. 37–46.

Zhang Yongyue, Brady Michael, Smith Stephen. Segmentation of Brain MR Images Through a Hidden Markov Random Field Model and the Expectation-Maximization Algorithm // IEEE Transactions on Medical Imaging. 2001. 20, 1. 45–57.

Chapter 6

Acoustic Radiation tractography reconstruction: optimization of MRI acquisition and tractography analysis choices for atlas reconstruction

6.1 Introduction

Diffusion-based MRI tractography allows *in-vivo* and non-invasive characterization of white matter architecture of the human brain (Chapter. 3). Since the introduction of the diffusion MRI tensor model, one of its major applications has been the localization and description of fibre bundles of the brain. Most of these well-known bundles are the large associative fibre pathways that, following the longitudinal plane, connect different cortical regions of the brain. However, these pathways represent the brain's "highways" and constitute only a small sample of all the white matter fibres, the architecture of which is much more complex.

The introduction of more advanced multi-fibre models (Chapter 2) has helped advance the knowledge of these main white matter pathways. However, some primary bundles are still only partially reconstructed, or not reconstructed at all. Chapter 4 introduces the topography of the acoustic radiation (AR), a primary sensory pathway that constitutes a notable omission in tractography studies. The AR, because of its location and anatomical features, goes undetected with the basic diffusion tensor model. In Chapter 5 we combined *post-mortem* dissections and ultra-high b-value tractography to better understand the topography of the AR and its correspondence and differences with

tractography reconstructions. Results showed that the AR fibres are characterized by a fully transversal course from the midline to the cortex, along which they cross some of the major fibre system of the human brain. We argue that the location and shape of this bundle has largely prevented the investigation of its anatomy in humans *in-vivo*. We also highlighted how successful and reliable reconstruction of this bundle using diffusion-based tractography techniques would allow for the exploration of the morphology and topography of these fibres in humans, and for correlation with anatomical and functional aspects of audition and language (Chapter 4 and 5). The combination of ultra-high b-values and probabilistic tractography shows that results comparable to *post-mortem* dissections can be obtained *in-vivo* (Chapter 5). However, acquisition of such high quality diffusion MRI data is challenging, in particular with the time constrains of typical clinical settings, which typically are consistent with single shell MRI diffusion acquisition protocols. It is therefore important to understand how single b-value MRI acquisition and analysis choices ultimately affect the reconstruction of the AR.

The final result of any tractography reconstruction intimately depends on both the acquisition and tractography parameters chosen. Different studies have investigated how changing analysis parameters such as angular resolution (Vos et al., 2012; Calabrese et al., 2014), spatial resolution (Vos et al., 2012), tractography algorithm (Bastiani et al., 2012), and tractography parameters (Thomas et al., 2014; Takemura et al., 2016; Chamberland et al., 2014; Domin et al., 2014; Girard et al., 2014) affect the reconstruction of well known white matter tract, focusing on finding optimal parameters. However, it remains unclear how these parameters affect the tractography reconstruction of the AR.

In this study, we systematically investigated the effects of MRI acquisition and tractography parameters on the diffusion-based tractography reconstruction of the AR using data publicly available from the Human Connectome Project. The main aims of this study are two: i) using a subgroup of subjects and a reference AR for each subject, define an optimum set of MRI acquisition and tractography analysis parameters for the reconstruction of the AR by systematically characterizing AR reconstruction effects as function of several parameters (MRI acquisition: b-value and number of diffusion encoding directions; diffusion model: probabilistic and deterministic; tractography: angle threshold and step size), and ii) use the optimum parameter set on the full group of subjects to build a tractography-based atlas of the AR.

6.2 Methods

Diffusion and structural data of 35 healthy adult subjects (16 females, mean age: 31.1) provided by the Human Connectome project (http://humanbrainconnectome.org) were analysed.

Diffusion data processing

Diffusion weighted data was pre-processed as previously described (Fan et al., 2015). The diffusion data is constituted by a multi-shell acquisition (b-factor=1000, 3000, 5000 and 10000 s/mm^2) for a total of 552 directions, of which 512 diffusion weighted (DW)

and 40 non-DW volumes (b=0), at a spatial resolution of 1.5mm isotropic. In order to investigate acquisition parameters, the four shells were divided and separately analysed in MRTrix3 (Tournier et al., 2012). For each shell, bias field correction and global intensity normalisation were performed and an average response function was calculated. The constrained spherical-deconvolution-based diffusion profile (FODs) was then reconstructed for each subject for each shell on the basis of the shell-specific average response function. The tensor model was also fit to the data and fractional anisotropy (FA) maps were extracted.

Structural Data Processing

The T1 weighted structural image of each subject was linearly registered through affine registration to the diffusion space of each subject in FSL. For better co-registration results, first the up-sampled FA map ($1 \times 1 \times 1\ mm^3$) was registered to the T1, and then the inverse transformation was applied to the T1 image. The registered T1 was then segmented in FSL using FAST (Zhang et al., 2001) to segment white matter, grey matter and CSF, and FIRST (Patenaude et al., 2012) to extract subcortical nuclei. This information was combined to create a five-tissue-type image to be used for anatomically constrained tractography (ACT) (Smith et al., 2012). The right and left thalami were segmented in FSL using FIRST for use as seeding regions of interest (ROI) to initiate tractography of the AR. The Heschl's gyrus was manually segmented in each subject as outlined in Chapter 5 and it was used as a target ROI.

Optimal AR tractography reconstruction

A subgroup of 5 subjects was used to determine the set of diffusion acquisition and analysis parameters that would reconstruct the AR with the highest volumetric and spatial agreement with respect to the reference AR reconstruction. The subjects considered were: MGH_1001, MGH_1002, MGH_1003, MGH_1004, MGH_1005. For each one of these subjects, the left and right hemisphere AR were reconstructed using one set of acquisition and analyses parameters as defined in Table 6.1. In other words, for each combination of single-shell b-value and number of gradient directions, deterministic and probabilistic AR reconstructions were performed sampling a range of tractography angle thresholds and step sizes (Table 6.1). The following parameters were considered to be the default: step size = 0.75 mm, angle = 45°. The following analysis parameters were kept constant: the maximum streamline length (80 mm), seed locations for tractography was in the thalamus (2000 seeds per voxel) using the Heschl's gyrus (HG) as an inclusion ROI. The algorithm was instructed to stop at the grey matter/white matter interface, as defined by the structural T1 data. Overall, this gave 72 different AR tractography reconstructions per subject, per hemisphere.

The effects of acquisition and analysis on AR reconstructions were evaluated in two ways: spatial extent (volume) and spatial overlap with a reference AR reconstruction. Spatial extent was defined as the sum of voxels traversed by at least one streamline belonging to the reconstructed tractogram (volume). The reference AR from each subject was reconstructed starting from the multishell dataset as follows: the multi-shell multi-

Shell	$1000, 3000, 5000, 10000\ s/mm^2$
DW Directions	$68, 68, 128, 256$
Algorithm	Probabilistic, Deterministic
Angle Threshold	$20, 30, 45, 60, 80°$
Step size	$0.25, 0.50, 0.75, 1, 1.25\ mm$
Maximum Streamline Length	$80\ mm$
Seeds per Voxel	2000

Table 6.1: Acquisition and Tractography Parameters
The table shows the acquisition and tractography parameters used in the study.

tissue constrained spherical deconvolution algorithm (Jeurissen et al., 2014) was fit to the data and anatomically-constrained (Smith et al., 2012) probabilistic tractography (ACT) was performed (0.75 mm step size, 45° angle threshold, 2000 seeds/voxel) (Chapter 5). To increase the topographical accuracy of the reference AR, these tractograms were first manually inspected and filtered (edited) by the neuro-surgeon (author S.S) that performed the *post-mortem* dissections in a previous study (Maffei et al., 2017). To quantify the anatomical correspondence between the reference tractograms and the reconstructed tractograms a binary mask was created for all voxels intersected by at least one streamline. From these binary masks the volumetric overlap was quantified as the Dice similarity coefficient (Dice, 1945):

$$overlap = \frac{2(mask_A \cap mask_B)}{mask_A + mask_B} \tag{6.1}$$

where 0 represents no overlap and 1 complete overlap. The Dice coefficient has been used before in tractography studies to assess reconstruction reproducibility (Vos et al., 2016; Bauer et al., 2013; Dayan et al., 2015).

Full group acoustic radiation tractography reconstruction

The set of acquisition and tractography parameters that better reconstructed the profile of the AR were then applied to the complete dataset (34 subjects). One subject was excluded (MGH_1020) because it had an incomplete acquisition (482 volumes instead of 552 b=10000 s/mm^2 volumes).

Hemispheric tract-specific AR measures were then extracted (volume, number of streamlines, FA, AFD). FA values were extracted from the FA scalar map computed for b=1000 s/mm^2, to avoid FA confounding at high b-values (Frank, 2001). Coefficients of variation (CV) were computed for each extracted measure and each subject in both hemispheres. CF is defined as the ratio of the standard deviation σ to the mean of the population. A laterality index (LI) was also computed ($LI = L - R/L + R$, R: right, L: left) on the tract-specific metrics to investigate the hemispheric asymmetry of the AR. The LI ranged from -1 (completely right$-$lateralized) to $+1$ (completely left$-$lateralized). In concordance with prior studies, bilateral representation was defined

in the -0.2 to $+0.2$ range (Springer et al., 1999). Paired t$-$tests were applied to evaluate the asymmetry of the AR. *Acoustic Radiation Atlas Construction*

The AR atlas was constructed using the optimal AR reconstructions from the 34 subjects. We first computed the warping images between the diffusion space of each participants and the standard MNI space through a two step diffeomorphic registration performed in ANTS software (Avants et al., 2008). The up-sampled subject's FA map ($1\times1\times1\ mm$) was first registered to the subject's T1; the subject's T1 was then registered to the MNI_152_1mm space. The inverse warps were then concatenated and applied to the reconstructed streamlines of each participant through the *tcknormalize* command implemented in MRtrix3.

We then computed the tract density image (TDI) of each streamline AR bundle in MNI space and binarized it with a threshold of 2 (at least 2 streamlines traversing the voxel) in MRtrix3. All binary images were then summed together to build the final AR atlas. In this way, the voxel value would represent the number of subject showing AR streamlines at that location. As a second alternative approach, we first merged together all the reconstructed streamlines warped in MNI space, and computed the TDI after that. In this way the final atlas could be thresholded based on absolute AR streamline number per voxel.

6.3 Results

6.3.1 Acoustic radiation reconstruction: small group study of MRI acquisition and tractography analysis effects

The main result is that tractography reconstructions of the AR showed notable differences depending on the choice of MRI shell, tractography algorithm (probabilistic versus deterministic), and tractography parameters. Figure 6.1 illustrates these effects on the right hemisphere AR in one of the 5 subjects using the default tractography parameters. To determine an optimal parameter set for the AR reconstruction we evaluated the obtained tractograms both on the base of their spatial extent, and on their anatomical accuracy relative to a reference AR.

Acoustic radiation: spatial extent evaluation

For the lowest b-value (b= 1000 s/mm^2) and for default parameters, the deterministic reconstruction provided almost no streamlines belonging to the AR in all 5 subjects. On the contrary, the probabilistic methods resulted in a great amount of streamlines reconstructed between the thalamus and HG (Figure 6.1). Many of these low b-value probabilistic streamlines, however, likely constitute false positive reconstructions, following the course of other fibre crossing the vertical axis. For higher b-values ($> b = 3000\ s/mm^2$) the deterministic reconstructions start providing more streamlines belonging to the AR, and the probabilistic reconstructions show less false positive streamlines on the vertical plane (Figure 6.1). Using the lowest b-value ($b = 10000\ s/mm^2$), the representations of

probabilistic and deterministic methods tend to converge to similar anatomical representations.

Figure 6.2 shows radius plots of how the hemispheric AR volume changes as a function of MRI acquisition (b-value and directions), diffusion model (probabilistic and deterministic) and tractography parameters (angle threshold and step size). The overall pattern is similar across the two hemispheres. The probabilistic approach gives volume estimates of the 3D AR reconstructions that are robust to different tractography analysis parameters, especially for low b-values (Figure 6.2). For b=1000 s/mm^2 the volume of the tract strongly decreases for angle = 20°, probably reflecting the elimination of most false positive artefacts. On the contrary, the volume of the tract increases for small angle thresholds at high b-values (Figure 6.2). The step size does not have a strong impact on the probabilistic reconstructions at any of the different shells. The same is true also for deterministic reconstructions. As for probabilistic, the angle threshold affects the deterministic reconstructions at all b-values, increasing the number of reconstructed streamlines. For low angles, no streamlines are reconstructed even at high b-values (Figure 6.2).

Acoustic radiation: topographical evaluation

The spatial extent, while giving information on the ease of tracking for a given number of seeds, does not give any information on the topographical accuracy of the reconstructed tractograms. Higher number of streamlines and thus larger spatial extents might correspond to higher numbers of false positive inaccurate reconstructions.

To improve the accuracy of our evaluation, reconstructed tractograms were compared with a reference AR. Figure 6.3 shows an example of how the reference AR were edited from those originally reconstructed. Most of the artefactual streamlines are situated at the level of the posterior dorsal portion of the external capsule, and at the level of the inferior portion of the posterior and middle thirds of the superior temporal gyrus (STG) (Figure 6.3). One subject (subject MGH_1003) was excluded from the reference generation, since both the automatically reconstructed and the filtered tractograms resulted in too few streamlines to allow for meaningful comparisons.

Figure 6.4 shows the group summary results of the Dice coefficient of spatial overlap (AR reconstruction relative to reference AR) for the same manipulations described in AR volume evaluations (Figure 6.2). As for the spatial extent, the pattern is extremely similar across the two hemispheres. Dice is overall higher for probabilistic reconstructions than for deterministic ones, and higher when using higher b-values. Increasing the angle decreases the overlap for high b-values, but increases the overlap for low b-values. At b=1000 s/mm^2, for angle = 20° the overlap is very close to the reconstruction of the AR at high b-values (Figure 6.4). For all shells the overlap slightly increases when bigger step sizes are used. For the deterministic reconstructions the overlap is strongly affected by the angle, increasing for higher angle values, while greater step sizes only slightly affects the reconstruction with no clear trend. Overall, the default tractography parameters seem to provide the best overlap with the reference AR, even if slightly better results are obtained increasing the step size at higher b-values for probabilistic tractography.

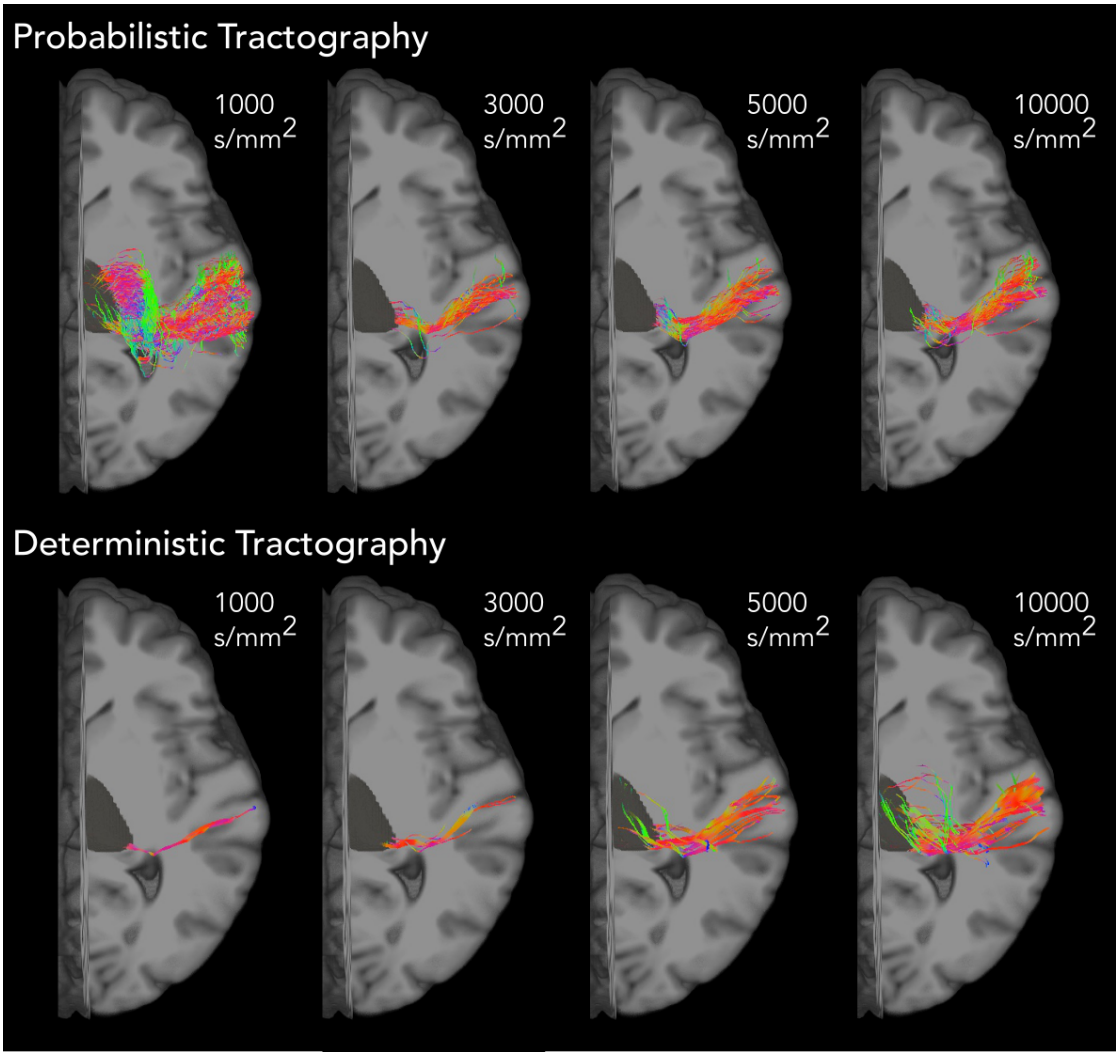

Figure 6.1: Acquisition Parameter Effects on Acoustic Radiation Reconstructions. The image shows the deterministic and probabilistic reconstruction of the right hemisphere AR for a representative subject for each shell at defaults tractography parameters (angle = 45°, step size = 0.75 mm). The reconstructed streamlines are shown on the the T1 image of the subject. The streamline color encodes directionality. The 3D reconstruction of the right thalamus is also shown in dark grey.

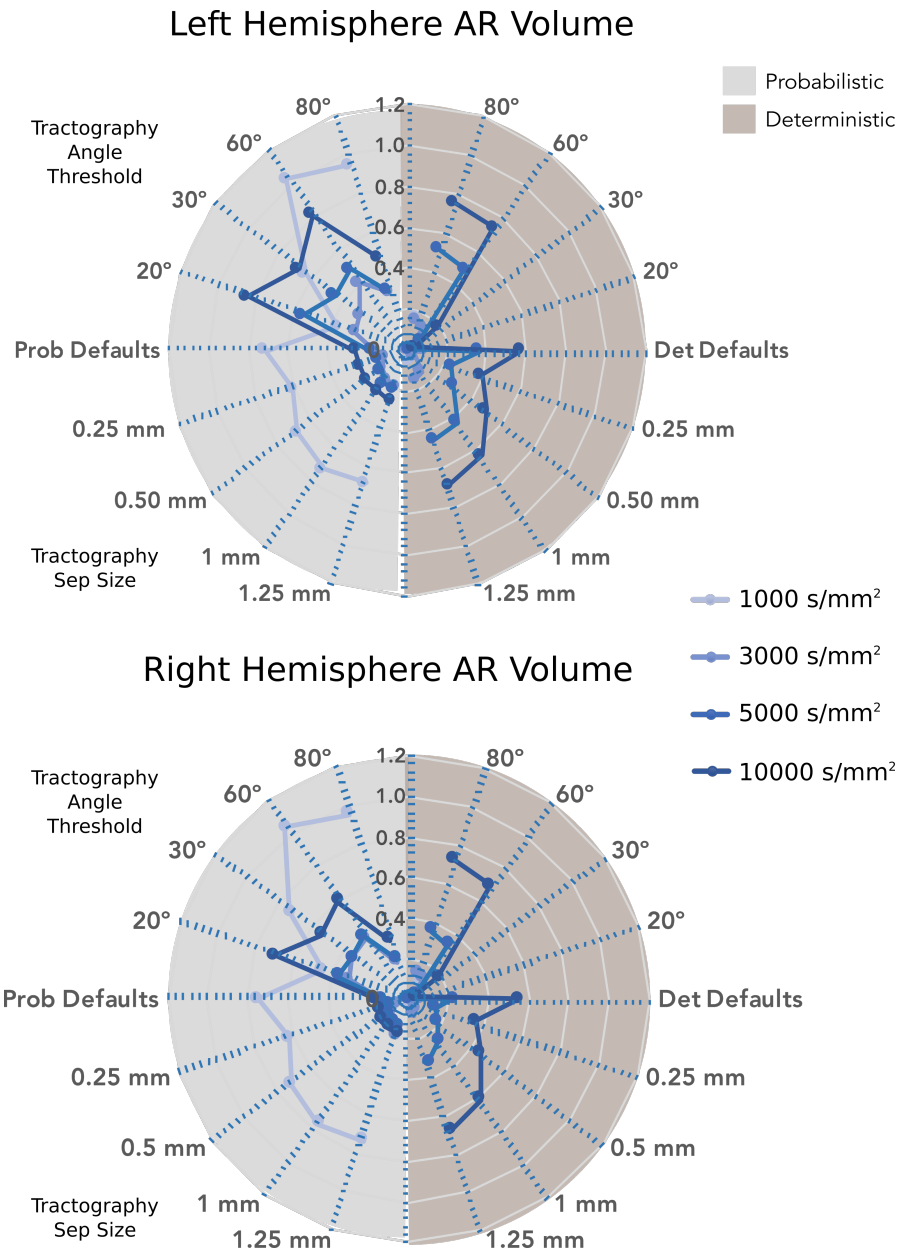

Figure 6.2: MRI Acquisition and Tractography Analysis Effects on AR Volume. The figure shows the radar plots where the radius denotes the mean AR volume (5 subjects, concentric circles from 0 to 1.2 10^4 ml in steps of 0.2 10^4 ml) for the two brain hemispheres. The volume (ml) is plotted for the two algorithms (probabilistic and deterministic) and the different angle and step size parameters at the four shells (indicated in different shades of blue).

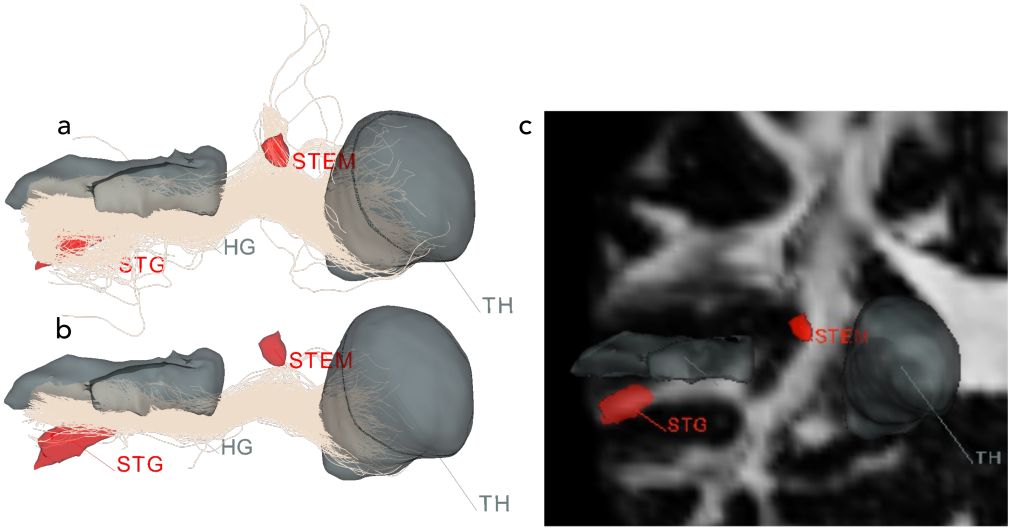

Figure 6.3: AR Manual Filtering. The image shows the AR reconstruction before (a) and after (b) the manual filtering for a representative subject (MGH_1001). The 3D reconstruction of the thalamus (TH) and the HG (grey) are shown together with the exclusion ROIs (red) used to filter the tract, the inferior part of the superior temporal gyrus (STG), and the stem region of the AR at the posterior part of the external capsule. The same ROIs are also shown on a coronal slice of the FA map of the same subject (c).

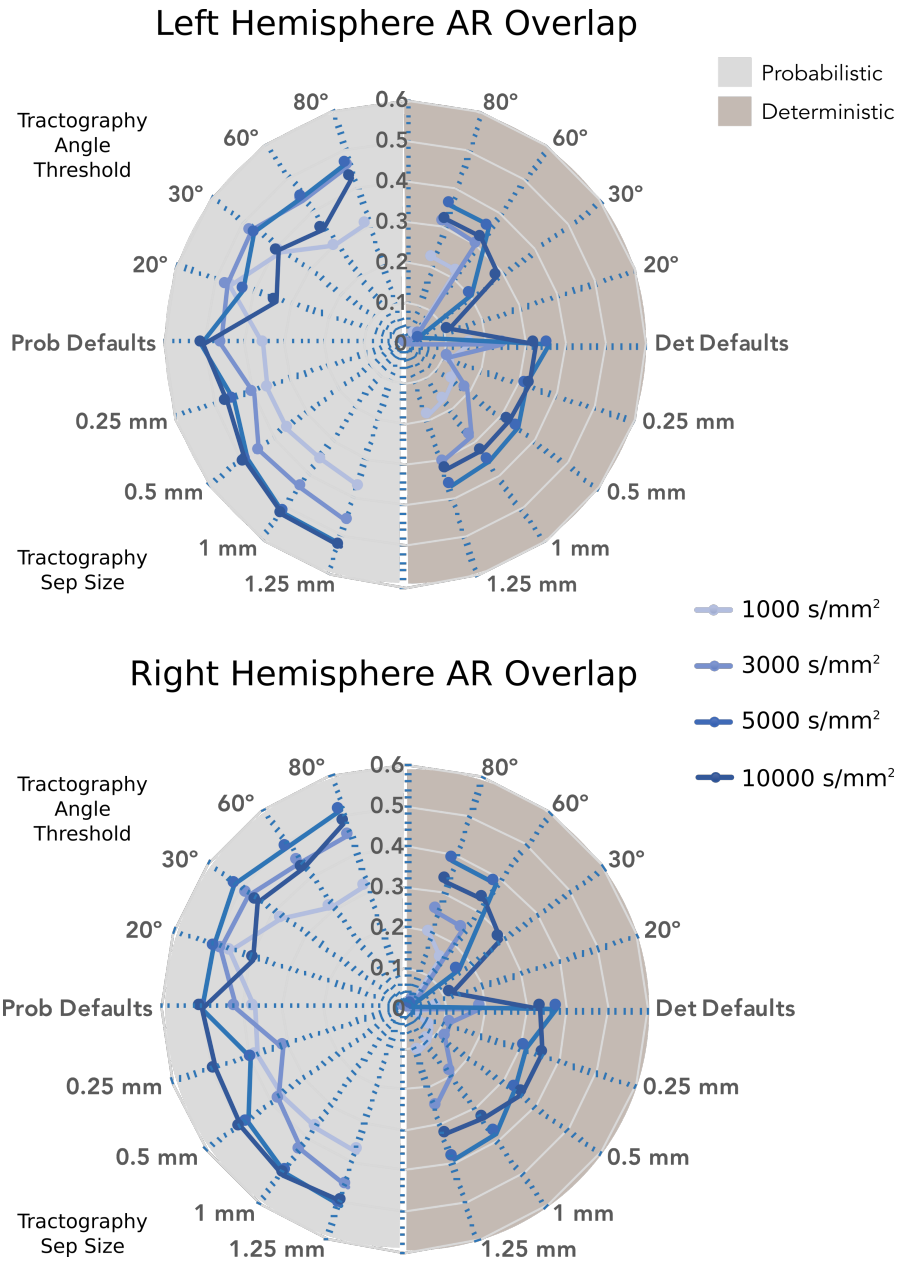

Figure 6.4: Topographical Evaluation. The image shows the radar plots of the mean dice coefficient values between the filtered AR and the different tractograms for the four subjects (mean values). The dice coefficient is plotted for the two algorithms (probabilistic and deterministic) and for the different angle and step size parameters at the four shells (indicated by different line colours).

For each algorithm (probabilistic/deterministic) we used a non-parametric Kruskall-Wallis test to evaluate whether varying b-value, step size, and angle threshold affected the spatial overlap of the tractograms with the reference AR. Significant effects are found only for deterministic tractography, for acquisition parameters and angle ($p > 0.05$).

Comparison of Spatial Extent and Topographical Evaluation

For higher b-values and number of diffusion directions both the volume and the spatial overlap increase for deterministic tractography (Figure 6.5). However, for b=10000 s/mm^2 the increase in spatial extent is not followed by an increase in the spatial overlap. This may reflect the fact that only spurious streamlines are added to the tractography reconstructions. Similarly, for low b-values, the probabilistic reconstruction shows greater spatial extent but lower overlap. For higher b-values the Dice coefficient increases while the volume strongly decreases (Figure 6.5).

Interim summary

Starting from the same data and the same low-level diffusion model, the use of different MRI acquisition parameters, tractography algorithm and tractography parameters lead to very different tractography reconstructions of the AR. Overall, probabilistic reconstructions resulted better in terms of topographical AR accuracy (Figure 6.5). In addition, probabilistic algorithms can recover the AR even at low b-values (e.g., b=1000 s/mm^2, commonly used in clinical protocols), for which the deterministic algorithm could not reconstruct any or only very few streamlines (Figure 6.1). Consistently, significant effects in the accuracy of AR reconstruction in comparison to the reference AR were found only for deterministic algorithms, for b-value and angle threshold. step size had minor effects on the AR reconstruction (Figure 6.4). Overall, optimal results in terms of topographical accuracy and correspondence to our AR reference where obtained for probabilistic tractography, using high b-values and default tractography parameters.

6.3.2 Acoustic radiation: full group and atlas reconstruction

Based on the parameter optimization results, to reconstruct the AR in the entire dataset (34 subjects) the following parameters were chosen: probabilistic algorithm, b-val=10000 s/mm^2, default parameters (step size = 0.75 mm, angle = 45°). The AR was successfully reconstructed in most of the subjects, correctly following macro-anatomical landmarks and showing a very low number of false positive reconstructions. Streamlines correctly leave the postero-lateral part of the thalamus and move first in a lateral and then antero-lateral direction, to terminate in HG. No streamlines erroneously following the direction of the external capsule fibres are visible. However, a high level of variability across subjects still emerged. Two subjects showed no reconstructed streamlines in the right hemisphere, and in 6 subjects only few streamlines were visible in one hemisphere. Variability in the reconstructions is confirmed by the variability of extracted tracts' volume (CV: LH=0.58, RH=0.69) and number of streamlines (CV: LH=RH=0.93) (Figure 6.7). FA values averaged over AR were very low for all subjects (< 0.3), and showed less

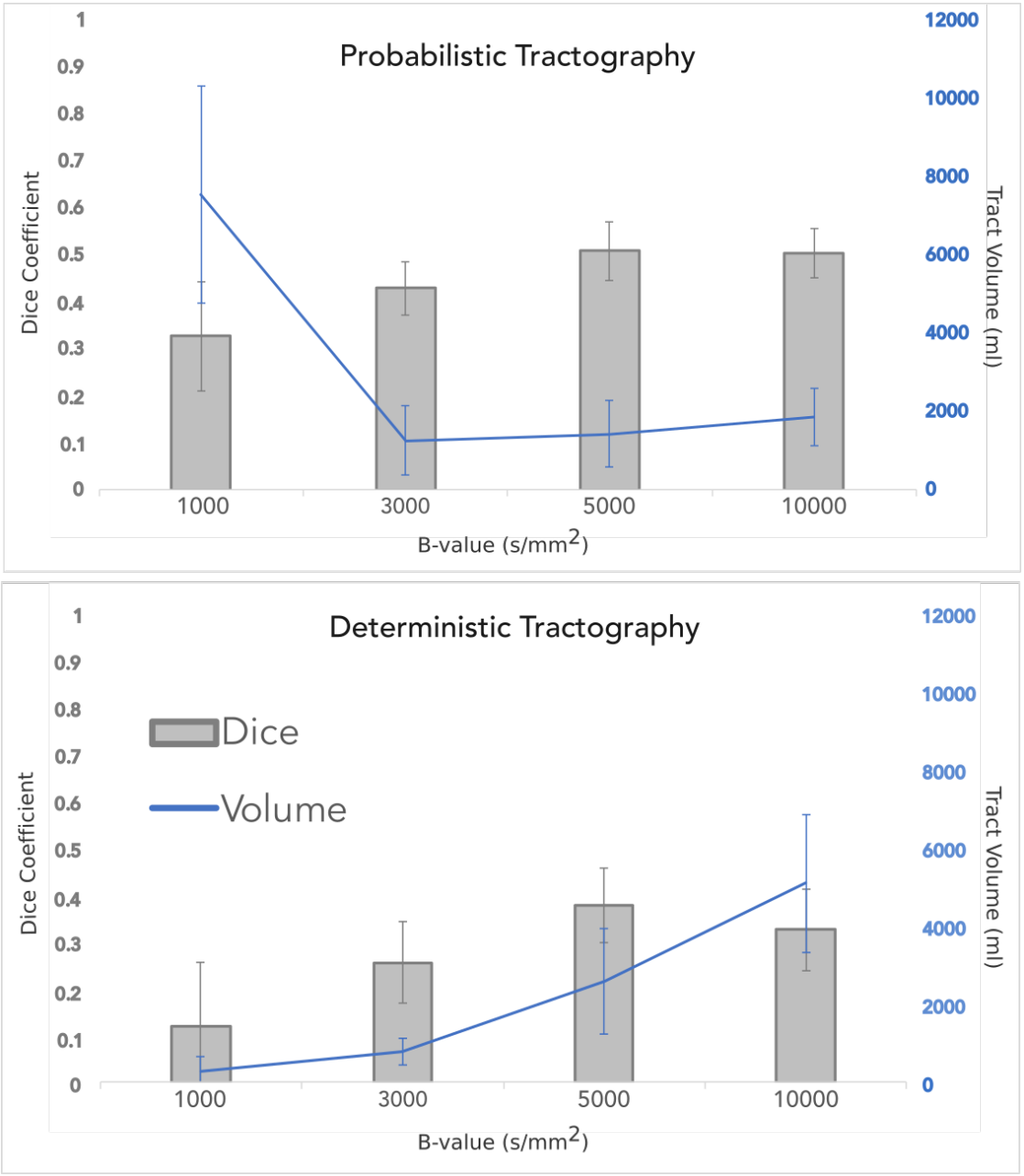

Figure 6.5: Effects of Acquisition Parameters on the AR Reconstruction. The image shows the relationship between the spatial and the topographical evaluations for MRI acquisition parameters. A bar graph of the Dice coefficient for default parameters for the four shells is shown for probabilistic and deterministic tractography (median values). The volume (ml) for the same tractograms is also shown (blue) (right-hand vertical axis).

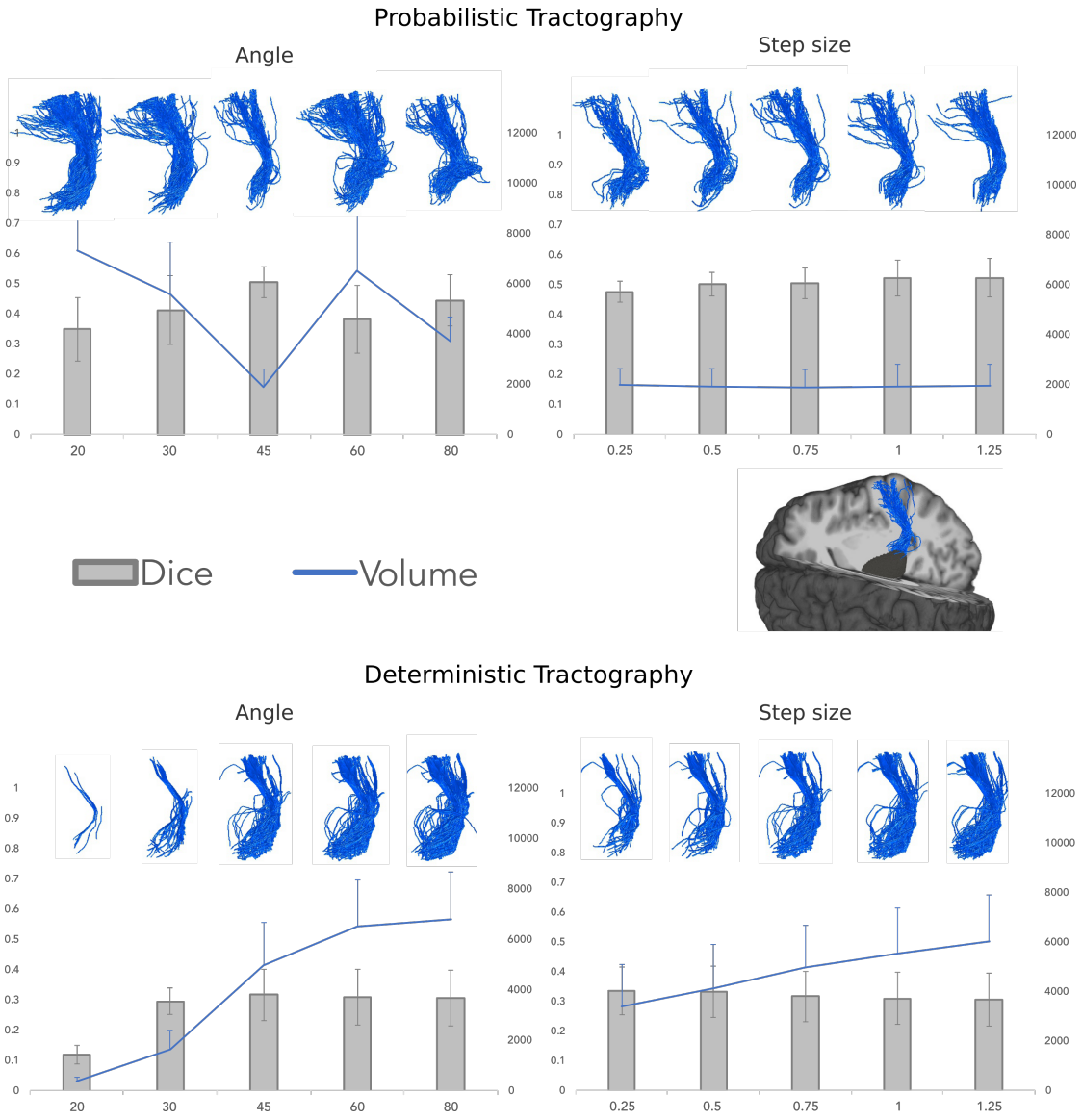

Figure 6.6: Effects of Tractography Parameters on the AR Reconstruction. The image shows the effect of tractography parameters (angle and step size) on the reconstruction of the AR at b=10000 s/mm^2 for both probabilistic and deterministic algorithms. Both median Dice coefficient and volume (ml) values for all subjects and both hemispheres (mean values) are displayed. The profile of the right AR for a representative subject is also shown. A 3D reconstruction of the subject's brain, the thalamus and the AR shows the plane and angle used to take the screenshots of all the other tractograms.

AR hemispheric lateralization: subject proportion and p-value				
	Left	**Bilateral**	**Right**	**p-value**
Apparent fibre Density	19/34	14/34	1/34	$p < 0.01$
Fractional Anisotropy	2/34	31/34	1/34	$p > 0.05$
Tract Volume	17/34	16/34	1/34	$p < 0.01$
Number of streamlines	24/34	8/34	2/34	$p < 0.01$

Table 6.2: Acoustic Radiation Hemispheric Lateralization. The table reports the number of subjects that show leftward, bilateral, or rightward lateralization of the different measures extracted from the acoustic radiation (apparent fiber density, fractional anisotropy, tract volume, and number of streamlines). The p value of the hemispheric difference of these measures is also reported.
.

variability across the group (CV: LH=0.08, RH=0.28). AFD also showed considerable variability across the group (CV: LH=0.55, RH=0.65) (Figure 6.7).

A lateralization index was computed for all the extracted quantitative measures (volume, N streamlines, FA, AFD) in each subject (Figure 6.8). Paired t-tests were applied to evaluate the asymmetry of the acoustic radiation. Results, summarized in Table 6.2, show a significant degree of left lateralization for AFD, volume and number of streamlines ($p < 0.01$). FA values show a bilateral distribution in almost all subjects (31/34) ($p > 0.05$) (Table 6.2). Overall, only two subjects showed a degree of right lateralization (Figure 6.8).

The AR atlas was reconstructed in MNI space from the group tractography reconstructions (Figure 6.9). The voxel-wise AR atlas was constructed to represent either number of streamlines (>5) or number of subjects (>3).

6.4 Discussion and conclusions

This study focuses on the tractography reconstruction of the human acoustic radiation, a bundle that is almost completely absent from previous tractography studies. We investigated the effect of MRI acquisition and tractography parameters on the final 3D reconstruction of this bundle. The main findings of the study are: i) higher b-values ($\geq 5000\ s/mm^2$) and more DW directions (≥ 128) increase the accuracy of the AR reconstruction for both probabilistic and deterministic tractography; ii) only probabilistic tractography can reconstruct the AR at low b-values ($\leq 3000\ s/mm^2$); iii) the AR reconstruction remains challenging and highly variable across subjects; and iv) the AR was found to be predominantly left lateralized. Additionally, we built a tractography-based atlas of the AR.

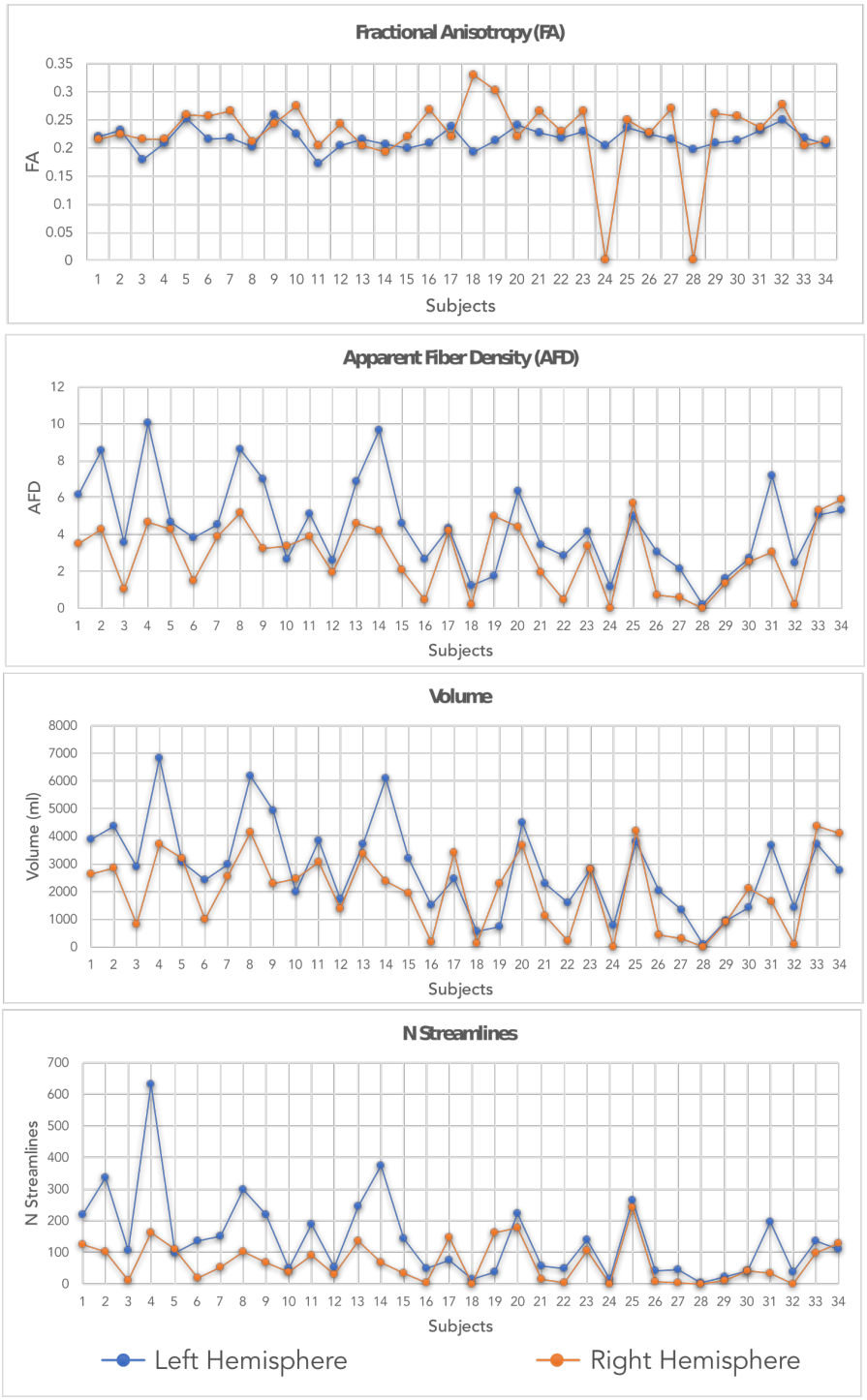

Figure 6.7: Acoustic Radiation Tract Specific Measures. Group variability of different tract-specific measures extracted for the AR: FA, AFD, volume, N streamlines. Measures are reported for the 34 subjects for each hemisphere.

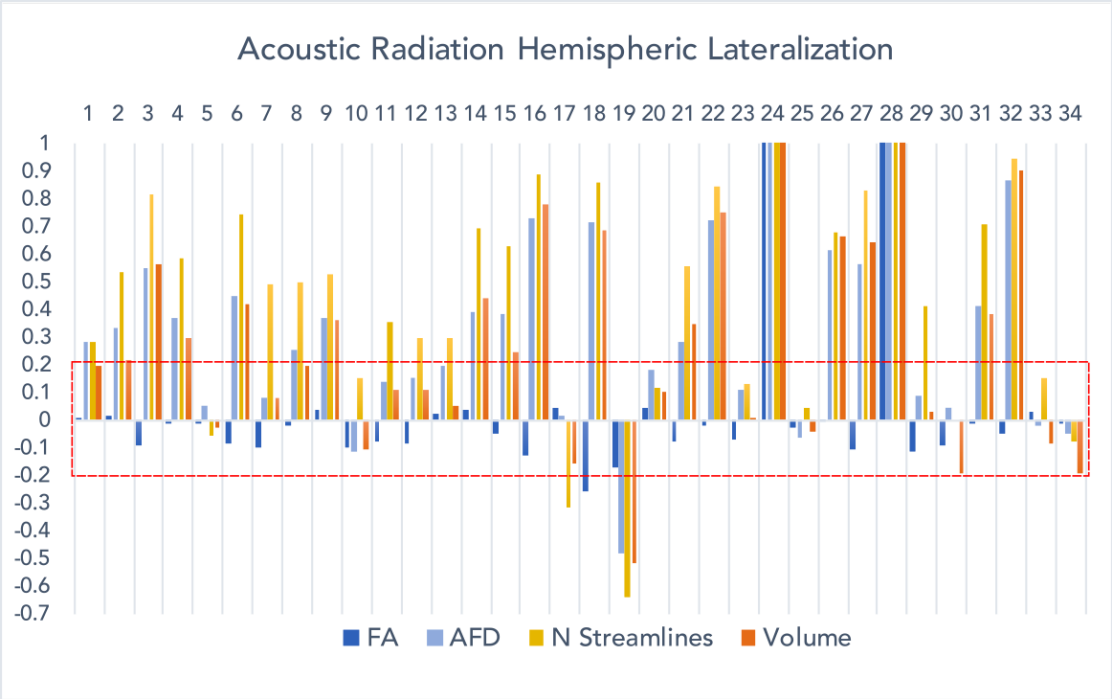

Figure 6.8: Lateralization Index of the Acoustic Radiation. The graph reports the lateralization index (LI) of the AR for the 34 subjects. The LI ranges from -1 (completely right−lateralized) to $+1$ (completely left−lateralized). Bilateral AR representation was defined in the -0.2 to $+0.2$ range, identified by the red dotted line.

Effects of acquisition and tractography parameters

The choice of tractography algorithm (probabilistic and deterministic), tractography parameters (angle threshold and step size), and acquisition parameters (b-value and number of diffusion directions) affected the sensitivity and specificity of tractography reconstructions. Previous studies investigated the dependence of tractography on user-defined parameters (Chamberland et al., 2014; Thomas et al., 2014; Bastiani et al., 2012; Takemura et al., 2016) and agreed that no absolute optimal set of parameters exists. The choice of parameters strictly depends on the white matter region of interest and the specific white matter bundle that is investigated.

In this study, in terms of the AR reconstruction, deterministic results were less robust than probabilistic tractography when using the parameters in this study. Significant effects in the Dice coefficient were shown for the b-value and angle threshold only for deterministic reconstructions. For low b-values (1000 and 3000 s/mm^2), no, or only a few (<5), streamlines were reconstructed, and results were slightly improved increasing the angle threshold up to 60° (Figure 6.2). For higher b-values (1000 and 3000 s/mm^2), more streamlines belonging to the AR could be reconstructed. However, their anatomical accuracy remained lower than probabilistic results (Figure 6.5). Visual inspection

of tractograms suggests there may be false positive reconstructions at the level of the thalamus, that are not present in probabilistic counterparts (Figure 6.1).

Probabilistic tractography always reconstructed AR streamlines, even at low b-values. However, many of these reconstructed streamlines constituted false positive reconstructions (Figure 6.1). Most streamlines erroneously followed the course of the external capsule on the inferior-superior axis. Results greatly improved when small angles were used in the reconstruction (20°), obtaining anatomical accuracy comparable to that given when using high b-values (Figure 6.4). This might be important when reconstructing the AR at clinical protocols. Increasing the angle at high b-values only increased the false positive reconstructions and decreased anatomical accuracy, as previously shown (Thomas et al., 2014). The effect of varying the step size were almost negligible (Figure 6.6). However when using very low step sizes (<0.5), reconstructions became very noisy, as previously reported (Chamberland et al., 2014).

In summary, we found that in terms of comparison with the reference AR, the optimal parameter choices for the atlas reconstruction were: probabilistic tractography based on the b=10000 s/mm^2 data using the default reconstruction parameters (angle threshold = 45°, step size = 0.75 mm).

Atlas of the acoustic radiation

The reconstructions of the AR using the optimal parameters showed a high level of inter-subject variability. For example, the number of streamlines ranged from 0 to 631, and the volume ranged from 0 to 6834 ml. Inter-subject variability in tractography reconstructions has been previously investigated and can be related to individual anatomical differences, and concomitant methodological limitations like uncertainty in fibre orientation estimation due to noise, head movements, and partial volume effects (Jones, Cercignani, 2010; Thiebaut de Schotten et al., 2011; Heiervang et al., 2006; Pujol et al., 2015). Individual anatomical variability might be a factor in AR reconstruction. Both the Heschl's gyrus (HG) and the MGN, are subject to extreme anatomical variability across individuals, both in location and size (Rademacher et al., 2002; Bürgel et al., 2006). The HG is characterized by very different configurations across subjects, and even across hemispheres (Marie et al., 2015). Narrower and smaller configurations might make the tractography reconstruction more challenging.

This group variability was lower for FA values, in agreement with previous studies (Heiervang et al., 2006). However, FA values were overall very low (min 0.17- max 0.32), even lower than previous studies looking at FA values in the AR (Crippa et al., 2010). This is most likely related to the dense fibre crossing of this region (Chapter 5), and lower than what it is usually considered to be the threshold to differentiate grey and white matter (0.2). This poses limits on the possible uses of this metric to evaluate this specific white matter bundle, and makes the implementation of more advanced quantitative measures necessary (Raffelt et al., 2017; Dell'Acqua et al., 2010). In this study we also evaluate the AFD of the AR, as implemented in MRtrix3. At high b-values (as used in this study) the integral for a particular FOD 'lobe' is considered proportional to the intra-axonal volume of axons associated with that lobe (Raffelt et al., 2012). Compared

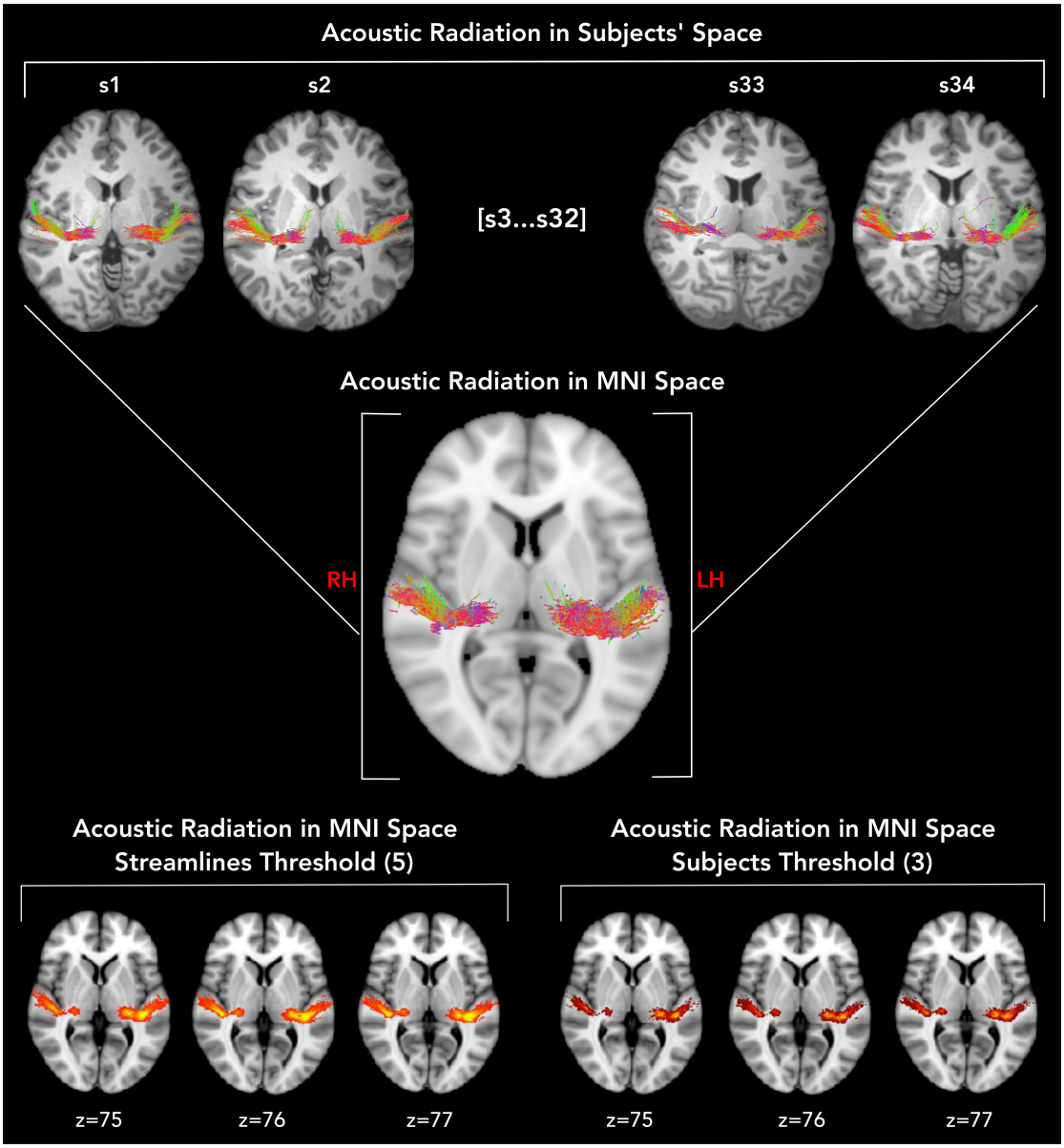

Figure 6.9: Atlas of the Acoustic Radiation. The figure shows the schematic pipeline for the construction of the AR atlas. As a first step, subject's specific reconstructed AR (top row) are non-linearly registered to the MNI152 T1 space. Then, the streamlines are transformed in track density images (TDI), with either number of streamlines or number of subjects as voxel value. The final AR atlas in MNI space is shown for each different types of threshold is shown, number of streamlines or number of subjects (bottom row).

to FA which is voxel-based, AFD is tract-specific. Only the lobes of the FOD that are associated to AR streamlines are used to compute the AFD. This makes AFD a more specific measure, less prone to complex fibre configuration biases. Similarly to tract volume, AFD showed high variability across subjects. This measures is been recently introduced (Raffelt et al., 2012, 2017) and used in clinical populations (Scheck et al., 2015). However, no studies have investigated its variability across subjects and white matter bundles.

Significant hemispheric difference was found in the AR reconstruction of the 34 subjects, showing a strong left lateralization (Figure 6.8). These results are in contrast with a previous histological study that found no significant asymmetry in the volume of the AR in 10 *post-mortem* brains (Rademacher et al., 2002). The small number of subjects we analyzed in this work limits the certainty of the results. More studies investigating this asymmetry in different populations, and using different methods are needed. However, our findings open interesting avenues for investigating the well-known relationship between the left hemisphere and language processing (Catani et al., 2005; Vernooij et al., 2007; Thiebaut de Schotten et al., 2011). For example, future research might investigate the relationship between this asymmetry and other features, such as handedness and gender.

Limitations and future directions

The results obtained in this study are restricted to the acquisition, diffusion and tractography parameters used. Different acquisition protocols, low level models, tractography parameters, and region of interests, could lead to different findings. In this study, for example, we did not investigate the effects of MRI spatial resolution (kept at 1.5 mm isotropic), which may affect tract reconstruction and diffusion metrics estimation (Laganà et al., 2010; Papinutto et al., 2013). However, previous studies showed that varying spatial resolution, up to certain limits ($< 2.5\ mm$ isotropic), did not affect tractography reconstructions as much as changes in angular resolution (Vos et al., 2016). Also, we did not specifically address whether it was the number of DW directions or the b-value that affected the reconstruction most. Given that optimal angular resolution might be obtained by a combination of the two, it is possible that the same results are obtainable for lower b-values and more DW directions (Vos et al., 2016; Tournier et al., 2007).

Comparing the tractograms with a reference AR allowed us to evaluate the results on an anatomical qualitative and quantitative basis. Increased number of streamlines, or increased volume, most often say nothing about the anatomical accuracy of the reconstruction. The reference allowed us to evaluate tractograms on the basis of their topographical accuracy. However, our reference had clear limitations. Being tractography-based itself, it suffers from the same limitations of the other reconstructions. The manual filtering was aimed at eliminating most false positive of the reconstruction. However, false negatives in the initial reconstruction may bias comparison with the other tractograms. Moreover, these references were reconstructed using probabilistic tractography, which might have favoured probabilistic tractograms in the comparison. Future studies might improve the quality of this comparison, using references obtained with different methods, such

as more advanced *post-mortem* validation techniques (Magnain et al., 2014). The Dice scores obtained in the study were overall low, and lower than other reports on different tracts (Kristo et al., 2013). However, those studies used the Dice coefficient to quantify test-retest reproducibility of the same tract over two different scans, thus making the comparison with our study not straightforward. As a further step of the study, we plan to evaluate the spatial extent (volume) of the tractograms in comparison to the spatial extent of the reference bundle. This could give us more information about the rate of false positive and false negative present in the tractography reconstructions.

In previous work on *post-mortem* dissections, we defined three sub-components of the AR bundle: the *genu*, the *stem*, and the *fan* (Maffei et al., 2017) (Chapter 5). Future steps of this study will include applying this knowledge on the reconstructed AR, by isolating the AR stem. Previous studies have shown that performing tractography from the stem improves the final tractography reconstruction, by minimizing the constrained posed by cortical terminations (Hau et al., 2016). We think this might help on different fronts in the tractography reconstruction of the AR : we would avoid seeding from the thalamus, which is well-known to be challenging in tractography (Thomas et al., 2014) and we might increase the number of streamlines that successfully reach the cortex on HG, given that the AR stem is lateral to the intermingling fibres of the internal capsule.

Conclusion

This study presents the first tractography atlas of the acoustic radiation from a population of 34 young healthy subjects. The atlas was constructed using high quality MRI data from the Human Connectome Project. The acoustic radiation reconstruction was optimized with a systematic evaluation of MRI acquisition and analysis parameters using as reference reconstructions validated from an *ex-vivo* dissection study from our group Maffei et al. (2017). The optimized reconstruction parameters and the atlas may be used in future studies interested in identifying and characterizing the acoustic radiation.

Bibliography

Avants B B, Epstein C L, Grossman M, Gee J C. Symmetric diffeomorphic image registration with cross-correlation: evaluating automated labeling of elderly and neurodegenerative brain. // Medical image analysis. feb 2008. 12, 1. 26–41.

Bastiani Matteo, Shah Nadim Jon, Goebel Rainer, Roebroeck Alard. Human cortical connectome reconstruction from diffusion weighted MRI: The effect of tractography algorithm // NeuroImage. 2012. 62, 3. 1732–1749.

Bauer Miriam H A, Kuhnt Daniela, Barbieri Sebastiano, Klein Jan, Becker Andreas, Freisleben Bernd, Hahn Horst K, Nimsky Christopher, Baron Jean-Claude. Reconstruction of White Matter Tracts via Repeated Deterministic Streamline Tracking – Initial Experience // PLoS ONE. 2013. 8, 5.

Bürgel Uli, Amunts Katrin, Hoemke Lars, Mohlberg Hartmut, Gilsbach Joachim M, Zilles Karl. White matter fiber tracts of the human brain: Three-dimensional mapping at microscopic resolution, topography and intersubject variability // NeuroImage. 2006. 29, 4. 1092–1105.

Calabrese Evan, Badea Alexandra, Coe Christopher L., Lubach Gabriele R., Styner Martin A., Johnson G. Allan. Investigating the tradeoffs between spatial resolution and diffusion sampling for brain mapping with diffusion tractography: Time well spent? // Human Brain Mapping. 2014. 5685, February 2013. n/a–n/a.

Catani Marco, Jones Derek K., Ffytche Dominic H. Perisylvian language networks of the human brain // Annals of Neurology. 2005. 57, 1. 8–16.

Chamberland Maxime, Whittingstall Kevin, Fortin David, Mathieu David, Descoteaux Maxime. Real-time multi-peak tractography for instantaneous connectivity display // Frontiers in Neuroinformatics. 2014. 8, May. 1–15.

Crippa Alessandro, Lanting Cris P, Dijk Pim van, Roerdink Jos B T M. A diffusion tensor imaging study on the auditory system and tinnitus. // The open neuroimaging journal. 2010. 4. 16–25.

Dayan Michael, Kreutzer Sylvia, Clark Chris A. Tractography of the optic radiation: a repeatability and reproducibility study // NMR in Biomedicine. apr 2015. 28, 4. 423–431.

Dell'Acqua Flavio, Scifo Paola, Rizzo Giovanna, Catani Marco, Simmons Andrew, Scotti Giuseppe, Fazio Ferruccio. A modified damped Richardson-Lucy algorithm to reduce isotropic background effects in spherical deconvolution // NeuroImage. 2010. 49, 2. 1446–1458.

Dice Lee R. Measures of the Amount of Ecologic Association Between Species // Ecology. jul 1945. 26, 3. 297–302.

Domin Martin, Langner Sönke, Hosten Norbert, Lotze Martin, Perry M. Comparison of Parameter Threshold Combinations for Diffusion Tensor Tractography in Chronic Stroke Patients and Healthy Subjects // PLoS ONE. may 2014. 9, 5. e98211.

Fan Qiuyun, Witzel Thomas, Nummenmaa Aapo, Van Dijk Koene R.A., Van Horn John D., Drews Michelle K., Somerville Leah H., Sheridan Margaret A., Santillana Rosario M., Snyder Jenna, Hedden Trey, Shaw Emily E., Hollinshead Marisa O., Renvall Ville, Zanzonico Roberta, Keil Boris, Cauley Stephen, Polimeni Jonathan R., Tisdall Dylan, Buckner Randy L., Wedeen Van J., Wald Lawrence L., Toga Arthur W., Rosen Bruce R. MGH–USC Human Connectome Project datasets with ultra-high b-value diffusion MRI // NeuroImage. 2015.

Frank Lawrence R. Anisotropy in high angular resolution diffusion-weighted MRI // Magnetic Resonance in Medicine. jun 2001. 45, 6. 935–939.

Girard Gabriel, Whittingstall Kevin, Deriche Rachid, Descoteaux Maxime. Towards quantitative connectivity analysis : reducing tractography biases // NeuroImage. 2014. 98. 266–278.

Hau Janice, Sarubbo Silvio, Perchey Guy, Crivello Fabrice, Zago Laure, Mellet Emmanuel, Jobard Gaël, Joliot Marc, Mazoyer Bernard M, Tzourio-Mazoyer Nathalie, Petit Laurent. Cortical Terminations of the Inferior Fronto-Occipital and Uncinate Fasciculi: Anatomical Stem-Based Virtual Dissection. // Frontiers in neuroanatomy. 2016. 10. 58.

Heiervang E., Behrens T.E.J., Mackay C.E., Robson M.D., Johansen-Berg H. Between session reproducibility and between subject variability of diffusion MR and tractography measures // NeuroImage. nov 2006. 33, 3. 867–877.

Jeurissen Ben, Tournier Jacques-Donald, Dhollander Thijs, Connelly Alan, Sijbers Jan. Multi-tissue constrained spherical deconvolution for improved analysis of multi-shell diffusion MRI data // NeuroImage. 2014. 103. 411–426.

Jones Derek K, Cercignani Mara. Twenty-five pitfalls in the analysis of diffusion MRI data // NMR in Biomedicine. 2010. 23, 7. 803–820.

Kristo Gert, Leemans Alexander, Raemaekers Mathijs, Rutten Geert-Jan, Gelder Beatrice de, Ramsey Nick F. Reliability of two clinically relevant fiber pathways reconstructed with constrained spherical deconvolution // Magnetic Resonance in Medicine. dec 2013. 70, 6. 1544–1556.

Laganà M., Rovaris M., Ceccarelli A., Venturelli C., Marini S., Baselli G. DTI Parameter Optimisation for Acquisition at 1.5T: SNR Analysis and Clinical Application // Computational Intelligence and Neuroscience. 2010. 2010. 1–8.

Maffei Chiara, Jovicich Jorge, De Benedictis Alessandro, Corsini Francesco, Barbareschi Mattia, Chioffi Franco, Sarubbo Silvio. Topography of the human acoustic radiation

as revealed by ex vivo fibers micro-dissection and in vivo diffusion-based tractography // Brain Structure and Function. sep 2017. 1–11.

Magnain Caroline, Augustinack Jean C., Reuter Martin, Wachinger Christian, Frosch Matthew P., Ragan Timothy, Akkin Taner, Wedeen Van J., Boas David A., Fischl Bruce. Blockface histology with optical coherence tomography: A comparison with Nissl staining // NeuroImage. jan 2014. 84. 524–533.

Marie D, Jobard G, Crivello F, Perchey G, Petit L, Mellet E, Joliot M, Zago L, Mazoyer B, Tzourio-Mazoyer N. Descriptive anatomy of Heschl's gyri in 430 healthy volunteers, including 198 left-handers. // Brain structure & function. mar 2015. 220, 2. 729–43.

Papinutto Nico Dario, Maule Francesca, Jovicich Jorge. Reproducibility and biases in high field brain diffusion MRI: An evaluation of acquisition and analysis variables // Magnetic Resonance Imaging. jul 2013. 31, 6. 827–839.

Patenaude Brian, Smith Stephen M, Kennedy David, Jenkinson Mark. A Bayesian model of shape and appearance for subcortical brain segmentation // Neuroimage. 2012. 56, 3. 907–922.

Pujol Sonia, Wells William, Pierpaoli Carlo, Brun Caroline, Gee James, Cheng Guang, Vemuri Baba, Commowick Olivier, Prima Sylvain, Stamm Aymeric, Goubran Maged, Khan Ali, Peters Terry, Neher Peter, Maier-Hein Klaus H, Shi Yundi, Tristan-Vega Antonio, Veni Gopalkrishna, Whitaker Ross, Styner Martin, Westin Carl-Fredrik, Gouttard Sylvain, Norton Isaiah, Chauvin Laurent, Mamata Hatsuho, Gerig Guido, Nabavi Arya, Golby Alexandra, Kikinis Ron. The DTI Challenge: Toward Standardized Evaluation of Diffusion Tensor Imaging Tractography for Neurosurgery. // Journal of neuroimaging : official journal of the American Society of Neuroimaging. 2015. 25, 6. 875–82.

Rademacher J, Bürgel U, Zilles K. Stereotaxic localization, intersubject variability, and interhemispheric differences of the human auditory thalamocortical system. // NeuroImage. sep 2002. 17, 1. 142–60.

Raffelt David, Tournier J. Donald, Rose Stephen, Ridgway Gerard R., Henderson Robert, Crozier Stuart, Salvado Olivier, Connelly Alan. Apparent Fibre Density: A novel measure for the analysis of diffusion-weighted magnetic resonance images // NeuroImage. 2012. 59, 4. 3976–3994.

Raffelt David A, Tournier J. Donald, Smith Robert E, Vaughan David N, Jackson Graeme, Ridgway Gerard R, Connelly Alan. Investigating white matter fibre density and morphology using fixel-based analysis // NeuroImage. jan 2017. 144, Pt A. 58–73.

Scheck Simon M., Pannek Kerstin, Raffelt David A., Fiori Simona, Boyd Roslyn N., Rose Stephen E. Structural connectivity of the anterior cingulate in children with

unilateral cerebral palsy due to white matter lesions // NeuroImage: Clinical. 2015. 9. 498–505.

Smith Robert E., Tournier Jacques-Donald, Calamante Fernando, Connelly Alan. Anatomically-constrained tractography: Improved diffusion MRI streamlines tractography through effective use of anatomical information // NeuroImage. 2012. 62, 3. 1924–1938.

Springer Jane A., Binder Jeffrey R., Hammeke Thomas A., Swanson Sara J., Frost Julie A., Bellgowan Patrick S. F., Brewer Cameron C., Perry Holly M., Morris George L., Mueller Wade M. Language dominance in neurologically normal and epilepsy subjects // Brain. nov 1999. 122, 11. 2033–2046.

Takemura Hiromasa, Caiafa Cesar F., Wandell Brian A., Pestilli Franco. Ensemble Tractography // PLoS Computational Biology. 2016. 12, 2. 1–22.

Thiebaut de Schotten Michel, Ffytche Dominic H, Bizzi Alberto, Dell'Acqua Flavio, Allin Matthew, Walshe Muriel, Murray Robin, Williams Steven C, Murphy Declan G M, Catani Marco. Atlasing location, asymmetry and inter-subject variability of white matter tracts in the human brain with MR diffusion tractography. // NeuroImage. jan 2011. 54, 1. 49–59.

Thomas Cibu, Ye Frank Q., Irfanoglu M. Okan, Modi Pooja, Saleem Kadharbatcha S., Leopold David A., Pierpaoli Carlo. Anatomical accuracy of brain connections derived from diffusion MRI tractography is inherently limited // Proceedings of the National Academy of Sciences. nov 2014. 111, 46. 16574–16579.

Tournier J. Donald, Calamante Fernando, Connelly Alan. Robust determination of the fibre orientation distribution in diffusion MRI: Non-negativity constrained super-resolved spherical deconvolution // NeuroImage. may 2007. 35, 4. 1459–1472.

Tournier J. Donald, Calamante Fernando, Connelly Alan. MRtrix: Diffusion tractography in crossing fiber regions // International Journal of Imaging Systems and Technology. 2012. 22, 1. 53–66.

Vernooij M.W., Smits M., Wielopolski P.A., Houston G.C., Krestin G.P., Lugt A. van der. Fiber density asymmetry of the arcuate fasciculus in relation to functional hemispheric language lateralization in both right- and left-handed healthy subjects: A combined fMRI and DTI study // NeuroImage. apr 2007. 35, 3. 1064–1076.

Vos Sjoerd B., Aksoy Murat, Han Zhaoying, Holdsworth Samantha J., Maclaren Julian, Viergever Max A., Leemans Alexander, Bammer Roland. Trade-off between angular and spatial resolutions in in vivo fiber tractography // NeuroImage. apr 2016. 129. 117–132.

Vos Sjoerd B, Jones Derek K, Jeurissen Ben, Viergever Max A, Leemans Alexander. The influence of complex white matter architecture on the mean diffusivity in diffusion tensor MRI of the human brain // NeuroImage. 2012. 59, 3. 2208–2216.

Zhang Yongyue, Brady Michael, Smith Stephen. Segmentation of Brain MR Images Through a Hidden Markov Random Field Model and the Expectation-Maximization Algorithm // IEEE Transactions on Medical Imaging. 2001. 20, 1. 45–57.

Chapter 7

Application of the acoustic radiation atlas in a study of congenitally deaf subjects

7.1 Introduction

Hearing loss is accompanied by functional and structural changes in the brain of deaf subjects. At the functional level, cross-modal reorganization mechanisms (Lomber et al., 2010) drive visual, linguistic, tactile, and somatosensory stimuli to be processed in the auditory cortex (Petitto et al., 2000; MacSweeney et al., 2002; Finney et al., 2001; Bola et al., 2017). Brain structural changes associated with hearing loss have been mostly seen in white matter rather than in gray matter. White matter changes in early deaf include increased mean (MD) and radial diffusivity (RD) in frontal regions (Lyness et al., 2014), reduced fractional anisotropy (FA) in the Heschl's gyrus (HG) and the anterior and posterior superior temporal gyrus (aSTG, pSTG), reduced FA in the posterior corpus callosum (CC), and decreased white matter volume in HG. (Li et al., 2012; Kim et al., 2009; Karns et al., 2017; Hribar et al., 2014; Emmorey et al., 2003). In contrast, although animal studies show neuronal degeneration for midbrain structures (Nishiyama et al., 2000), no reduction in grey matter volume has been reported in the auditory cortices of early deaf subjects (Emmorey et al., 2003; Shibata, 2007).

These changes are consistent with the view that in congenital deafness, while thalamocortical afferent pathways are subject to degeneration because of sensory deprivation, auditory cortices get involved in processing other types of stimuli, thus remaining physiologically preserved (Lomber et al., 2010; Petitto et al., 2000; MacSweeney et al., 2002; Finney et al., 2001; Bola et al., 2017).

It remains unclear which specific white matter structural changes accompany congenital and early deafness. A few recent studies agree in showing that structural hemispheric

asymmetry is different between deaf and healthy controls, yet the anatomical features changing are different across studies. Karns et al. (2017) found the largest differences between hearing and deaf subjects in the right STG; Hribar et al. (2014) found decreased white matter volume only in left HG; while Amaral et al. (2016) showed that for deaf, but not for hearing individuals, the right thalamus, right lateral geniculate nucleus and right inferior colliculus are larger than their left counterparts; Shibata (2007) reported decreased white matter volume in the left STG of deaf subjects.

These differences in reported hemispheric differences might be related to the fact that in deaf subjects altered sensory experience is concomitant with altered language experience (*e.g.*, a lifetime experience with sign language), and different deaf populations might have very different language experiences (*i.e.*lip reading and sign language, only sign language, only lip reading).

It has been suggested that the decrease in white matter observed in the left STG and HG in deaf subjects is due to a decreased volume of auditory tracts (Shibata, 2007). However, to our knowledge, no study has investigated the deafness-induced changes in the acoustic radiation pathways. This is mainly due to the difficulties in reconstructing these fibres *in-vivo* using tractography techniques (Chapter 6).

Even though animal studies suggest absence of large-scale connectional changes in thalamo-cortical projections (Meredith, Allman, 2012; Butler et al., 2016), white matter changes in auditory areas in humans suggest at least partial degeneration of these connections (Shibata, 2007; Emmorey et al., 2003). Understanding the deafness-induced mechanisms on these connections may help elucidate how the deaf brain reorganizes, also in relation to language experience.

The goal of this study is to investigate how deafness affects the acoustic radiation (AR) by comparing diffusion-related quantitative measures between a group of deaf subjects and a group of age and gender matched hearing controls. To define the acoustic radiation region of interest (ROI), the acoustic radiation atlas built in 6 was used. This study constitutes both a preliminary investigation and a first "application case" for our AR atlas.

7.2 Methods

Subjects

10 congenital deaf subjects (5 females, mean age= 33 years, SD=7.9) and 10 age and gender matched hearing controls (5 females, mean age = 30.5 years, SD=3.9) participated in the study, which was approved by the Ethical Committee of the University of Trento. Subject recruitment was done by the group of Prof. Olivier Collignon. Both deaf subjects and hearing controls had no previous history of neurological or psychiatric illness. The hearing subjects had no history of hearing disorders.

Brain MRI Acquisition

A 4T Bruker Medspec MRI scanner was used to acquire diffusion (2.3 mm isotropic voxel, 60 DW volumes, 10b=0 volumes, b=1500 s/mm^2, $TE = 99$ ms) and T1 anatomical (MPRAGE, 1 mm isotropic) data. MRI scanning was done by the group of Prof. Collignon using a protocol defined in collaboration with the MRI methods group.

Brain Data Processing

Diffusion data were corrected for eddy currents and head motion in FSL followed by bias field correction and global intensity normalization in MrTrix3 (Tournier et al., 2012). A response function was estimated in each subject from voxels containing only one fiber direction ($lmax = 6$). Diffusion data were then up-sampled ($1 \times 1 \times 1$ mm^3) to improve anatomical accuracy. Fiber orientation distributions (FODs) were estimated for each voxel starting from a group-specific average response function. The tensor model was also fit to the data to estimate fractional anisotropy (FA) , radial, mean and axial diffusivity (RD, MD and AD, respectively) scalar maps. Apparent fiber density (AFD) scalar maps were also computed for each subject taking the first spherical harmonic coefficient. This describes the total size (integral) of the FOD at each voxel.

To isolate the AR, the atlas built in Chapter 6 was used. First the diffusion space of each participant was warped into the standard MNI space, through a two steps diffeomorphic registration performed in ANTS software, using the T1 image as a middle anchoring step (FA subject to T1 subject to T1 MNI). The inverse registrations were then applied to bring the AR atlas ROI into the diffusion space of each subject.

Once the AR atlas was mapped to each subject, the mean FA and AFD were computed, separately for each hemispheric AR. Group differences of diffusion measures (FA, RD, MD, AD and AFD) in the AR were then tested using a non-parametric 2-tailed paired Wilcoxon rank sum test between the deaf group and the matched hearing controls. Statistics were done using RStudio.

7.3 Results and discussion

Results showed reduction in FA extracted values between deaf and hearing controls in both hemispheres (Figure 7.1). However, this difference was significant in the left ($p < 0.01$) but not in the right hemisphere ($p > 0.05$). Deaf subjects had lower AFD values in the left hemisphere, compared to controls, but the difference was not significant ($p > 0.05$). The remaining DTI measures (MD, RD and AD) showed all bilateral significant increase in deaf relative to hearing subjects (Figure 7.2).

The altered micro- and macrostructure of the WM in the auditory areas are the most documented differences in brain structure between deaf and normal hearing subjects (Shibata, 2007; Emmorey et al., 2003; Karns et al., 2017; Amaral et al., 2016). In agreement with this, relative to healthy controls, we found a significant reduction of FA in the left hemisphere AR of the deaf subjects, and significant bilateral increases of MD, RD and AD. Non significant effects were found for AFD. These results are in line with previous findings on FA reduction in the left HG (Hribar et al., 2014). They support the hypothesis that auditory differentiation, following sensory deprivation,

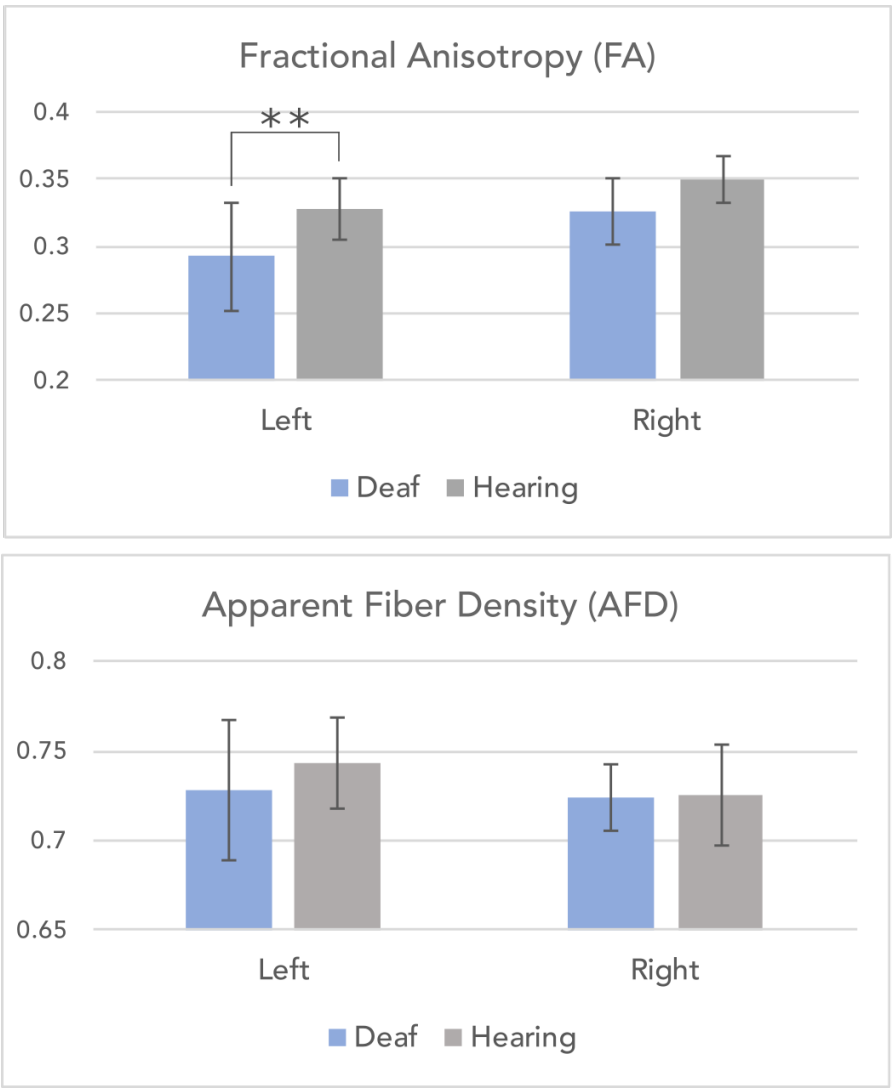

Figure 7.1: Acoustic Radiation Differences Between Deaf and Hearing Controls. The graph reports group means of diffusion measures averaged on the acoustic radiation ROI in deaf and hearing controls. Stars indicate significant differences (** $= p < 0.01$).

results in less myelination, fewer fibers projecting to and from auditory cortices, or greater axonal pruning in the congenitally deaf (Emmorey et al., 2003; Butler et al., 2016). Demyelination or axonal degeneration often cause the anisotropy to decrease, which may result in increased radial diffusivity and reduced or unaffected axial diffusivity (Alexander et al., 2007). In our study we also found significant increases of MD, RD, and also AD in deaf subjects relative to controls. Increases in MD and AD may be associated to both axonal damage and demyelination (Alexander et al., 2007), and have been associated to aging (Bennett et al., 2010).

However, even if it might be tempting to interpret these differences of diffusion scalar metrics in terms of biological changes in deaf compared to hearing subjects, caution must be taken. Interpretation of DTI measures is challenging because of the indirect nature of DWI and the presence of multiple fibre configuration per voxel (Jones, Cercignani, 2010; Alexander et al., 2007, 2001; Vos et al., 2012). The AR is located in a region with dense crossing fibres inside voxels 5, and as observed in 6 FA values are lower in AR than what commonly reported for other white matter bundles. In crossing fibre configurations, degeneration of one fiber bundle could cause the other fiber bundle to become more dominant, resulting in an increase in FA or MD, making difficult to interpret results (Vos et al., 2012; Song et al., 2002; Jones, Cercignani, 2010). As anticipated in Chapter 6, different quantitative measures are necessary in order to draw more reliable conclusions on the acoustic radiation. In this study we complement DTI with apparent fiber density (AFD) measures. Results did not show significant differences in the two groups for this measure. Interestingly, while FA is higher in the right hemisphere of hearing subjects, AFD shows the opposite trend, in agreement with results we report in chapter 6. However, we note that in this study the AFD still represents a voxel-based measure, and thus is influenced from the same averaging issues related to tensor measures. In the future we will consider the combination of these measures with other imaging measures (*e.g.*, T1, T2), which may help to improve the precision of AR quantification in these subjects. Also, we will perform tractography reconstruction of the AR to improve the anatomical specificity in defining the auditory pathways in the deaf and hearing subjects. Tractography reconstructions will allow us to extract sub-voxel orientation-specific quantitative measures (Raffelt et al., 2017), that are less influenced by complex fibre configuration inside the voxel. Tractography will also allow us to compare the reproducibility of the atlas-based AR results, as well as to evaluate the sensitivity of the atlas to subject-specific anatomy, both in the control and deaf group. This might be particularly important considering the leftward asymmetry that we found in the reconstructed AR (Chapter 6, which might be different in deaf subjects. We observed leftward asymmetry in hearing subjects for AFD, MD, and RD measures, while FA was right lateralized and AD bilateral (Figure 7.2). Significant hemispheric differences were found for FA ($p < 0.01$), MD ($p < o.05$), and RD ($p < 0.01$). AFD was not significantly different between hemispheres. Deaf subjects exhibit the same asymmetry as control hearing subjects for all measures but AFD, which is more bilaterally distributed. Significant hemispheric differences in deaf subjects were found for FA ($p < 0.01$), MD ($p < 0.01$) and RD ($p < 0.01$). Previous studies investigated asymmetry in deaf subjects. They report that for deaf, but not for

hearing individuals, the right thalamus, right lateral geniculate nucleus and right inferior colliculus are larger than their left counterparts deafness(Amaral et al., 2016). Other studies report STG, HG, and planum temporale (PT) grey matter asymmetry in both deaf and control groups, while others report grey matter asymmetry in STG for hearing subjects but not for deaf (Shibata, 2007).

The discrepancy of areas with altered white matter structure among previous studies, and the different results on asymmetry, might lie in the differences between the groups of deaf participants, the number of subjects, the methods used, and the different regions of interested. In particular, a challenge in assessing deafness is that altered sensory experience is concomitant with altered language experience. Participants differ in their speech-reading and sign language skills. Therefore, it is difficult to make attributions solely to auditory deprivation. In this preliminary analysis we included hearing subjects who have no signing experience. In future steps of this project we will include hearing subjects who learn sign language from birth, to differentiate sensory and language experience.

In conclusion, preliminary results of this study show for the first time a characterization and comparison of the acoustic radiation in congenital blind subjects relative to healthy controls. Relative to healthy controls, congenitally deaf subjects with no sign language knowledge, showed a left hemisphere reduction of FA with bilateral increases of MD, RD and AD. These findings, with the known limitations of scalar diffusion tensor data from an area with fiber crossing, support the idea of axonal damage in the acoustic radiation related to auditory deprivation. Further studies are needed to further clarify the role of learning sign language. The reconstruction of the auditory pathways in deaf subjects will add important information on the reorganization of brain structures after sensory deprivation.

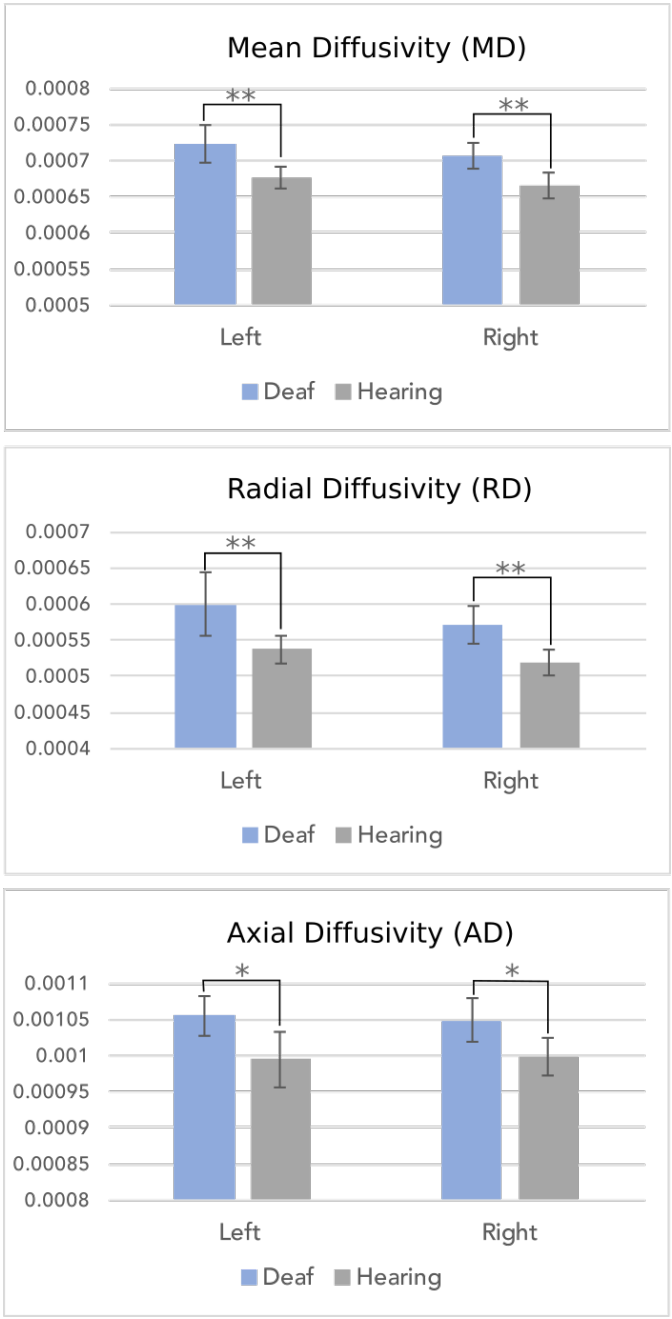

Figure 7.2: Acoustic Radiation Differences Between Deaf and Hearing Controls. The graph reports group means of diffusion measures averaged on the acoustic radiation ROI in deaf and hearing controls. Stars indicate significant differences (** $= p < 0.01$, ** $= p < 0.05$).

Bibliography

Alexander Andrew L., Hasan Khader M., Lazar Mariana, Tsuruda Jay S., Parker Dennis L. Analysis of partial volume effects in diffusion-tensor MRI // Magnetic Resonance in Medicine. may 2001. 45, 5. 770–780.

Alexander Andrew L, Lee Jee Eun, Lazar Mariana, Field Aaron S. Diffusion tensor imaging of the brain. // Neurotherapeutics : the journal of the American Society for Experimental NeuroTherapeutics. jul 2007. 4, 3. 316–29.

Amaral L., Ganho-Ávila A., Osório A., Soares M. J., He D., Chen Q., Mahon B. Z., Gonçalves O. F., Sampaio A., Fang F., Bi Y., Almeida J. Hemispheric asymmetries in subcortical visual and auditory relay structures in congenital deafness // European Journal of Neuroscience. sep 2016. 44, 6. 2334–2339.

Bennett Ilana J, Madden David J, Vaidya Chandan J, Howard Darlene V, Howard James H, Jr. . Age-related differences in multiple measures of white matter integrity: A diffusion tensor imaging study of healthy aging. // Human brain mapping. mar 2010. 31, 3. 378–90.

Bola Łukasz, Zimmermann Maria, Mostowski Piotr, Jednoróg Katarzyna, Marchewka Artur, Rutkowski Paweł, Szwed Marcin. Task-specific reorganization of the auditory cortex in deaf humans. // Proceedings of the National Academy of Sciences of the United States of America. jan 2017. 114, 4. E600–E609.

Butler Blake E., Chabot Nicole, Lomber Stephen G. Quantifying and comparing the pattern of thalamic and cortical projections to the posterior auditory field in hearing and deaf cats // Journal of Comparative Neurology. oct 2016. 524, 15. 3042–3063.

Emmorey Karen, Allen John S, Bruss Joel, Schenker Natalie, Damasio Hanna. A morphometric analysis of auditory brain regions in congenitally deaf adults // PNAS. 2003. 100, 17. 10049–10054.

Finney Eva M., Fine Ione, Dobkins Karen R. Visual stimuli activate auditory cortex in the deaf. // Nature Neuroscience. dec 2001. 4, 12. 1171–1173.

Hribar Manja, Šuput Dušan, Carvalho Altiere Araujo, Battelino Saba, Vovk Andrej. Structural alterations of brain grey and white matter in early deaf adults // Hearing Research. 2014. 318. 1–10.

Jones Derek K, Cercignani Mara. Twenty-five pitfalls in the analysis of diffusion MRI data // NMR in Biomedicine. 2010. 23, 7. 803–820.

Karns Christina M., Stevens Courtney, Dow Mark W., Schorr Emily M., Neville Helen J. Atypical white-matter microstructure in congenitally deaf adults: A region of interest and tractography study using diffusion-tensor imaging // Hearing Research. jan 2017. 343. 72–82.

Kim Dae-Jin, Park Seong-Yong, Kim Jinna, Lee Dong Ha, Park Hae-Jeong. Alterations of white matter diffusion anisotropy in early deafness // NeuroReport. jul 2009. 20, 11. 1032–1036.

Li Yanyan, Ding Guosheng, Booth James R., Huang Ruiwang, Lv Yating, Zang Yufeng, He Yong, Peng Danling. Sensitive period for white-matter connectivity of superior temporal cortex in deaf people // Human Brain Mapping. feb 2012. 33, 2. 349–359.

Lomber Stephen G, Meredith M Alex, Kral Andrej. Cross-modal plasticity in specific auditory cortices underlies visual compensations in the deaf // Nature Neuroscience. nov 2010. 13, 11. 1421–1427.

Lyness Rebecca C, Alvarez I, Sereno Martin I, MacSweeney Mairéad. Microstructural differences in the thalamus and thalamic radiations in the congenitally deaf. // NeuroImage. oct 2014. 100, 100. 347–57.

MacSweeney Mairéad, Woll Bencie, Campbell Ruth, McGuire Philip K, David Anthony S, Williams Steven C R, Suckling John, Calvert Gemma A, Brammer Michael J. Neural systems underlying British Sign Language and audio-visual English processing in native users. // Brain : a journal of neurology. jul 2002. 125, Pt 7. 1583–93.

Meredith M Alex, Allman Brian L. Early hearing-impairment results in crossmodal reorganization of ferret core auditory cortex. // Neural plasticity. 2012. 2012. 601591.

Nishiyama N, Hardie N A, Shepherd R K. Neonatal sensorineural hearing loss affects neurone size in cat auditory midbrain. // Hearing research. feb 2000. 140, 1-2. 18–22.

Petitto L. A., Zatorre R. J., Gauna K., Nikelski E. J., Dostie D., Evans A. C. Speech-like cerebral activity in profoundly deaf people processing signed languages: Implications for the neural basis of human language // Proceedings of the National Academy of Sciences. dec 2000. 97, 25. 13961–13966.

Raffelt David A, Tournier J. Donald, Smith Robert E, Vaughan David N, Jackson Graeme, Ridgway Gerard R, Connelly Alan. Investigating white matter fibre density and morphology using fixel-based analysis // NeuroImage. jan 2017. 144, Pt A. 58–73.

Shibata D. K. Differences in brain structure in deaf persons on MR imaging studied with voxel-based morphometry // American Journal of Neuroradiology. 2007. 28, 2. 243–249.

Song Sheng-Kwei, Sun Shu-Wei, Ramsbottom Michael J, Chang Chen, Russell John, Cross Anne H. Dysmyelination revealed through MRI as increased radial (but unchanged axial) diffusion of water. // NeuroImage. nov 2002. 17, 3. 1429–36.

Tournier J. Donald, Calamante Fernando, Connelly Alan. MRtrix: Diffusion tractography in crossing fiber regions // International Journal of Imaging Systems and Technology. 2012. 22, 1. 53–66.

Vos Sjoerd B, Jones Derek K, Jeurissen Ben, Viergever Max A, Leemans Alexander. The influence of complex white matter architecture on the mean diffusivity in diffusion tensor MRI of the human brain // NeuroImage. 2012. 59, 3. 2208–2216.

Chapter 8

Other Applications

8.1 Introduction

This chapter focuses on two studies that used diffusion-based tractography techniques to investigate different aspects of brain reorganization, both using expertise gained from the acoustic radiation studies described in the previous Chapters.

The first study evaluates brain plasticity effects resulting from visual deprivation, in particular by characterizing changes in the optic radiation in early and late blind subjects relative to sighted controls. The second study evaluates post infarct brain reorganization and related language disorders, in particular by characterizing the structure of the middle longitudinal fasciculus in two patients affected by pure word deafness.

These studies represent examples of diffusion tractography applications in special and clinical populations.

8.2 A study of structural brain plasticity of the visual system in blind subjects

8.2.1 Introduction

Ample evidence shows that the visually deprived brain is capable of both major structural and functional reorganization (Merabet, Pascual-Leone, 2010). Functional studies in humans showed that the occipital cortex of blind subjects can process tactile (Burton et al., 2002) and auditory information (Poirier et al., 2006) and that engages in many other higher cognitive functions, such as memory and language (Burton et al., 2002; Melzer et al., 2001).

At the structural level, animal studies showed that in conditions of early visual deprivation reorganization of the thalamo-cortical interconnections can occur (Ghazanfar, Schroeder, 2006). Using voxel-based-morphometry (VBM), several human studies reported atrophy in both grey and white matter structures of the visual system of blind

subjects compared to sighted controls (SC). These regions include the LGN, the pulvinar nuclei, visual striate and extrastriate areas, the inferior temporal gyrus (ITG), the lateral orbital cortex, the optic tract and optic chiasm, the optic radiation, and the splenium of the corpus callosum (Beatty et al., 1982; Bridge et al., 2009; Leporé et al., 2010; Noppeney et al., 2005; Pan et al., 2007; Bauer et al., 2017; Shu et al., 2009; Wang et al., 2014).

The optic radiation (OR) represents the main white matter pathway to convey visual input from the lateral geniculate nucleus (LGN) of the thalamus to the occipital cortex, where this information is elaborated. Its anatomy has been largely investigated in post-mortem dissection and tractography studies in healthy subjects (Kammen et al., 2016; Lim et al., 2015; Renauld et al., 2016; Sarubbo et al., 2015; Clatworthy et al., 2010). However, little is known about the anatomical profile of the OR fibres in blind subjects. In particular, it remains unclear whether changes to this structure differ between blind subjects with visual deprivation before and after a critical developmental period. Using diffusion tensor imaging (DTI) and a region of interest (ROI)-based approach, some studies have found widespread fractional anisotropy (FA) differences in early blind (EB) relative to SC, but no differences between late blind (LB) and SC. Others have found significant atrophy in the visual cortex and optic radiation of both EB and LB (Leporé et al., 2010; Wang et al., 2013). In addition, the white matter volume in the optic radiation of the EB has been found to decrease progressively with aging and with increasing duration of blindness, suggesting that the reduction of white matter volume in the OR of the EB might occur progressively later in life, presumably through disuse-related mechanisms (Pan et al., 2007). Despite the large number of studies investigating the white matter anatomical reorganization of the blind brain, only few of them have used diffusion-based tractography to look at the profile of the optic radiation in visually deprived subjects (Shimony et al., 2006; Schoth et al., 2006).

The OR mainly includes connections between the LGN and the primary visual area (V1), representing the geniculo-striate pathway. However other exstrastriate connections between the LGN and secondary visual areas have been reported (exstrastriate pathway). Among these, direct connections between the LGN and the secondary middle temporal areas (V5) have been described (Abed Rabbo et al., 2015). These connections were first put forward by the observation of Riddochs syndrome in patients with lesions to primary visual cortex, that maintained visual processing abilities (Riddoch, 1917). This phenomenon was later described as blindsight and direct connections between LGN and V5 were considered responsible for this mechanism. These connections have been observed in macaques (Sincich et al., 2004) and more recently reconstructed using diffusion-based tractography (Bridge et al., 2009; Arrigo et al., 2016). Functional studies show that in early blind subjects visual motion areas (V5) are recruited for auditory motion processing , as a consequence of cross-modal mechanisms (Poirier et al., 2006; Saenz et al., 2008). However the structural re-organization of these pathways in blind subjects remains unknown.

Within the general goal of characterizing brain plasticity changes in early and late blind relative to normal sighted subjects, the specific goals of this study are to: i) charac-

terize white matter changes in the optic radiation, particularly in LGN-V1 and LGN-V5 tractography reconstructions; ii) characterize grey matter structural differences in visual areas, particularly in V1 and V5; iii) test whether sight deprivation age onset and years of blindness affects the reorganization of OR's and visual areas.

8.2.2 Methods

Subjects

17 early blind (6 males, mean age 33, blindness age onset $\leq$ 3 years old) and 11 late blind (8 males, mean age 42, blindness age onset $>$ 3 years old) subjects were investigated in comparison with two gender- and age-matched groups of healthy sighted controls. None of the EB subjects had visual memory. Etiology of blindness included: retinitis pigmentosa, retinopathy prematurity, leber congenital amaurosis, congenital glaucoma, retrolentar fibroplasia.

Brain MRI acquisition

A 4T Bruker Medspec MRI scanner was used to acquire diffusion ($2.3mm$ isotropic voxel, 60 DW volumes and $10b = 0volumes, b = 1500s/mm^2$, $TE = 99ms$) and T1 anatomical (MPRAGE, 1 mm isotropic) data.

Brain diffusion analysis

Diffusion data were corrected for eddy currents and head motion in FSL followed by bias field correction and global intensity normalization in MrTrix3 (Tournier et al., 2012). A response function was estimated in each subject from voxels containing only one fibre direction ($lmax = 6$). Diffusion data were then up-sampled ($1 \times 1 \times 1\ mm^3$) to improve anatomical accuracy and FODs were estimated for each voxel starting from a group-specific average response function. The tensor model was also fit to the data and scalar maps were computed (FA, MD, RD, AD).

Brain morphometry analysis

The T1-weighted structural image was skull stripped and non-linearly registered to the diffusion data in ANTS using an up-sampled FA map ($1 \times 1 \times 1\ mm^3$). The registered T1 was then segmented in FSL using FAST in white matter, grey matter and CSF tissues. This information was combined to form a five tissue type image to be used for anatomically constrained tractography (Smith et al., 2012).

The LGN was extracted from the Juelich atlas (threshold= 25%), inflated (2 mm in every direction) in order to account for inter-subject variability, and non-linearly registered to the diffusion space of each subject in FSL (FNIRT).

The pericalcarine area (V1) and the middle temporal area (V5) were automatically parcellated in Freesurfer v5.3.0 (http://surfer.nmr.mgh.harvard.edu). The preprocessing steps for the anatomical images included skull striping, transformation to standard Talairach space, white and grey matter segmentation, intensity normalization, topology correction, surface inflation, and atlas registration (Dale et al., 1999; Fischl et al., 1999).

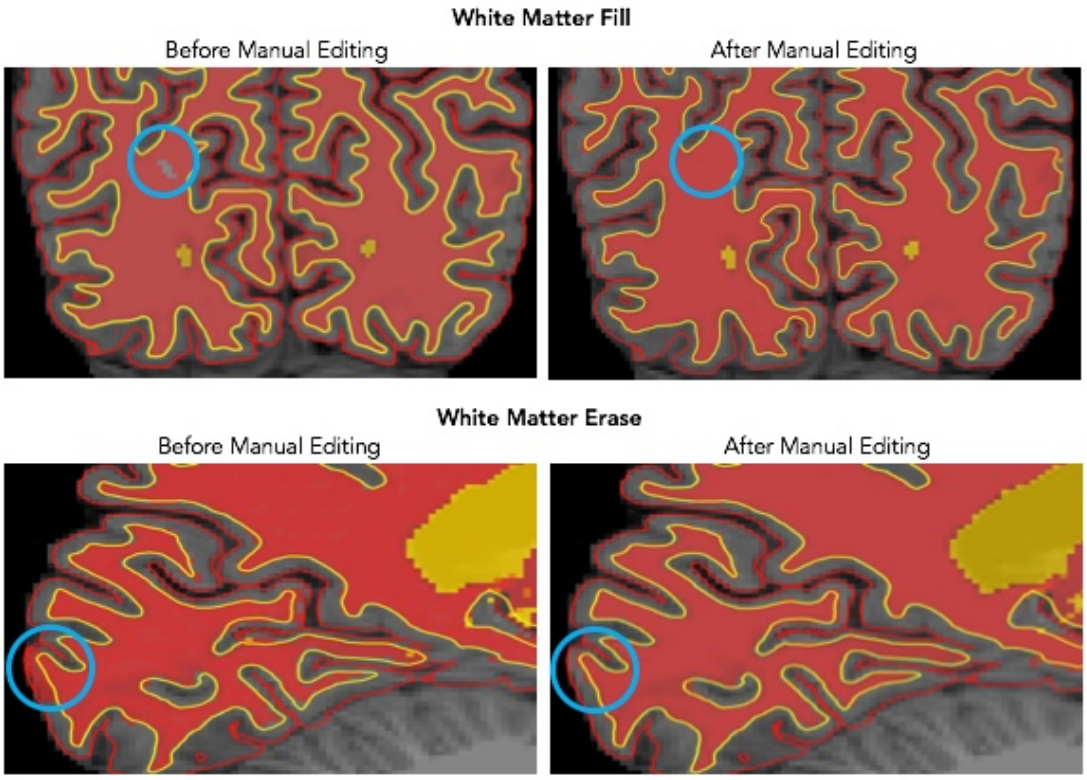

Figure 8.1: Manual Editing of Freesurfer Parcellations. The image shows an example for one representative subject before (left) and after (right) manual edits (inside blue circle) of segmentation maps in the occipital lobe: white matter voxel filling (upper panel), white matter erosion (lower panel).

The cerebral parcellation was performed according to the Desikan-Killiany Atlas (Desikan et al., 2006) and the pericalcarine/V1 parcel from each hemisphere was used as a ROI. To parcellate V5/MT, we used Freesurfer's Brodmann Area Maps. Parcellations were visually inspected in each subject and, if necessary, manual editing of the occipital lobe was performed by an expert operator (H.T). Wrong classification of white matter voxels was corrected either by filling (10/56 subjects) or eroding voxels (56/56 subjects) (Figure 8.1). The following morphological measures were then extracted for V1 and V5: total surface area (mm^2), total grey matter volume (mm^3), average cortical thickness $\pm$ standard deviation (mm), mean curvature, Gaussian curvature.

Optic radiation tractography

Anatomically constrained probabilistic tractography (ACT)(Smith et al., 2012) was performed on the up-sampled DW data at the following parameters: 0.5 mm step size, 45° maximum angle threshold, 1000 seeds per voxel. A preliminary investigation was

conducted in order to define the number of seeds per voxel. Probabilistic tractography was computed for different number of seeds until no new information was added. Tracking was randomly initiated from each voxel in the LGN and the primary visual cortex (V1) and the middle temporal area (V5) were used as targets. Volume (number of voxels traversed by at least one streamline belonging to the reconstructed bundle) and tensor-derived scalar metrics (fractional anisotropy (FA), mean diffusivity (MD), radial diffusivity (RD), axial diffusivity (AD)) were extracted for each bundle.

Statistics

To investigate group differences in morphometry and diffusion measures we applied a non-parametric 2-tailed paired Wilcoxon rank sum test between the blind groups and matched sighted controls. To investigate correlations between diffusion or morphometry measures and the onset age of blindness and/or the years of darkness in the late blind subjects we performed Spearman's partial correlations controlling for biological age. Analyses were performed in Matlab R2015a.

8.2.3 Results

Blindness effects on brain morphometry in visual areas

Brain morphometry data from V1 and V5 were compared in each of the blind groups (EB and LB) relative to their sighted control groups (Figure 8.2). Both blind groups showed no V5 morphometry differences with respect to their sighted controls. V1, instead, showed morphometry differences with blindness, differently for EB and LB, as summarized in table 8.1. Both EB and LB showed significant decreases of V1 cortical surface area and V1 cortical volume ($p < 0.01$). LB, in addition, showed significant decrease of V1 cortical thickness standard deviation and mean V1 thickness ($p < 0.05$). The other morphometry data gave non-significant differences between blind groups and their respective sighted controls.

Blindness effects on the optic radiation

Qualitative assessment of OR tractography reconstructions (LGN-V1 and LGN-V5) show visible differences in blind subjects relative to their age and gender matched sighted controls (Figure 8.3). Overall, the OR in the EB group presents less reconstructed streamlines in LGN-V1 relative to its SC group, while LGN-V5 shows a similar but weaker effect. The LB group presents comparable results but with apparent less differences relative to its SC group (Figure 8.3).

The analysis of tract-specific measures revealed significant differences between blind subjects and sighted controls mainly for LGN-V1 reconstructions. In agreement with visual inspection of the reconstructed OR, the volume resulted significantly reduced in LGN-V1 and and LGN-V5 for EB ($p < 0.01$), and only in LGN-V1 for LB, although to a lesser extent ($p < 0.05$). LGN-V1 in EB showed significant decrease in FA and significant increase in MD ($p < 0.01$). RD was also significantly higher in LGN-V1 for both EB

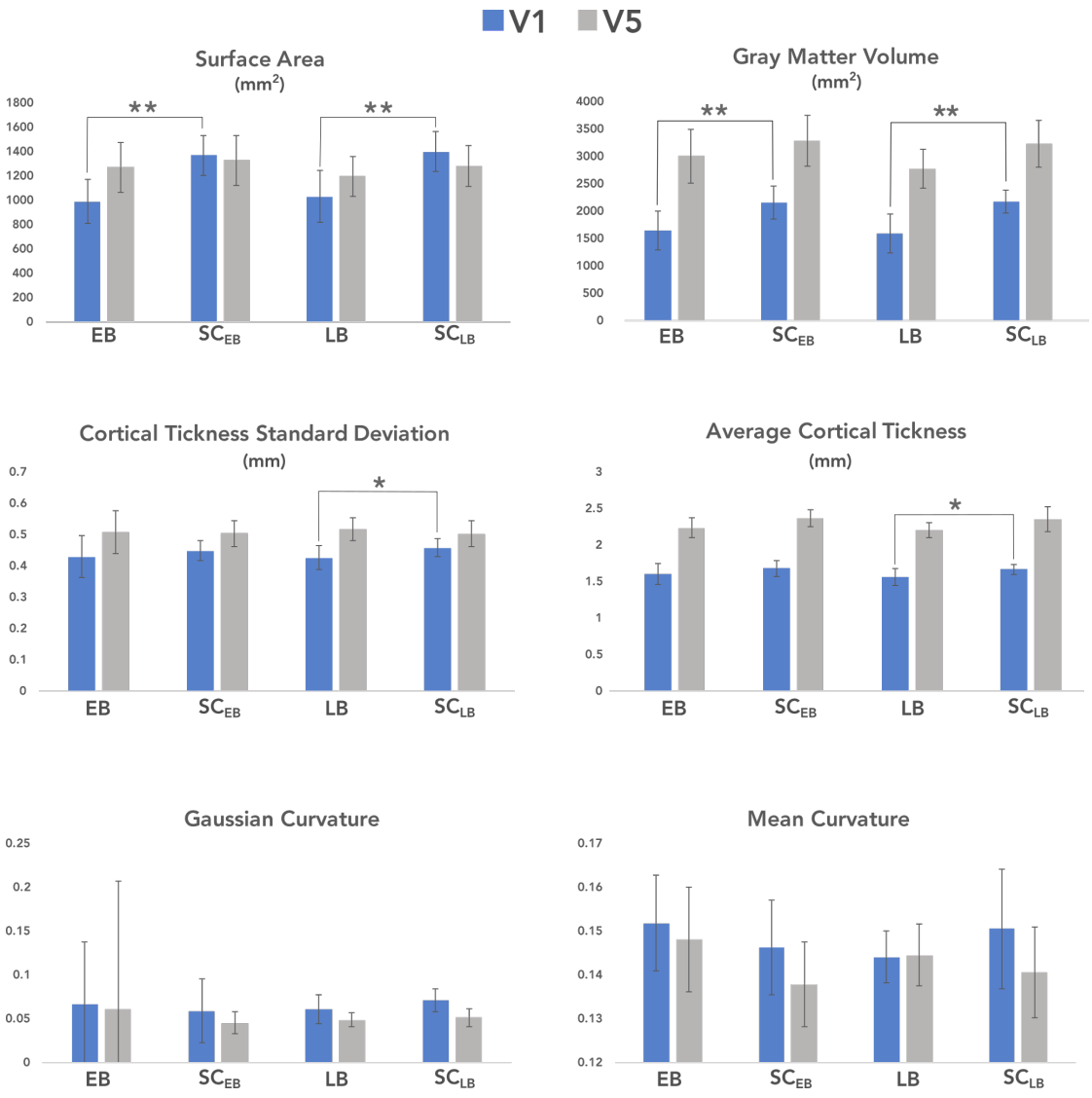

Figure 8.2: Brain Morphometry in Visual Areas: Early and Late Blind versus Sighted controls. The image shows the median values ($\pm sd$) of each group, left and right hemisphere data averaged, for all the measures extracted from V1 (blue) and V5 (grey) in FreeSurfer: total surface area (mm^2), total grey matter volume (mm^3), average cortical thickness $\pm$ standard deviation (mm), mean curvature, Gaussian curvature. Stars indicate significant differences between blind and sighted groups ($* = p < 0.05, ** = p < 0.01$).

	Blindness Effects in V1 Morphometry (p-value)					
	Surface area	grey matter volume	Cortical thickness standard deviation	Average cortical thickness	Gaussian curvature	Mean curvature
EB vs SC_{EB}	0.01	0.01	n.s.	n.s.	n.s.	n.s.
LB vs SC_{LB}	0.01	0.01	0.05	0.05	n.s.	n.s.

Table 8.1: Summary of Blindness Effects in Human V1 Morphometry. Comparison of Freesurfer morphometry results from V1 in early blind (EB) and late blind (LB), each relative to its own group of age and gender matched sighted controls (SC_{EB}, SC_{LB}).

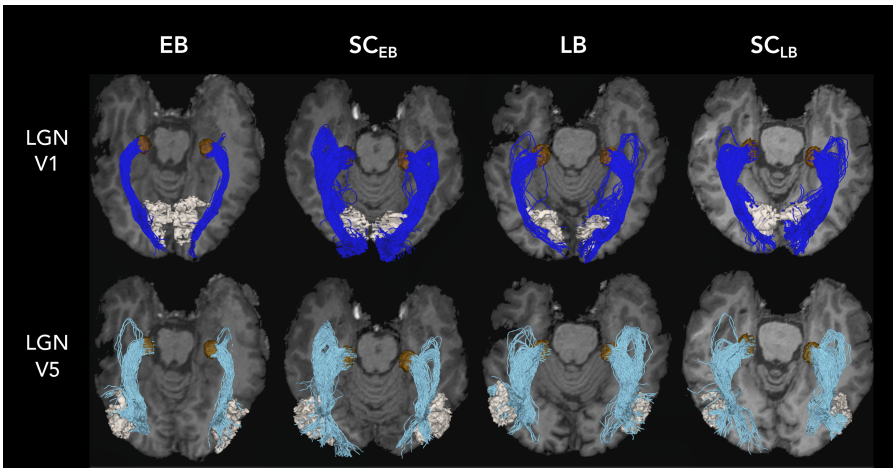

Figure 8.3: Optic Radiation Tractography Results. The figure presents the tractography results for a representative subject for each of the four groups (EB, SC_{EB}, LB, SC_{LB}). For each subject, the reconstruction of the streamlines between LGN (orange) and V1 (blue, top row) and between LGN and V5 (light blue, bottom row) are shown on the subject's T1 weighted image. The 3D reconstruction of the parcellations of V1 (top row) and V5 (bottom row) are also shown

	Blindness Effects in LGN-V1 Tractography (p-value)				
	Volume	FA	MD	RD	AD
EB vs SC_{EB}	0.01	0.01	0.01	0.01	n.s.
LB vs SC_{LB}	0.01	n.s	n.s	0.01	n.s.

	Blindness Effects in LGN-V5 Tractography (p-value)				
	Volume	FA	MD	RD	AD
EB vs SC_{EB}	0.05	n.s	n.s.	n.s.	n.s
LB vs SC_{LB}	n.s	n.s	n.s	n.s	n.s.

Table 8.2: Summary of Blindness Effects in Human optic radiation. Summary of blindness effects in human optic radiation. Comparison of LGN-V1 (top) and LGN-V5 (bottom) tract-specific measures extracted from tractography reconstructions in early blind (EB) and late blind (LB), each relative to its own group of age and gender matched sighted controls (SC_{EB}, SC_{LB}).

and LB. No significant differences were found in AD values, which were slightly higher in LGN-V1 compared to LGN-V5 for all groups.

Correlation analysis

Correlations between diffusion and morphometry measures with blindness onset and duration in LB did not reveal any significant correlation ($p > 0.05$)(Table 8.3).

8.2.4 Discussion

This study aimed at characterizing brain structural differences in the visual system in early and late blind subjects relative to age and gender matched sighted controls. Both blind groups showed significant grey and white matter differences in the visual system relative to sighted controls, but with differences across groups, suggesting that the role of visual experience plays a role in affecting the integrity of visual structures. Specifically, the main results of this study are: i) grey matter differences were significant only in V1 (not in V5), with effects that were similar in both EB and LB groups (reduced surface area and grey matter volume) and effects that were only detected in the LB group (reduced thickness standard deviation and average cortical thickness); ii) white matter related differences in the OR were mainly significant for connections to V1 in the EB group (reduced volume and FA, and increased MD and RD), and to a lesser extent in the LB group (reduced volume and increased RD). Connections to V5 only showed significant

	LGN-V1		**LGN-V5**	
	Onset	Duration	Onset	Duration
FA	-0.067	0.15	-0.08	0.10
MD	0.32	-0.17	0.29	-0.12
RD	0.17	-0.07	0.16	-0.04
AD	0.43	-0.22	0.29	-0.17
VOL	0.01	-0.09	-0.26	-0.04
	V1		**V5**	
	Onset	Duration	Onset	Duration
Surface Area (mm^2)	-0.23	0.36	-0.50	0.58
GM Volume (mm^3)	-0.42	0.48	-0.46	0.36
Thickness Mean (mm)	-0.44	0.38	-0.04	-0.18
Thickness SD (mm)	-0.32	0.07	-0.05	-0.14
Mean Curvature	-0.07	-0.15	0.01	0.28
Gaussian Curvature	-0.36	0.40	0.19	0.00

Table 8.3: Brain Structural Correlations in the Visual System with Blindness Onset and Duration. Summary of correlation coefficients between diffusion and morphometry measures, and blindness age onset and duration of blindness (years) in late blind subjects. In all correlations biological age has been used as controlling variable.

volume reduction in the EB group; iii) correlation analyses between grey/white matter related measures and blindness onset/duration did not show any significant result.

Our results showed significant reduction in surface area and grey matter volume in V1 in early blind subjects compared to controls. This is in agreement with previous studies that reported grey matter losses in primary visual striate areas of congenital and early blind subjects (Park et al., 2009; Dietrich et al., 2015; Bauer et al., 2017; Ptito et al., 2008; Pan et al., 2007). Grey matter changes in early blind subjects might reflect neuronal degeneration, and are probably due to deprivation of visual inputs coming from the LGN. In agreement with this we found that the connections between LGN and V1 showed reduced volume and FA, and increased RD and MD compared to sighted controls reconstructions. These results are in agreement with previous studies showing higher MD and lower FA (Shimony et al., 2006; Shu et al., 2009), and reduced white matter density (Noppeney et al., 2005) in the OR of EB subjects. The interpretation of differences in diffusion-derived metrics remains difficult, because of the indirect nature of the diffusion MRI measurement (Jones, Cercignani, 2010). However, lower FA values have been associated to deafferentation and axonal degeneration mechanisms, that can follow sensory deprivation (Beaulieu et al., 1996). Absence of visual input could lead to such degeneration in the connections to primary visual areas.

These results suggest that, as a consequence of sensory deprivation early in life, the visual cortex of these individuals and its afferent pathways reorganize following plasticity mechanisms. Studies investigating cross-modal reorganization in blind showed that the occipital cortex of blind individuals is activated in response to non-visual stimuli (Burton et al., 2002; Melzer et al., 2001; Poirier et al., 2006). One important question is how these non-visual stimuli reach the visual cortex. These results suggest the hypothesis that non-visual information reaches the visual cortex by other existing cortico-cortical pathways. The idea is supported by the preservation of connections between V1 and prefrontal and temporal cortices (Shimony et al., 2006) and by increased connectivity between auditory and visual areas in EB but not in SC (Klinge et al., 2010).

This reorganization appears to be experience-dependent. Our LB group showed differences in grey and white matter changes compared to EB, suggesting that blindness onset before and after a critical period differently affects brain reorganization. Grey matter changes in primary visual areas were found to a greater extent than in the EB group. Not only surface area and grey matter volume were reduced, but also the cortical thickness. This is in agreement with previous literature that found cortical thinning in the primary visual areas of LB subjects (Park et al., 2009), and with the idea that plasticity can happen later in life, even after short deprivation periods. Subjects who were blindfolded for even only a week showed posterior occipital lobe activation during tactile discrimination tasks (Merabet et al., 2008).

Contrary to cortical regions, we found that in LB reconstructed LGN-V1 connections were less affected than in EB. Tract volume was reduced compared to age-matched sighted controls and the RD increased. In agreement with previous studies we did not find differences in FA in these reconstructed connections (Schoth et al., 2006; Reveley et al., 2015). Opposite evidence did show strong FA reduction in the optic radiation of late blind subjects (Dietrich et al., 2015; Qin et al., 2013). Other studies found no difference between LB and SC in fractional anisotropy and mean diffusivity indices (Zhang et al., 2012). However, the blindness age onset used to define LB groups in these studies differed significantly (LB: $>$ 12 or 18 yrs versus $>$ 3 yrs in our study), making difficult to compare results.

These results suggest that reorganization of primary visual areas and its afferent connections differs in EB and LB groups. In EB thalamo-cortical connections are more damaged than in LB, while the opposite is true for cortical areas. This is in line with the idea that cross-modal reorganization mechanisms have critical developmental periods. Cortical areas in EB might be better preserved because devoted to processing non-visual stimuli, mostly conveyed by cortico-cortical, and not thalamo-cortical, connections. In acquired blindness, the level of cross-modal reorganization might not be the same. In agreement, the recruitment of occipital regions for non-visual tasks' processing seems to happen at a lesser degree in late compared to early blind subjects (Collignon et al., 2013; Bedny et al., 2012; Burton et al., 2002).

In this study we also investigated the reorganization of secondary middle temporal visual areas (V5), and their connections. Overall, the blindness-induced changes in these structures were less affected than primary counterparts. No morphometry differences

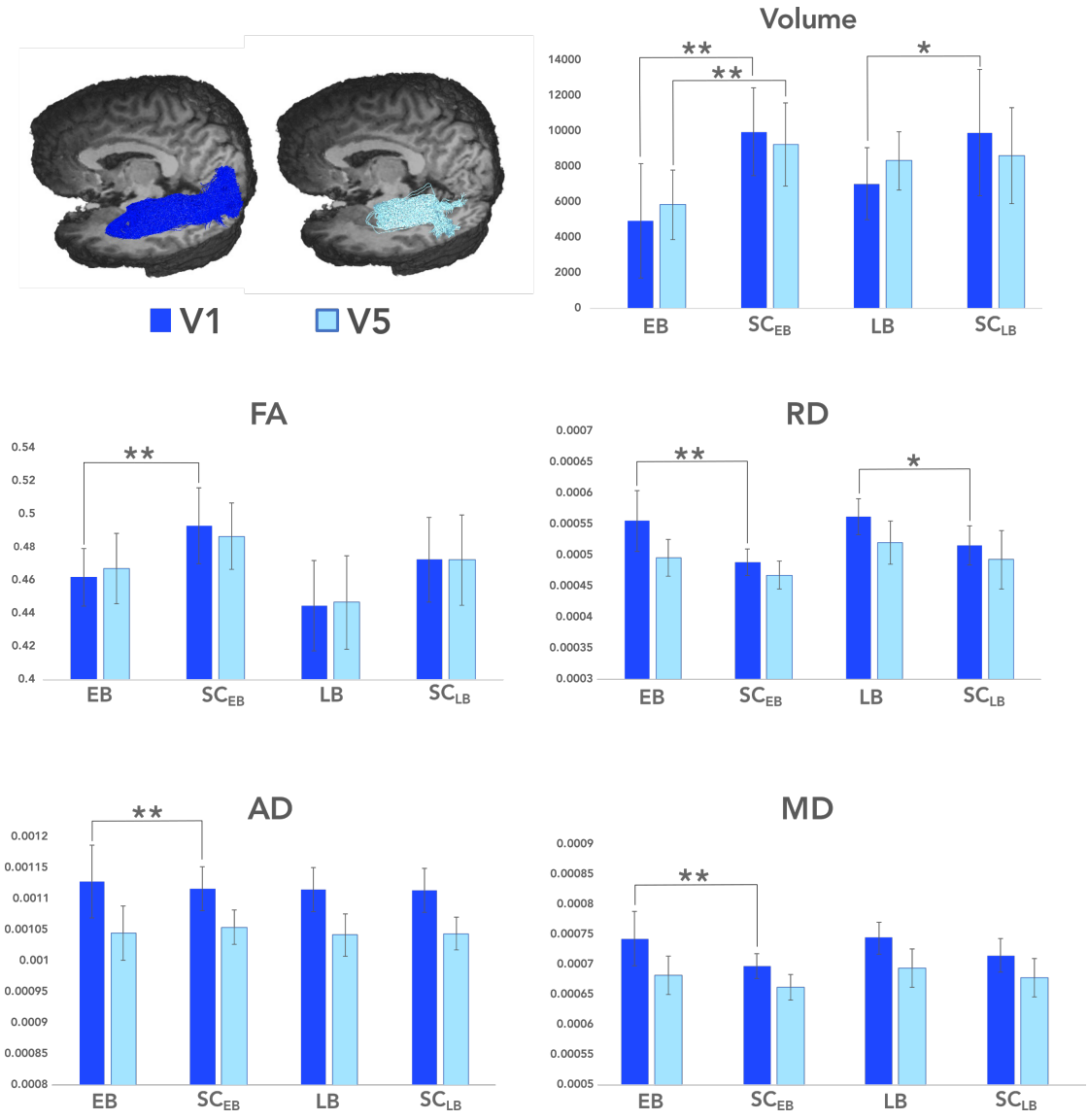

Figure 8.4: Tract-specific Measures. The figure reports the median group values for each of the tract-specific mean diffusion measures for each group (EB, SC_EB, LB, SC_LB) and each streamline bundle: LGN-V1 (shown in blue), and LGN-V5 (shown in light blue). The values represent the average between right and left OR. A 3D reconstruction of the brain in sagittal view for a representative subject is also shown together with the bundle reconstructions (top left). FA: fractional anisotropy, RD: radial diffusivity, MD: mean diffusivity, AD: axial diffusivity, Volume: number of voxels traversed by at least one streamline in the reconstructed bundle.

were found in EB or LB, and contained decrease in tract volume was found only for EB subjects. This is in agreement with previous studies reporting none or minor differences in higher exstrastriate cortices (Ptito et al., 2008; Pan et al., 2007). This is likely due to the fact that most of the projections fibres contacting V1 come from the LGN, which no longer receives inputs from the optic nerve. On the contrary, secondary visual areas instead, also receive inputs from other higher secondary association areas (Pan et al., 2007). The better preservation of V5 might be due to the higher potential for cross-modal plasticity in associative regions (Pan et al., 2007), and the task-specific reorganization of this area. Various functional studies report the recruitment of V5 in auditory motion tasks (Poirier et al., 2006; Saenz et al., 2008; Collignon et al., 2011).

Finally, although our results suggest experience-dependent changes in visual structures of blind individuals, we did not find significant correlation between the blindness onset age and the blindness duration and extracted brain measures in the late blind subjects. This is in agreement with previous studies, where no significant correlations between the FA values in OR and the age of blindness onset were found (Wang et al., 2013). Other studies did find significant negative correlation between FA and grey matter volume and the duration of blindness (Pan et al., 2007), and between WM loss and blindness age onset (Noppeney et al., 2005). Our negative results might be due to the small sample size of our study. However, more studies are needed to clarify this.

Study limitations and future research

Large variability in reported results exists in the literature. These differences might be due to the different methodologies implemented and the generally small and differently categorized samples of blind subjects (CB, EB, LB). For this reason, uncertainty remains in the extent of atrophy in visual areas and integrity of afferent and efferent projections. Regions of interest between these studies are different, and so the results are not directly comparable.

Most of these studies used ROI-based approach to define the OR. To increase anatomical specificity, in this study we used probabilistic tractography to reconstruct the profile of the AR. However, reconstructing the topography of the optic radiation fibres with diffusion-based tractography remains somehow challenging (Martínez-Heras et al., 2015; Hofer et al., 2010). This is mainly related to the complicated anatomical shape of the Meyers loop, where fibres first project anteriorly to the temporal horn and then extend posteriorly towards the occipital lobe. Also, in their course from the LGN to the visual cortex these fibres run in close proximity to the fibres of the inferior fronto-occipital fasciculus (IFOF) and the splenium of the corpus callosum (Sarubbo et al., 2015; Renauld et al., 2016). These characteristics are challenging for the tractography algorithm, that can easily result in false negative at the level of the Meyer's loop and false positive along the AR course. To decrease the possible artefacts arising from crossing and kissing situations, we up-sampled our diffusion data to increase location accuracy, and used a multi-fibre based probabilistic algorithm, previously shown to well behave in reconstructing the OR (Kammen et al., 2016). The spherical deconvolution-based probabilistic algorithm used in this study, together with the anatomical information derived from the structural

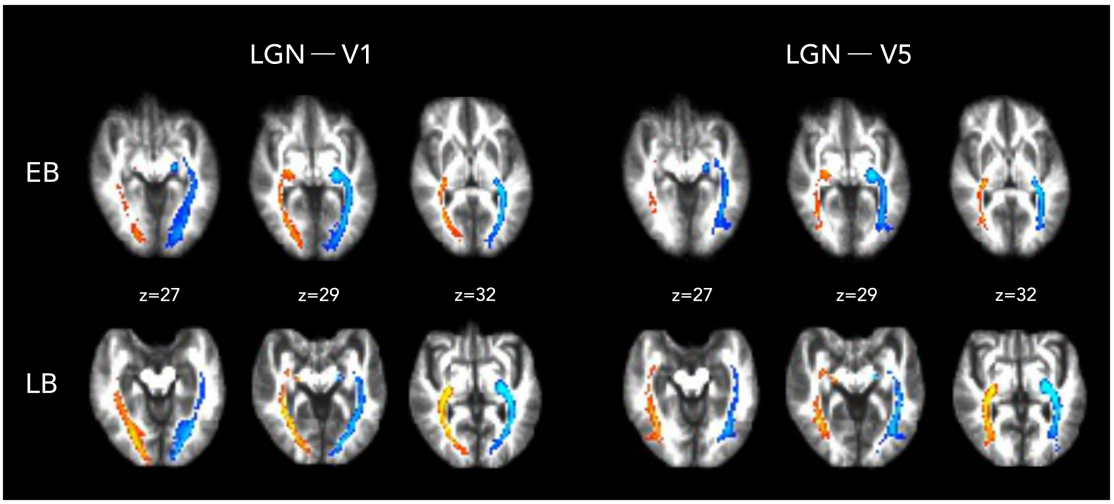

Figure 8.5: Population Template of the Optic Radiation. The image shows the FA population template for the EB-SC and LB-SC groups. For each group (EB and LB) and each connection (LGN-V1 and LGN-V5) the tractography reconstruction for blind subjects (yellow-red) and sighted controls (light blue-blue) is shown. Reconstructions are shown in the form of probabilistic maps where the voxel value corresponds to the number of subjects presenting connections at that location. Reconstructions are shown at 25% threshold.

data, successfully reconstructed OR bundles following macroanatomical knowledge of the OR. Streamlines belonging to the Meyer's loop were visible in all sighted controls. Nevertheless, reconstructions showed a high degree of variability in the volume of the reconstructed tracts across subjects and hemispheres in all four groups. This variability in OR has been previously reported, particularly at the level of the Meyer loop (Nilsson et al., 2007).

Another limitations might be related to the use of an atlas for defining the LGN seed ROI, which may introduce false positives and wrong tract terminations (Cecchetti et al., 2016). Using a subject-specific LGN segmentation should increase the accuracy of the tractography results. However, common acquisition protocols like ours, do not have the contrast to allow for this segmentation. Improvements in tractography and segmentation techniques will allow to better and more precisely define the reconstruction of the OR.

Conclusion

In conclusion, our study shows that the grey and white matter structures of the visual system are differently affected by early blindness relative to age and gender matched sighted controls. Somehow surprisingly, it seems that even late-acquired blindness, and even for a relatively short period, is sufficient to induce those modifications in the primary visual cortex and its afferent pathways. This is in line with the idea that significant

potential for plastic changes exists throughout the lifespan, but may differ in the extent and the underlying neurophysiological mechanisms following different periods of development. More precise and reliable quantification of the integrity of the structures of the visual system in these individuals may have clinical value to assess the potential suitability of sight restoration and retinal implants.

8.3 A study of the middle longitudinal fasciculus in two word deaf patients

8.3.1 Introduction

The middle longitudinal fasciculus (MdLF) was first delineated in monkeys as an independent white matter bundle connecting the parietal lobe and the superior temporal gyrus (STG), down to the temporal pole (TP) (Schmahmann et al., 2007; Seltzer, Pandya, 1984). Description of this tract in humans is sparse, and classical neuroanatomical studies of gross dissections failed to describe it (Ludwig, Klingler, 1956). However, recent studies using diffusion-based tractography methods have added information about the anatomy of the MdLF in humans *in-vivo* (Makris et al., 2009, 2013; Menjot De Champfleur et al., 2013). The MdLF can be identified as a distinct fascicle that runs superior to the inferior longitudinal fasciculus (ILF) and the inferior fronto-occipital fasciculus (IFOF) and medial to the arcuate fasciculus (AF). Aiming at validating these tractography reconstructions, a few works recently investigated the anatomy of this bundle using post-mortem gross dissections (Maldonado et al., 2013; Wang et al., 2012). While neuroimaging and neuroanatomical studies agree that the MdLF courses the white matter core of the STG, they disagree on posterior terminations; some tractography studies suggest its fibres terminate in the posterior portion of the angular gyrus (AG) and inferior parietal lobule (IPL), confirming findings in monkeys (Makris et al., 2009), other tractography studies and post-mortem investigations show they continue to the cortex caudal to the IPL, reaching the parieto-occipital regions and the superior parietal lobule (SPL) (Wang et al., 2012). A solution was recently proposed by Makris et al. (2013) who demonstrated a subdivision of the MdLF, in which a ventro-lateral branch would connect STG to AG and a dorso-medial branch STG to SPL.

The functional role of the MdLF remains largely unknown. Given its topographical location, a role in language processing is been often proposed (Makris et al., 2009; Schmahmann et al., 2007). Both the IPL and the STG are part of the language network (Hickok, Poeppel, 2007) and are connected by the arcuate fasciculus (Catani et al., 2005). However, resection of a large part of the left MdLF in 8 patients did not cause permanent language deficits postoperatively, suggesting this tract is not essential for language processing (De Witt Hamer et al., 2011). In addition, no evident left hemisphere lateralization of the MdLF has been found, suggesting this tract might not be language-specific. The functional role of the cortical areas it connects has also prompted the hypothesis that this bundle is involved in audio-visual integration (Makris et al., 2013; Wang et al., 2012). According to functional neuroimaging studies, both the AG and the STG/STS have been related to audiovisual speech perception processing (Bernstein et al., 2008; Möttönen et al., 2004; Stevenson, James, 2009; Wright et al., 2003). Bilateral lesion of the SPL is characterized by auditory and visual spatial localization deficits (Phan et al., 2000), and direct electrophysiological evidence from intracranial recordings show audio-visual multisensory processing in the SPL (Molholm et al., 2006).

A fascinating example of auditory and visual multisensory integration is the McGurk

effect. This is an audiovisual illusion in which incongruent audiovisual combinations alter the perception of syllables (Mcgurk, Macdonald, 1976). For example, when presented visually with /ga/ and auditorily with /ba/, subjects often incorrectly perceive a third syllable /da/. Neuroimaging studies investigating the neurofunctional substrate of the McGurk illusion highlighted the role of the supramarginal gyrus, the IPL (Jones, Callan, 2003), and the STS (Beauchamp, 2010) in processing incongruous audio-visual stimuli. Interestingly, a recent study demonstrates that bilateral cathodal transcranial direct current stimulation (tDCS) of these areas can interfere with the McGurk illusion effect (Marques et al., 2014).

It has been often observed that patients with circumscribed left temporal lesions show speech perception deficits in the presence of spared writing and reading abilities. This syndrome has been described as pure word deafness (PWD) (Buchman et al., 1986; Nakakoshi et al., 2001; Saffran et al., 1976; Hemphill, Stengel, 1940). These patients show a strong tendency to rely on lip reading to understand speech (Shindo et al., 1991). Therefore, PWD provides a unique opportunity to investigate audio-visual integration mechanisms.

In this study we aim to clarify the role of the MdLF in audiovisual integration comparing the anatomy of the MdLF in two pure word deaf patients and 20 healthy controls. The specific goals of this study are i) to evaluate the profile of the MdLF in the two patients in comparison to healthy controls, ii) to test audio-visual integration mechanisms in the two patients in comparison to healthy controls through the McGurk test and iii) to evaluate the claim that MdLF plays a critical role in audiovisual integration.

8.3.2 Methods

Subjects

Patient FO and patient GB suffered from an ischemic infarct in the left hemisphere (Figure 8.6). In patient FO the lesion mainly affects the primary auditory cortex (PAC or A1) on the transverse temporal gyrus of Heschl (HG), and the posterior portion of the insula. The lesion also involves the anterior and middle portions of the superior temporal gyrus (STG), only marginally affecting its posterior part. In patient GB the lesion is larger and extends for the entire length of the superior temporal sulcus (STS). Both patients completed the Italian battery for aphasic deficits (Miceli et al., 2004) and presented with pure word deafness (PWD).

FO, GB and 20 control subjects (15 female; mean age: 25.8, SD=3.5; mean years of formal education: 16.8, SD=1.7) participated in the McGurk experiment. The control subjects had no previous history of neurological deficits. No formal audiometric test was carried out in these subjects, but none reported subjective or objective auditory problems.

McGurk test

Nine videos were presented, each corresponding to the combination of an auditorily-presented syllable (/ba/, /da/, /ga/) and a visually-presented syllable (/ba/, /da/, /ga),

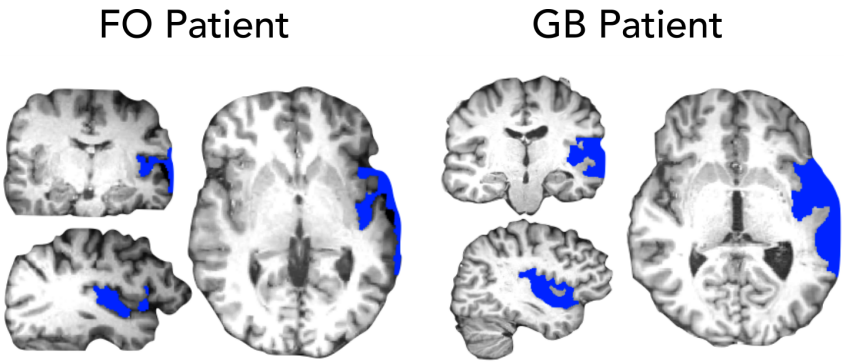

Figure 8.6: Lesion Quantification. Structural T1 weighted scans of the 2 patients. Semi-automatic segmentation of the lesion as performed in ITK-snap is shown in blue.

produced by the same female speaker. Each auditory/visual pair was presented 20 times in random order, for a total of 180 trials. Of these, 80 stimuli were incongruent (*e.g.* /ga/, /da/), 40 were "illusive" (*e.g.* /ga/, /ba/), 60 were congruent (*e.g.* /ba/, /ba/) Participants were seated in front of a monitor on which the videos were presented. The auditory stimuli were played via headphones. Participants were instructed to verbally report which syllable they perceived.

Data acquisition

Diffusion weighted MRI data of GB were acquired in Paris using a 3T Siemens Magnetom Verio scanner with following parameters: 60 diffusion-weighted directions at $b = 1500\ s/mm^2$, 6 volumes with no diffusion gradient applied ($b = 0$), spatial resolution of $2 \times 2 \times 2\ mm^3$, $TE = 85\ ms$. Data from 10 healthy age-matched controls (5 males, mean age=47) subjects were acquired at same parameters. FO data were acquired on a 4T whole-body Bruker MedSpec scanner with following parameters: 30 diffusion-weighted volume directions at $b = 1000\ s/mm^2$ and 5 volumes with no diffusion gradient applied, a spatial resolution of $2 \times 2 \times 2\ mm^3$, TE=94 ms. 10 healthy controls were acquired using the same sequence (8 females, mean age=25).

Diffusion Data Processing

Diffusion weighted data were corrected for eddy currents distortion and head movement in FSL (http://www.fmrib.ox.ac.uk/fsl) and the b-matrix was rotated accordingly (Leemans, Jones, 2009). Data were then processed in MrTrix3 (http://www.mrtrix.org) (Tournier et al., 2012). Bias field correction and global intensity normalization were applied to the data and the response function was computed for each subject ($lmax = 6$). Diffusion data was then up-sampled to improve anatomical accuracy and FODs were then estimated from the group-specific average response function. The tensor model was also fit to the data and tensor-derived scalar maps were computed. Apparent fibre density (AFD) scalar maps were also computed for each subject taking the first spherical

harmonic coefficient. This describes the total size (integral) of the FOD at each voxel.

Tractography

Whole brain tractography was performed starting from the spherical-deconvolution-based fibre orientation distribution profiles (FODs). Seeding was randomly started from each voxel (100 seeds per voxel) inside a binary FA-derived white matter mask of the brain. A deterministic algorithm was propagated with a step-size=$0.5mm$, and an angle threshold=45°.

Virtual dissection of the MdLF was performed in MrTrix using a two-regions of interest approach. The ROIs were manually defined on the FA template of each group: a first ROI was drawn to encompass the entire white matter of the superior temporal gyrus (STG), and a second ROI to include the white matter of the parietal lobe. Only those streamlines passing through the two ROIs were visualized and tract-specific measures were extracted. From each dissected bundle mean FA, mean length, volume (ml) and mean AFD were extracted. For each quantitative measure, we computed within-subject hemispheric differences and compared patients and control groups within each MR acquisition protocol.

8.3.3 Results

Behavioral Results

The two word-deaf patients showed an increased McGurk effect as compared to control subjects (Figure 8.7). Controls perceived the McGurk illusion on average 3/40 times (7.5%), and reported the auditory presented syllable on the remaining 37/40 instances. They never reported the visual stimulus. By contrast, GB and FO perceived the McGurk illusion 23/40 (57.5%) and 13/40 (32.5%) times, respectively. When this did not happen, GB and FO reported the auditory presented syllable respectively 8/40 and 13/40 times, and the visual stimulus 9/40 and 12/40.

Tractography Results

Visual assessment of the tractography reconstructions show clear differences between the reconstructed MdLF in the left hemisphere of patients and controls (Figure 8.8). Overall, the reconstruction of the left MdLF in GB resulted more extensively damaged. The tract appeared smaller and shorter if compared to reconstructions in controls. The left MdLF in FO resulted overall less damaged, and apparently more similar to controls reconstructions (Figure 8.8).

Tract specific measures revealed significant differences between patients and matched controls, in agreement with visual assessment. In patient GB, tract volume, tract mean length and apparent fibre density (AFD) were significantly different from those of controls (respectively $< 3\sigma, < 1\sigma, < 5\sigma$) (Figure 8.9). In patient FO, volume and length were not significantly different from controls, but microstructural measures revealed significant difference in AFD ($> 5\sigma$) (Figure 8.9). The right MdLF in the two patients was

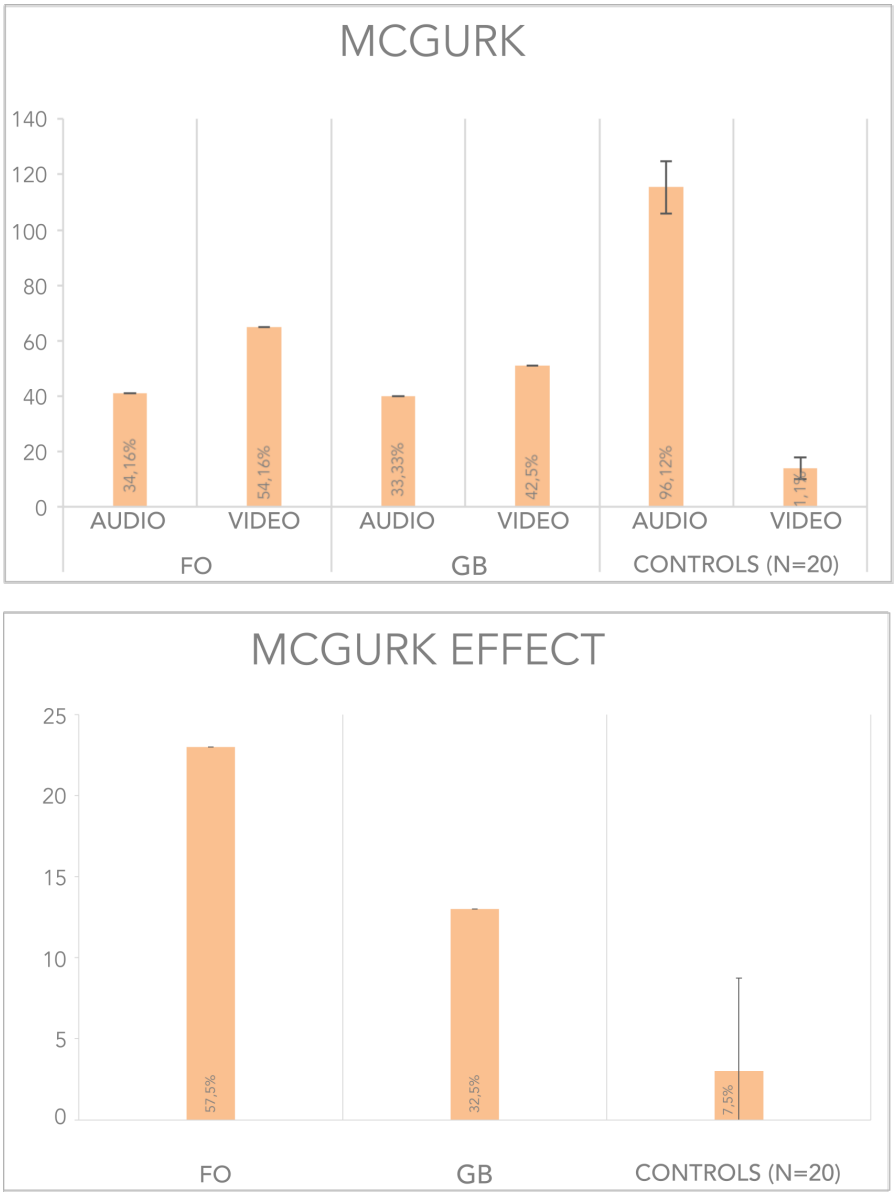

Figure 8.7: McGurck Results. Results of the McGurk experiment are shown for FO, GB and control group ($N = 20$). The top plot shows the number of times the acoustic or the visual information were reported out of all 120 stimuli. The bottom plot shows the number of times subjects perceive the McGurk illusion.

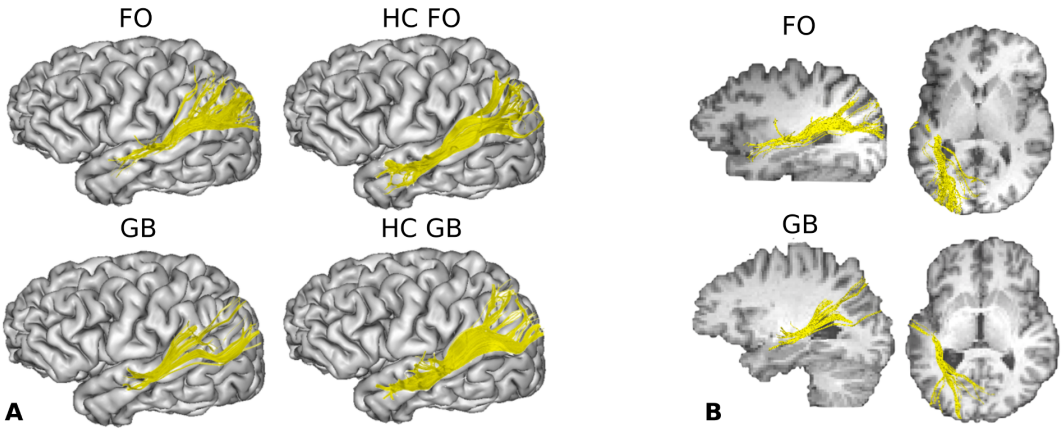

Figure 8.8: Middle longitudinal fasciculus tractography in word-deaf patients. A) Tractography reconstructions of the left MdLF in two word-deaf patients (FO, GB) and representative age and gender matched healthy controls for each patient (HC FO, HC GB). B) Left MdLF in FO and GB shown on the anatomical T1 MRI of each subject.

indistinguishable from that of controls.

8.3.4 Discussion

This study aimed at characterizing the profile of the MdLF in two word deaf patients and healthy controls, in the context of audio-visual integration mechanisms. The main results show: i) an increase of the McGurk effect in the patients compared to controls, with a stronger effect for patient GB; ii) a difference in the reconstructed profile of the left MdLF in patients versus controls, that is stronger for patient GB.

Somehow surprisingly, both PWD subjects showed an increased McGurk effect in comparison to controls. In particular patient GB, for whom tractography results showed more extensive damage to the MdLF, presented a more pronounced McGurk effect than subject FO. These results seem to argue against the view that MdLF plays a direct critical role in audiovisual integration. If the MdLF was directly responsible for audio-visual integration, damage to this bundle would predict a reduced McGurk effect in these patients. However, results from this study show the opposite trend. Also, considering the lesion profile of the two patients, these results are in disagreement with previous functional studies suggesting that the pSTG is necessary to generate the McGurk effect (Erickson et al., 2014). GB's brain lesion extends for the entire length of the superior temporal sulcus (STS), including damage to the Heschl's gyrus and the STG. Some of these studies draw upon the evidence that applying transcranic magnetic stimulation (TMS) or transcranial direct current stimulation (tDCS) on the STS can strongly interfere with the McGurk effect, resulting in less illusion-type responses being perceived (Beauchamp, 2010; Marques et al., 2014). However, the results of our study are in agree-

ment with previous studies showing that patients with left hemisphere lesions affected by Broca's aphasia and concomitant speech comprehension deficits can still perceive the McGurk illusion (Andersen, Starrfelt, 2015; Campbell ' et al., 1990). In addition, electrophysiological evidence suggest that, while the STG is a locus of multimodal integration, the perception of this integration depends on a larger distributed network (Keil et al., 2012).

The hypothesis that the MdLF has a role in audio-visual integration has not been directly demonstrated yet. This hyposthesis has been put forward based on the fact that the cortical regions connected by the MdLF bundle (STG and TP) have been found to be functionally involved in processing integration of auditory and visual stimuli (Bernstein et al., 2008; Möttönen et al., 2004; Phan et al., 2000). Together with STG and STS regions, intracranial electrical recordings in humans identified a region in the lateral superior parietal lobule that responded to both auditory and visual stimulation, with auditory inputs arriving considerably earlier ($30ms$) than visual inputs (Molholm et al., 2006). A second hyothesis is that MdLF is involved in language processing (Saur et al., 2008; Menjot De Champfleur et al., 2013; Makris et al., 2009), and more specifically in acoustic-phonetic processing (Makris et al., 2013).Perhaps this bundle, not being responsible for audio-visual integration itself, transfers auditory information from the STG and HG to the inferior and superior parietal lobules (IPL and SPL). In this view, direct or indirect damage to the MdLF, would prevent the auditory information from reaching audiovisual integration centers in the parietal regions. When presented with incongruent stimuli, due to incomplete auditory information, patients might be actually more likely to perceive the McGurk illusion.

This hypothesis is possibly reinforced by the fact that, when the McGurf effect is not perceived, patients report the visual stimulus more often than the acoustic one, in contrast to controls that always report the acoustic stimulus. This is in line with the ability of these patients to rely on lip reading to improve language comprehension (Shindo et al., 1991). Our results are in agreement with previous studies reporting patients with left hemisphere lesion preferring visual responses over auditory responses (Campbell ' et al., 1990). The patient evaluated in that study, consistently with our findings, was able to improve comprehension rate by lip-reading. However, our results are in disagreement with more recent experiments, in which by creating virtual lesions through the use of single-pulse TMS, healthy subjects did not show the McGurk effect and rather more often reported the acoustic part of the stimulus (Beauchamp, 2010). These differences need to be further investigated, but they may be due to to a number of factors, including lip reading ability differences between the deaf subjects and the healthy controls, as well as experimental protocol differences, such as specific limitations of TMS to reversely affect a focused target area together with its connected areas.

Study limitations and future research

Besides the fundamental limitation of having evaluated only two word-deaf patients, limitations of this study include both behavioral and diffusion MRI methods. Regarding behavioral methods, in our McGurk test only few control subjects actually experienced

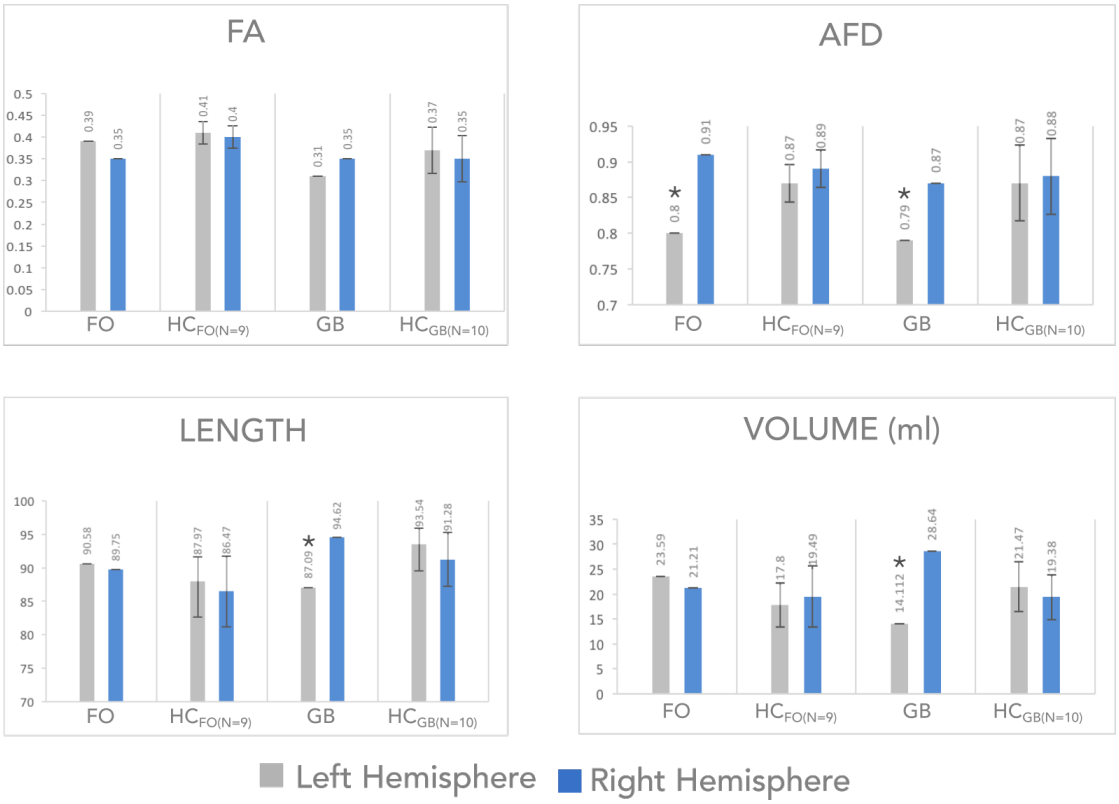

Figure 8.9: Tract-specific Quantitative Measures. FA and AFD measures are shown for the left (blue) and right (grey) MdLF for the 2 patients and each sequence-matched healthy control (HC) group (mean values).

the McGurk illusion. They almost always correctly report the auditory stimulus, and on average the illusion percept was reported only in 7.5% of the trials. This rate is lower than usually reported in previous studies (40-80%) (Mcgurk, Macdonald, 1976; Keil et al., 2012). However, studies have shown that the illusory percept does not occur with equal probability in all participants (from 0% to 100%) (Stevenson et al., 2012; Benoit et al., 2010; Basu Mallick et al., 2015) and also fluctuates on a trial-by-trial basis within one participant (Keil et al., 2012). In our case the low number of incongruent presented trials (40) might have influenced the results (Basu Mallick et al., 2015).

Limitations related to dMRI involve the common difficulties in interpreting the biological meaning of the quantitative measures extracted from the tractography reconstructed bundles. In particular, even though in this study AFD resulted more sensitive than FA in showing differences between patients and controls, it should be mentioned that in this report AFD was calculated in a voxel-based way, and thus was still influenced from the same averaging issues related to tensor measures. Moreover the interpretation of this measure at low b-values ($< 3000\ s/mm^2$) is not straight forward since it might be confounded by diffusivity in the extra-axonal space (Raffelt et al., 2012, 2017). Also, the virtual dissection of the MdLF has been performed on the base of ROIs manually drawn on the FA population template. Reconstructions show a typical course of the MdLF from STG/HG to parietal regions. However, variability in cortical termination especially in the parietal lobe existed. The definition of these ROIs in subject's space, either manually or through automatic parcellation, might improve the anatomical accuracy of the reconstructed bundles. In addition to improving anatomical accuracy, future steps of this study will evaluate the profile of other white matter bundles involved in language perception. The posterior segment of the arcuate fasciculus, for example, is been involved in the processing of auditory linguistic stimuli and word comprehension (Catani et al., 2005). This bundle connects the inferior parietal regions and the STG, and it is in close proximity of the MdLF. Investigating the anatomical profile of this bundle would help to understand and interpret results of the study, and to correlate these results with previous studies.

Conclusion

Opposing views exist about a fundamental functional role of the middle longitudinal fasciculus in audio visual-visual integration. This behavioural and diffusion MRI study provides supporting evidence that the middle longitudinal fasciculus is not directly involved in audio-visual integration processing in humans. Two patients with lesions to the left temporal lobe and damage to the MdLF showed increased perception of the McGurk effect, an audiovisual illusion in which incongruent audiovisual combinations alter the perception of syllables. The results are in agreement with the view that incomplete auditory information retrieval makes the McGurk effect more likely to happen. Given that the lesions of these patients were localized on the Heschl's gyrus and the superior temporal gyrus, our study questions the hypothesis that the superior temporal gyrus is fundamental for audio-visual integration.

Bibliography

Abed Rabbo Francis, Koch Guillaume, Lefèvre Christian, Seizeur Romuald. Direct geniculo-extrastriate pathways: a review of the literature. oct 2015. 891–899.

Andersen Tobias S, Starrfelt Randi. Audiovisual integration of speech in a patient with Broca's Aphasia. // Frontiers in psychology. 2015. 6. 435.

Arrigo Alessandro, Calamuneri Alessandro, Mormina Enricomaria, Gaeta Michele, Quartarone Angelo, Marino Silvia, Anastasi Giuseppe Pio, Aragona Pasquale. New Insights in the Optic Radiations Connectivity in the Human Brain. // Investigative ophthalmology & visual science. jan 2016. 57, 1. 1–5.

Basu Mallick Debshila, F. Magnotti John, S. Beauchamp Michael. Variability and stability in the McGurk effect: contributions of participants, stimuli, time, and response type // Psychonomic Bulletin & Review. oct 2015. 22, 5. 1299–1307.

Bauer Corinna M, Hirsch Gabriella V, Zajac Lauren, Koo Bang Bon, Collignon Olivier, Merabet Lotfi B. Multimodal MR-imaging reveals large-scale structural and functional connectivity changes in profound early blindness // PLoS ONE. 2017. 12, 3. e0173064.

Beatty Rm, Sadun Aa, Smith Leh, Vonsattel Jp, Richardson Ep. Direct demonstration of transsynaptic degeneration in the human visual system: a comparison of retrograde and anterograde changes // Journal of Neurology Neurosurgery, and Psychiatry. feb 1982. 45, 2. 143–146.

Beauchamp Michael S. fMRI-guided TMS reveals that the STS is a Cortical Locus of the McGurk Effect // Journal of Neuroscience. 2010. 30, 7. 2414–2417.

Beaulieu C, Does M D, Snyder R E, Allen P S. Changes in water diffusion due to Wallerian degeneration in peripheral nerve. // Magnetic resonance in medicine. oct 1996. 36, 4. 627–31.

Bedny Marina, Pascual-Leone Alvaro, Dravida Swethasri, Saxe Rebecca. A sensitive period for language in the visual cortex: Distinct patterns of plasticity in congenitally versus late blind adults // Brain and Language. sep 2012. 122, 3. 162–170.

Benoit Margo Mckenna, Raij Tommi, Lin Fa-Hsuan, Jääskeläinen Iiro P, Stufflebeam Steven. Primary and Multisensory Cortical Activity is Correlated with Audiovisual Percepts // Human Brain Mapping. 2010. 31. 526–538.

Bernstein Lynne E, Auer Edward T, Wagner Michael, Ponton Curtis W. Spatiotemporal dynamics of audiovisual speech processing. // NeuroImage. jan 2008. 39, 1. 423–35.

Bridge Holly, Cowey Alan, Ragge Nicola, Watkins Kate. Imaging studies in congenital anophthalmia reveal preservation of brain architecture in 'visual' cortex // Brain. dec 2009. 132, 12. 3467–3480.

Buchman a S, Garron D C, Trost-Cardamone J E, Wichter M D, Schwartz M. Word deafness: one hundred years later. // Journal of neurology, neurosurgery, and psychiatry. 1986. 49, 5. 489–499.

Burton H, Snyder A Z, Conturo T E, Akbudak E, Ollinger J M, Raichle M E. Adaptive changes in early and late blind: a fMRI study of Braille reading. // Journal of neurophysiology. jan 2002. 87, 1. 589–607.

NEUROPSYCHOLOGICAL STUDIES OF AUDITORY-VISUAL FUSION ILLUSIONS. FOUR CASE STUDIES AND THEIR IMPLICATIONS. // . 1990. 2, 8. 7–7.

Catani Marco, Jones Derek K., Ffytche Dominic H. Perisylvian language networks of the human brain // Annals of Neurology. 2005. 57, 1. 8–16.

Cecchetti Luca, Ricciardi Emiliano, Handjaras Giacomo, Kupers Ron, Ptito Maurice, Pietrini Pietro. Congenital blindness affects diencephalic but not mesencephalic structures in the human brain // Brain Structure and Function. apr 2016. 221, 3. 1465–1480.

Clatworthy P. L., Williams G. B., Acosta-Cabronero J., Jones S. P., Harding S. G., Johansen-Berg H., Baron J. C. Probabilistic tractography of the optic radiations-An automated method and anatomical validation // NeuroImage. feb 2010. 49, 3. 2001–2012.

Collignon Olivier, Dormal Giulia, Albouy Geneviève, Vandewalle Gilles, Voss Patrice, Phillips Christophe, Lepore Franco. Impact of blindness onset on the functional organization and the connectivity of the occipital cortex // Brain. 2013. 136, 9. 2769–2783.

Collignon Olivier, Vandewalle Gilles, Voss Patrice, Albouy Geneviève, Charbonneau Geneviève, Lassonde Maryse, Lepore Franco. Functional specialization for auditory-spatial processing in the occipital cortex of congenitally blind humans. // Proceedings of the National Academy of Sciences of the United States of America. mar 2011. 108, 11. 4435–40.

Dale Anders M., Fischl Bruce, Sereno Martin I. Cortical Surface-Based Analysis // NeuroImage. feb 1999. 9, 2. 179–194.

De Witt Hamer Philip C., Moritz-Gasser Sylvie, Gatignol Peggy, Duffau Hugues. Is the human left middle longitudinal fascicle essential for language? A brain electrostimulation study // Human Brain Mapping. 2011. 32, 6. 962–973.

Desikan Rahul S, Ségonne Florent, Fischl Bruce, Quinn Brian T, Dickerson Bradford C, Blacker Deborah, Buckner Randy L, Dale Anders M, Maguire R Paul, Hyman Bradley T, Albert Marilyn S, Killiany Ronald J. An automated labeling system for subdividing the human cerebral cortex on MRI scans into gyral based regions of interest. // NeuroImage. jul 2006. 31, 3. 968–80.

Dietrich Susanne, Hertrich Ingo, Kumar Vinod, Ackermann Hermann. Experience-related structural changes of degenerated occipital white matter in late-blind humans - a diffusion tensor imaging study. // PloS one. 2015. 10, 4. e0122863.

Erickson Laura C., Zielinski Brandon A., Zielinski Jennifer E. V., Liu Guoying, Turkeltaub Peter E., Leaver Amber M., Rauschecker Josef P. Distinct cortical locations for integration of audiovisual speech and the McGurk effect // Frontiers in Psychology. jun 2014. 5. 534.

Fischl Bruce, Sereno Martin I., Dale Anders M. Cortical Surface-Based Analysis // NeuroImage. feb 1999. 9, 2. 195–207.

Ghazanfar Asif A., Schroeder Charles E. Is neocortex essentially multisensory? jun 2006. 278–285.

Hemphill R E, Stengel E. a Study on Pure Word-Deafness. // Journal of neurology and psychiatry. 1940. 3, 3. 251–262.

Hickok Gregory, Poeppel David. The cortical organization of speech processing. // Nature reviews. Neuroscience. may 2007. 8, 5. 393–402.

Hofer Sabine, Karaus Alexander, Frahm Jens. Reconstruction and dissection of the entire human visual pathway using diffusion tensor MRI // Frontiers in Neuroanatomy. 2010. 4-15, April. 1–77.

Jones Derek K, Cercignani Mara. Twenty-five pitfalls in the analysis of diffusion MRI data // NMR in Biomedicine. 2010. 23, 7. 803–820.

Jones Jeffery A, Callan Daniel E. Brain activity during audiovisual speech perception: an fMRI study of the McGurk effect. // Neuroreport. jun 2003. 14, 8. 1129–33.

Kammen Alexandra, Law Meng, Tjan Bosco S, Toga Arthur W, Shi Yonggang. Automated retinofugal visual pathway reconstruction with multi-shell HARDI and FOD-based analysis. // NeuroImage. jan 2016. 125. 767–79.

Keil J., Muller N., Ihssen N., Weisz N. On the Variability of the McGurk Effect: Audiovisual Integration Depends on Prestimulus Brain States // Cerebral Cortex. jan 2012. 22, 1. 221–231.

Klinge C., Eippert F., Roder B., Buchel C. Corticocortical Connections Mediate Primary Visual Cortex Responses to Auditory Stimulation in the Blind // Journal of Neuroscience. sep 2010. 30, 38. 12798–12805.

Leemans Alexander, Jones Derek K. The B-matrix must be rotated when correcting for subject motion in DTI data // Magnetic Resonance in Medicine. 2009. 61, 6. 1336–1349.

Leporé Natasha, Voss Patrice, Lepore Franco, Chou Yi-Yu, Fortin Madeleine, Gougoux Frédéric, Lee Agatha D, Brun Caroline, Lassonde Maryse, Madsen Sarah K, Toga Arthur W, Thompson Paul M. Brain structure changes visualized in early- and late-onset blind subjects. // NeuroImage. jan 2010. 49, 1. 134–40.

Lim Jeremy C, Phal Pramit M, Desmond Patricia M, Nichols Andrew D, Kokkinos Chris, Danesh-Meyer Helen V, Kaye Andrew H, Moffat Bradford A. Probabilistic MRI tractography of the optic radiation using constrained spherical deconvolution: a feasibility study. // PloS one. 2015. 10, 3. e0118948.

Ludwig E, Klingler J. Atlas Cerebri Humani (The Inner Structure of the Brain Demonstrated on the Basis of Macroscopical Preparations). Boston, 1956.

Makris N, Preti M G, Asami T, Pelavin P, Campbell B, Papadimitriou G M, Kaiser J, Baselli G, Westin C F, Shenton M E, Kubicki M. Human middle longitudinal fascicle: variations in patterns of anatomical connections. // Brain structure & function. jul 2013. 218, 4. 951–68.

Makris Nikos, Papadimitriou George M., Kaiser Jonathan R., Sorg Scott, Kennedy David N., Pandya Deepak N. Delineation of the middle longitudinal fascicle in humans: A quantitative, in vivo, DT-MRI study // Cerebral Cortex. 2009. 19, 4. 777–785.

Maldonado Igor Lima, De Champfleur Nicolas Menjot, Velut St??phane, Destrieux Christophe, Zemmoura Ilyess, Duffau Hugues. Evidence of a middle longitudinal fasciculus in the human brain from fiber dissection // Journal of Anatomy. 2013. 223, 1. 38–45.

Marques Lucas Murrins, Lapenta Olivia Morgan, Merabet Lotfi B, Bolognini Nadia, Boggio Paulo Sérgio. Tuning and disrupting the brain-modulating the McGurk illusion with electrical stimulation. // Frontiers in human neuroscience. 2014. 8, August. 533.

Martínez-Heras Eloy, Varriano Federico, Prčkovska Vesna, Laredo Carlos, Andorrà Magí, Martínez-Lapiscina Elena H, Calvo Anna, Lampert Erika, Villoslada Pablo, Saiz Albert, Prats-Galino Alberto, Llufriu Sara. Improved Framework for Tractography Reconstruction of the Optic Radiation. // PloS one. 2015. 10, 9. e0137064.

Mcgurk Harry, Macdonald John. Hearing lips and seeing voices // Nature. dec 1976. 264, 5588. 746–748.

Melzer P, Morgan V L, Pickens D R, Price R R, Wall R S, Ebner F F. Cortical activation during Braille reading is influenced by early visual experience in subjects with severe visual disability: a correlational fMRI study. // Human brain mapping. nov 2001. 14, 3. 186–95.

Menjot De Champfleur Nicolas, Lima Maldonado Igor, Moritz-Gasser Sylvie, MacHi Paolo, Le Bars Emmanuelle, Bonafé Alain, Duffau Hugues. Middle longitudinal fasciculus delineation within language pathways: A diffusion tensor imaging study in human // European Journal of Radiology. 2013. 82, 1. 151–157.

Merabet Lotfi B., Hamilton Roy, Schlaug Gottfried, Swisher Jascha D., Kiriakopoulos Elaine T., Pitskel Naomi B., Kauffman Thomas, Pascual-Leone Alvaro. Rapid and Reversible Recruitment of Early Visual Cortex for Touch // PLoS ONE. aug 2008. 3, 8. e3046.

Merabet Lotfi B., Pascual-Leone Alvaro. Neural reorganization following sensory loss: the opportunity of change // Nature Reviews Neuroscience. jan 2010. 11, 1. 44–52.

Miceli Gabriele, Laudanna A, Burani C, Capasso R. Batteria per l'analisi dei deficit afasici // EMS, Bologna. 2004.

Molholm Sophie, Sehatpour Pejman, Mehta Ashesh D, Shpaner Marina, Gomez-Ramirez Manuel, Ortigue Stephanie, Dyke Jonathan P, Schwartz Theodore H, Foxe John J. Audio-visual multisensory integration in superior parietal lobule revealed by human intracranial recordings. // Journal of neurophysiology. 2006. 96, 2. 721–729.

Möttönen Riikka, Schürmann Martin, Sams Mikko. Time course of multisensory interactions during audiovisual speech perception in humans: A magnetoencephalographic study // Neuroscience Letters. 2004. 363, 2. 112–115.

Nakakoshi S, Kashino M, Mizobuchi a, Fukada Y, Katori H. Disorder in sequential speech perception: a case study on pure word deafness. // Brain and language. 2001. 76, 2. 119–129.

Nilsson Daniel, Starck Göran, Ljungberg Maria, Ribbelin Susanne, Jönsson Lars, Malmgren Kristina, Rydenhag Bertil. Intersubject variability in the anterior extent of the optic radiation assessed by tractography // Epilepsy Research. 2007. 77, 1. 11–16.

Noppeney Uta, Friston Karl J., Ashburner John, Frackowiak Richard, Price Cathy J. Early visual deprivation induces structural plasticity in gray and white matter. 2005. R488–R490.

Pan Wen Ju, Wu Guangyao, Li Chun Xia, Lin Fuchun, Sun Junmo, Lei Hao. Progressive atrophy in the optic pathway and visual cortex of early blind Chinese adults: A voxel-based morphometry magnetic resonance imaging study // NeuroImage. aug 2007. 37, 1. 212–220.

Park Hae-Jeong, Lee Jong Doo, Kim Eung Yeop, Park Bumhee, Oh Maeng-Keun, Lee SungChul, Kim Jae-Jin. Morphological alterations in the congenital blind based on the analysis of cortical thickness and surface area // NeuroImage. aug 2009. 47, 1. 98–106.

Phan M L, Schendel K L, Recanzone G H, Robertson L C. Auditory and visual spatial localization deficits following bilateral parietal lobe lesions in a patient with Balint's syndrome. // Journal of cognitive neuroscience. jul 2000. 12, 4. 583–600.

Poirier C., Collignon O., Scheiber C., Renier L., Vanlierde A., Tranduy D., Veraart C., De Volder A.G. Auditory motion perception activates visual motion areas in early blind subjects // NeuroImage. may 2006. 31, 1. 279–285.

Ptito Maurice, Schneider Fabien C. G., Paulson Olaf B., Kupers Ron. Alterations of the visual pathways in congenital blindness // Experimental Brain Research. may 2008. 187, 1. 41–49.

Qin Wen, Liu Yong, Jiang Tianzi, Yu Chunshui. The development of visual areas depends differently on visual experience. // PloS one. 2013. 8, 1. e53784.

Raffelt David, Tournier J. Donald, Rose Stephen, Ridgway Gerard R., Henderson Robert, Crozier Stuart, Salvado Olivier, Connelly Alan. Apparent Fibre Density: A novel measure for the analysis of diffusion-weighted magnetic resonance images // NeuroImage. 2012. 59, 4. 3976–3994.

Raffelt David A, Tournier J. Donald, Smith Robert E, Vaughan David N, Jackson Graeme, Ridgway Gerard R, Connelly Alan. Investigating white matter fibre density and morphology using fixel-based analysis // NeuroImage. jan 2017. 144, Pt A. 58–73.

Renauld Emmanuelle, Descoteaux Maxime, Bernier Michaël, Garyfallidis Eleftherios, Whittingstall Kevin. Semi-automatic segmentation of optic radiations and LGN, and their relationship to EEG alpha waves // PLoS ONE. 2016. 11, 7.

Reveley Colin, Seth Anil K., Pierpaoli Carlo, Silva Afonso C., Yu David, Saunders Richard C., Leopold David A., Ye Frank Q. Superficial white matter fiber systems impede detection of long-range cortical connections in diffusion MR tractography // Proceedings of the National Academy of Sciences. may 2015. 112, 21. E2820–E2828.

Riddoch G. On the Relative Perceptions of Movement and a Stationary Object in Certain Visual Disturbances due to Occipital Injuries. // Proceedings of the Royal Society of Medicine. 1917. 10, Neurol Sect. 13–34.

Saenz Melissa, Lewis Lindsay B, Huth Alexander G, Fine Ione, Koch Christof. Visual Motion Area MT+/V5 Responds to Auditory Motion in Human Sight-Recovery Subjects. // The Journal of neuroscience : the official journal of the Society for Neuroscience. may 2008. 28, 20. 5141–8.

Saffran E M, Marin O S, Yeni-Komshian G H. An analysis of speech perception in word deafness. // Brain and language. apr 1976. 3, 2. 209–28.

Sarubbo Silvio, De Benedictis Alessandro, Milani Paola, Paradiso Beatrice, Barbareschi Mattia, Rozzanigo Umbero, Colarusso Enzo, Tugnoli Valeria, Farneti Marco, Granieri Enrico, Duffau Hugues, Chioffi Franco. The course and the anatomo-functional relationships of the optic radiation: a combined study with post mortem dissections and in vivo direct electrical mapping. // Journal of anatomy. jan 2015. 226, 1. 47–59.

Saur Dorothee, Kreher Björn W, Schnell Susanne, Kümmerer Dorothee, Kellmeyer Philipp, Vry Magnus-Sebastian, Umarova Roza, Musso Mariacristina, Glauche Volkmar, Abel Stefanie, Huber Walter, Rijntjes Michel, Hennig Jürgen, Weiller Cornelius. Ventral and dorsal pathways for language. // Proceedings of the National Academy of Sciences of the United States of America. 2008. 105, 46. 18035–40.

Schmahmann Jeremy D., Pandya Deepak N., Wang Ruopeng, Dai Guangping, D'Arceuil Helen E., De Crespigny Alex J., Wedeen Van J. Association fibre pathways of the brain: Parallel observations from diffusion spectrum imaging and autoradiography // Brain. 2007. 130, 3. 630–653.

Schoth F., Burgel U., Dorsch R., Reinges M.H.T., Krings T. Diffusion tensor imaging in acquired blind humans // Neuroscience Letters. may 2006. 398, 3. 178–182.

Seltzer B, Pandya DN. Further observations on parieto-temporal connections in the rhesus monkey. - PubMed - NCBI // Experimental Brain Research. 1984. 55. 301–312.

Shimony J.S., Burton H., Epstein A.A., McLaren D.G., Sun S.W., Snyder A.Z. Diffusion Tensor Imaging Reveals White Matter Reorganization in Early Blind Humans // Cerebral Cortex. nov 2006. 16, 11. 1653–1661.

Shindo M, Kaga K, Tanaka Y. Speech discrimination and lip reading in patients with word deafness or auditory agnosia // Brain and Language. 1991. 40, 2. 153–161.

Shu Ni, Liu Yong, Li Jun, Li Yonghui, Yu Chunshui, Jiang Tianzi. Altered anatomical network in early blindness revealed by diffusion tensor tractography. // PloS one. sep 2009. 4, 9. e7228.

Sincich Lawrence C, Park Ken F, Wohlgemuth Melville J, Horton Jonathan C. Bypassing V1: a direct geniculate input to area MT // Nature Neuroscience. oct 2004. 7, 10. 1123–1128.

Smith Robert E., Tournier Jacques-Donald, Calamante Fernando, Connelly Alan. Anatomically-constrained tractography: Improved diffusion MRI streamlines tractography through effective use of anatomical information // NeuroImage. 2012. 62, 3. 1924–1938.

Stevenson Ryan A., James Thomas W. Audiovisual integration in human superior temporal sulcus: Inverse effectiveness and the neural processing of speech and object recognition // NeuroImage. 2009. 44, 3. 1210–1223.

Stevenson Ryan A, Zemtsov Raquel K, Wallace Mark T. Individual differences in the multisensory temporal binding window predict susceptibility to audiovisual illusions. // Journal of experimental psychology. Human perception and performance. dec 2012. 38, 6. 1517–29.

Tournier J. Donald, Calamante Fernando, Connelly Alan. MRtrix: Diffusion tractography in crossing fiber regions // International Journal of Imaging Systems and Technology. 2012. 22, 1. 53–66.

Wang Dawei, Qin Wen, Liu Yong, Zhang Yunting, Jiang Tianzi, Yu Chunshui. Altered white matter integrity in the congenital and late blind people. // Neural plasticity. 2013. 2013. 128236.

Wang Dawei, Qin Wen, Liu Yong, Zhang Yunting, Jiang Tianzi, Yu Chunshui. Altered resting-state network connectivity in congenital blind // Human Brain Mapping. jun 2014. 35, 6. 2573–2581.

Wang Yibao, Fernandez-Miranda Juan C., Verstynen Timothy, Pathak Sudhir, Schneider Walter, Yeh Fang Cheng. Rethinking the role of the middle longitudinal fascicle in language and auditory pathways // Cerebral Cortex. 2012. 23, 10. 2347–2356.

Wright Tarra M., Pelphrey Kevin A., Allison Truett, McKeown Martin J., McCarthy Gregory. Polysensory interactions along lateral temporal regions evoked by audiovisual speech // Cerebral Cortex. 2003. 13, 10. 1034–1043.

Zhang Yan, Wan Sihai, Ge Jian, Zhang Xuelin. Diffusion tensor imaging reveals normal geniculocalcarine-tract integrity in acquired blindness // Brain Research. jun 2012. 1458. 34–39.

Chapter 9

Concluding Remarks

The advent of diffusion magnetic resonance imaging (MRI) (Basser et al., 1994), and successively, of tractography techniques (Mori et al., 1999), opened previously unforseen opportunities for revealing the microscopic anatomical organization of brain tissue in the living human brain. Before diffusion MRI, only *post-mortem* investigations in humans, and istochemical studies in monkeys were available to explore the axonal connections of nerve fibres.

For the first time, diffusion-based tractography made possible to visualize and reconstruct the architecture of white matter bundles *in-vivo* and non-invasively. This allowed to assess the the relationship between white matter architecture and function, both in health and in disease. It's now clearer that every complex human behaviour is represented in the brain by a distributed network of areas that work together to accomplish the function at issue (Mesulam, 1990). And in the same way, it's every day clearer that the cause of a "malfunctioning brain" can be associated with a "malfunctioning network" as opposed to a damaged localized region (Catani, 2007). However, as Johansen-Berg advises, it is easy to fall in love with these pretty pictures of colourful streamlines ignoring the massive methodological limitations involved in these reconstructions (Johansen-Berg, Behrens, 2006).

The inherent indirect nature of the diffusion MRI measurement makes tractography inaccurate and difficult to quantify (Jbabdi, Johansen-Berg, 2011). Tractography techniques rely on the diffusion of water molecules inside the brain to indirectly infer the geometry of tissue microstructure. However, "Trying to infer information on the actual orientation of fibres direction from a water diffusion displacement profile is fundamentally a complex, undetermined inverse problem that cannot be solved."(Thomas et al., 2014). Moreover, the spatial resolution at which we can observe these phenomena is far from the scale at which these phenomena actually take place. This makes difficult to disentangle the different processes happening inside the imaging voxel. Beside its intrinsic limitations, we should not forget that diffusion MRI is the only technique at our disposal to investigate architecture of the human white matter *in-vivo* and in less than 10 minutes scanning time. For this reason, tractography has been extensively applied in

both basic research and clinical contexts, and has been more recently became routine in surgical applications (Catani et al., 2005; Scheck et al., 2015; Saur et al., 2008; Yu et al., 2006; Sigalovsky et al., 2006; Winston et al., 2011; Chen et al., 2015). Tensor-derived diffusion metrics have provided a way to characterize tissue microstructure in healthy subjects and patients, and plays an important role as biomarkers in neurodegenerative diseases (Schouten et al., 2016; Shibata, 2007; Wang et al., 2013; Schoth et al., 2006; Budde et al., 2007; Lee et al., 2015; Stebbins, Murphy, 2009). Diffusion tractography is thus imperfect, but useful, if we understand and acknowledge its limitations.

The most successful application of diffusion tractography has been the definition and localization of the major white matter bundles of the human brain (Catani, Mesulam, 2008; Makris et al., 2013; Maldonado et al., 2013; Takemura et al., 2016), and their use as regions of interest to improve the individual anatomical precision in extracting microstructural information. However, it has been difficult to go beyond this main application and the major well known white matter bundles. The reason for this in part lies on the fact that the very elements of brain anatomical connectivity that are poorly known are the ones that are more challenging for diffusion tractography (Jbabdi, Johansen-Berg, 2011). We can reliably visualize the main associative cortico-cortical fascicles that run anterior-posteriorly in the human brain (Lawes et al., 2008), but secondary bundles are hard to track, especially if they are medio-laterally oriented. Moreover, while locating a bundle in the brain can easily be achieved, precisely determining its cortical terminations remains challenging because of low spatial resolution and partial volume effects. These limits restrict some applications of tractography, such as grey matter parcellation and connectomic analysis (Pestilli et al., 2014). The introduction of more advanced low-level models that can better characterize the profile of the fibres inside the voxel has improved the accuracy in detecting secondary white matter pathways (Tournier et al., 2004; Dell'Acqua et al., 2007; Descoteaux et al., 2009). However, the detailed organization of axons within a voxel remains often ambiguous, because of kissing, bending, crossing, and fanning fibres.

So, how can we improve the sensitivity and specificity of tractography? Innovations in MRI hardware, sequence optimization, diffusion models, and tractography algorithms will certainly improve the accuracy of the results, and will expand the potential application of the technique. Improvement of segmentation and clustering techniques will help the topographical definition of fibre bundles and correct visualization of fibre terminations Smith et al. (2012); Girard et al. (2014). Today, it is clear that anatomical *a-priori* knowledge is fundamental to increase the specificity of the 3D reconstructions. The choice of tractography parameters strictly depends on the specific white matter region and white matter bundle under investigation. "Black box tractography" is hardly gonna give us reliable answers. In this sense, validation of tractography results at the micro-anatomical level is fundamental, both to improve tractography methods and to expand our knowledge on the complex white matter architecture of the human brain. Finally, in the field of virtual dissection, there is an urgent need for new quantitative measures that can better describe the tissue microstructure. Tensor-derived metrics are useful in defining some aspects about brain connectivity, but their interpretation is limited (Jones,

Cercignani, 2010).

Continuous improvement in methods of white matter characterization along with with other developments in electrophysiology and functional neuroimaging techniques will contribute to expand our knowledge on large-scale network. Knowing about the structure of a network informs our understanding of its function. *"[...] Any attempt to disclose the nature of cortical processes — that is, the fate of the incoming impulses from the external world — must commence by tracing the afferent paths traversed by these external impulses on their way to the cortex."* Polyak (1932)

Bibliography

Basser P J, Mattiello J, LeBihan D. MR diffusion tensor spectroscopy and imaging. // Biophysical journal. 1994. 66, 1. 259–267.

Budde Matthew D, Kim Joong Hee, Liang Hsiao-Fang, Schmidt Robert E, Russell John H, Cross Anne H, Song Sheng-Kwei. Toward accurate diagnosis of white matter pathology using diffusion tensor imaging // Magnetic Resonance in Medicine. 2007. 57, 4. 688–695.

Catani Marco. From hodology to function // Brain. 2007. 130, 3. 602–605.

Catani Marco, Jones Derek K., Ffytche Dominic H. Perisylvian language networks of the human brain // Annals of Neurology. 2005. 57, 1. 8–16.

Catani Marco, Mesulam Marsel. What is a disconnection syndrome? // Cortex. 2008. 44, 8. 911–913.

Chen Zhenrui, Tie Yanmei, Olubiyi Olutayo, Rigolo Laura, Mehrtash Alireza, Norton Isaiah, Pasternak Ofer, Rathi Yogesh, Golby Alexandra J., O'Donnell Lauren J. Reconstruction of the arcuate fasciculus for surgical planning in the setting of peritumoral edema using two-tensor unscented Kalman filter tractography // NeuroImage: Clinical. 2015. 7. 815–822.

Dell'Acqua F, Rizzo G, Scifo P, Clarke R a, Scotti G, FAzio F. A ModelBased Deconvolution Approach to Solve Fiber Crossing in DiusionWeighted MR Imaging // Biomedical Engineering, IEEE Transactions on. 2007. 54, 3. 462472.

Descoteaux Maxime, Deriche Rachid, Knösche T, Anwander Alfred. Deterministic and Probabilistic Tractography Based on Complex Fiber Orientation Distributions // IEEE Transactions on Medical Imaging. 2009. 28, 2. 269–286.

Girard Gabriel, Whittingstall Kevin, Deriche Rachid, Descoteaux Maxime. Towards quantitative connectivity analysis : reducing tractography biases // NeuroImage. 2014. 98. 266–278.

Jbabdi Saad, Johansen-Berg Heidi. Tractography: Where Do We Go from Here? // Brain Connectivity. 2011. 1, 3. 169–183.

Johansen-Berg Heidi, Behrens Timothy E J. Just pretty pictures? What diffusion tractography can add in clinical neuroscience. // Current opinion in neurology. aug 2006. 19, 4. 379–85.

Jones Derek K, Cercignani Mara. Twenty-five pitfalls in the analysis of diffusion MRI data // NMR in Biomedicine. 2010. 23, 7. 803–820.

Lawes I Nigel C, Barrick Thomas R, Murugam Vengadasalam, Spierings Natalia, Evans David R, Song Marie, Clark Chris A. Atlas-based segmentation of white matter tracts of the human brain using diffusion tensor tractography and comparison with classical dissection. // NeuroImage. jan 2008. 39, 1. 62–79.

Lee Dong-Hoon, Park Ji Won, Park Sung-Hee, Hong Cheolpyo. Have You Ever Seen the Impact of Crossing Fiber in DTI?: Demonstration of the Corticospinal Tract Pathway // Plos One. 2015. 10, 7. e0112045.

Makris N, Preti M G, Asami T, Pelavin P, Campbell B, Papadimitriou G M, Kaiser J, Baselli G, Westin C F, Shenton M E, Kubicki M. Human middle longitudinal fascicle: variations in patterns of anatomical connections. // Brain structure & function. jul 2013. 218, 4. 951–68.

Maldonado Igor Lima, De Champfleur Nicolas Menjot, Velut St??phane, Destrieux Christophe, Zemmoura Ilyess, Duffau Hugues. Evidence of a middle longitudinal fasciculus in the human brain from fiber dissection // Journal of Anatomy. 2013. 223, 1. 38–45.

Mesulam M-marsel. Large-Scale Neurocognitive Networks and Distributed Processing for Attention, Language, and Memory // Annals of Neurology. 1990. 28. 597–613.

Mori S, Crain B J, Chacko V P, Zijl P C van. Three-dimensional tracking of axonal projections in the brain by magnetic resonance imaging. // Annals of neurology. 1999. 45, 2. 265–269.

Pestilli Franco, Yeatman Jason D, Rokem Ariel, Kay Kendrick N, Wandell Brian A. Evaluation and statistical inference for human connectomes. // Nature methods. 2014. 11, 10. 1058–63.

The Main Afferent Fiber Systems of the Cerebral Cortex in Primates, VoL 2. // . 1932. 370.

Saur Dorothee, Kreher Björn W, Schnell Susanne, Kümmerer Dorothee, Kellmeyer Philipp, Vry Magnus-Sebastian, Umarova Roza, Musso Mariacristina, Glauche Volkmar, Abel Stefanie, Huber Walter, Rijntjes Michel, Hennig Jürgen, Weiller Cornelius. Ventral and dorsal pathways for language. // Proceedings of the National Academy of Sciences of the United States of America. 2008. 105, 46. 18035–40.

Scheck Simon M., Pannek Kerstin, Raffelt David A., Fiori Simona, Boyd Roslyn N., Rose Stephen E. Structural connectivity of the anterior cingulate in children with unilateral cerebral palsy due to white matter lesions // NeuroImage: Clinical. 2015. 9. 498–505.

Schoth F., Burgel U., Dorsch R., Reinges M.H.T., Krings T. Diffusion tensor imaging in acquired blind humans // Neuroscience Letters. may 2006. 398, 3. 178–182.

Schouten Tijn M., Loitfelder Marisa, Vos Frank de, Seiler Stephan, Grond Jeroen van der, Lechner Anita, Hafkemeijer Anne, Möller Christiane, Schmidt Reinhold, Rooij Mark de, Rombouts Serge A.R.B. Combining anatomical, diffusion, and resting state functional magnetic resonance imaging for individual classification of mild and moderate Alzheimer's disease // NeuroImage: Clinical. jan 2016. 11. 46–51.

Shibata D. K. Differences in brain structure in deaf persons on MR imaging studied with voxel-based morphometry // American Journal of Neuroradiology. 2007. 28, 2. 243–249.

Sigalovsky Irina S, Fischl Bruce, Melcher Jennifer R. Mapping an intrinsic MR property of gray matter in auditory cortex of living humans: a possible marker for primary cortex and hemispheric differences. // NeuroImage. oct 2006. 32, 4. 1524–37.

Smith Robert E., Tournier Jacques-Donald, Calamante Fernando, Connelly Alan. Anatomically-constrained tractography: Improved diffusion MRI streamlines tractography through effective use of anatomical information // NeuroImage. 2012. 62, 3. 1924–1938.

Stebbins G T, Murphy C M. Diffusion tensor imaging in Alzheimer's disease and mild cognitive impairment. // Behavioural neurology. 2009. 21, 1. 39–49.

Takemura Hiromasa, Caiafa Cesar F., Wandell Brian A., Pestilli Franco. Ensemble Tractography // PLoS Computational Biology. 2016. 12, 2. 1–22.

Thomas Cibu, Ye Frank Q., Irfanoglu M. Okan, Modi Pooja, Saleem Kadharbatcha S., Leopold David A., Pierpaoli Carlo. Anatomical accuracy of brain connections derived from diffusion MRI tractography is inherently limited // Proceedings of the National Academy of Sciences. nov 2014. 111, 46. 16574–16579.

Tournier J. Donald, Calamante Fernando, Gadian David G., Connelly Alan. Direct estimation of the fiber orientation density function from diffusion-weighted MRI data using spherical deconvolution // NeuroImage. 2004. 23, 3. 1176–1185.

Wang Dawei, Qin Wen, Liu Yong, Zhang Yunting, Jiang Tianzi, Yu Chunshui. Altered white matter integrity in the congenital and late blind people. // Neural plasticity. 2013. 2013. 128236.

Winston Gavin P, Mancini Laura, Stretton Jason, Ashmore Jonathan, Symms Mark R, Duncan John S, Yousry Tarek A. Diffusion tensor imaging tractography of the optic radiation for epilepsy surgical planning: a comparison of two methods. // Epilepsy research. nov 2011. 97, 1-2. 124–32.

Yu C S, Lin F C, Li K C, Jiang T Z, Zhu C Z, Qin W, Sun H, Chan P, Smith S M, Paulson O B, Jelsing J. Diffusion tensor imaging in the assessment of normal-appearing brain tissue damage in relapsing neuromyelitis optica. // AJNR. American journal of neuroradiology. 2006. 27, 5. 1009–1015.